The Thesis Committee for Jose Carlos Davila Labastida
Certifies that this is the approved version of the following thesis:

Reverse-Selective Polymer-Ionic Liquid Membranes

for Light Paraffin Gas Separations

APPROVED BY

SUPERVISING COMMITTEE:

Joan F. Brennecke, Co-Supervisor

Benny D. Freeman, Co-Supervisor

Reverse-Selective Polymer-Ionic Liquid Membranes

for Light Paraffin Gas Separations

by

Jose Carlos Davila Labastida, B.S.

Thesis

Presented to the Faculty of the Graduate School of

The University of Texas at Austin

in Partial Fulfillment

of the Requirements

for the Degree of

Master of Science in Engineering

The University of Texas at Austin

August 2021

Dedication

To Joe, Laura and Luis

Possunt, quia posse videntur

Acknowledgements

It is hard to overstate the importance of collaboration in intellectual work. It is almost as hard to adequately recognize everyone who has directly or indirectly contributed a puzzle piece, which were all undoubtedly held by individuals other than the author, of the work hereby reported. Nonetheless, an effort will be made.

Firstly, the four undergraduates and one high school student who contributed their time and energy to learn the ropes of laboratory work and independent thought must be recognized: the Jack-of-all-trades Maximilian Strauss, the highly meticulous Nathalie Debelle, the interdisciplinary Sarah Sam, the always ready to go Mikaela Rey, and the tech-savvy Matthew Santoso. As the reader will notice, Max contributed immensely to this work and wholly deserves co-authorship in at least two journal articles had the author managed to publish in peer-reviewed journals. Thanks to the sponsoring programs, the CISTAR Outreach fund for supporting Max for over 2 years, the tireless Ana Dison from the Women in Engineering Program for connecting Sarah, Nathalie and Mikaela to the author via the GLUE initiative, and the CISTAR Summer Young Scholars program for supporting Matthew.

Secondly, I must acknowledge my peers. Thanks to Dr. Jaesung Park for teaching the author of permeation systems, both constant-volume and mixed-gas. Thanks to Dr. Tangqiumei "Maggie" Song for illuminating the author on how to use the MSB, how most of the Brennecke lab equipment is used, and how to be extra safe. Thanks to Dr. Michelle Dose for showing her syntheses, allowing the author to get in the way of her GC troubleshooting, and leading the Freeman group lab move and outreach efforts. Thanks to Caitlin Bentley for her 101 ways of troubleshooting anything experimental, her hearty

counsel and heartier baked goods. Thanks to Dr. Kristofer Gleason for automating most of our permeators, for his design expertise crucial to getting Bespin built, and for sharing where to find even the most obscure part numbers. Thanks to Edwin Torres Cuevas for his help with polymerizations and castings, his GUM and safety officer initiatives, and his being a great listener. Thanks to Constanza for sharing her regulators, gas cylinders and valuable experiences. Thanks to Dr. Manuel Aguilar for letting the author tap his expertise in selecting the best membrane science models and the best Mennonite cheeses. Thanks to Phiwat Klomkaew for always making our visiting scholars feel welcome and offering a helping hand to the local graduate students. Thanks also to Dr. Melanie Merrick for her expertise in EOS selection and Kaleidagraph, and for her abundant feedback that is usually the perfect blend of constructive and encouraging. Thanks to Dr. Josh Moon for his aiding the author in design of experiments and sample preparation early on and for his making very thorough points during group meetings, despite not being a presenter in most of them. Thanks to Matt Davenport for his insightful research discussions, for his candid encouragement and leadership within CISTAR. Thanks to Sejoon Park for his admirable perseverance, for his aid with equipment calibrations, and for sharing Chewbacca with the author.

In addition, the author would like to acknowledge T.J. Dilenshneider, Marshall Allen, Kimi Bourland, Alexander Bridge, Hyeonji Oh, Mariam Balogun, and Dr. Oscar Morales-Collazo (as well as Phiwat, Edwin and Melanie) for their helping the author with the madness of setting up the Girl Day Frozen Chemistry Show and other outreach efforts. Thanks also to Zhichao Chen, Mike Lubben, Yuanyuan Lyu, Janakey Devi, Heewok Yoon, Eui Soung Jang, Rahul Sujanani, Kevin Reimund, Christina Rodriguez, Kimi Bourland, Austin Keller, Oscar Nordness, Hadi Khani, Yu-Heng Cheng, Horacio Lopez Marques, Seungmin Oh, Gabriela Avelar-Bonilla, William Sullivan, Julian

Abstract

Reverse-Selective Polymer-Ionic Liquid Membranes
for Light Paraffin Gas Separations

Jose Carlos Davila Labastida, M.S.E.

The University of Texas at Austin, 2021

Co-Supervisor: Benny D. Freeman

Co-Supervisor: Joan F. Brennecke

Natural gas plays a major role as both a relatively clean-burning fossil fuel and a precursor to hydrogen, ethylene, and numerous chemical commodities. With advancements in horizontal drilling and hydraulic fracturing, abundant shale resources are a growing piece of the global energy transition puzzle. Shale gas is richer in C_{2+} hydrocarbons than conventional natural gas which presents challenges and opportunities to centralized gas processing infrastructure. Membranes offer an energy efficient alternative separation technology for fractionating the light C_{2+} hydrocarbons at modular scales.

Reverse-selective membranes may offer an economic advantage given their typically high productivities. Reverse-selective polymers, much like ionic liquids and other solvents, discriminate between gas molecules based primarily on solubility differences. Unlike traditional solvents, however, ionic liquids are negligibly volatile and

can be combined with polymers into stable membrane platforms, albeit with lesser understood transport properties.

In this thesis, a comprehensive study of the light paraffin gas transport properties of 1-hexyl-3-methylimidazolium bis(trifluoromethylsulfonyl)imide, or [hmim][Tf_2N], ionic liquid supported in poly(1-trimethylsilyl-1-propyne), or PTMSP, membranes is presented, along with preliminary work on some alternative polymer-ionic liquid combinations. The thermal, mechanical, and swelling properties of these supported ionic liquid membranes (SILMs) were initially characterized for various ionic liquid loadings. The pure-gas permeation, sorption, and diffusion properties of SILMs were then determined and compared with those of the neat parent materials.

While prior work on SILMs for gas separations is widespread, few studies focus on light paraffin separations, and fewer still evaluate mixed-gas transport properties or pronounced plasticizing effects of the polymer support on the gas transport properties. A mixed-gas permeation system was built and validated to probe the more industrially relevant mixture properties. Unlike in the neat PTMSP, pronounced permeability increases with rising C_{2+} activities were noted in SILMs. A plasticization model was fit to the diffusion data of the three lightest paraffin gases to better understand the impact of ionic liquid content on plasticization.

With increasing ionic liquid content, a clear transition in the C_{2+} sorption behavior was observed from a rigid, open glass (dual-mode) to a dense, softer material (Flory-Huggins). A new hybrid model was proposed to fit sorption isotherms in all regimes of this transition. Lastly, an atypical volume expansion behavior was observed in preliminary SILM dilation studies and an optical transition matching the inflection in the C_{2+} sorption isotherms and permeability curves was identified.

Table of Contents

List of Tables

List of Figures

Chapter 1: Introduction

1.1 NATURAL GAS LIQUID RECOVERY FROM METHANE IN NATURAL GAS PROCESSING

Advancements in horizontal drilling and hydraulic fracturing have allowed the U.S. energy industry to exploit previously untapped shale oil and gas resources. Rich in hydrocarbons other than methane, shale resources have enabled the inexpensive production of not only methane gas but also associated C_2-C_{4+} natural gas liquids, or NGLs. As illustrated by Figure 1.1, the proportion of NGLs in shale gas ($\sim29_{vol}\%$) exceeds that in conventional natural gas (from $4_{vol}\%$ for dry gas to $15.4_{vol}\%$ for wet gas) [1,2]. Due in part to their growing surplus, NGLs have been increasingly displacing traditional naphtha feedstocks for fuel and chemical manufacturing [3].
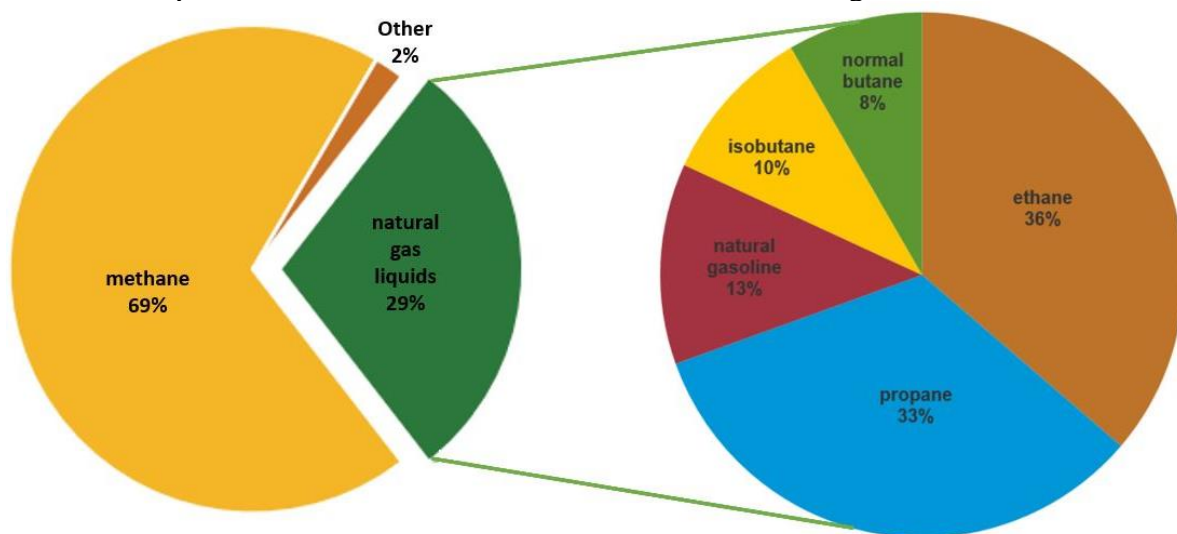
Figure 1.1:   Left: Typical U.S. natural gas composition as averaged from production in the Bakken, Marcellus, Utica, Niobrara, and Eagle Ford shales, 2014. Right: U.S. hydrocarbon gas liquids production from natural gas processing, 2016 (3.51 million barrels per day in 2016). Adapted from [2, 4]

5.43 million barrels per day (MMBD) of NGLs were being produced in 2019, of which roughly a third (1.83 MMBD) were ethane and a third (1.88 MMBD) were

propane [5]. Most raw NGLs are transported in Y-grade pipelines to midstream natural gas plants. Y-grade pipelines are limited to low capacities due to pooling of the heavier NGLs when they reach their vapor pressures. The mid-purity NGL pipelines, such as E-P (80% ethane-20% propane), P-P (refinery-grade propane-propylene mixtures), and L-P (liquified petroleum gas, mostly liquid propane, n-butane, and isobutane), are more efficient than Y-grade infrastructure. These mid-purity streams can be readily used as feedstocks for processes downstream (e.g., thermal cracking, dehydrogenation and oligomerization), used as fuels, or, since 2010, exported to offshore markets. [6] Nonetheless, inherent transportation and separation infrastructure limitations keep more than 12% of NGLs from being usefully consumed. In fact, of the 5.43 MMBD produced in the U.S. in 2019, only 3.14 MMBD were consumed in U.S. markets, while 1.83 MMBD were exported and 0.21 MMBD were imported [5].

The fate of the remainder 0.67 MMBD NGLs, except for a minute fraction allocated for long-term storage, is the flare. For by-product NGLs at the growing number of smaller (<500 BOE/d) drilling operations, flaring is often the only financially sound alternative. In 2016, as much as 10_{vol}% of natural gas (29_{vol}% of which are unrecovered NGLs) of the 6 BCFD being produced in the Eagle Ford were flared [7]. This figure can be higher in less developed shale formations, as much as 32_{vol}% in North Dakota's Bakken in 2013.

Separation of the NGLs from shale gas is typically done via cryogenic turboexpansion and distillation in a demethanizer, following the drying, sweetening and upgrading of raw natural gas shown in Figure 1.2. Further fractionation steps, depending on purity targets, may involve one or several of the following distillation units: deethanizer, depropanizer, debutanizer, deisobutanizer [8]. Note that the U.S. average

NGL yield is 84 barrels per million standard cubic feet of gas [4].
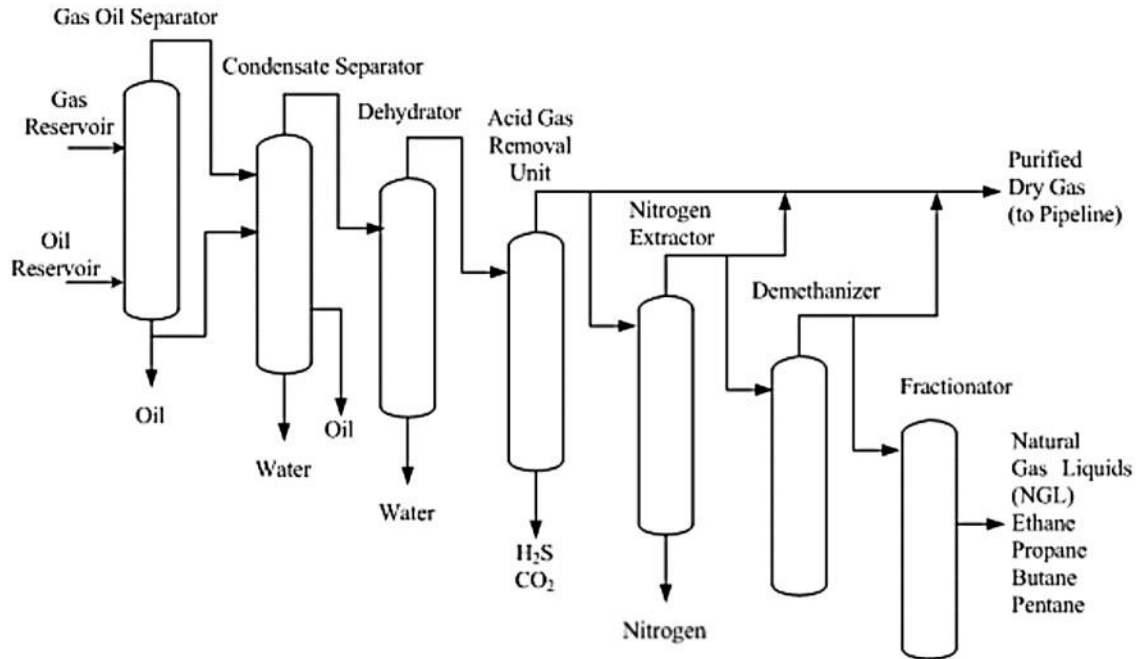
Figure 1.2:   A summary of typical natural gas treatment steps as presented by [9].

Given the importance of refrigeration in conventional NGL fractionation processes, midstream gas plants are built to benefit from the economies of scale. As a result, the raw gas must be transported upstream from dozens to hundreds of wells to a relatively large NGL fractionation facility (the smallest gas plants process 100-200 MSCFD, though a typical capacity in Texas is 200-300 MSCFD) while the mid-purity product stream is transported either to further processing downstream or to various industrial, commercial, and residential markets [10, 11]. This makes the viability of any one new drilling operation dependent not only on its throughput but also on its accessibility by Y-grade hydrocarbon infrastructure or suitable alternatives.

3

To reduce the gap between produced and consumed NGLs and to facilitate the expansion of U.S. shale resource production projects, more modular, smaller scale gas processing units closer to the wellhead could prove advantageous [6]. Such units may benefit from mass transfer-based rather than heat transfer-based separation technologies, such as pressure-swing adsorption or membrane separations.

1.2 POLYMER MEMBRANES FOR GAS SEPARATIONS

Polymer membranes have found commercial success in applications such as hydrogen recovery, air separation, and natural gas sweetening [12-15]. While there is rising interest in using membranes for paraffin and hydrocarbon vapor separations, studies of light hydrocarbon vapor transport through polymers are not as numerous as those for the permanent gases. Nonetheless, there are nascent industrial-scale efforts in the light hydrocarbon separations space involving polymer membranes:

- Monomer recovery in polyolefin plants [16, 17]
- Gasoline vapor recovery from purge streams [18, 19]
- Membrane-assisted liquified petroleum gas (LPG) recovery [20]

Membrane-based separations offer several advantages. The energy requirement can be as little as 10% of that of the distillation equivalent, translating to lower operational and environmental costs [21]. A membrane unit scales with surface area rather than volume and needs little to no refrigeration, yielding less prohibitive capital costs than other methods for small-scale, modular systems. Membrane modularization permits the easier adaptation of separation processes to fit the changing composition and capacity needs of a process [15]. In the context of shale gas processing, treating the raw natural gas closer to the wellhead rather than transporting it to a centralized midstream gas plant could reduce processing energy and Y-grade infrastructure costs. Figure 1.3

depicts commonly employed hollow fiber and spiral-wound membrane module architectures in many gas separations.
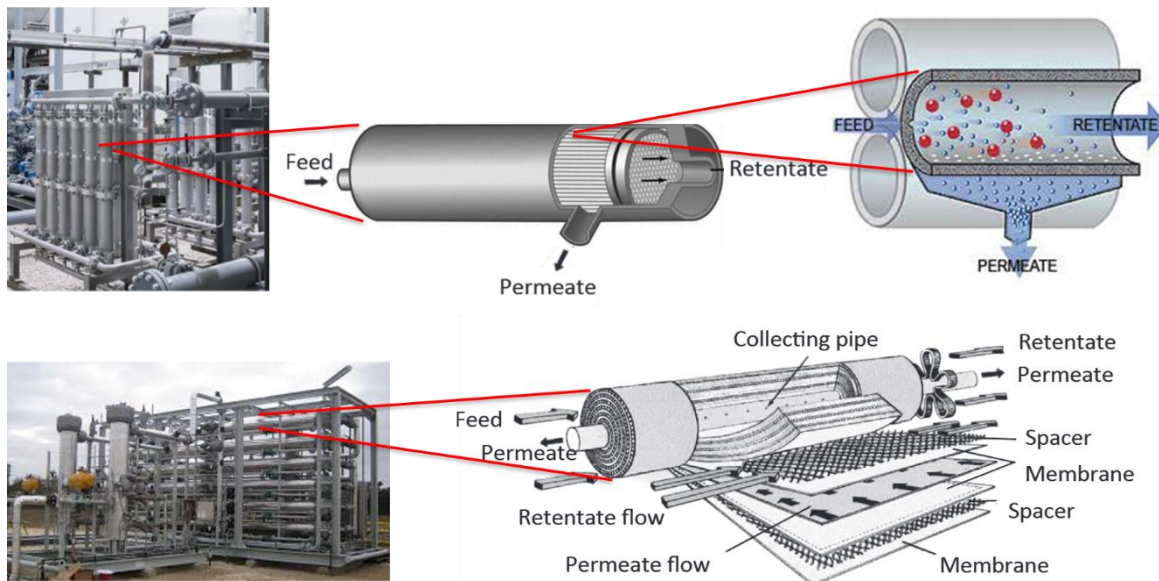
Figure 1.3:   Top: a skid of Sepuran® Noble He separation hollow-fiber modules developed by Evonik Industries. They are part of the largest industrial facility of its kind to purify He from N_2 in Mankota, Saskatchewan, Canada, designed by Linde Engineering and operated by the Weil Group. Bottom: a skid of Separex^{TM} cellulose acetate spiral-wound modules for CO_2 removal developed by Honeywell UOP. Such modules are used in very large CO_2 removal plants in Kadanwari and Qadirpur, Pakistan, installed by UOP. Adapted from [14-15, 22].

1.3 IONIC LIQUIDS FOR GAS SEPARATIONS

Ionic liquids, or ILs, are salts with melting points below 100 °C. They have been extensively studied for separations applications due to their negligible volatility, high thermal stability, and tunable functionalities [23, 24]. As implied by Figure 1.4, ILs have been investigated as CO_2 capture absorbents, as media for the safe storage of hazardous gases (e.g., H_2S and C_2H_2), as solvents for liquid-liquid extractions, and as active components of stationary phases in GC columns [25-27]. Like other organic solvents, ILs

can discriminate between gas molecules based on solubility differences and thus make attractive candidates for solubility-driven separation techniques [28, 29].

Figure 1.4:   The utility of ionic liquids goes beyond applications in separations.

In the context of gas separation membranes, organic liquids with favorable solubility-selectivity or plasticizing properties can be combined with polymers to enhance their transport properties. However, traditional supported liquid membranes often face challenges with low accessible transmembrane pressure (limited by capillary force supporting the liquid in the largest pores), short lifetimes due to the organic liquid volatility, and, in the case of polymeric supports, reduced mechanical and thermal stability compared to the pristine polymers. Given their negligible volatility, high thermal stability, and moderate to high viscosities permitting augmented capillary forces, [24] ILs can address these challenges.

6

ILs can be incorporated into a polymer membrane in multiple ways: a) by supporting the IL in a porous polymeric support; b) by blending a compatible IL and polymer into a casting solution to form a composite membrane; and c) by building a poly-ionic liquid. The last can be achieved through polymerization of either the anions or cations (with its balance of complementary free ions) or through functionalization of an anion or cation into an existing polymer chain [30]. The first approach, making supported ionic liquid membranes (SILMs), is also the most common.

1.4 REVERSE-SELECTIVE AND SIZE-SELECTIVE MEMBRANES

Membrane materials can be categorized as size-selective or reverse-selective for a given separation. Size-selective materials discriminate amongst molecules based primarily on their relative diffusivities. Size-sieving effects are most significant when the size of the average free volume elements available for diffusion lies between the effective sizes of the two penetrants to be separated. Penetrant size is often characterized by the kinetic diameter or by the Lennard Jones diameter. Separations in reverse-selective materials are mainly solubility-driven, permitting penetrants to permeate in the order of most to least condensable [28, 29]. Condensability is characterized by gas critical temperature and is sometimes correlated to penetrant volume or the Lennard Jones well depth of the gas, ε/k.

For NGL recovery from methane, reverse-selective membranes may offer the advantage of keeping the methane-rich stream at high pressure in the retentate side. As implied in Figure 1.5, the compression duties of the permeate streams (overall and between stages in a membrane cascade) in the reverse-selective system are smaller than in its size-selective analogue. Prior studies on solubility-selective membranes have

considered both glassy and rubbery polymers for CO_2 from H_2, [29, 31-33] light paraffin (C_3H_8 and n-C_4H_{10}) from CH_4 and H_2 [34-38], and H_2S from CH_4 separations [39].
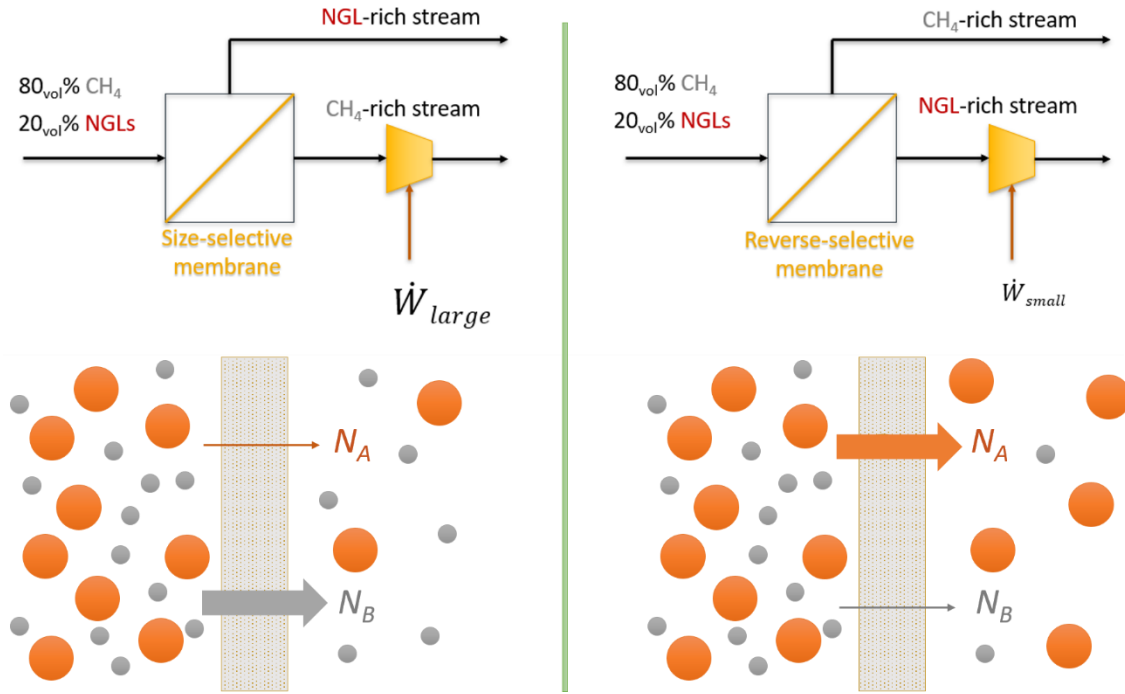
Figure 1.5:   Comparing size-selective and reverse-selective membrane systems in the context of NGL recovery from CH_4.

1.5 IMPORTANCE OF MIXED-GAS VS PURE-GAS STUDIES

Across the membrane science literature, it is practical to obtain permeation and sorption properties with pure-gas feeds. Pure-gas measurements are relatively simple to carry out and interpret, but they derive only a good approximation of properties obtained from mixed-gas experiments, provided that there are minimal mixture interactions (i.e., that all species in the mixture are near ideal gases and the material permeation properties do not change significantly due to exposure to all species). Mixed-gas measurements yield transport properties that are more representative of the real material performance

8

and, in tandem with pure-gas measurements, help researchers quantify the effects of mixture interactions on material transport properties. Membrane materials are often subject to highly condensable penetrant-induced effects such as conditioning, plasticization and competitive-sorption.

Prior mixed-gas studies of light paraffin transport in polymers include CH_4-C_4H_{10} in PDMS [38, 40], CO_2-C_2H_6 in a crosslinked PEO-based copolymer [41], CH_4-C_4H_{10} in PTMSP and PIM-1 [34, 42] and CO_2-CH_4 in 6FDA-mPDA polyimide [43] (see Appendix A for the full name of these polymers). Alhazmi summarized the observed differences between CH_4 permeabilities from pure-gas and $98_{vol}\%CH_4$-$2_{vol}\%C_4H_{10}$ mixed-gas studies of various polymers, shown in Figure 1.6. These mixed-gas/pure-gas differences can also be quite significant, albeit not as extreme, for mixtures involving the 2-carbon and 3-carbon paraffins, yet few studies consider them for binary mixed-gas studies, as C_4H_{10} has been a preferred model NGL molecule.

Mixed-gas permeation and sorption measurements, while more complex and time intensive than the pure-gas equivalents, are essential for a complete understanding of light paraffin gas and vapor mixture transport in membrane materials.

1.6 GOALS AND STRUCTURE OF THIS THESIS

The objectives of this thesis are (1) to investigate the viability of hybridizing ionic liquids that have large C_{2+}/CH_4 solubility-selectivities with highly permeable substituted polyacetylenes, (2) to assess the potential of these polyacetylene supported ionic liquid membranes for NGL recovery, (3) to evaluate the impact of mixture nonidealities on the transport properties, and (4) to add to the growing literature on material transport properties derived from mixed-gas studies.

This thesis is organized into eight chapters. This first chapter serves as the introduction and motivation for the work documented in later chapters. Chapter 2 covers the most relevant theory of permeation and sorption in membrane materials, as well as some background on polyacetylenes and ionic liquids. Materials and experimental methods are the subject of Chapter 3.
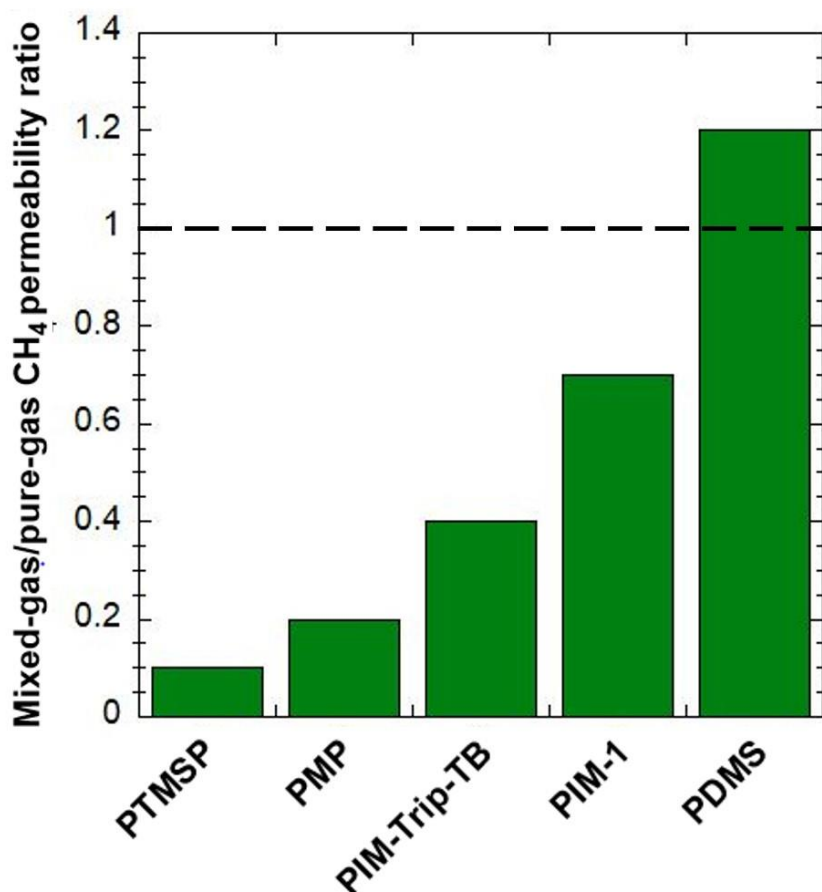
Figure 1.6:   The mixed-gas over pure-gas methane permeability ratio of 5 membrane materials as tested with a $98_{vol}\%$ CH_4-$2_{vol}\%C_4H_{10}$ mixed-gas feed at 25 °C and CH_4, C_4H_{10} pure-gas feeds at 25 °C. The transmembrane pressure was fixed between 3.5 bar and 5 bar in all cases, except when testing the pure C_4H_{10} feed, which was held at 2 bar. Note that all but PDMS are glassy polymers, while PDMS is a rubbery polymer. Adapted from [44].

Chapter 4 presents basic membrane characterization studies complementary to the transport properties explored in later chapters. Chapter 5 reports pure-gas permeation studies of PTMSP and PMP, both as neat polymers and with various loadings of an ionic liquid, primarily 1-hexyl-3-methylimidazolium bis(trifluoromethylsulfonyl)imide ([hmim][Tf$_2$N]). Chapter 6 focuses on CH$_4$-C$_2$H$_6$ and CH$_4$-C$_3$H$_8$ mixed-gas permeation studies of select compositions of the [hmim][Tf$_2$N]-PTMSP system of SILMs. Chapter 7 explores CH$_4$, C$_2$H$_6$, and C$_3$H$_8$ sorption and dilation studies for the same [hmim][Tf$_2$N]-PTMSP system, as well as pure-gas derived diffusivities in these materials.

Chapter 8 completes the thesis with the conclusions and suggestions for future work.

1.7 REFERENCES

[1]   S. Faramawy, T. Zakib, A.A.-E. Sakr, Natural gas origin, composition, and processing: A review, Journal of Natural Gas Science and Engineering, 34 (2016) 34-54.

[2]   M.W. Conder, K.A. Lawlor, Production Characteristics Of Liquids-Rich Resource Plays Challenge Facility Design, American Oil & Gas Reporter (2014).

[3]   S.E. DeRosa, D.T. Allen, Impact of Natural Gas and Natural Gas Liquids Supplies on the United States Chemical Manufacturing Industry: Production Cost Effects and Identification of Bottleneck Intermediates, ACS Sustainable Chemistry and Engineering, 3 (2015) 451-459.

[4]   U.S. Energy Information Administration, Petroleum Supply Annual, 2017.

[5]   U.S. Energy Information Administration, Monthly Crude Oil and Natural Gas Production, 2020.

[6]   T. Ridha, Y. Li, E. Gençer, J, Siirola, J. Miller, F. Ribeiro, R. Agrawal, Valorization of Shale Gas Condensate to Liquid Hydrocarbons through Catalytic Dehydrogenation and Oligomerization, Processes, 6 (2018) 139.

[7]   M. Franklin, K. Chau, L.J. Cushing and J.E. Johnston, Characterizing Flaring from Unconventional Oil and Gas Operations in South Texas Using Satellite Observations, *Environmental Science & Technology, 53* (2019) 2220-2228.

[8]   S. Lee, N. V.D. Long, M.Lee, Design and Optimization of Natural Gas Liquefaction and Recovery Processes for Offshore Floating Liquefied Natural Gas Plants, Industrial & Engineering Chemistry Research, 51 (2012) 10021-10030.

[9]   T. James, S. Phil, M. Erin, Natural Gas Processing, Energy Information Administration, Office of Oil and Gas, 2006.

[10]   A. Pederstad, Improving utilization of associated gas in US tight oil fields (Rep. No. 988 457 930), Carbon Limits, Oslo, Norway, 2015.

[11]   A. Keller, The Lower Carbon Hydrocarbons Leading a US Manufacturing Renaissance, Wood Mackenzie, 2018, 5-12.

[12]   P. Bernardo, E. Drioli, G. Golemme, Membrane Gas Separation: A Review/State of the Art, Industrial Engineering and Chemistry Research, 48 (2009) 4638-4663.

[13]   C.A. Scholes, G.W. Stevens, S.E. Kentish, Membrane gas separation applications in natural gas processing, Fuel 96 (2012) 15-28.

[14]   R.W. Baker, K. Lokhandwala, Natural Gas Processing with Membranes: An Overview, Industrial Engineering Chemistry Research 47 (2008) 2109-2121.

[15]   A. Iulianelli, E. Drioli, Membrane engineering: Latest advancements in gas separation and pre-treatment processes, petrochemical industry and refinery, and future perspectives in emerging applications, Fuel Processing Technology, 206 (2020) 106464.

[16]   G. Tu, Z. Liao, Z. Huang, B. Jiang, J. Wang, Y. Yang, Strategy of effluent recovery technology selection in polyolefin plants, Process Safety and Environmental Protection, 103 (2016) 405-412.

[17]   R.J. Lahiere, M.W. Hellums, J.G. Wijmans, J. Kaschemekat, A Membrane Vapor Separation: Recovery of Vinyl Chloride Monomer from PVC Reactor Vents,

Industrial Engineering and Chemistry Research, 32 (1993) 2236-2241.

[18]   K. Ohlrogge, J. Wind, A Method and Apparatus for reducing Emissions from
        Breather lined Storage Tanks, U.S. Patent 6,059,856 (May 2000).

[19]   X. Wang, R. Daniels, R.W. Baker, A Recovery of VOCs from High-Volume Low
        Concentration Air Streams, AIChE Journal 47 (2001) 1094-1097.

[20]   B.S. Minhas, D.W. Staubs, Membrane process for LPG recovery U.S. Patent
        7,799,964 B2 (April 2006).

[21]   T. Harlacher, M. Wessling, Gas–gas separation by membranes. In Progress in
        Filtration and Separation, Elsevier: New York, NY, USA (2015) 557–584.

[22]   R.P. Lively, D.S. Scholl, Seven Separations to Change the World, Nature 532
        (2016) 435-437.

[23]   M.B. Shiflett, E.J. Maginn, The solubility of gases in ionic liquids. AIChE
        Journal, 63 (2017) 4722-4737.

[24]   R.D. Noble, D.L. Gin, Perspective on ionic liquids and ionic liquid membranes,
        Journal of Membrane Science, 369 (2011) 1-4.

[25]   L.C. Tomé, I.M. Marrucho, Ionic liquid-based materials: A platform to design
        engineered CO_2 separation membranes. Chemical Society Reviews, 45 (2016),
        2785-2824.

[26]   R.I. Canales, J.F.; Brennecke, Comparison of Ionic Liquids to Conventional
        Organic Solvents for Extraction of Aromatics from Aliphatics. Journal of
        Chemical Engineering Data, 61 (2016) 1685-1699.

[27]   C.F. Poole, S.K. Poole, Ionic liquid stationary phases for gas chromatography,
        Journal of Separation Science, 34 (2011) 888-900.

[28]   A. Khakpay, P. Scovazzo, Reverse-selective behavior of room temperature ionic
        liquid-based membranes for natural gas processing. Journal of Membrane

Science, 545 (2018) 204-212.

[29] C.H. Lau, P. Li, F. Li, T. Chung, D.R. Paul, Reverse-selective polymeric membranes for gas separations, Progress in Polymer Science, 38 (2013) 740-766.

[30] V. Polevaya, V. Geiger, G. Bondarenko, S. Shishatskiy, V. Khotimskiy, Chemical Modification of Poly(1-Trimethylsylil-1-Propyne) for the Creation of Highly Efficient CO_2-Selective Membrane Materials, Materials, 12 (2019) 2763.

[31] H. Zhao, X. Ding, Z. Wei, Q. Xie, Y. Zhang, X. Tan, H_2/CO_2 Gas Transport Performance in Poly (Ethylene Oxide) Reverse-selective Membrane with Star-like Structures, Journal of Wuhan University of Technology-Mater. Sci. Ed., 34 (2019) 195-200.

[32] M. Klepić, K. Setničková, M. Lanč, M. Žák, P. Izák, M. Dendisová, A. Fuoco, J.C. Jansen, K. Friess, Permeation and sorption properties of CO2-selective blend membranes based on polyvinyl alcohol (PVA) and 1-ethyl-3-methylimidazolium dicyanamide ([EMIM][DCA]) ionic liquid for effective CO_2/H_2 separation, Journal of Membrane Science, 597 (2020) 117623.

[33] C.L. Bentley, T. Song, B.J. Pedretti, M.J. Lubben, N.A. Lynd, J.F. Brennecke, Effects of Poly(glycidyl ether) Structure and Ether Oxygen Placement on CO2 Solubility, Journal of Chemical & Engineering Data, 66 (2021) 2832-2843.

[34] S. Thomas, I. Pinnau, N. Du, M.D. Guiver, Pure- and mixed-gas permeation properties of a microporous spirobisindane-based ladder polymer (PIM-1), Journal of Membrane Science, 333 (2009) 125-131.

[35] L.E. Starannikova, N.A. Belov, V.P. Shantorovich, T. Suzuki, T.G. Golenko, K.L. Makovetskii, Y.P. Yampol'skii, Transport and physicochemical parameters of polypentenamer, Polymer Science Series A, 49 (2007) 509-516.

[36] M.V. Bermeshev, A.V. Syromolotov, L.E. Starannikova, M.L. Gringolts, V.G. Lakhtin, Y.P. Yampolskii, E.S. Finkelshtein, Glassy Polynorbornenes with Si–O–Si Containing Side Groups. Novel Materials for Hydrocarbon Membrane Separation, Macromolecules, 46 (2013) 8973-8979.

[37]   S. Thomas, I. Pinnau, N. Du, M.D. Guiver, Hydrocarbon/hydrogen mixed-gas permeation properties of PIM-1, an amorphous microporous spirobisindane polymer, Journal of Membrane Science, 338 (2009) 1-4.

[38]   I. Pinnau, Z. He, Pure- and mixed-gas permeation properties of polydimethylsiloxane for hydrocarbon/methane and hydrocarbon/hydrogen separation, Journal of Membrane Science, 244 (2004) 227-233.

[39]   S. Yi, B. Ghanem, Y. Liu, I. Pinnau, W.J. Koros, Ultraselective glassy polymer membranes with unprecedented performance for energy-efficient sour gas separation, Science Advances, 5 (2019) eaaw5459.

[40]   R.D. Raharjo, B.D. Freeman, D.R. Paul, G.C. Sarti, E.S. Sanders, Pure and mixed gas CH_4 and $n-C_4H_{10}$ permeability and diffusivity in poly(dimethylsiloxane), Journal of Membrane Science, 306 (2007) 75-92.

[41]   C.P. Ribeiro, B.D. Freeman, D.R. Paul. Pure- and mixed-gas carbon dioxide/ethane permeability and diffusivity in a cross-linked poly(ethylene oxide) copolymer. Journal of Membrane Science, 377 (2011) 110-123.

[42]   R.D. Raharjo, B.D. Freeman, D.R. Paul, E.S. Sanders, Pure and mixed gas CH_4 and $n-C_4H_{10}$ permeability and diffusivity in poly(1-trimethylsilyl-1-propyne), Polymer, 48 (2007) 7329-7344.

[43]   G. Genduso, B.S. Ghanem, I. Pinnau, Experimental Mixed-Gas Permeability, Sorption and Diffusion of CO_2-CH_4 Mixtures in 6FDA-mPDA Polyimide Membrane: Unveiling the Effect of Competitive Sorption on Permeability Selectivity, Membranes, 9 (2019).

[44]   A.T. Alhazmi, Tröger's Base Ladder Polymer for Membrane-Based Hydrocarbon Separation, M.S. Thesis, King Abdullah University of Science and Technology, Thuwal, Saudi Arabia, 2017.

Chapter 2: Background and Theory

2.1 GAS PERMEATION IN POLYMER MEMBRANES

This section addresses the basics of gas molecule transport through polymer membranes.

2.1.1: Solution-diffusion

Permeability in membranes is typically expressed in units of $10^{-10}\,\text{cm}^3(\text{STP})\text{cm}/(\text{cm}^2\text{s cmHg})$, also known as Barrer, and is defined by Equation 2.1 as the transmembrane pressure and thickness normalized molar flux [1]:

$$P_A = \frac{N_A l}{p_{us} - p_{ds}} \tag{2.1}$$

where p_{us} is the upstream (or retentate) pressure and p_{ds} is the downstream (or permeate) pressure, l is the membrane thickness, and N_A is the molar flux of species A. The latter can be defined by Fick's law (simplified to 1 dimension):

$$N_A = -D_A \frac{dC_A}{dx} \tag{2.2}$$

In this context, D_A is the effective diffusion coefficient of species A in the membrane phase, C_A is the concentration, and x is the spatial coordinate parallel to the membrane thickness [2]. While it is useful to think of the concentration gradient as a proxy for the driving force of gas transport across a membrane, the true driving force involves a gradient in chemical potential, $-\frac{1}{T}\frac{d\mu_A}{dx}$. The chemical potential is defined as [3]:

$$\mu_A = \left(\frac{\partial G}{\partial n_A}\right)_{p,T,n_{B \neq A}} = \mu_A^0 + RT \ln(a_A) \tag{2.3}$$

where μ_A is the chemical potential, μ_A^0 is the reference state chemical potential, G is the Gibbs free energy, a_A is the activity of species A (typically p_A/p_A^{ref} for ideal gases with

16

the reference pressure selected as the saturation pressure for the vapors), and n_A is the number of molecules of A (the chemical potential is also linked to concentration and partial pressure by $p_A = y_A p = \frac{n_A}{n_A + n_B + \cdots} p$).
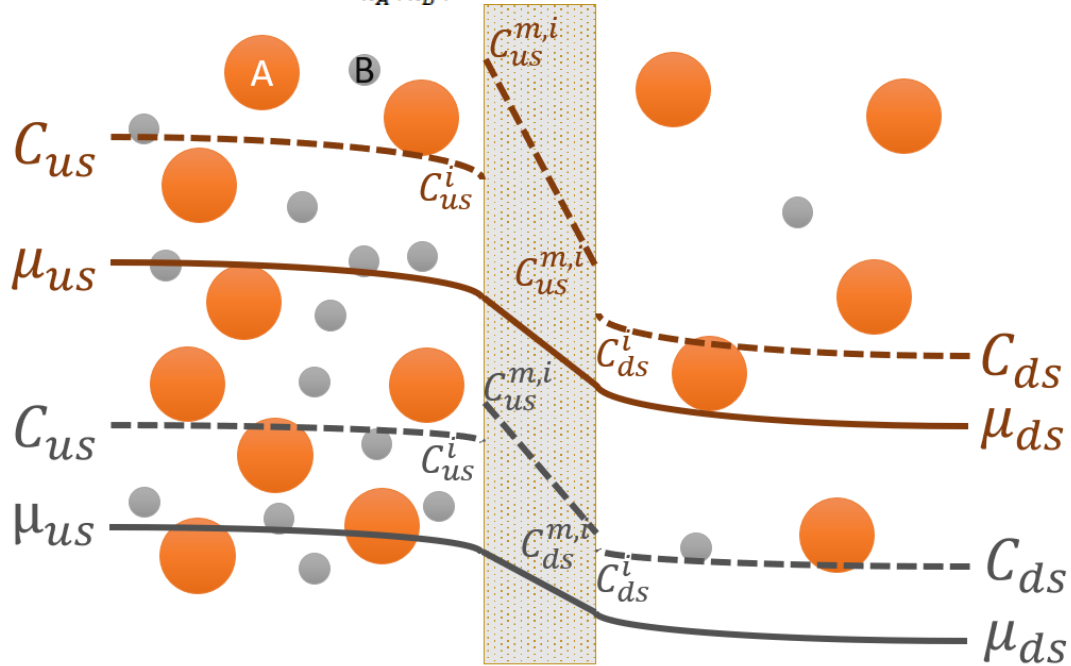
Figure 2.1: Qualitative chemical potential and concentration profiles of two penetrants in steady-state permeation through a dense membrane. The partial pressure, and thus the chemical potential and concentration, of both species is greater at the upstream (left) than it is in the downstream (right). Any gas (A or B) concentration in the solid phase at either interface of the membrane can be related to the gas-phase concentration through a partition coefficient: $: C_{us,i}^{m} = K_{us} C_{us,i}.$ Conveniently, if we assume negligible concentration polarization, the gas concentration in the (upstream or downstream) gas side of the interphase can be approximated as the bulk (upstream or downstream) gas-phase concentration and the partition coefficient defined in terms of the partial pressure: $K_{A,us} = C_{A,us}^{m,i} / p_{A,us}^{i}$.. Adapted from [4].

Depicted in Figure 2.1are the concentration and chemical potential profiles of two species permeating at constant flux (i.e., steady state) in a reverse-selective membrane.

Note that the chemical potential profiles are continuous, emphasizing the equality of chemical potential at the upstream and downstream interfaces of the membrane.

For cases where gases do not behave as ideal gases (i.e., the pressures are not a good approximation of fugacities), it is more meaningful to define permeability as the transmembrane fugacity and thickness normalized flux (see Section 2.5, Equation 2.20).

If the gas partial pressure and concentration are much greater in the upstream than in the downstream, permeability can be reduced to Equation 2.4, the familiar solution-diffusion mechanism [5]:

$$P_A = S_A \bar{D}_A \qquad (2.4)$$

Here, S_A is the solubility of A, and $\bar{D}_A$ is the concentration-averaged diffusivity of A.

The ideal selectivity of a membrane is the ratio of the pure-gas permeabilities of two species, Equation 2.5:

$$\alpha_{A/B} = \frac{P_A}{P_B} = \left(\frac{S_A}{S_B}\right)\left(\frac{\bar{D}_A}{\bar{D}_B}\right) \qquad (2.5)$$

Selectivity is not to be confused with the separation factor, $\alpha^*_{A/B}$: the two quantities differ when the simplifying assumption that $p_{i,us} \gg p_{i,ds} \, y_{i,ds}/y_{i,us}$ is not true [2]:

$$\alpha^*_{A/B} = \frac{y_{A,ds}/y_{B,ds}}{y_{A,us}/y_{B,us}} = \alpha_{A/B} \frac{p_{us} - p_{ds}\dfrac{y_{A,ds}}{y_{A,us}}}{p_{us} - p_{ds}\dfrac{y_{B,ds}}{y_{B,us}}} \qquad (2.6)$$

Further differences arise when considering nonideal gas mixtures (see section 2.5) [5].

Note that any further discussion of diffusivities in this work will be specific to effective concentration-averaged diffusivities, $\bar{D}_i$, and will be expressed simply as D_i

from this point forward. It should be mentioned that other common types of diffusion coefficients in membrane transport have been defined and contrasted in other works [6].

2.1.2: The upper-bound

Traditional size-selective upper bound plots for the CH_4-C_2H_6 and CH_4-C_3H_8 gas pairs were developed, as shown in Figures 2.2a and 2.2b. In this case, the upper bound is defined by relating ideal selectivity to the permeability of the more permeable gas by Equation 2.7, as proposed by Robeson [7]:

$$\alpha_{A/B} = \frac{P_A}{P_B} = \frac{1}{k_p P_A^{n_p-1}} \cong \frac{\beta_{\frac{A}{B}}}{P_A^{\frac{\lambda_A}{B}}} \tag{2.7}$$

where k_p, the front factor, has units of Barrer, and n_p, the slope of the correlation between P_A and P_B, is unitless. Freeman proposed a method to readily estimate these two parameters (albeit rearranged as $\lambda_{A/B}$ and $\beta_{A/B}$) for any given gas pair using Equation 2.8 and Equation 2.9 [8]:

$$n_p - 1 \cong \lambda_{\frac{A}{B}} = \left(\frac{d_B}{d_A}\right)^2 - 1 \tag{2.8}$$

$$\frac{1}{k_p} \cong \beta_{A/B} = \frac{S_A}{S_B} S_A^{\lambda_{A/B}} \exp\left\{-\lambda_{A/B}\left[b - \frac{f(1-a)}{RT}\right]\right\} \tag{2.9}$$

Typically, the d_A and d_B size parameters used are the kinetic diameters of the more and less permeable species, respectively. However, for species larger than methane (the largest of the permanent gases), other size parameters that better describe the relative sizes of the penetrant molecules are often used, such as the Lennard-Jones diameters for olefin-paraffin gas pairs [9].

For the CH_4-C_2H_6 and CH_4-C_3H_8 gas pair upper bounds in this work, diameters derived from the Chung correlation were selected: $d_{C,i} = 0.809 V_{C,i}^{1/3}$, where $V_{C,i}$ is the critical volume of species i. Note that the Chung correlation assumes spherical gas molecules [10].

19

Figures 2.2c and 2.2d show the reverse-selective upper bound analogues for the

C_2H_6-CH_4 and C_3H_8-CH_4 gas pairs, respectively.
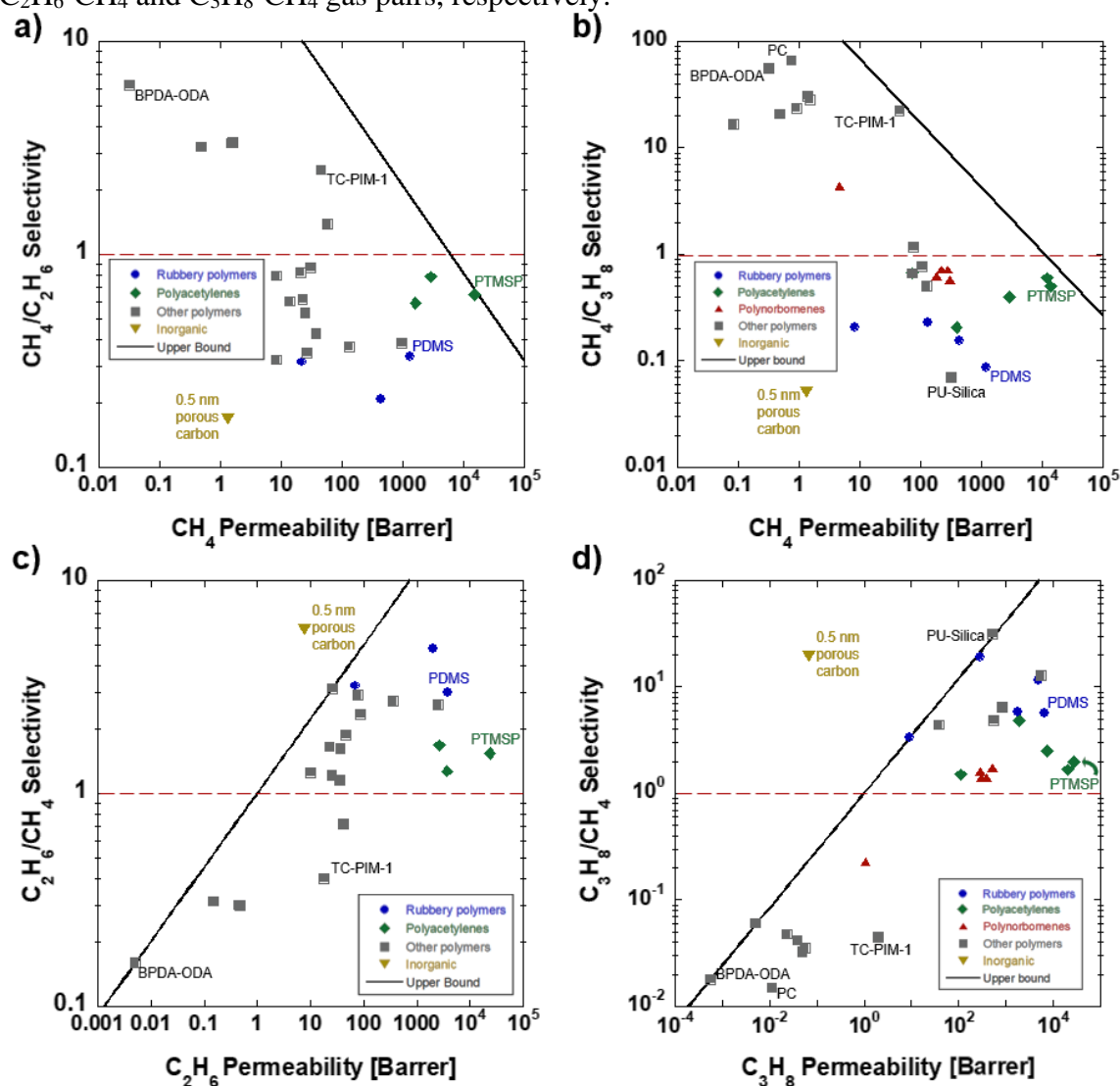
Figure 2.2: a) CH_4-C_2H_6 and b) CH_4-C_3H_8 size-selective upper bound plots. The solubility coefficients for CH_4, C_2H_6, and C_3H_8 are 0.00146, 0.00667, and 0.00936 [cm^3(STP) cm^{-3} polymer $cmHg^{-1}$], respectively, as derived by van Krevelen [11]. Parameters a, b, and f (in equation 2.9) were kept as their typical values of 0.64, -11.513 and 12600, respectively [8].
c) C_2H_6-CH_4 and d) C_3H_8-CH_4 reverse-selective upper bound plots. The upper bounds were drawn by eye. d) was adapted from [12]. Experimental data were compiled from [12-31].

For membranes where the larger species also happens to be the most permeable, Equation 2.5 yields a positive $\lambda_{A/B}$. In general, the upper bounds for reverse-selective gas pairs like CO_2-H_2, C_2H_6-CH_4 and C_3H_8-CH_4 are not drawn from Equation 2.4, if an upper bound is drawn at all [31]. Nonetheless, reverse-selective analogues to these upper bound plots permit more meaningful comparisons of material properties. Note that Figures 2.2c and 2.2d show the same data as Figures 2.2a and 2.2b, respectively.

2.1.3: Permeability and free volume

Membrane materials vary widely in morphology, but, in general, the fractional free volume, or FFV, of a material is a very telling parameter of the expected magnitude of permeabilities. Materials with a larger FFV tend to have not only a greater proportion of large enough free volume elements to be accessible to a penetrant but also more interconnected pathways for longer distance and more frequent diffusion steps. The usual correlation takes the form of Equation 2.10 [2, 32]:

$$P_A = A \, exp\left(-\frac{B}{FFV}\right) \tag{2.10}$$

where A and B are gas-specific empirical constants that scale somewhat with penetrant solubility and size, respectively.

While FFV does not directly inform us of the polydispersity of free volume elements or whether their distribution is unimodal, its ease of calculation by the Bondi method makes it an accessible parameter in membrane materials research [33, 34]:

$$FFV = \frac{(v_s - v_o)}{v_s} \cong \frac{(v_s - 1.3v_{vdW})}{v_s} \tag{2.11}$$

Here, v_s is the material specific volume and v_o is the occupied volume, which is generally approximated from v_{vdW}, the van der Waals volume, as computed by group contribution methods.

2.2 PRIOR WORK IN REVERSE-SELECTIVE MEMBRANE MATERIALS

This section reviews the gas separations literature with a focus on polyacetylenes and supported liquid membranes.

2.2.1: Substituted polyacetylenes

Polyacetylenes are a family of glassy polymers with highly constrained rotational chain mobility due to the double bond in their repeat unit [35]. Among these, poly(1-trimethylsilyl-1-propyne), PTMSP, was the substituted polyacetylene with highest gas permeability when developed by Masuda *et al.* [36]. Chemists have documented over 100 different substituted polyacetylenes. Among those investigated for gas separations are PTMSP, PMP, PTMGP, PTMSDPA, PCIPA, PTBA, PPP, PVTMS, PBTMST, and PTMST [27, 29, 35-40]. Their full names appear in Appendix A.

Polyacetylenes, like other glassy polymers, are susceptible to physical aging, where gas permeability decreases over time [41]. The thermal history of glassy polymers can usually be reset by heat treating to slightly over the glass transition temperature. However, PTMSP degrades before reaching its glass transition temperature. As shown in Table 2.1, the theoretical T_g of PTMSP, PMP, and other "super-glassy" polymers can be estimated [42].

To reset the thermal history of a PTMSP sample, it is customary to treat the sample with a conditioning agent (*e.g.*, methanol). The large gas permeability of PTMSP is mainly attributed to an exceptionally high fractional free volume of up to 0.34 and average free volume element radii of 3 Å for the smaller mode and 5.3 Å for the larger mode (assuming spherical cavities) [43]. Gas permeation in PTMSP has been characterized for light hydrocarbon separations [1, 20, 24, 44-45].

22

PTMSP has been studied extensively, given its compatibility with many industrially relevant solvents, ease of synthesis, and high permeabilities [36, 45]. The superior gas transport through PTMSP is at least partly due to a third of its volume comprising free volume (the highest of any known dense polymer) [46]. This large nonequilibrium free volume makes PTMSP soluble in a relatively large number of solvents but also prone to pronounced swelling by a variety of non-solvents, as summarized by Kappert *et al.* [47] (and implied by Figure 2.3).

Substituted polyacetylenes present challenges for their use as commercially viable membrane materials. While very permeable to gases and light hydrocarbon vapors, PTMSP and its cousin materials have only modest selectivities. Most polyacetylenes have limited thermal stability, and their reverse-selectivities are often less desirable at moderately high temperatures [48]. Glassy polymers, and especially polyacetylenes, are susceptible to physical aging, which reduces gas permeability over time [41]. Although the thermal history of glassy polymers can be reset by heat treating to or above the glass transition temperature, PTMSP degrades before reaching its glass transition temperature. The accepted alternative method of resetting the thermal history effects of a PTMSP membrane is through treatment with a conditioning agent like methanol [49].

PTMSP and fumed silica (particles with estimated diameter of 12 nm) mixed-matrix membranes (MMMs) have been shown to improve both C_3H_8/H_2 selectivity and its permeability, mainly due to the shift of the large free volume element mode (r_4) to radii up to 5.8 Å and the insertion of a third mode of interstitial free volume elements (r_5) with radii in the range of 10-12 Å [55-56]. A similar observation was made in poly(4-methyl-2-pentyne), PMP. The $n\text{-}C_4H_{10}/CH_4$ selectivity and permeability in PMP MMMs significantly improve for fumed silica particles smaller than 50 nm in diameter, although
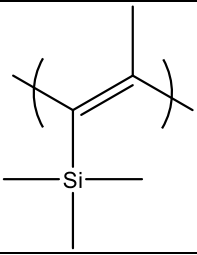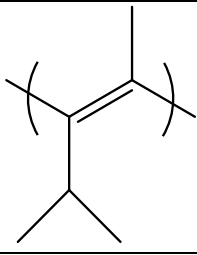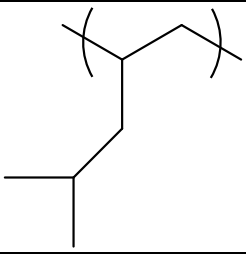
	PTMSP	PMP	PMPentene
Structure			
Degradation temperature, T_d [°C]	~360	~230	>424
Melting temperature, T_m [°C]	>360	>230	235
Glass transition temperature, T_g [°C]	>400 (est. 473)	>230	30
Density, ρ [g/cm³]	0.73-0.75	0.78-0.80	0.83
Fractional free volume, *FFV*	0.29-0.34	0.28	0.18
Average FVE cavity radii, *r* [Å]	3, 5.3	2.5, 5	2
CH₄ permeability (25 °C), *P* [Barrer]	12,000-15,000	1,500-2,000	11

Table 2.1:   Contrasting some properties of the super-glassy, highly permeable, reverse-selective substituted polyacetylenes PTMSP and PMP with the structurally similar, semicrystalline poly-α-olefin PMPentene. Data compiled from [48, 50-54].

the free volume element size modes in PMP MMMs remain slightly smaller than in the PTMSP MMMs [57].

2.2.2: Ionic liquid membranes

Extensive reviews have been written to guide polymer and ionic liquid-based separation membrane materials design [58-60]. The most prevalent supported ionic liquid membrane, or SILM, supports are PVDF, PTFE, PES, and inorganic Al_2O_3. In contrast with a ceramic support, a polymer support may offer secondary transport pathways through the polymer phase. Moreover, the polymer support can become plasticized (swollen) by the IL or the vapor penetrants [61-62]. Some SILM materials have been investigated for light hydrocarbon separations and exhibited promising selectivity [63-64]. Common assumptions in these studies are that the support is rigid and highly impermeable compared to the IL and that any polymer swelling by the liquid is negligible.

These assumptions may not be appropriate for PTMSP, as prior studies have found PTMSP is prone to high degrees of swelling when exposed to a variety of non-solvents [47, 65]. This characteristic of PTMSP gave rise to a discrepancy between geometric and pycnometric (*i.e.*, skeletal) density measurements of PTMSP, as described by Paul [66].

In selecting an IL for a polymeric support, it is useful to consider its affinity for the support. If it is too favorable, the IL will dissolve in the polymer and tend to form a single phase, whether a plasticized polymer or an ionogel. If it is too unfavorable, the IL will only weakly wet the free volume cavities and tend to form its own disperse phase or leach out of the support. One can gauge the IL-support interactions by comparing their

Kamlet-Taft parameters, contact angles, or Hansen solubility parameters, as shown in Figure 2.3.
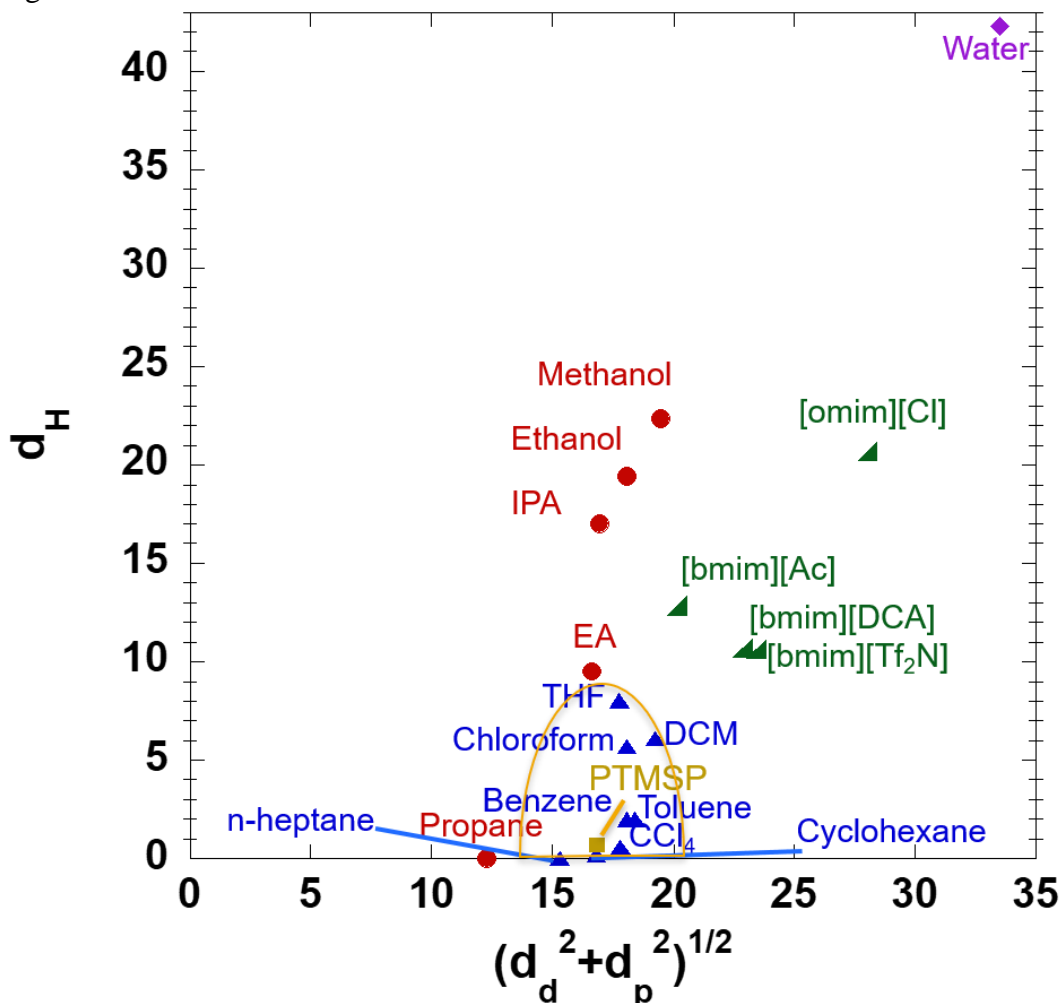
Figure 2.3: Hansen solubility parameter map of various PTMSP solvents and non-solvents, including 4 ionic liquids and water. The y-axis parameter, d_H, stands for the hydrogen-bonding Hansen solubility parameter [MPa$^{1/2}$]. The x-axis combines the dispersive and polar Hansen solubility parameters, d_D and d_P, respectively. The yellow half-oval is a qualitative representation of the solubility boundary for PTMSP. Note that the typical solubility sphere drawn in Hansen space uses $(2d_D)$, d_P, and d_H as axes [67-69].

Studies of SILMs for CO_2 separations are more abundant than those for hydrocarbon separations, and much can be learned from conclusions drawn in this space.

26

CO_2 is also a highly condensable, plasticizing gas, and SILMs are often reverse-selective for the CO_2/H_2 gas pair [31, 41, 70]. Because CO_2 has a smaller kinetic diameter than CH_4, many SILM systems developed have shown promise in exceeding the CO_2/CH_4 Robeson upper-bound [71-72]. This is due in part to a facilitated-transport mechanism available to CO_2 in many protic ILs (i.e., a chemisorption mode, in addition to physisorption in the IL). A corrected upper bound for SILMs has been developed for CO_2/CH_4 and CO_2/N_2 [73].

2.2.3: Other reverse-selective materials

It is worth mentioning that most low T_g, high-permeability rubbery polymers are reverse-selective in the context of light hydrocarbon separations. In particular, the properties of siloxane-based rubbers (*e.g.*, PDMS and POMS) and other rubbers, like cis-polypentenamer (cis-PPM), have been evaluated for light paraffin transport [16-17, 25].

Other classes of glassy polymers that sometimes exhibit reverse-selectivity including some high free volume polyimides, polynorbornenes, dibenzodioxin-based polymers and other ladder polymers have also been reported [21-23, 41].

Inorganic membrane materials with highly monodisperse pore sizes in the range of surface flow have also been studied for their reverse-selective separations potential. These include 0.5-2 nm porous carbon membranes, metal-organic framework (MOF) mixed matrix membranes, and zeolite MFI nanosheet membranes [19, 30, 41, 74].

2.3 GAS SORPTION IN POLYMERS

This section presents commonly used models for predicting gas and vapor sorption in glassy and rubbery polymers.

2.3.1: Dual-mode model

As its name implies, the dual-mode model is a combination of two simpler sorption models: Henry's law and Langmuir's model [2]. The dual-mode model is appropriate for describing gas sorption in most glassy polymers with both absorption (*e.g.*, gas dissolved in the dense polymer phase) and adsorption (i.e., Langmuir sites around the accessible free volume) characteristics. Together, Figure 2.4a) and b) and Equations 2.12-2.13 show the contributions from each of the modes to the concentration and solubility curves, respectively. For pure-gas sorption:

$$C_A = k_{D,A} p_A + \frac{C'_{H,A} b_A p_A}{1 + b_A p_A} \tag{2.12}$$

where C_A is the concentration of species A in the membrane, $k_{D,A}$ is the dense phase Henry's solubility constant, $C'_{H,A}$ is the Langmuir capacity parameter (proportional to the amount of available Langmuir sites) and b_A is the Langmuir affinity parameter (related to the penetrant condensability in the membrane). Similarly, in terms of solubility,

$$S_A = k_{D,A} + \frac{C'_{H,A} b_A}{1 + b_A p_A} \tag{2.13}$$

This expression can be combined with equation 2.4 to yield dual mode fitting parameters for permeability data [20]. Glassy polymers with more accessible free volume will typically have both a larger proportion of their concentration from the Langmuir mode and a larger solubility pressure-dependence as a result.
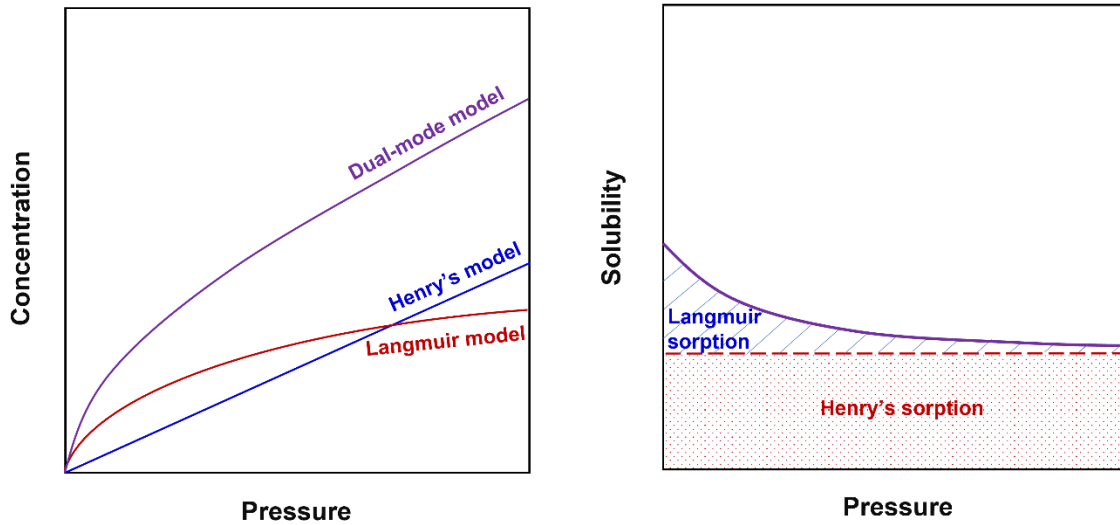
Figure 2.4: The dual-mode model results from the superposition of Henry's law and a Langmuir sorption model. At high equilibrium pressure, the slope from the dual-mode model approaches that of Henry's law, as the contribution from Langmuir sorption becomes insignificant. Adapted from [74]

The mixed-gas analogue, Equation 2.14, hints at the mixture phenomenon of competitive sorption, where the interaction of multiple species competing for limited Langmuir sites can result in significantly lower solubilities (and, thus, permeabilities) of a given species A, particularly if $b_B p_B \gg b_A p_A$ [2, 44]:

$$S_A = k_{D,A} + \frac{C'_{H,A} b_A}{1 + b_A p_A + b_B p_B + \cdots} \tag{2.14}$$

This model can be extended beyond binary mixtures, as implied by the ellipsis.

2.3.2: Flory-Huggins model

For rubbery polymers or other relatively dense glassy polymers near their glass transition temperature, sorption isotherms are better described by the Flory-Huggins model, Equation 2.15 [2, 75]:

$$\ln(a_A) = \ln(\varphi_A) + (1 - \varphi_A) + \chi(1 - \varphi_A)^2 \tag{2.15}$$

29

where φ_A is the volume fraction of A in the membrane, χ is the penetrant-polymer Flory-Huggins interaction parameter (and the single fitting parameter in this model), and a_A is the activity of A in the membrane phase.

Volume fraction can be related to concentration by Equation 2.16 [2,76-77],

$$\varphi_A = \left(\frac{1}{1 + \frac{\vartheta_a V_{STP}^{ig}}{C_A \bar{V}_A}} \right) \tag{2.16}$$

with $\bar{V}_A$ representing the partial molar volume of A in the membrane (either experimentally determined or estimated as the liquid molar volume of the species at its normal boiling point, V_A^0 [76]), ϑ_a signifying the fraction of amorphous phase (equal to 1 for non-semicrystalline polymers) and V_{STP}^{ig} being the molar volume of an ideal gas at standard temperature and pressure (here used as a conversion factor of 22,414 [cm^3(STP)/mol]).

The Flory-Huggins model reduces to Henry's law at the limit of infinite dilution [77-78]:

$$S_A = k_{D,A} \exp \left[2(1 + \chi) \frac{\bar{V}_A}{V_{STP}^{ig}} C_A \right] \tag{2.17}$$

where $k_{D,A} = \frac{\vartheta_a V_{STP}^{ig}}{\bar{V}_A \, p_A^0} \exp(-(1 + \chi))$. Note that the saturation pressure, p_A^0, can be replaced with the saturation fugacity for a nonideal gas (see Section 2.5).

2.3.3: Berens-Hopfenberg model

Some sorption isotherms exhibit an inflection point such that the data are concave-down at low activities but is well fit by the Flory-Huggins model at high activities. Figure 2.5 shows that the inflection occurs at lower activity the closer a

polymer is to its glass transition temperature, but in all cases the data converge to the expected Flory-Huggins curve at high enough activity.
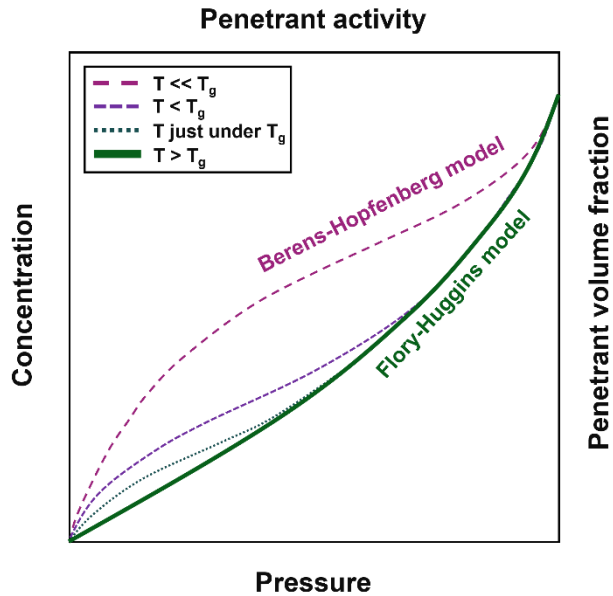
Figure 2.5:   Qualitative depiction of the isotherms described by Berens and Hopfenberg. The sorption in excess of that predicted by the Flory-Huggins theory at low penetrant activity is attributed to Langmuir-like sorption to non-equilibrium free volume sites characteristic of glassy polymers. Adapted from [80].

These isotherms are commonly observed for highly condensable gas or vapor sorption in glassy polymers, particularly those susceptible to penetrant-induced swelling, or plasticization, though they have also been observed in vapor sorption of more rigid, porous materials [79]. On such isotherms, one could fit the data with Equation 2.18. Note that the Langmuir-like parameters $C_{H,A}^{\prime,*}$ and b_A^* will be smaller than (and should not be compared directly with) the dual-mode $C_{H,A}^{\prime}$ and b_A parameters. In the literature, it is common to fit the high activity (concave-up) portion of the data with Flory-Huggins

independently from the low pressure (concave-down) portion of the data, which is fit with the dual-mode model [81-82].

$$S_A = k_{D,A} \exp\left[2(1+\chi)\frac{\bar{V}_A}{V_{STP}^{ig}}C_A\right] + \frac{C_{H,A}^{\prime,*}b_A^*}{1+b_A^*p_A} \tag{2.18}$$

2.3.4: Other sorption models

The sorption models presented earlier in this section are by no means the only models used to describe isotherms with inflection. Among lattice-fluid models, there is an extension to Equation 2.13, the Flory-Rehner model, which polymer scientists use to account for the effects of crosslinks in dense polymers [78]. The Sanchez-Lacombe model further extends this analysis by also accounting for the effects of cavities [83]. Some researchers have also adapted non-random and non-equilibrium lattice fluid (NRLF and NELF) models for polymer-gas systems, including butane in PET, xylene/nonane in polystyrene, and N_2 and CO_2 in polypropylene [84].

Multilayer sorption models originally developed for analysis of hard materials have also found applications in polymer systems. For instance, the Brunauer-Emmett-Teller (BET) type II model has been used not only for cryogenic N_2 and He porosimetry measurements of high FFV polymers but also for fitting vapor sorption data near-room temperatures, including methanol in cellulose acetate [85]. Likewise, the Guggenheim-Anderson-DeBoer model has been used for fitting data of butanol sorption in PTMSP [86].

2.4 GAS SOLUBILITY AND DIFFUSIVITY IN IONIC LIQUID MEMBRANES

At low pressures, gases are generally sparingly soluble in ILs, as they are in most organic liquids, so Henry's law (i.e., Equation 2.13 truncated to the first term) is generally a good model to describe most gas-IL systems [87]. In the IL literature,

solubilities are typically reported as Henry's constants. Appendix B shows how to convert Henry's constants to volume-based solubilities (*e.g.*, [mol L^{-1} bar^{-1}] or [cm^3 (STP) cm^{-3} cmHg^{-1}]), as generally reported in membrane science literature.

Solubility behavior of gases does deviate from the infinite dilution limit (Henry's law) at high pressures. The Krichevsky-Kasarnovsky model can better describe non-linear (concave towards the pressure axis) isotherms in gas-IL systems [88]. For the relatively more condensable CO_2 or C_{2+} hydrocarbon vapors, other deviations from Henry's law may arise at relatively low pressures. In these cases, researchers may rely on regular-solution theory, Pierroti's theory, various lattice fluid models, or predictive models (such as UNIFAC or COSMO-based models) [47, 89-90].

Both solubility and diffusivity depend on the fractional free volume of the confined liquid [47]. IL molar volume is often used as a proxy for free volume, as it is easily determined (only density needs to be measured). Banu *et al.* showed that confined IL properties can vary significantly from bulk IL properties and cautioned against using bulk IL properties for analyzing systems with a confined IL phase [91], in part because ionic liquid-based membranes can be affected by plasticization effects. A typical diffusion model for plasticizing membranes accounts for the increase in free volume due to increasing concentration of penetrant [20, 78]:

$$\bar{D}_A = \bar{D}_{0,A} \exp(\beta_A \bar{C}_A) \tag{2.19}$$

where β_A is the penetrant-specific plasticization constant, $\bar{C}_A$ is the average concentration of penetrant A in the membrane and the infinite dilution concentration-averaged diffusivity, $\bar{D}_{0,A}$, mimics the FFV-dependent form of Equation 2.10.

Scovazzo *et al*. developed gas diffusivity correlations in a variety of supported IL systems and showed that penetrant molar volume (while dissolved in the IL phase) and

liquid viscosity are useful in determining gas diffusivities, in addition to IL molar volume [92]. These correlations have the form:

$$\bar{D}_{0,A} = A \frac{V_{IL}^a}{\mu_{IL}^b V_A^c} \tag{2.20}$$

where $A, a, b,$ and c are empirical constants specific to a class of ILs, V_{IL} is the molar volume of the IL, μ_{IL} is the viscosity of the IL, and V_A is the molar volume of penetrant A.

2.5 ACCOUNTING FOR NON-IDEALITIES IN GAS MIXTURES

For gases that behave nonideally, the partial pressure of a species A is not a good approximation of their fugacity, f_A. In those situations, it is more meaningful to replace pressure with fugacity in all preceding equations, including any reference or saturation pressures for vapors, when defining vapor activity (e.g., f_A/f_A^0 in place of p_A/p_A^0 in Equation 2.15).

When studying gas mixtures that behave non-ideally, the fugacity coefficients should reflect the effect of interspecies interactions on the deviation from ideality. Doing so fundamentally refines the initially presented definition of permeability, Equation 2.1:

$$P_A = \frac{N_A l}{\hat{f}_{A,us} - \hat{f}_{A,ds}} = \frac{y_{A,ds} Q l}{A(\hat{f}_{A,us} - \hat{f}_{A,ds})} \frac{T_S}{T} \tag{2.21}$$

where $\hat{f}_{A,us}$ and $\hat{f}_{A,ds}$ are the fugacity of component A in a mixture either upstream or downstream of the membrane, Q is the total gas volumetric flowrate across the membrane, A is the effective membrane surface area, T_S is the standard temperature (273.15 [K]) and T is the temperature at which the permeation experiment is done.

$$\hat{f}_A = \hat{\phi}_A y_A p \tag{2.22}$$

where $\hat{\phi}_A$ is the mixture fugacity coefficient of A, y_A is the mol fraction of A in the gas mixture, and p is the total pressure [3, 93].

To further extend Equation 2.6 for a binary mixture (assuming that, for both species A and B, $f_{i,us} \gg f_{i,ds} \, y_{i,ds}/y_{i,us}$) [93]:

$$\alpha^*_{A/B} = \frac{y_{A,ds}/y_{B,ds}}{y_{A,us}/y_{B,us}} = \frac{P_A \hat{f}_{A,ds}}{P_B \hat{f}_{B,ds}} \frac{y_{B,us}}{y_{A,us}} = \alpha_{A/B} \frac{\hat{\phi}_{A,us}}{\hat{\phi}_{B,us}} = \alpha_{A/B} \Phi_{A/B} \qquad (2.23)$$

Here the $\Phi_{A/B}$ parameter is defined as the ratio of the mixture fugacity coefficients of A and B.

In determining an appropriate mixture fugacity, it is important to balance the accuracy and practicality of our thermodynamic model of choice. The model should consider how both mixture conditions and interspecies interactions vary with changing state variables (*e.g.*, temperature and pressure). Figure 2.6 compares the fugacity coefficients as calculated from three equations of state (EOS) in a binary CH_4-C_2H_6 system.
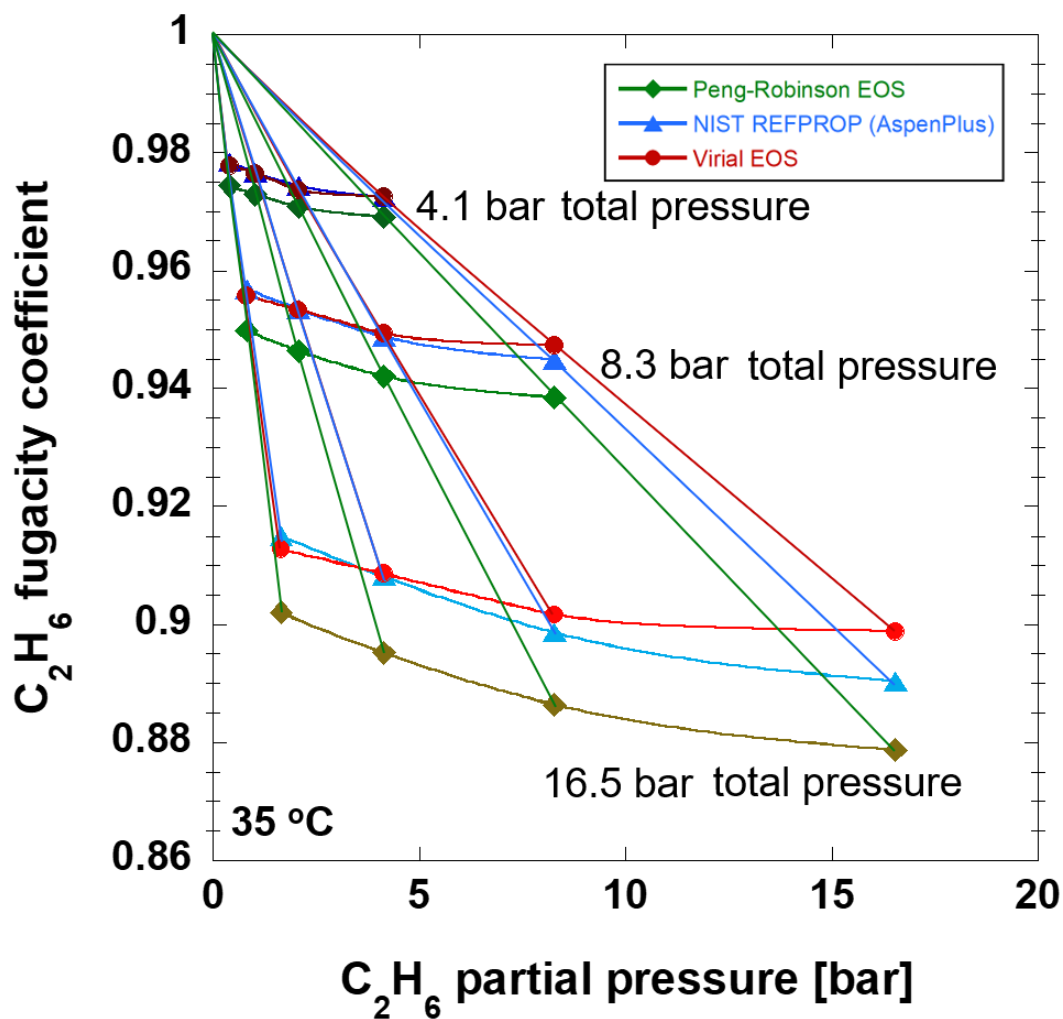
Figure 2.6: Comparing C_2H_6 fugacity coefficients for CH_4-C_2H_6 binary mixtures at 35 °C and three different total mixture pressures obtained from Peng-Robinson and the Virial equation truncated to the second term with those obtained from the NIST reference properties library in AspenPlus. The rightmost data represent pure-gas ethane fugacity coefficients, $\phi_{C_2H_6}$, because the partial ethane pressure equals the total pressure. Second virial coefficients were interpolated from [94].

Note that for all three EOS, the C_2H_6 fugacity coefficient at a constant partial pressure (vertical line) varies greatly depending on the total mixture pressure. The employed forms of the NIST REFPROP, Peng-Robinson and truncated virial EOS, along

with fugacity coefficients for CH_4, C_2H_6, and C_3H_8 over the range of studied pressures, are presented in Appendix C.

2.6 REFERENCES

[1]   I. Pinnau, L.G. Toy, Transport of organic vapors through poly(1-trimethylsilyl-1-propyne), Journal of Membrane Science, 116 (1996) 199-209.

[2]   S. Matteucci, Y. Yampol'skii, B. D. Freeman, I. Pinnau, Transport of gases and vapors in glassy and rubbery polymers, in: Y. Yampol'skii, I. Pinnau, B. D. Freeman (Eds.) Materials Science of Membranes, John Wiley & Sons, Chichester, 2006.

[3]   J.R. Elliot and C.T. Lira, Introductory Chemical Engineering Thermodynamics, 2nd Ed, Prentice Hall, Upper Saddle River, NJ, 2012.

[4]   X. Li, J. Li, Fluxes and Driving Forces in Membrane Separation Processes, in: E. Drioli, L. Giorno (Eds.) Encyclopedia of Membranes, Springer Berlin Heidelberg, Berlin, Heidelberg, 2015, pp. 1-3.

[5]   R.D. Raharjo, H. Lin, D.F. Sanders, B.D. Freeman, S. Kalakkunnath, D.S. Kalika, Relation between network structure and gas transport in crosslinked poly(propylene glycol diacrylate), Journal of Membrane Science, 283 (2006) 253-265.

[6]   J.D. Moon, Impact of Humidity and Polymer Blending on the Gas Transport Properties of Polybenzimidazoles, PhD dissertation, The University of Texas at Austin, Austin, TX, 2019.

[7]   L.M. Robeson, The upper bound revisited, Journal of Membrane Science, 320 (2008) 390-400.

[8]   B.D. Freeman, Basis of Permeability/Selectivity Tradeoff Relations in Polymeric Gas Separation Membranes, Macromolecules, 32 (1999) 375-380.

[9]   M. Rungta, C. Zhang, W.J. Koros, L. Xu, Membrane-based ethylene/ethane separation: The upper bound and beyond, AIChE Journal, 59 (2013) 3475-3489.

[10]   J.-J. Shieh, T.S. Chung, Gas permeability, diffusivity, and solubility of poly(4-vinylpyridine) film, Journal of Polymer Science Part B: Polymer Physics, 37 (1999) 2851-2861.

[11]   D.W. van Krevelen, Properties of Polymers, 3rd Ed, Elsevier, Amsterdam, 1990.

[12]   B.D. Freeman, I. Pinnau, Separation of gases using solubility-selective polymers, Trends in Polymer Science 5 (1997) 167-173.

[13]   Y. Alqaheem, A. Alomair, M. Vinoba, A. Pérez, Polymeric Gas-Separation Membranes for Petroleum Refining, International Journal of Polymer Science, 2017 (2017) 4250927.

[14]   F.I Alghunaimi, The Performance of a Thermally Cross-Linked Polymer of Intrinsic Microporosity (PIM-1) for Gas Separation, M.S. Thesis, King Abdullah University of Science and Technology, Thuwal, Saudi Arabia, 2013.

[15]   K. Haraya, K. Obata, T. Hakuta, H. Yoshitom, The permeation of gases through a new type polyimide membrane, Membrane 11 (1986) 48-52.

[16]   L. Starannikova, Y. Yampol'skii, K. Makovet'skii, T. Golenko, A novel high permeability rubbery membrane material – cis-polypentenamer, Desalination, 200 (2006) 18-19.

[17]   I. Pinnau, Z. He, Pure- and mixed-gas permeation properties of polydimethylsiloxane for hydrocarbon/methane and hydrocarbon/hydrogen separation, Journal of Membrane Science, 244 (2004) 227-233.

[18]   A. Khosravi, M. Sadeghi, H.Z. Banadkohi, M.M. Talakesh, Polyurethane-silica nanocomposite membranes for separation of propane/methane and ethane/methane, Industrial Engineering and Chemistry Research 53 (2014) 2011-2021.

[19]   M.B. Rao, S. Sircar, Nanoporous carbon membranes for separation of gas mixtures by selective surface flow, Journal of Membrane Science, 85 (1993) 253-264.

[20]   T.C. Merkel, V.I. Bondar, K. Nagai, B.D. Freeman, Sorption and Transport of Hydrocarbon and Perfluorocarbon Gases in Poly(1-trimethylsilyl-1-propyne), Journal of Polymer Science Part B: Polymer Physics 38 (2000) 415-434.

[21]   S. Thomas, I. Pinnau, N. Du, M.D. Guiver, Hydrocarbon/hydrogen mixed-gas permeation properties of PIM-1, an amorphous microporous spirobisindane polymer, Journal of Membrane Science, 338 (2009) 1-4.

[22]   N.Y. Alaslai, Gas Sorption, Diffusion and Permeation in a Polymer of Intrinsic Microporosity (PIM-7), M.S. Thesis, King Abdullah University of Science and Technology, Thuwal, Saudi Arabia, 2013.

[23]   M.V. Bermeshev, A.V. Syromolotov, L.E. Starannikova, M.L. Gringolts, V.G. Lakhtin, Y.P. Yampolskii, E.S. Finkelshtein, Glassy Polynorbornenes with Si–O–Si Containing Side Groups. Novel Materials for Hydrocarbon Membrane Separation, Macromolecules, 46 (2013) 8973-8979.

[24]   A. Morisato, B.D. Freeman, I. Pinnau, C.G. Casillas, Pure hydrocarbon sorption properties of poly(1-trimethylsilyl-1-propyne) (PTMSP), poly(1-phenyl-1-propyne) (PPP), and PTMSP/PPP blends, Journal of Polymer Science Part B: Polymer Physics, 34 (1996) 1925-1934.

[25]   E.A. Grushevenko, I.L. Borisov, D.S. Bakhtin, G.N. Legkov, G.N. Bondarenko, A.V. Volkov, Membrane Material Based on Octyl-Substituted Polymethylsiloxane for Separation of C_3/C_1 Hydrocarbons, Petroleum Chemistry 57 (2017) 334-340.

[26]   S.S. Chang, R. Wang, T.-S. Chung, Y. Liu, C_2 and C_3 hydrocarbon separations in poly(1,5-naphthalene-2,2′-bis(3,4-phthalic) hexafluoropropane)diimide (6FDA-1,5-NDA) dense membranes, Journal of Membrane Science 210 (2002) 55–64.

[27]   L.G. Toy, K. Nagai, B.D. Freeman, I. Pinnau, Z. He, T. Masuda, M. Teraguchi, Y.P. Yampolskii, Pure-Gas and Vapor Permeation and Sorption Properties of Poly[1-phenyl-2-[p-(trimethylsilyl)phenyl]acetylene] (PTMSDPA), Macromolecules, 33 (2000) 2516-2524.

[28] M.E. Arnold, K. Nagai, B.D. Freeman, R.J. Spontak, D.E. Betts, J.M. DeSimone, I. Pinnau, Gas Permeation Properties of Poly(1,1'-dihydroperfluorooctyl acrylate), Poly(1,1'-dihydroperfluorooctyl methacrylate), and Poly(styrene)-b-poly(1,1'-dihydroperfluorooctyl acrylate) Block Copolymers, Macromolecules, 34 (2001) 5611-5619.

[29] K. Nagai, L.G. Toy, B.D. Freeman, M. Teraguchi, G. Kwak, T. Masuda, I. Pinnau, Gas permeability and n-butane solubility of poly(1-trimethylgermyl-1-propyne), Journal of Polymer Science Part B: Polymer Physics, 40 (2002) 2228-2236.

[30] C. Altintas, S. Keskin, Molecular simulations of MOF membranes for separation of ethane/ethene and ethane/methane mixtures, RSC Advances, 7 (2017) 52283-52295.

[31] O. Shekhah, V. Chernikova, Y. Belmabkhout, M. Eddaoudi, Metal–Organic Framework Membranes: From Fabrication to Gas Separation, Crystals, 8 (2018).

[32] S.D. Kelman, B.W. Rowe, C.W. Bielawski, S.J. Pas, A.J. Hill, D.R. Paul, B.D. Freeman, Crosslinking poly[1-(trimethylsilyl)-1-propyne] and its effect on physical stability, Journal of Membrane Science, 320 (2008) 123-134.

[33] M.S. Shannon, J.M. Tedstone, S.P.O. Danielsen, M.S. Hindman, A.C. Irvin, J.E. Bara, Free Volume as the Basis of Gas Solubility and Selectivity in Imidazolium-Based Ionic Liquids, Industrial & Engineering Chemistry Research, 51 (2012) 5565-5576.

[34] A. Bondi, van der Waals volumes and radii. The Journal of Physical Chemistry 68 (1964) 441-451.

[35] Y. Yampol'skii, A Current Position of Polyacetylenes Among Other Highly Permeable Membrane Materials, Polymer Reviews, 57 (2017) 200-212.

[36] T. Masuda, E. Isobe, T. Higashimura, K. Takada, Poly[1-(trimethylsilyl)-1-propyne]: A new high polymer synthesized with transition-metal catalysts and characterized by extremely high gas permeability. Journal of the American Chemical Society, 105 (1983) 7473-7474.

[37]   T.C. Merkel, B.D. Freeman, R.J. Spontak, Z. He, I. Pinnau, P. Meakin, A.J. Hill, Ultrapermeable, Reverse-Selective Nanocomposite Membranes, Science, 296 (2002) 519.

[38]   A. Yushkin, A. Grekhov, S. Matson, M. Bermeshev, V. Khotimsky, E. Finkelstein, P.M. Budd, V. Volkov, T.J.H. Vlugt, A. Volkov, Study of glassy polymers fractional accessible volume (FAV) by extended method of hydrostatic weighing: Effect of porous structure on liquid transport, Reactive and Functional Polymers, 86 (2015) 269-281.

[39]   T. Masuda, Substituted Polyacetylenes: Synthesis, Properties, and Functions, Polymer Reviews, 57 (2016) 1-14.

[40]   T. Nakagawa, T. Watanabe, M. Mori, K. Nagai, Aging of Gas Permeability in Poly[1-(trimethylsilyl)-1-propyne]   (PTMSP)   and   PTMSP-Poly(tert-butylacetylene) Blends. ACS Symposium Series Polymer Membranes for Gas and Vapor Separation, 733 (1999) 68-84.

[41]   M. Galizia, W.S. Chi, Z.P. Smith, T.C. Merkel, R.W. Baker, B.D. Freeman, 50th Anniversary Perspective: Polymers and Mixed Matrix Membranes for Gas and Vapor Separation: A Review and Prospective Opportunities, Macromolecules, 50 (2017) 7809-7843.

[42]   W. Ogieglo, H. Wormeester, M. Wessling, N. E. Benes, Effective medium approximations for penetrant sorption in glassy polymers accounting for excess free volume, Polymer (Guildf), 55 (2014) 1737-1744.

[43]   X. Wang, A. Hill, B.D. Freeman, I.C. Sanchez, Structural, sorption and transport characteristics of an ultrapermeable polymer. Journal of Membrane Science 314 (2008) 15–23.

[44]   R.D. Raharjo, B.D. Freeman, D.R. Paul, E.S. Sanders, Pure and mixed gas CH_4 and $n-C_4H_{10}$ permeability and diffusivity in poly(1-trimethylsilyl-1-propyne), Polymer, 48 (2007) 7329-7344.

[45]   I. Pinnau, C. G. Casillas, A. Morisato, B.D. Freeman, Hydrocarbon/Hydrogen Mixed Gas Permeation in Poly(1 -trimethylsilyl-1 -propyne) (PTMSP), Poly(1 -

phenyl-1 -propyne) (PPP), and PTMSP/PPP Blends. Journal of Polymer Science: Part B: Polymer Physics, 34 (1996) 2613-2621.

[46]   V. Volkov, Free Volume Structure and Transport Properties of Glassy Polymers—Materials for Separating Membranes, Nature Polymer, 23 (1991) 457– 466.

[47]   E.J. Kappert, M.J.T. Raaijmakers, K. Tempelman, F.P. Cuperus, W. Ogieglo, N.E. Benes, Swelling of 9 polymers commonly employed for solvent-resistant nanofiltration membranes: A comprehensive dataset, Journal of Membrane Science, 569 (2019) 177-199.

[48]   M.T. Demko, J.C. Cheng, A.P. Pisano, Rigid, Vapor-Permeable Poly(4-methyl-2-pentyne) Templates for High Resolution Patterning of Nanoparticles and Polymers, ACS Nano, 6 (2012) 6890-6896.

[49]   K. Nagai, T. Masuda, T. Nakagawa, B.D. Freeman, I. Pinnau, Poly[1-(trimethylsilyl)-1-propyne] and related polymers: synthesis, properties and functions, Progress in Polymer Science, 26 (2001) 721-798.

[50]   V. Polevaya, A. Vorobei, A. Gavrikov, S. Matson, O. Parenago, S. Shishatskiy, V. Khotimskiy, Modification of Poly(4-methyl-2-pentyne) in the Supercritical Fluid Medium for Selective Membrane Separation of CO_2 from Various Gas Mixtures, Polymers, 12 (2020) 2468.

[51]   S. Markova, V. Zhmakin, T. Gries, V. Teplyakov, Combination of the Experimental and Theoretical Approaches for the Estimation of the C_1–C_4 Alkane Permeability Parameters in Poly (4-Methyl-2-Pentyne) and Poly (4-Methyl-1-Pentene), Applied Sciences, 10 (2020) 1735.

[52]   C.H. Lau, P.T. Nguyen, M.R. Hill, A.W. Thornton, K. Konstas, C.M. Doherty, R.J. Mulder, L. Bourgeois, A.C.Y. Liu, D.J. Sprouster, J.P. Sullivan, T.J. Bastow, A.J. Hill, D.L. Gin, R.D. Noble, Ending Aging in Super Glassy Polymer Membranes, Angewandte Chemie International Edition, 53 (2014) 5322-5326.

[53]   V.P. Shantarovich, I.B. Kevdina, Y.P. Yampol'skii, A.Y. Alentiev, Positron Annihilation Lifetime Study of High and Low Free Volume Glassy Polymers:

Effects of Free Volume Sizes on the Permeability and Permselectivity, Macromolecules, 33 (2000) 7453-7466.

[54] E.Y. Sultanov, A.A. Ezhov, S.M. Shishatskiy, K. Buhr, V.S. Khotimskiy, Synthesis, Characterization, and Properties of Poly(1-trimethylsilyl-1-propyne)-block-poly(4-methyl-2-pentyne) Block Copolymers, Macromolecules, 45 (2012) 1222-1229.

[55] T.C. Merkel, Z. He, I. Pinnau, B.D. Freeman, P. Meakin, A.J. Hill, Effect of Nanoparticles on Gas Sorption and Transport in Poly(1-trimethylsilyl-1-propyne), Macromolecules, 36 (2003) 6844-6855.

[56] K. De Sitter, P. Winberg, J. D'Haen, C. Dotremont, R. Leysen, J.A. Martens, S. Mullens, F.H.J. Maurer, I.F.J. Vankelecom, Silica filled poly(1-trimethylsilyl-1-propyne) nanocomposite membranes: Relation between the transport of gases and structural characteristics, Journal of Membrane Science, 278 (2006) 83-91.

[57] T.C. Merkel, B.D. Freeman, R.J. Spontak, Z. He, I. Pinnau, P. Meakin, A.J. Hill, Sorption, Transport, and Structural Evidence for Enhanced Free Volume in Poly(4-methyl-2-pentyne)/Fumed Silica Nanocomposite Membranes, Chemistry of Materials, 15 (2003) 109-123.

[58] J. Wang, J. Luo, S. Feng, H. Li, Y. Wan, X. Zhang, Recent development of ionic liquid membranes, Green Energy & Environment, 1 (2016) 43-61.

[59] M.G. Cowan, D.L. Gin, R.D. Noble, Poly(ionic liquid)/Ionic Liquid Ion-Gels with High "Free" Ionic Liquid Content: Platform Membrane Materials for CO2/Light Gas Separations, Accounts of Chemical Research, 49 (2016) 724-732.

[60] L.C. Tomé, I.M. Marrucho, Ionic liquid-based materials: a platform to design engineered CO_2 separation membranes, Chemical Society Reviews, 45 (2016) 2785-2824.

[61] H.A. Mannan, D.F. Mohshim, H. Mukhtar, T. Murugesan, Z. Man, M.A. Bustam, Synthesis, characterization, and CO_2 separation performance of polyether sulfone/[EMIM][Tf_2N] ionic liquid-polymeric membranes (ILPMs), Journal of Industrial and Engineering Chemistry, 54 (2017) 98-106.

[62] A. Volkov, A. Yushkin, A. Grekhov, A. Shutova, S. Bazhenov, S. Tsarkov, V. Khotimsky, T.J.H. Vlugt, V. Volkov, Liquid permeation through PTMSP: One polymer for two different membrane applications, Journal of Membrane Science, 440 (2013) 98-107.

[63] A. Khakpay, P. Scovazzo, Reverse-selective behavior of room temperature ionic liquid based membranes for natural gas processing, Journal of Membrane Science, 545 (2018) 204-212.

[64] M. Althuluth, J.P. Overbeek, H.J. van Wees, L.F. Zubeir, W.G. Haije, A. Berrouk, C.J. Peters, M.C. Kroon, Natural gas purification using supported ionic liquid membrane, Journal of Membrane Science, 484 (2015) 80-86.

[65] G.S. Golubev, I.L. Borisov, V.V. Volkov, Performance of Commercial and Laboratory Membranes for Recovering Bioethanol from Fermentation Broth by Thermopervaporation, Russian Journal of Applied Chemistry, 91 (2018) 1375-1381.

[66] D.R. Paul, Y. P. Yampol'skii, Gas Separation Membranes, CRC Press, Boca Raton, 2018, 116-118.

[67] Y. Lan, M.G. Corradini, X. Liu, T.E. May, F. Borondics, R.G. Weiss, M.A. Rogers, Comparing and Correlating Solubility Parameters Governing the Self-Assembly of Molecular Gels Using 1,3:2,4-Dibenzylidene Sorbitol as the Gelator, Langmuir, 30 (2014) 14128-14142.

[68] S.O. Ilyin, V.V. Makarova, M.P. Arinina, E.G. Litvinova, V.S. Khotimskii, V.G. Kulichikhin, Phase equilibrium and rheology of poly(1-trimethylsilyl-1-propyne) solutions, Polymer Science, Series A, 59 (2017) 1-11.

[69] Y. Agata, H. Yamamoto, Determination of Hansen solubility parameters of ionic liquids using double-sphere type of Hansen solubility sphere method, Chemical Physics, 513 (2018) 165-173.

[70] A.S.L. Gouveia, M. Yáñez, V.D. Alves, J. Palomar, C. Moya, D. Gorri, L.C. Tomé, I.M. Marrucho, CO_2/H_2 separation through poly(ionic liquid)–ionic liquid membranes: The effect of multicomponent gas mixtures, temperature and gas feed pressure, Separation and Purification Technology, 259 (2021) 118113.

[71]   S. Elhenawy, M. Khraisheh, F. AlMomani, M. Hassan, Key Applications and Potential Limitations of Ionic Liquid Membranes in the Gas Separation Process of CO_2, CH_4, N_2, H_2 or Mixtures of These Gases from Various Gas Streams, Molecules, 25 (2020).

[72]   F. Moghadam, E. Kamio, A. Yoshizumi, H. Matsuyama, An amino acid ionic liquid-based tough ion gel membrane for CO_2 capture, Chemical Communications, 51 (2015) 13658-13661.

[73]   Z. Dai, R.D. Noble, D.L. Gin, X. Zhang, L. Deng, Combination of ionic liquids with membrane technology: A new approach for CO_2 separation, Journal of Membrane Science, 497 (2016) 1-20.

[74]   S. Kanehashi, K. Nagai, Analysis of dual-mode model parameters for gas sorption in glassy polymers, Journal of Membrane Science, 253 (2005) 117-138.

[75]   P.J. Flory, Principles of polymer chemistry. Cornell University Press, Ithaca, NY, 1953.

[76]   T.C. Merkel, V.I. Bondar, K. Nagai, B.D. Freeman, I. Pinnau, Gas sorption, diffusion, and permeation in poly(dimethylsiloxane), Journal of Polymer Science Part B: Polymer Physics, 38 (2000) 415-434.

[77]   Y. Kamiya, Y. Naito, K. Terada, K. Mizoguchi, A. Tsuboi, Volumetric Properties and Interaction Parameters of Dissolved Gases in Poly(dimethylsiloxane) and Polyethylene, Macromolecules, 33 (2000) 3111-3119.

[78]   C.A. Scholes, G.W. Stevens, S.E. Kentish, Modeling syngas permeation through a poly dimethyl siloxane membrane by Flory–Rehner theory, Separation and Purification Technology, 116 (2013) 13-18.

[79]   H. Zhao, Z. Lai, A. Firoozabadi, Sorption Hysteresis of Light Hydrocarbons and Carbon Dioxide in Shale and Kerogen, Scientific Reports, 7 (2017) 16209.

[80]   A.R. Berens, Gravimetric and volumetric study of the sorption of gases and vapors in poly(vinyl chloride) powders, Polymer Engineering & Science, 20 (1980) 95-101.

[81] L.C. Witchey-Lakshmanan, H.B. Hopfenberg, R.T. Chern, Sorption and transport of organic vapors in poly[1-(trimethylsilyl)-1-propyne], Journal of Membrane Science, 48 (1990) 321-331.

[82] P. Chandra, Multi-Component Transport of Gases and Vapors in Poly(ethylene terephthalate), M.S. Thesis, Georgia Institute of Technology, Atlanta, GA, 2006.

[83] I.C. Sanchez, R.H. Lacombe, Statistical Thermodynamics of Polymer Solutions, Macromolecules, 11 (1978) 1145–1156.

[84] D. Tammaro, L. Lombardi, G. Scherillo, E. Di Maio, N. Ahuja, G. Mensitieri, Modelling Sorption Thermodynamics and Mass Transport of n-Hexane in a Propylene-Ethylene Elastomer, Polymers 13 (2021) 1157.

[85] H. Feng, Modeling of vapor sorption in glassy polymers using a new dual mode sorption model based on multilayer sorption theory, Polymer, 48 (2007) 2988-3002.

[86] V.P. Talluri, P. Patakova, T. Moucha, O. Vopicka, Transient and Steady Pervaporation of 1-Butanol–Water Mixtures through a Poly[1-(Trimethylsilyl)-1-Propyne] (PTMSP) Membrane, Polymers, 11 (2019) 1943.

[87] P.G.T. Fogg, W. Gerrard, Solubility of gases in liquids, John Wiley & Sons, Chichester, 1991.

[88] X. Liu, W. Afzal, M. He, J.M. Prausnitz, Solubilities of small hydrocarbons, viscosities of diluted tetraalkylphosphonium bis(2,4,4-trimethylpentyl) phosphinates, AIChE Journal, 60 (2014) 2607-2612.

[89] A. Finotello, J.E. Bara, S. Narayan, D. Camper, R.D. Noble, Ideal Gas Solubilities and Solubility Selectivities in a Binary Mixture of Room-Temperature Ionic Liquids, The Journal of Physical Chemistry B, 112 (2008) 2335-2339.

[90] Z. Lei, C. Dai, B. Chen, Gas Solubility in Ionic Liquids, Chemical Reviews, 114 (2014) 1289-1326.

[91]   L.A. Banu, D. Wang, R.E. Baltus, Effect of Ionic Liquid Confinement on Gas Separation Characteristics, Energy & Fuels, 27 (2013) 4161-4166.

[92]   P. Scovazzo, Determination of the upper limits, benchmarks, and critical properties for gas separations using stabilized room temperature ionic liquid membranes (SILMs) for the purpose of guiding future research, Journal of Membrane Science, 343 (2009) 199-211.

[93]   C.P. Ribeiro, B.D. Freeman, D.R. Paul, Pure- and mixed-gas carbon dioxide/ethane permeability and diffusivity in a cross-linked poly(ethylene oxide) copolymer, Journal of Membrane Science, 377 (2011) 110-123.

[94]   J.H. Dymond, K.N. Marsh, R.C. Wilhoit, K.C. Wond, The Virial Coefficients of Pure Gases and Mixtures, Springer, Darmstadt, 2001.

Chapter 3: Materials and Methods

3.1 MATERIALS

Poly(1-trimethylsilyl-1-propyne), PTMSP, was purchased from Gelest, Inc. The batch used in these experiments was characterized by Malgorzata Chwatko using gel permeation chromatography (GPC) with chloroform and had a weight average molar mass of 300,900 g/mol and a polydispersity index of 2.28. The poly(4-methyl-2-pentyne), PMP, was synthesized with the assistance of Maximilian Strauss. No GPC characterization was possible, as PMP is insoluble in the available GPC solvents [1].

4.0 research grade C_2H_6, 4.0 research grade C_3H_8, UHP 300 grade H_2, and UHP 300 grade CH_4 gas cylinders were obtained from Airgas. H-NMR spectra of [hmim][Tf$_2$N], PTMSP, and PMP are included in Figure D.2 through Figure D.4 (see Appendix D). The ionic liquids in this work were synthesized by Dr. Oscar Morales. Details of the syntheses are discussed next.

3.1.1: Synthesis of [hmim][Tf$_2$N]

The ionic liquid 1-hexyl-3-methylimidazolium bis(trifluoromethyl sulfonyl)imide, [hmim][Tf$_2$N], was synthesized by Dr. Oscar Morales as detailed in literature [2]. The precursors 1-bromohexane (>98%), 1-methylimidazole (99%), and lithium bis(trifluoromethyl sulfonyl)imide (99%), [Li][Tf$_2$N], were obtained from Sigma-Aldrich. The 1-methylimidazole was mixed with a small excess of 1-bromohexane in acetonitrile at 40 °C under a dry argon atmosphere. The highly exothermic reaction was carried out over the course of three days, and the produced 1-hexyl-3-methylimidazolium bromide, [hmim][Br], was purified using activated charcoal while stirring for 24 hrs. The solution was then diluted in acetonitrile and passed first through a Celite plug (7 cm long, 3 cm in

diameter) and then through a column of acidic alumina (20 cm long, 2.5 cm in diameter). The acetonitrile was then removed from solution via a rotary evaporator at 40 °C, followed by drying at high vacuum and 50 °C for 48 hrs. The dry bromide salt was then mixed with the [Li][Tf$_2$N] to allow for anion exchange. The [hmim][Tf$_2$N] was then decanted, washed 5-8 times with water until no halides were detectable by a silver nitrate test (~30 ppm halide detection limit), and dried under high vacuum for 48 hrs.

3.1.2: Synthesis of PMP

The batch of poly(4-methyl-2-pentyne) used in this work was synthesized by following procedures in the literature [3-4] using 96% 4-methyl-2-pentyne from Aldrich, extra dry (<50 ppm water) toluene from Acros Organics, and 99% niobium (V) chloride, NbCl$_5$, powder from Sigma-Aldrich. A catalyst solution was prepared in a dry (<2% relative humidity) N$_2$ environment by dissolving 0.24 g (0.85 mmol) of NbCl$_5$ in 36 mL anhydrous toluene. A clear solution of 10 grams of liquid 4-methyl-2-propyne, or MP, monomer and 14 mL of anhydrous toluene was then added dropwise to the gently stirred (~200 rpm) yellow catalyst solution at 30 °C and allowed to react for 24 hours. The viscosity of the dark brown reaction solution increased rapidly, such that the stirring settings in the magnetic plate had to be increased gradually over the first 30 minutes of the reaction (and until the magnetic stir bar became unable to spin even at the maximum stirring setting). After 24 hours, 3-5 mL of methanol were added to the reaction vessel to deactivate the catalyst. The thick, dark brown gel was recovered and redissolved overnight in 200 mL of cyclohexane while stirring at 400 rpm and 30 °C. The PMP was then precipitated by adding the cyclohexane solution dropwise to a rapidly stirred (1000 rpm) excess of methanol (~2 L). The methanol wash solution slowly turned yellow as it extracted the catalyst. Most of the excess methanol was removed by decanting, and the

remaining slurry was centrifuged for 20 minutes at 4000 rpm. The solids were then filtered with a Büchner funnel and dried with a diaphragm pump vacuum (in order not to expose the polymer to pump oil vapors) for 48 hours.

3.1.2: Synthesis of PDMS

Neat PDMS elastomer membrane samples were prepared by allowing a 5-fold molar excess of epoxypropoxypropyl-terminated PDMS to react with aminopropyl-terminated telechelic PDMS [5]. The epoxypropoxypropyl-terminated polymer reactant was roughly 550 g/mol, while the aminopropyl terminated PDMS had a molar mass of approximately 25,000 g/mol. The mixture was solution cast in a PTFE plate and annealed at 160 °C. A similar procedure was followed for PDMS-IL composite membrane preparation, but the amount of IL specified (e.g., $20_{wt}\%$) was added to the reaction mixture and stirred vigorously until a homogeneous dispersion was achieved. It should be noted that some of the less viscous (and/or some of the more hydrophylic) ILs aggregate into macroscopic droplets during the annealing step or prior to the permeation test.

3.2 MEMBRANE SAMPLE PREPARATION

Neat PTMSP films were cast from a $2_{wt}\%$ PTMSP dope cyclohexane solution. The casting solution was filtered in 0.45 µm PVDF/glass microfiber filters to remove dust and undissolved particles. Air bubbles were allowed to settle out prior to adding the dope solution to a glass casting plate partially covered by an inverted funnel with a plug at the neck. This set-up allowed slow evaporation of the cyclohexane over a period of 8-12 hours. The neat PTMSP membrane was delaminated from the casting plate and washed with methanol for conditioning.

SILMs were prepared by weighing neat polymer films and then immersing the neat sample for 10-15 minutes in a closed container with a methanol-[hmim][Tf$_2$N] solution of known concentration (refer to Figure 4.1 in Chapter 4). The soaked sample was removed from the closed container, immediately blotted dry with a laboratory tissue, and exposed to a diaphragm pump vacuum for 1 hour, as depicted in Figure 3.1. Using a diaphragm pump ensured that the samples were not exposed to pump oil vapors [6-7]. The dry SILM was then weighed, and the IL loading was computed as the weight of IL over the total weight of the SILM.
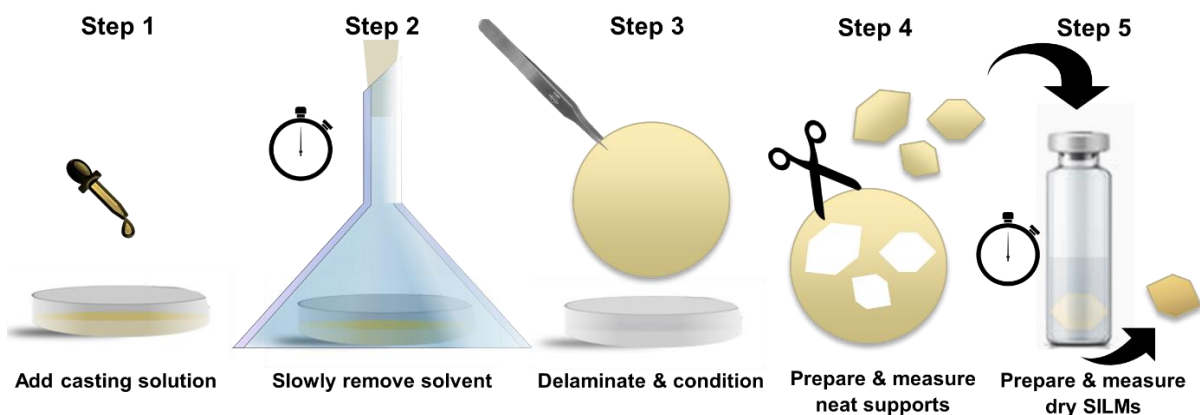
Figure 3.1:   Simplified SILM sample preparation protocol.

Membrane sample thicknesses, which ranged from 25 to 45 µm (+/- 1 µm), were measured using a Mitutoyo digital micrometer (293MDC-MX series). For permeation measurements, membrane samples were mounted on brass disks with orifice diameter ranging from 0.375 to 0.75 inches and adhered in place with 5-minute epoxy gel. Area measurements were carried out with a (CanoScan LiDE 400) computer scanner at 600 DPI resolution. Permeation measurements were conducted a minimum of 72 hours after

removal of the SILM from the methanol solution (or the neat PTMSP from the methanol conditioning).

3.3 PURE-GAS PERMEATION

Generally, gas permeabilities in neat PTMSP are high. Assuming that the permeability in PTMSP of the most impermeable species studied, CH_4, is on the order of 10,000 Barrer at 35 °C, the flowrate through a 30 μm-thick membrane sample with an area of 0.5 cm^2 is roughly 1.0 cm^3/min. In contrast, the CH_4 permeability in a 60_{wt}% [hmim][Tf$_2$N] in PTMSP SILM sample is 3 orders of magnitude lower (~10 Barrer), so a membrane sample with the same dimensions would yield a flowrate of around 0.001 cm^3/min.

A good rule of thumb is that samples with a permeate gas flowrate lower than 0.05 mL/min should be measured in a constant-volume, variable-pressure system, while samples yielding flowrates greater than 0.05 mL/min are more easily measured with a constant-pressure, variable-volume system.

3.3.1: Constant-pressure, variable-volume method

Neat PTMSP and PMP, as well as SILM samples, were measured using a constant-pressure, variable-volume apparatus. Once steady-state has been reached, permeability is calculated using Equation 3.1:

$$P_A = T_S \cdot l \cdot \frac{dV}{dt} / [A \cdot T \cdot (p_{us} - p_{ds})] \cdot 10^{10} \tag{3.1}$$

Where the permeability of species A, P_A, has units of Barrer, l is the membrane thickness in cm, $\frac{dV}{dt}$ is the pseudo-steady state volumetric flowrate of permeate gas in cm^3/s, and A is the membrane area in cm^2 [8]. Throughout this study, the downstream pressure, p_{ds}, is atmospheric (76 cmHg), T_S is the standard temperature (273.15 K), and the experimental

temperature, T, is controlled to a constant (usually 308.15 K). Figure 3.2 illustrates a typical constant-pressure, variable-volume apparatus.
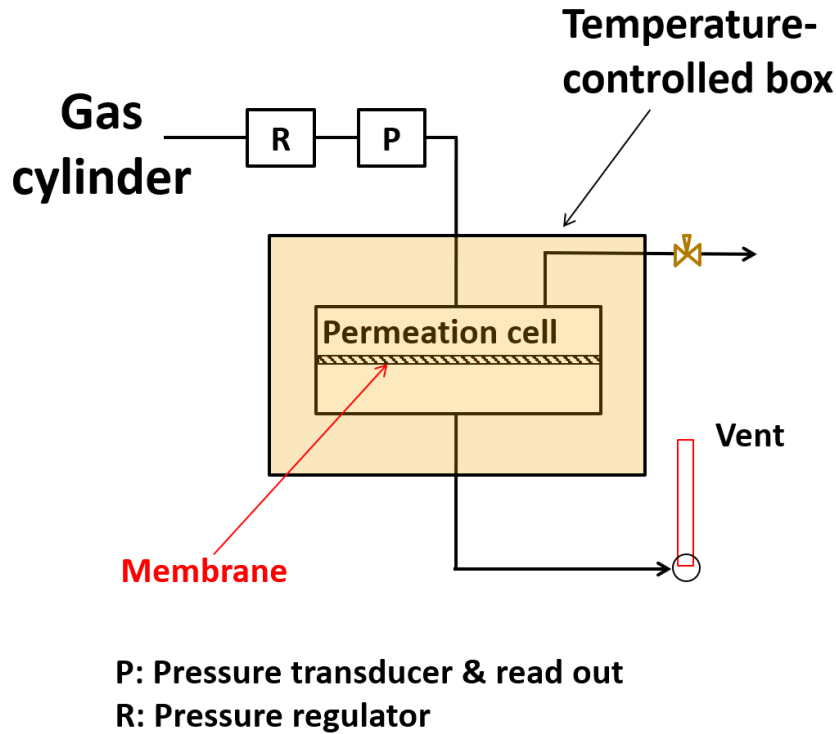
Figure 3.2   Constant-pressure, variable-volume permeation system schematic. The permeate flowrates can be measured with a variety of flowmeters but typically are limited to not less than 0.05 mL/min (with the 1 mL bubble flowmeter) and no more than 5,000 mL/min (with the 1 L bubble flowmeter).

3.3.2: Constant-volume, variable-pressure method

SILM samples of IL loading $42_{wt}\%$ and higher were measured using a constant-volume, variable pressure system. Permeability can be calculated by Equation 3.2:

$$P_A = T_S \cdot l \cdot V \cdot \left(\frac{dp_{ds}}{dt} - \frac{dp_{ds}}{dt}_{leak}\right)/(A \cdot T \cdot p_{us}) \cdot 10^{10} \qquad (3.2)$$

Where P_A has units of Barrer, l is the membrane thickness in cm, V is the downstream chamber volume in cm^3, $\frac{dp_{ds}}{dt} - \frac{dp_{ds}}{dt}_{leak}$ is the steady state downstream pressure

increment due to gas permeation in atm/s, A is the membrane area in cm^2, T is the experiment temperature in kelvin, and p_{us} is the applied (upstream) pressure in cmHg [9].

It is desired that the overall rising pressure rate $\frac{dp_{ds}}{dt}$ be at least ten times larger than the leak rate, $\frac{dp_{ds}}{dt}_{leak}$, otherwise the sample flowrate is too small to measure reliably with a constant-pressure, variable-volume system. Because this method exposes samples to a high vacuum line for extended periods of time, a liquid nitrogen trap (with sacrificial PTMSP powder as an absorbent) was used during measurement to prevent vacuum pump oil from accumulating in any permeation samples [6-7]. Figure 3.3 shows a simplified constant-volume, variable-pressure system diagram.
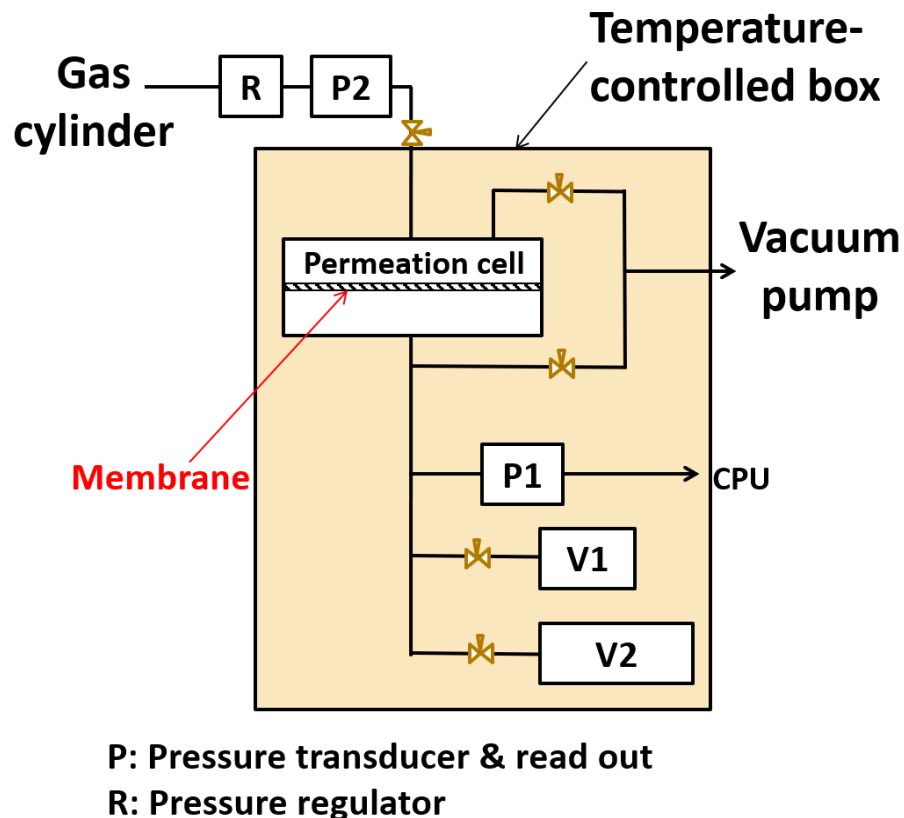
Figure 3.3   Constant-volume, variable-pressure permeation system schematic.

3.4 MIXED-GAS PERMEATION

Mixed-gas permeation experiments utilized a constant-pressure sweep system. Mixed-gas feeds of up to 3 different species can be custom made with the appropriate mass flow controllers calibrated for any of the six species depicted in the lower left-hand corner of Figure 3.4. The temperature can be controlled within the range of 5 to 200 °C, and samples with permeate flowrates as low as 0.0001 mL/min can be measured. A GC equipped with a TCD and an FID is used for compositional analysis.
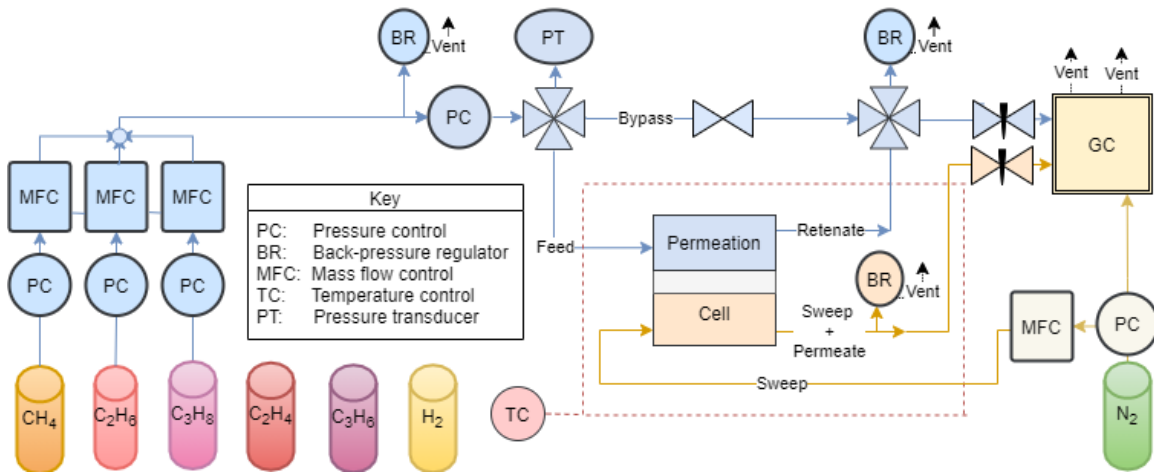
Figure 3.4:   Mixed-gas sweep system schematic.

To minimize concentration polarization, the sweep rate on both the upstream and downstream sides should be one hundred times larger than the gas flowrate across the membrane sample. This can also be defined as operating at a stage-cut of 0.01:

$$\theta_{ds} = \frac{Q_{permeate}}{Q_{sweep}}, \quad \theta_{us} = \frac{Q_{permeate}}{Q_{feed}} \tag{3.3}$$

where θ_{ds} is the downstream stage-cut, θ_{us} is the upstream stage-cut, and Q_i are volumetric flowrates. Figure 3.5 shows the various streams around the sweep system permeation cell.

Much like in the pure-gas constant-pressure, variable-volume system, we can calculate the permeability of a species in the mixture with Equations 3.4 and 3.5:

$$P_A = T_S \cdot l \cdot \frac{dV}{dt} / [A \cdot T \cdot (x_{A,us}\hat{f}_{A,us} - x_{A,ds}\hat{f}_{A,ds})] \cdot 10^{10} \tag{3.4}$$

$$\frac{dV}{dt} = x_{A,ds}Q_{sweep+permeate} = F_A\left(\frac{\Lambda_{TCD}}{\Lambda_{TCD}^0}\right)Q_{sweep+permeate} \tag{3.5}$$

Where $\hat{f}_A$ is the component A fugacity in a mixture, while the volume fraction of A in the downstream is a function, F_A, of Λ_{TCD}, the area of the TCD peak of component A, and Λ_{TCD}^0, the area of a TCD peak of $100_{vol}\%$ component A in the sample loop [10].

Feed in (e.g., C_3H_8, C_2H_6 and CH_4)

→ **Retentate**

Sweep in
(N_2)

Sweep + Permeate
(N_2 + analyte)
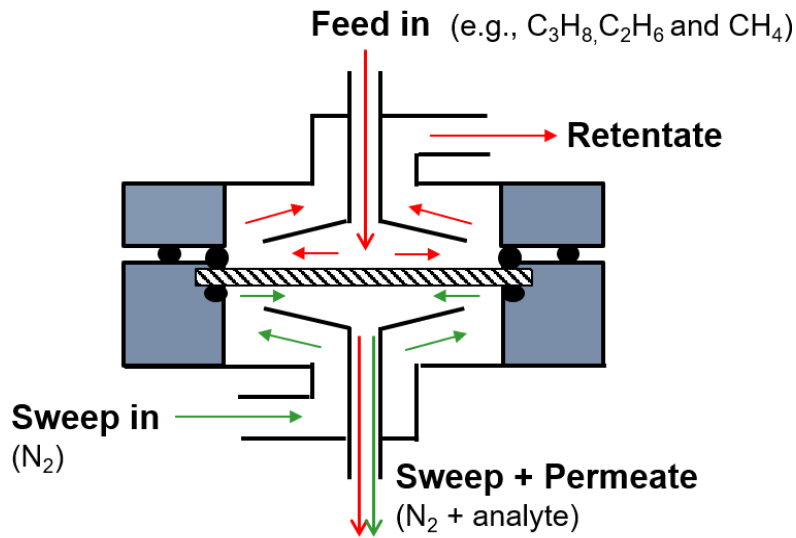
Figure 3.5:   Modified permeation cell design for upstream and downstream sweep.

3.5 PURE-GAS SORPTION

Of the many possible methods for characterizing isothermal gas sorption in liquids and solids, we focus on two: the pressure-decay and the gravimetric methods.

3.5.1: Pressure-decay method

This method involves inserting a material sample into a sample chamber of known volume V_2 and degassing it along with a known charge volume, V_1. After a known pressure of gas is loaded into the charge volume, V_1, the valve dividing V_1 and V_2 is opened momentarily and then closed again. The pressure in both chambers is monitored by pressure transducers and logged by a computer, as shown in Figure 3.6. As the gas in V_2 equilibrates with the sample, the pressure decays asymptotically. Once the pressure in the sample chamber equilibrates, a new higher pressure can be loaded to the charge volume, and the valve may be briefly opened once more to record a second equilibrium pressure. This process can be repeated for m charge steps. The amount of gas sorbed into the sample can be determined from a mol balance (Equation 3.6) and an equation of state [11].

$$n_{A,s}^m = n_{A,s}^{m-1} + n_{A,1}^{m-1} + n_{A,2}^{m-1} - n_{A,1}^m - n_{A,2}^m$$

$$= n_{A,s}^{m-1} + \frac{p_1^{m-1} V_1}{R\,T\,Z_1^{m-1}} + \frac{p_2^{m-1}(V_2 - V_s)}{R\,T\,Z_2^{m-1}} - \frac{p_1^m V_1}{R\,T\,Z_1^m} - \frac{p_2^m(V_2 - V_s)}{R\,T\,Z_2^m} \qquad (3.6)$$

where $n_{A,s}^m$ are the moles of A sorbed in the sample at any charge step m, $n_{A,1}^m$ are the moles of A in the charge volume, and $n_{A,2}^m$ are the moles of A in the headspace of the sample volume (*i.e.*, the portion of V_2 not occupied by the sample). p_1^m and p_2^m are the pressures in the charge and sample volumes, respectively, at any step m. Similarly, Z_1^m and Z_2^m are the compressibility factors corresponding to the gas pressure in the charge and sample volumes, respectively, at any charge step m.

For an ideal gas, Boyle's law is an appropriate equation of state, and all $Z_i^m = 1$. Otherwise, Z_i^m can be related to the fugacity coefficient obtained from any equation of state by Equation 3.7 [12]:

$$\ln \phi = \int_0^p \frac{Z(p, V_m) - 1}{p} dp \qquad (3.7)$$

where the compressibility factor, Z, is a function of only pressure and molar volume, $V_m = V/n$ for isothermal measurements.
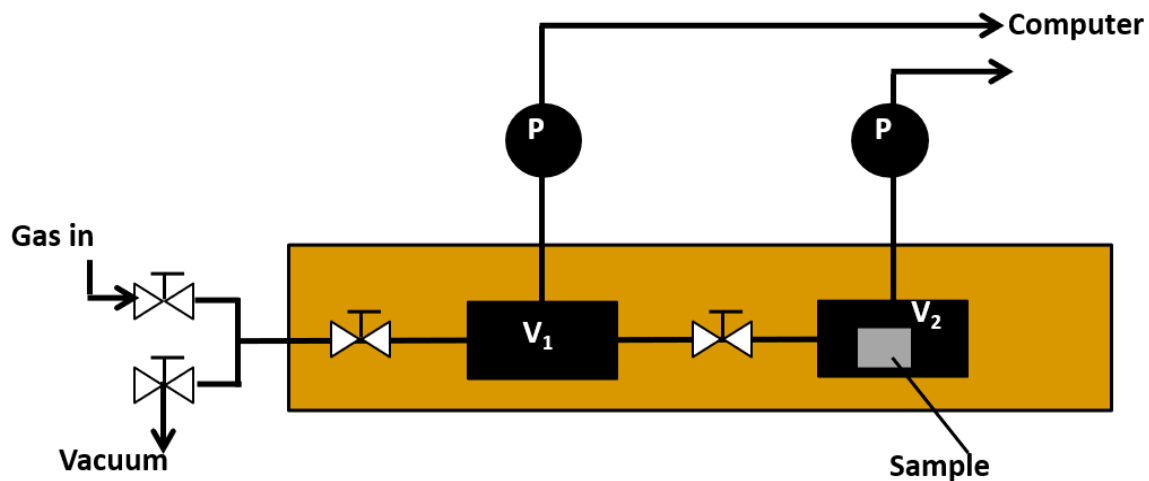
Figure 3.6: Pressure-decay apparatus schematic.

3.5.2: Gravimetric method

Gravimetric sorption measurements were carried out in a magnetic suspension balance. The sample is loaded in a bucket in a temperature- and pressure-controlled chamber, as shown in Figure 3.7. The measurement begins by degassing the sample until its mass change stabilizes to within the last two digits (tenths and hundredths of a

microgram). During measurement, the computer tracks the mass change over time after addition of the gas at a set pressure. The mass asymptotically approaches a new stable value as the sample reaches equilibrium with the gas in the chamber.

The instrument reports the bucket plus sample weight while lifting the bucket with the hook (that is, at the measuring point). The microbalance is tared every two minutes while the bucket is supported by the cone rather than the hook (that is, at the zero point) and the corrected weight reported by the instrument accounts for any balance drift by referencing the most recent tared mass. The sample mass is calculated from the following force balance [13-14]:

$$W_s(P,T) = W_m(P,T) - W_0 + \rho(P,T) \, g \, [V_0 + V_S(P,T)] \qquad (3.8)$$

where $W_m(P,T)$ is the measured, corrected weight (of the sample plus bucket), W_0 is the weight of the empty bucket under vacuum (at the measurement temperature), $\rho(P,T)$ is the density of the gas or vapor in the chamber, $V_S(P,T)$ is the volume of the sample, g is the acceleration due to gravity, and V_0 is the volume of the empty bucket as obtained from a buoyancy calibration run. The sample mass is obtained by dividing the weight of the sample, $W_s(P,T)$ by g. It should be noted that $V_S(P,T)$ is often assumed constant when measuring sorption of sparingly soluble gases, but for getting sorption isotherms of more condensable species, characterizing the $V_S(P,T)$ change with increasing pressure (*e.g.*, through dilatomery) is critical.
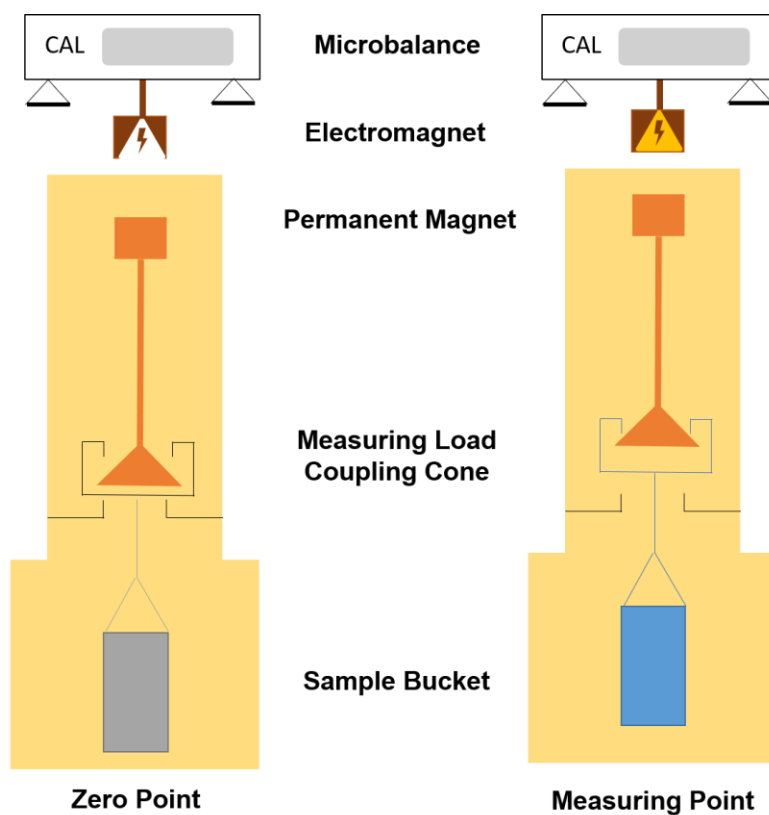
Figure 3.7:   Simplified schematic of a magnetic suspension balance. Adapted from [15].

3.6 DILATOMETRY

The one-dimensional length change of polymer and SILM samples when exposed to the light hydrocarbon gases was measured with a dilatometer, as pictured in Figure 3.8. Sample dimensions were approximately 80-90 mm long, 8-10 mm wide and 60-70 μm thick. The samples were held in place by a clamp within a Jerguson gauge and kept from curling by a wire track but were otherwise free to expand unconstrained. A Ricoh DMK 23U274 digital camera was used to record sample photographs continuously in a CPU. The minimum detectable length change is approximately 0.03 mm. The pressure readout is a 700 psia Heise gauge with an accuracy of 0.1% of the maximum grading. The oil

bath temperature was controlled with water flow through a glass jacket from a Thermo Neslab circulator.
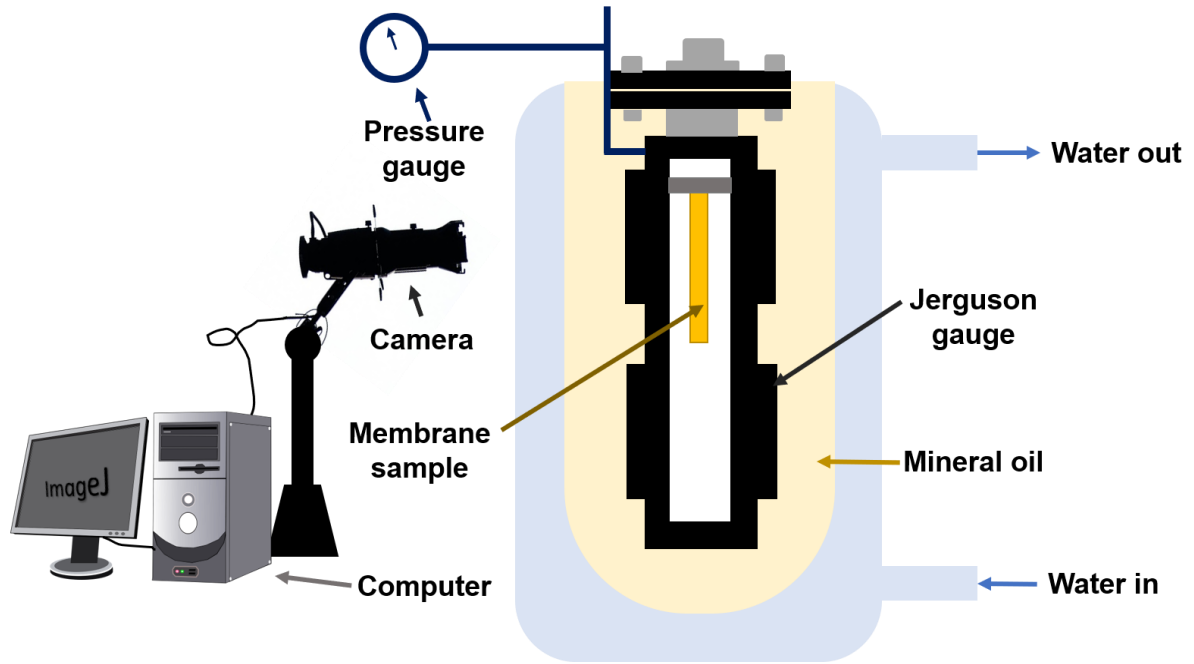
Figure 3.8:   A simplified schematic of the dilatometer. Adapted from [16].

3.7 DENSITY

Geometric densities were derived from sample mass from a Sartorius balance (model MSU225P-1TR-DA), thickness measurements from a Mitutoyo digital micrometer (293MDC-MX series), and area measurements from a (CanoScan LiDE 400) computer scanner.

Experimental densities were also determined with the buoyancy method by using Equation 3.11:

$$\rho_s = \frac{m_{s,a}}{m_{s,a} - m_{s,b}}(\rho_b - \rho_a) + \rho_a \qquad (3.9)$$

Where ρ_s is the density of the sample, $m_{s,a}$ is the mass of the sample in air, $m_{s,b}$ is the mass of the sample in an auxiliary liquid, ρ_a is the density of air and ρ_b is the density of the auxiliary liquid. The auxiliary liquid used was deionized water to prevent sample swelling mid-measurement [17].

3.8: DIFFERENTIAL SCANNING CALORIMETRY AND THERMOGRAVIMETRIC ANALYSIS

TGA and DSC scans were made in a Mettler Toledo TGA/DSC 3+ and a Mettler Toledo DSC 3. Because scan temperatures did not exceed 500 °C, standard aluminum crucibles were used. The TGA scanning rate was 5 °C/min, while the DSC scanning rate was 10 °C/min, and the 2nd heating curves are reported.

3.9: CROSS SECTIONAL SCANNING ELECTRON MICROSCOPY–ENERGY DISPERSIVE X-RAY (CS-SEM-EDX) SPECTROSCOPY

Cross sectional SEM was done using the secondary electron scanning and energy dispersive X-ray spectroscopy modes in a Hitachi S-5500 SEM. Samples were sputter-coated with gold nanoparticles for 90 seconds. An acceleration voltage of 20 kV and probe current of 10 µA were used, and magnification ranged from 1.2k to 1.4k. A slow scanning rate (capture speed integration of 20 s) was used. EDX spectra were collected for 180 s per frame.

3.10: MECHANICAL PROPERTIES ANALYSIS

Mechanical properties were measured with a Shimadzu Autograph AGS-X 500N, a Universal Testing Machine (UTM) adhering to the ASTM D-1708-13 standard; the tensile test method is outlined in standards D 882 and D 638. The UTM was operated with Bluehill Materials Testing software. Dogbone specimens (adhering to the D 882 standard) were between 60 and 70 µm in thickness. Averages and standard deviations of

properties from at least 5 dogbone specimens from the same membrane sample are reported [18].

3.11 REFERENCES

[1]   M.T. Demko, J.C. Cheng, A.P. Pisano, Rigid, Vapor-Permeable Poly(4-methyl-2-pentyne) Templates for High Resolution Patterning of Nanoparticles and Polymers, ACS Nano, 6 (2012) 6890-6896.

[2]   A. Ahosseini, B. Sensenich, L.R. Weatherley, A.M. Scurto, Phase Equilibrium, Volumetric, and Interfacial Properties of the Ionic Liquid, 1-Hexyl-3-methylimidazolium Bis(trifluoromethylsulfonyl)amide and 1-Octene, Journal of Chemical & Engineering Data, 55 (2010) 1611-1617.

[3]   K. Nagai, A. Sugawara, S. Kazama, B.D. Freeman, Effects of physical aging on solubility, diffusivity, and permeability of propane and n-butane in poly(4-methyl-2-pentyne), Journal of Polymer Science Part B: Polymer Physics, 42 (2004) 2407-2418.

[4]   E.Y. Sultanov, M.Y. Gorshkova, E.N. Semenistaya, V.S. Khotimsky, Living polymerization of 4-methyl-2-pentyne and 1-trimethylsilyl-1-propyne initiated by $NbCl_5$-Ph_4Sn catalyst, Polymer Science Series B, 50 (2008) 330-333.

[5]   J. Park, H. Ha, H.W. Yoon, J. Noh, H.B. Park, D.R. Paul, C.J. Ellison, B.D. Freeman, Gas sorption and diffusion in poly(dimethylsiloxane) (PDMS)/graphene oxide (GO) nanocomposite membranes, Polymer, 212 (2021) 123185.

[6]   L.C. Witchey-Lakshmanan, H.B. Hopfenberg, R.T. Chern, Sorption and transport of organic vapors in poly[1-(trimethylsilyl)-1-propyne], Journal of Membrane Science, 48 (1990) 321-331.

[7]   S.V. Dixon-Garrett, K. Nagai, B.D. Freeman, Sorption, diffusion, and permeation of ethylbenzene in poly(1-trimethylsilyl-1-propyne), Journal of Polymer Science Part B: Polymer Physics, 38 (2000) 1078-1089.

[8]   T.C. Merkel, Z. He, I. Pinnau, B.D. Freeman, P. Meakin, A.J. Hill, Effect of Nanoparticles on Gas Sorption and Transport in Poly(1-trimethylsilyl-1-propyne), Macromolecules, 36 (2003) 6844-6855.

[9]   D.G. Pye, H.H. Hoehn, M. Panar, Measurement of gas permeability of polymers. I. Permeabilities in constant volume/variable pressure apparatus, Journal of Applied Polymer Science, 20 (1976) 1921-1931.

[10]   C.P. Ribeiro, B.D. Freeman, D.R. Paul, Pure- and mixed-gas carbon dioxide/ethane permeability and diffusivity in a cross-linked poly(ethylene oxide) copolymer, Journal of Membrane Science, 377 (2011) 110-123.

[11]   H. Lin, B.D. Freeman, Chapter 7: Permeation and Diffusion, in: Springer Handbook of Materials Measurement Methods, 2006, pp. 371-387.

[12]   J.R. Elliot, C.T. Lira, Introductory Chemical Engineering Thermodynamics, 2nd Ed, Prentice Hall, Upper Saddle River, NJ, 2012.

[13]   T. Song, O. Morales-Collazo, J.F. Brennecke, Solubility and Diffusivity of Oxygen in Ionic Liquids, Journal of Chemical & Engineering Data, 64 (2019) 4956-4967.

[14]   C.P. Ribeiro, B.D. Freeman, Sorption, Dilation, and Partial Molar Volumes of Carbon Dioxide and Ethane in Cross-Linked Poly(ethylene oxide), Macromolecules, 41 (2008) 9458-9468.

[15]   Y. Changtao, L. Shuyuan, W. Hailong, Y. Fei, x. Xu, Pore structure characteristics and methane adsorption and desorption properties of marine shale in Sichuan Province, China, RSC Advances, 8 (2018) 6436-6443.

[16]   R.D. Raharjo, Mixed Gas Sorption and Transport Study in Solubility Selective Polymers, PhD dissertation, The University of Texas at Austin, Austin, TX, 2007.

[17]   E.J. Kappert, M.J.T. Raaijmakers, K. Tempelman, F.P. Cuperus, W. Ogieglo, N.E. Benes, Swelling of 9 polymers commonly employed for solvent-resistant nanofiltration membranes: A comprehensive dataset, Journal of Membrane Science, 569 (2019) 177-199.

[18]   J.D. Moon, Impact of Humidity and Polymer Blending on the Gas Transport Properties of Polybenzimidazoles, PhD dissertation, The University of Texas at Austin, Austin, TX, 2019.

Chapter 4: Characterization of [hmim][Tf$_2$N]-PTMSP SILMs

4.1 EQUILIBRIUM IL CONCENTRATION CURVES

SILMs were made following the procedure described in Section 3.2. For the [hmim][Tf$_2$N]-PTMSP SILMs, the IL was dissolved in methanol at various concentrations. After equilibrating a neat PTMSP sample of known mass in these solutions, the sample was removed from solution, the excess liquid immediately blotted off, and the sample dried under vacuum provided by a diaphragm pump. The IL loading of the dry SILM corresponding to each of the IL-methanol concentration solutions used was noted. From Figure 4.1, it is evident that sample thickness affects the IL loading. Matthew Santoso and Nathalie Debelle assisted in the making of other equilibrium IL loading versus IL-methanol concentration curves similar to Figure 4.1 for other alcohols or other ILs, respectively.

Other than functioning as the volatile component in the IL solutions, methanol serves at least two purposes: (1) it swells the PTMSP matrix, facilitating the diffusion of IL into the membrane and (2) it dissolves the IL, reducing the viscosity of the liquid mixture and thus the time to reach equilibrium. The viscosity of neat [hmim][Tf$_2$N] at 25 °C is 70.6 mPa s [1]. Given the high viscosities of some ILs, submerging PTMSP in a neat IL can take multiple days to reach equilibrium. For instance, Bazhenov et al. equilibrated their 21 μm PTMSP samples with various ILs, including [P$_{66614}$][Br] with a reported viscosity of 2988 mPa s at 25 °C, for a minimum of 40 days [2].
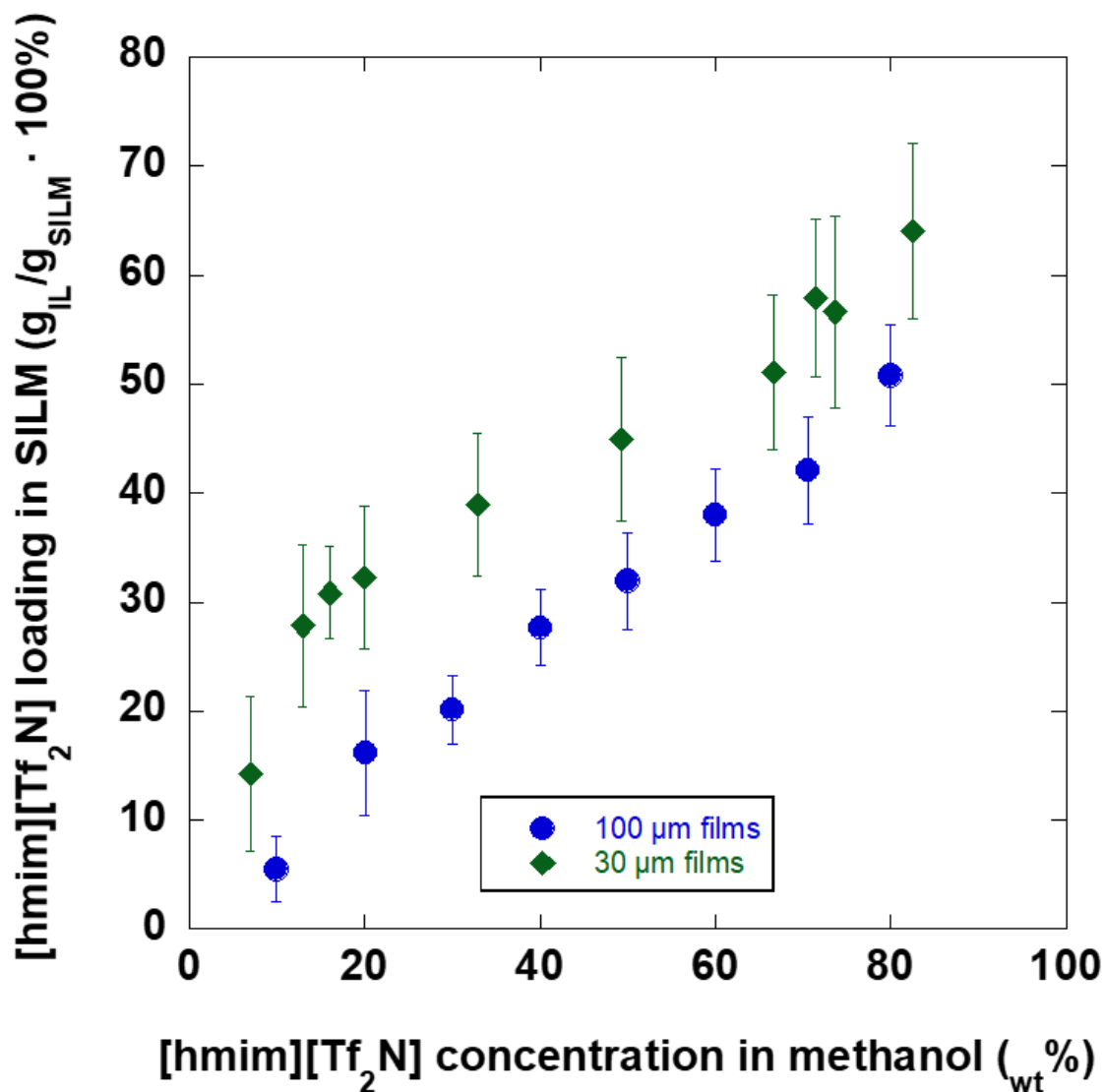
Figure 4.1: Equilibrium [hmim][Tf₂N] loading in dry SILMs post immersion in IL-
methanol solution of known concentration.

4.2 TGA AND DSC OF PTMSP SILMS

Figure 4.2 compares the thermal decomposition behavior of the neat PTMSP, the

neat [hmim][Tf$_2$N], and SILMs of various compositions. The tangent-extrapolated onset

temperature of the neat PTMSP was 356 °C, while that of [hmim][Tf$_2$N] was 411 °C. For

SILMs, the onset temperatures were 354, 358, 359, and 364 °C for the 21, 41, 50, and

59$_{wt}$% loadings, respectively. A secondary mass loss step associated with the degradation

of the ionic liquid was observed for the 42$_{wt}$% and higher loadings.
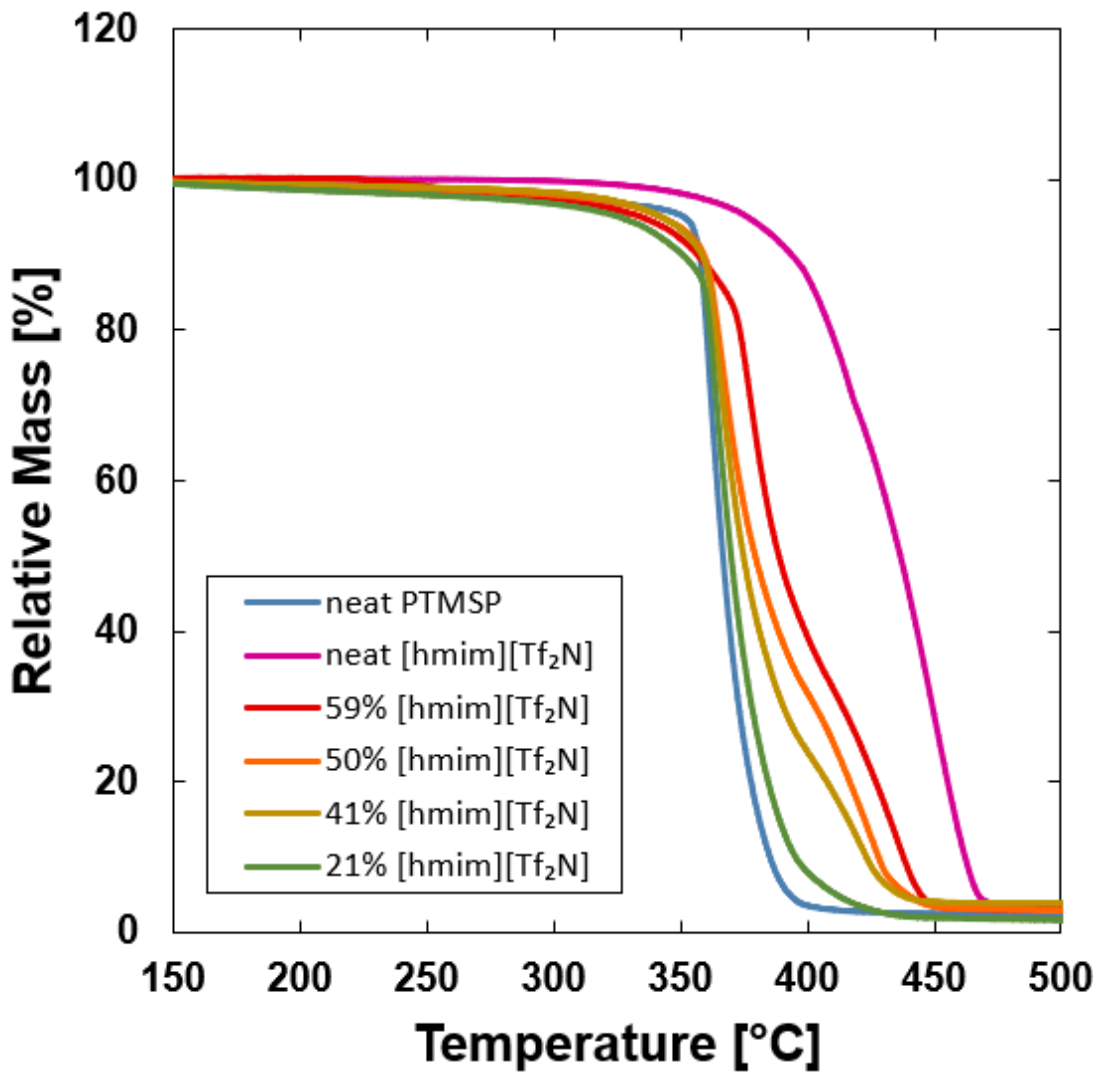
Figure 4.2:   Thermal decomposition curves of [hmim][Tf$_2$N]-PTMSP SILMs and the
neat components. Reported onset temperatures were determined by the
intersection of tangents method.

DSC analyses are summarized in Figure 4.3. The glass, crystallization, and

melting transitions (T_g, T_c and T_m) of the neat [hmim][Tf$_2$N] were identified at -85, -22,

and -6 °C, respectively. No characteristic features were observed in the neat PTMSP or

68

21$_{\text{wt}}$% loading SILM scans, whereas a small feature matching the melting temperature, T_m, of the IL was observed in the 41$_{\text{wt}}$% and 60$_{\text{wt}}$% SILM scans.
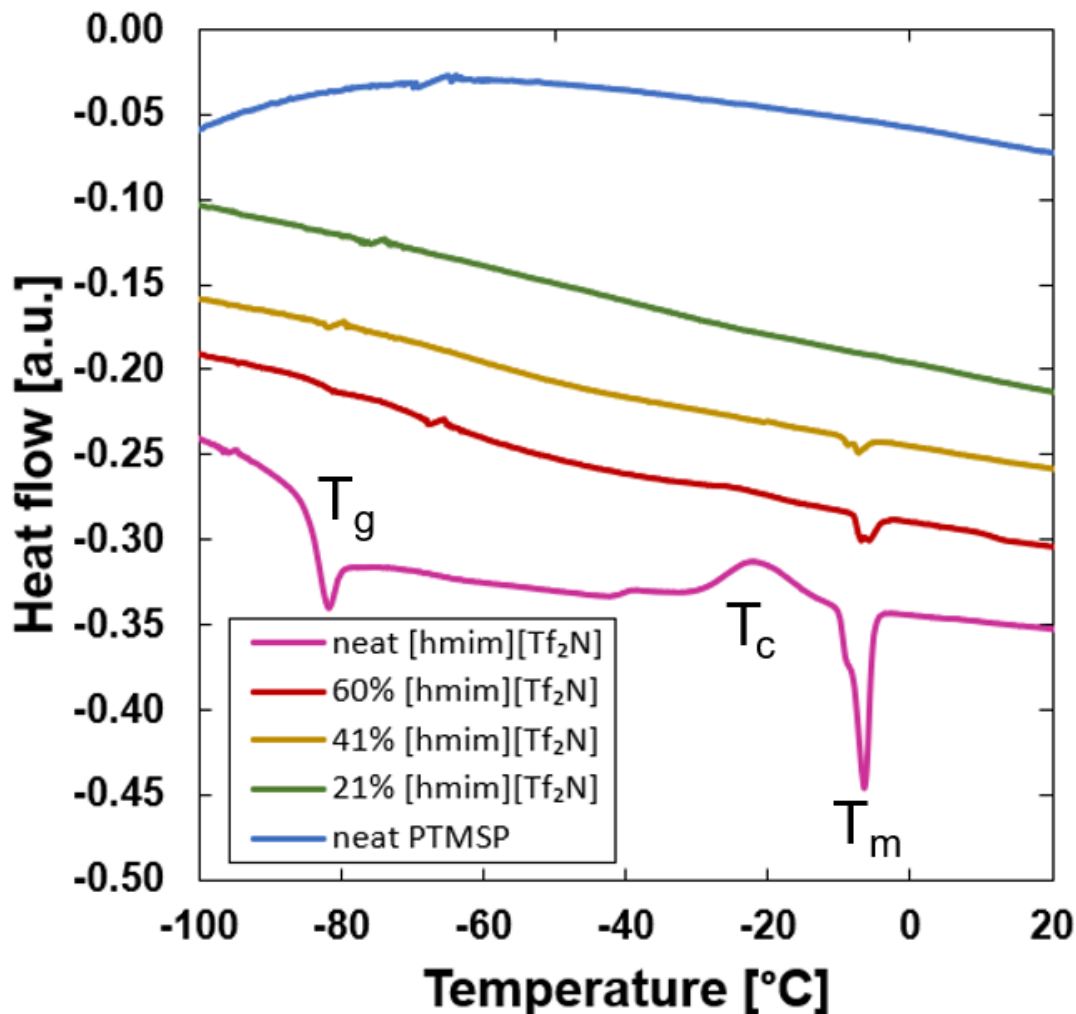
Figure 4.3: Second heating differential scanning calorimetry curves of [hmim][Tf$_2$N]-PTMSP SILMs and the neat components. The features labelled T_g, T_c, and T_m correspond to the glass transition, crystallization, and melting temperatures of the ionic liquid, respectively.

A small baseline shift matching the IL glass transition was also observed for the 60$_{\text{wt}}$% SILM curve. The IL confinement within the polymer matrix is likely to inhibit the crystallization transition, as was observed in SPI-[bmim][Tf$_2$N] membranes [3].

4.3 CROSS-SECTIONAL SCANNING ELECTRON MICROSCOPY WITH ENERGY DISPERSIVE SPECTROSCOPY OF SILMs

Elemental analysis via energy dispersive x-ray spectroscopy was conducted to investigate the IL dispersion in a $60_{wt}\%$ SILM. Figure 4.4 displays the relevant cross-sectional SEM images. Fluorine, nitrogen, and sulfur elemental analysis revealed that the IL was homogeneously dispersed across the membrane thickness, within the resolution of the detector, for all IL loadings studied.
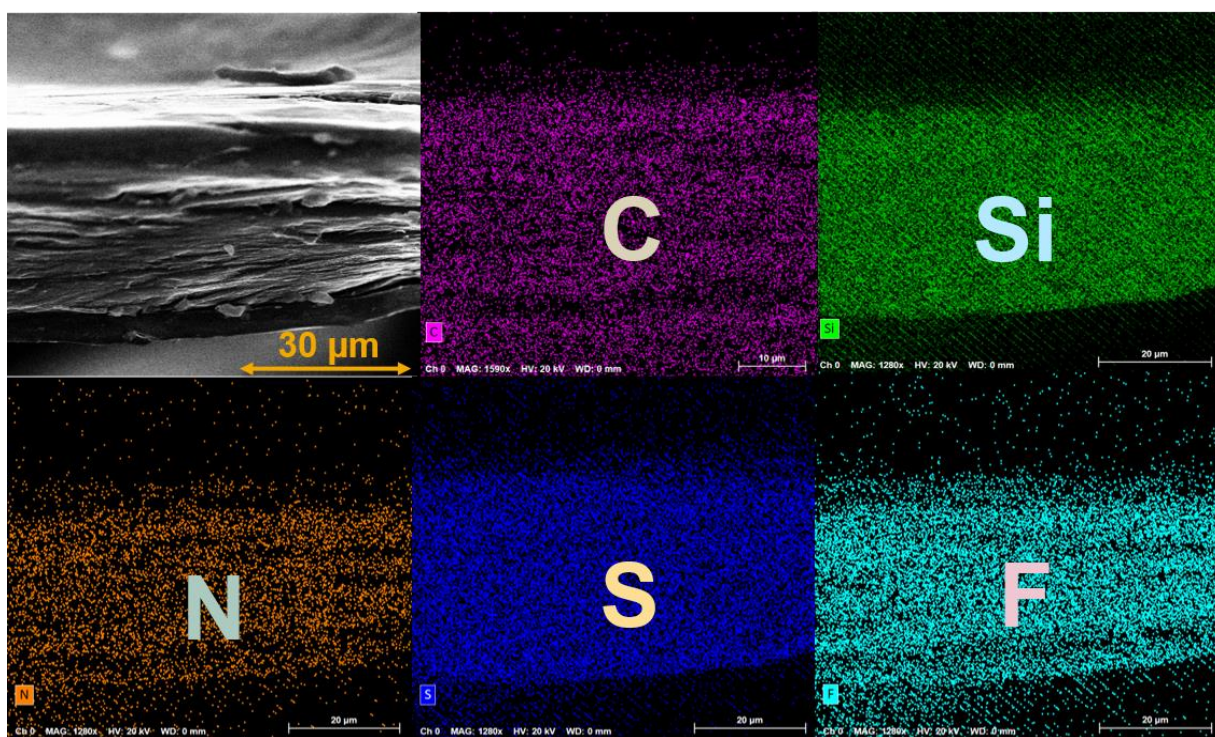
Figure 4.4:   Secondary electron and corresponding EDX elemental maps of C, Si, N, S, and F for a roughly 35 μm thick $60_{wt}\%$ [hmim][Tf$_2$N] in PTMSP SILM.

4.4 DENSITY OF SILMs AND NEAT PTMSP

As seen in Figure 4.5, uncertainties from densities determined by the geometric method are typically greater than those obtained from the buoyancy method or other

pycnometric methods. Other methods for measuring densities of polymers include gas pycnometers and density gradient columns. A helium pycnometer can measure skeletal density, which may differ from the geometric density if the sample is porous or a high free volume polymer [4]. Care must also be taken when making use of the density gradient column or buoyancy methods, one must keep in mind any pronounced effects of sample swelling when submerged into auxiliary fluids that are also swelling agents. The auxiliary fluid chosen should only minimally swell the sample, if at all, during measurement. For PTMSP, water was chosen as the auxiliary fluid given its negligible swelling degree on PTMSP [5] and the large immiscibility gap between [hmim][Tf$_2$N] and water [6].

The green curve in Figure 4.5 was obtained by assuming volume additivity and doing a mass balance [7]:

$$\varphi_{IL} = \frac{1}{1 + \frac{\rho_{IL}}{\rho_p}(\frac{1}{\omega_{IL}} - 1)} \tag{4.1}$$

where φ_{IL} is the volume fraction of IL in the SILM, ρ_{IL} is the density of neat IL, ω_{IL} is the IL mass fraction or fractional IL loading, and ρ_p is the density of neat polymer. From the mass balance, Equation 4.2 ensues:

$$\rho_{SILM} = \rho_{IL}\varphi_{IL} + \rho_p(1 - \varphi_{IL}) = \frac{1}{\frac{\omega_{IL}}{\rho_{IL}} + \frac{1 - \omega_{IL}}{\rho_p}} \tag{4.2}$$
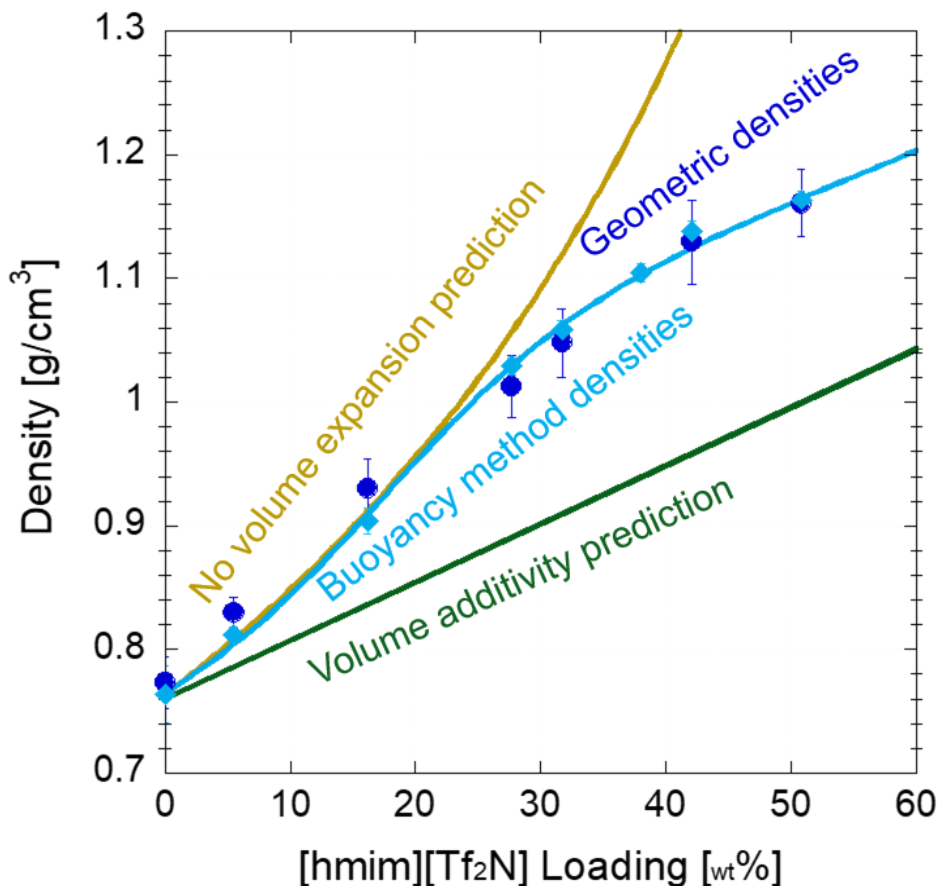
Figure 4.5: Densities of [hmim][Tf₂N]-PTMSP SILMs as determined by the geometric and buoyancy methods. The bounds represent theoretical predictions by the volume additivity assumption (lower) and the fixed-volume or no swelling assumption (upper). The buoyancy method data were fit using Equation 4.3 with $\Psi=12 \pm 0.7$, $\Omega=0.185 \pm 0.006$ and an R^2 of 0.998.

The yellow curve is obtained by fixing the original volume occupied by the polymer and computing the density increase with the addition of IL. The experimental density data are bound by the predictions made from either of these assumptions, so a more elaborate model is needed to fit the data. Given the large free volume of the neat polymer support, one could make a better model by making ρ_p a function of ω_{IL} to account for the apparent densification of the polymer phase as its accessible free volume

is occupied by, or shared with, the IL. Absent free volume, the maximum density of the polymer equals its skeletal density, as conveniently measured by a helium pycnometer [8]. The resulting model used for fitting the buoyancy method density data is Equation 4.3:

$$\rho_{SILM} = \cfrac{1}{\cfrac{\omega_{IL}}{\rho_{IL}} + \cfrac{1 - \omega_{IL}}{\rho_{p,geo} + \cfrac{\rho_{p,ske} - \rho_{p,geo}}{1 + \exp\left(-\Psi(\omega_{IL} - \Omega)\right)}}} \qquad (4.3)$$

Where $\rho_{p,ske}$ is the skeletal density of the polymer, $\rho_{p,geo}$ is its geometric density, and Ψ and Ω are fitting parameters related to the sharpness of the curvature transition and the weight fraction of IL at which the transition begins, respectively.

The densities and corresponding volume fractions of IL are shown in Table 4.1. In determining the volume fractions of [hmim][Tf$_2$N] of the SILMs from the density data, the following assumptions were made: (1) that the IL first occupies the accessible free volume in the PTMSP, prior to causing any matrix swelling; (2) that the swelling is isotropic; and (3) that the bulk phase IL and confined phase IL have the same density.

Table 4.1: Comparing densities obtained by the buoyancy, geometric, and pycnometric methods for neat PTMSP and [hmim][Tf$_2$N] in PTMSP SILMs and corresponding volume fraction of IL.

IL loading [$_{wt}$%]	Geometric density [g/cm^3]	Buoyancy method density [g/cm^3]	IL volume fraction [$_{vol}$%]
0	0.77 (±0.02)	0.764 (±0.023)	0
5.5	0.83 (±0.01)	0.812 (±0.006)	3.2
16.2	0.93 (±0.02)	0.904 (±0.010)	10.6
27.7	1.01 (±0.03)	1.029 (±0.007)	20.4
31.7	1.05 (±0.03)	1.059 (±0.008)	24.1
38.0	-	1.105 (±0.007)	30.1
42.1	1.13 (±0.03)	1.138 (±0.009)	34.0
50.8	1.16 (±0.03)	1.164 (±0.007)	42.4

4.5 MECHANICAL PROPERTIES OF A SILM AND OF NEAT PTMSP

Tensile tests of 42$_{wt}$% [hmim][Tf$_2$N] SILMs and PTMSP samples (14 days after methanol exposure) reveal the effects on the film's mechanical properties of incorporating IL into the polymer matrix. The IL-containing samples are both more ductile and tougher than the neat polymer samples, but their elastic modulus and yield strength are more modest than those of the neat polymer. Figure 4.6 shows the typical stress-strain behavior of PTMSP and 42$_{wt}$% SILM samples. PTMSP, like other brittle polymers, exhibits elastic and plastic regions prior to the point of fracture, which overlaps with the maximum applied stress, or the tensile strength. This is not the case in the typical 42$_{wt}$% SILM curves, as the maximum corresponds to the onset of necking, and the samples fail at a slightly greater strain.
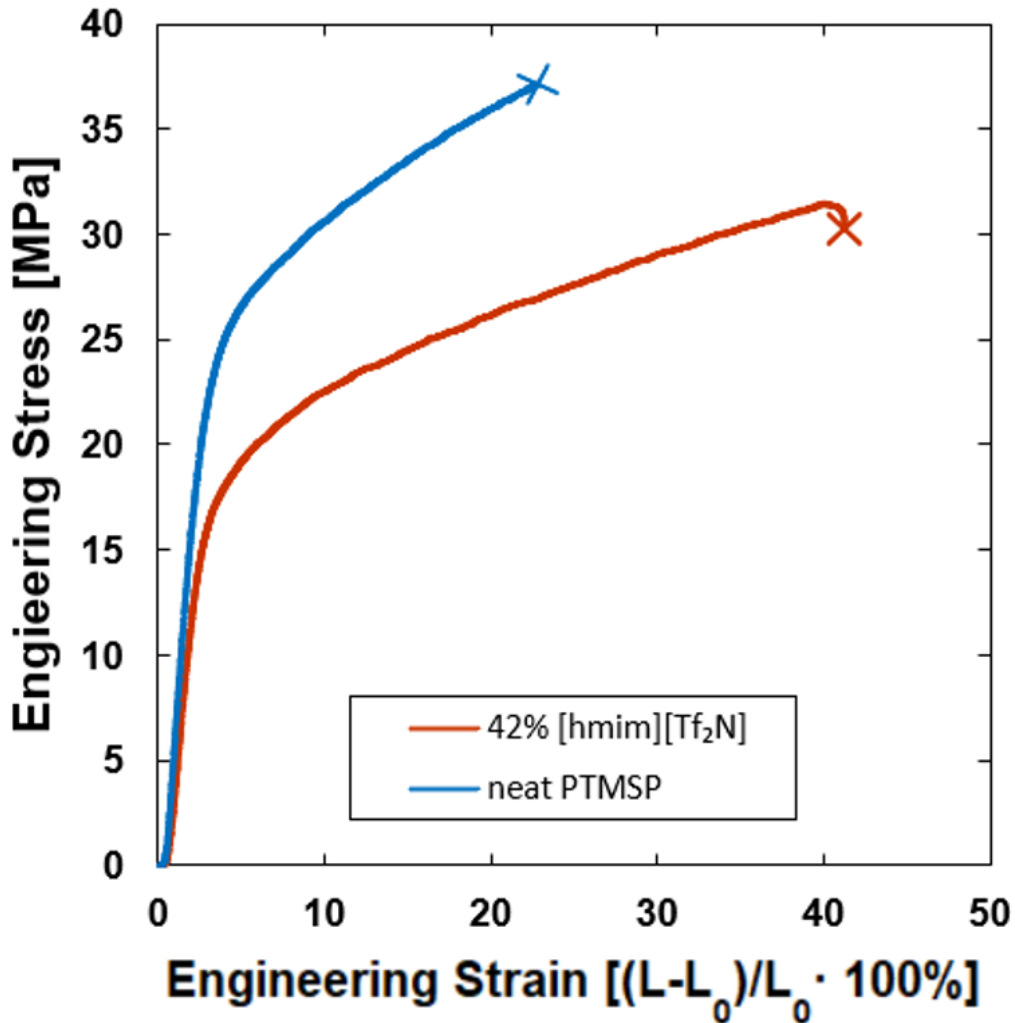
Figure 4.6: Representative engineering stress-strain curves of a neat PTMSP and a 42_{wt}% [hmim][Tf$_2$N] in PTMSP SILM dogbone specimens. Engineering strain is calculated as the length increase normalized over the initial sample length and expressed as a percentage length change.

The Young's modulus is 580 MPa, which is over 50% smaller than the 946 MPa measured in neat PTMSP. On the other hand, the elongation at break in the 42_{wt}% SILM is 42.0%, compared to 25.6% for the neat polymer. This translates to a more than 80% greater ductility for the SILM than for the neat support. These and other relevant SILM

mechanical properties are summarized in Table 4.2. The properties of the neat PTMSP compare favorably with the elastic modulus reported previously for as-cast PTMSP and PTMSP aged for 30 days [9].

Material	PTMSP	42_{wt}% [hmim][Tf$_2$N] in PTMSP SILM
Young's Modulus [MPa]	946 ($\pm$21)	578 ($\pm$33)
Yield Strength [MPa]	29.4 ($\pm$0.6)	19.1 ($\pm$1.9)
Yield Strain [%]	9.3 ($\pm$0.4)	7.0 ($\pm$1.0)
Toughness [MJ/m^3]	7.8 ($\pm$0.6)	10.4 ($\pm$2.1)
Elongation at Break [%]	25.6 ($\pm$2.6)	42.1 ($\pm$6.1)
Ductility [%]	16.3 ($\pm$2.2)	35.0 ($\pm$5.3)

Table 4.2:   Summary of mechanical properties for neat PTMSP and 42_{wt}% [hmim][Tf$_2$N] in PTMSP SILM obtained from at least 5 dogbone specimens.

4.6 REFERENCES

[1]   A. Ahosseini, A.M. Scurto, Viscosity of Imidazolium-Based Ionic Liquids at Elevated Pressures: Cation and Anion Effects, International Journal of Thermophysics, 29 (2008) 1222-1243.

[2]   S. Bazhenov, A. Malakhov, D. Bakhtin, V. Khotimskiy, G. Bondarenko, V. Volkov, M. Ramdin, T.J.H. Vlugt, A. Volkov, CO$_2$ stripping from ionic liquid at elevated pressures in gas-liquid membrane contactor, International Journal of Greenhouse Gas Control, 71 (2018) 293-302.

[3]   A. Ito, T. Yasuda, T. Yoshioka, A. Yoshida, X. Li, K. Hashimoto, K. Nagai, M. Shibayama, M. Watanabe, Sulfonated Polyimide/Ionic Liquid Composite Membranes for CO$_2$ Separation: Transport Properties in Relation to Their Nanostructures, Macromolecules, 51 (2018) 7112-7120.

[4]   D.R. Paul, Y.P. Yampol'skii, Gas Separation Membranes, CRC Press, Boca Raton, 2018, 116-118.

[5]   E.J. Kappert, M.J.T. Raaijmakers, K. Tempelman, F.P. Cuperus, W. Ogieglo, N.E. Benes, Swelling of 9 polymers commonly employed for solvent-resistant nanofiltration membranes: A comprehensive dataset, Journal of Membrane Science, 569 (2019) 177-199.

[6]   A. Chapeaux, L.D. Simoni, T.S. Ronan, M.A. Stadtherr, J.F. Brennecke, Extraction of alcohols from water with 1-hexyl-3-methylimidazolium bis(trifluoromethylsulfonyl)imide, Green Chemistry, 10 (2008) 1301-1306.

[7]   C. Casado-Coterillo, M. Del Mar López-Guerrero, Á. Irabien, Synthesis and Characterisation of ETS-10/Acetate-based Ionic Liquid/Chitosan Mixed Matrix Membranes for CO_2/N_2 Permeation, Membranes, 4 (2014) 287-301.

[8]   A.V. Volkov, D.S. Bakhtin, L.A. Kulikov, M.V. Terenina, G.S. Golubev, G.N. Bondarenko, S.A. Legkov, G.A. Shandryuk, V.V. Volkov, V.S. Khotimskiy, A.A. Belogorlov, A.L. Maksimov, E.A. Karakhanov, Stabilization of gas transport properties of PTMSP with porous aromatic framework: Effect of annealing, Journal of Membrane Science, 517 (2016) 80-90.

[9]   C.H. Lau, P.T. Nguyen, M.R. Hill, A.W. Thornton, K. Konstas, C.M. Doherty, R.J. Mulder, L. Bourgeois, A.C.Y. Liu, D.J. Sprouster, J.P. Sullivan, T.J. Bastow, A.J. Hill, D.L. Gin, R.D. Noble, Ending Aging in Super Glassy Polymer Membranes, Angewandte Chemie International Edition, 53 (2014) 5322-5326.

Chapter 5: Pure-gas permeation of polymer-IL SILMs and composites

5.1 PTMSP AND PTMSP-BASED SILMS

This section presents permeation data for (1) the neat polymer support as well as PTMSP-SILMs made with (2) [hmim][Tf₂N] at various IL loadings, (3) the imidazolium-based $[C_xmim][Tf_2N]$ and $[C_xmmim][Tf_2N]$ series at similar IL loadings, and (4) the ammonium based $[N_{xxxy}][Tf_2N]$ series at similar IL loadings. Unless otherwise specified, gases were measured in order of increasing condensability at 35 °C, all neat PTMSP measurements were carried out in a constant-pressure, variable-volume system, and all SILM measurements were done in a constant-volume, variable-pressure system.

5.1.1: PTMSP

Figure 5.1 shows the pure-gas permeabilities at 35 °C as a function of pressure for neat PTMSP. For the natural gas liquids (C₂₊), it is especially evident that permeabilities decrease asymptotically with increasing transmembrane pressure. The neat PTMSP permeation data is shown in tabular form in Table E.1 (see Appendix E).
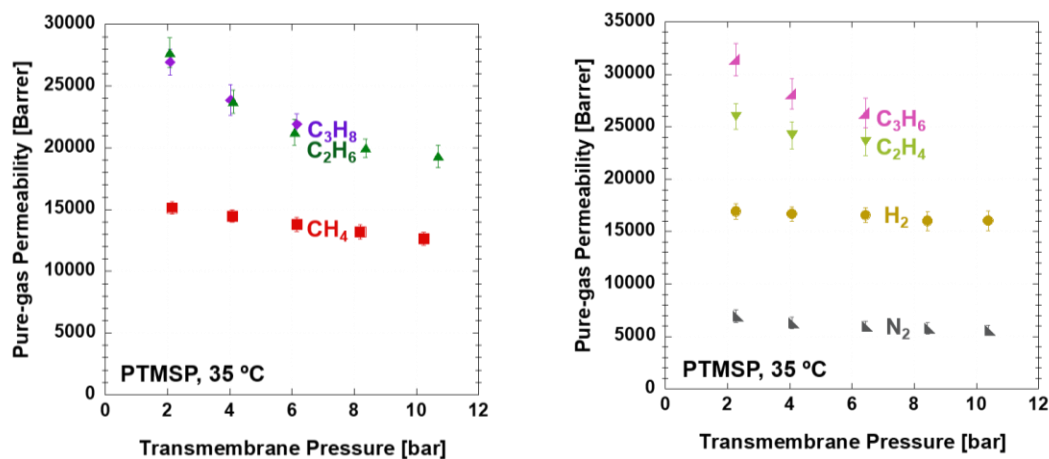
Figure 5.1:   Pure-gas permeability in neat PTMSP cast from cyclohexane at 35 °C

All studied gas permeabilities at 35 °C in neat PTMSP can be fit with the dual-mode transport model, as discussed in section 7.2 [1]. Nathalie Debelle assisted in measuring some of the N_2 and CH_4 permeabilities in neat PTMSP and [hmim][Tf$_2$N] SILMs.

5.1.2: [hmim][Tf$_2$N] in PTMSP SILMs

As shown in Figure 5.2, in contrast to the dual-mode behavior observed in the neat polymer, the permeability pressure dependence of the C_{2+} hydrocarbons in the [hmim][Tf$_2$N] in PTMSP SILMs is not only inverted but also much more pronounced. For instance, the propane permeability in a 42_{wt}% SILM at an applied pressure of 7 atmospheres is two orders of magnitude greater than that at a transmembrane pressure of 1 atmosphere, as shown in Figure 5.2. This dramatic increase is attributed to SILM plasticization by the C_{2+}. Section 7.2 discusses coupling the SILM permeability data presented here with solubility data to infer pure-gas effective concentration-averaged diffusivities and the penetrant-specific plasticization constant, β_A, for the C_{2+} using Equation 2.19.

As a testament to defect-free samples, the hydrogen permeability is not pressure dependent for either the neat polymer or the 42_{wt}% SILM. Figure 5.2 also shows that the gas permeabilities for all species in the 42_{wt}% SILM are nearly three orders of magnitude smaller than those in the neat polymer. Similar observations were made for SILMs of different IL compositions. Permeation data for SILMs ranging from 20_{wt}% to 64_{wt}% [hmim][Tf$_2$N] loading are presented in Figure E.1 and Tables E.1 and E.2 (see Appendix E). Dr. Jaesung Park aided in the data collection for the 20_{wt}% and 64_{wt}% SILMs. A sample constant-volume, variable-pressure permeation test protocol refined by Maximilian Strauss is outlined in Table E.3.
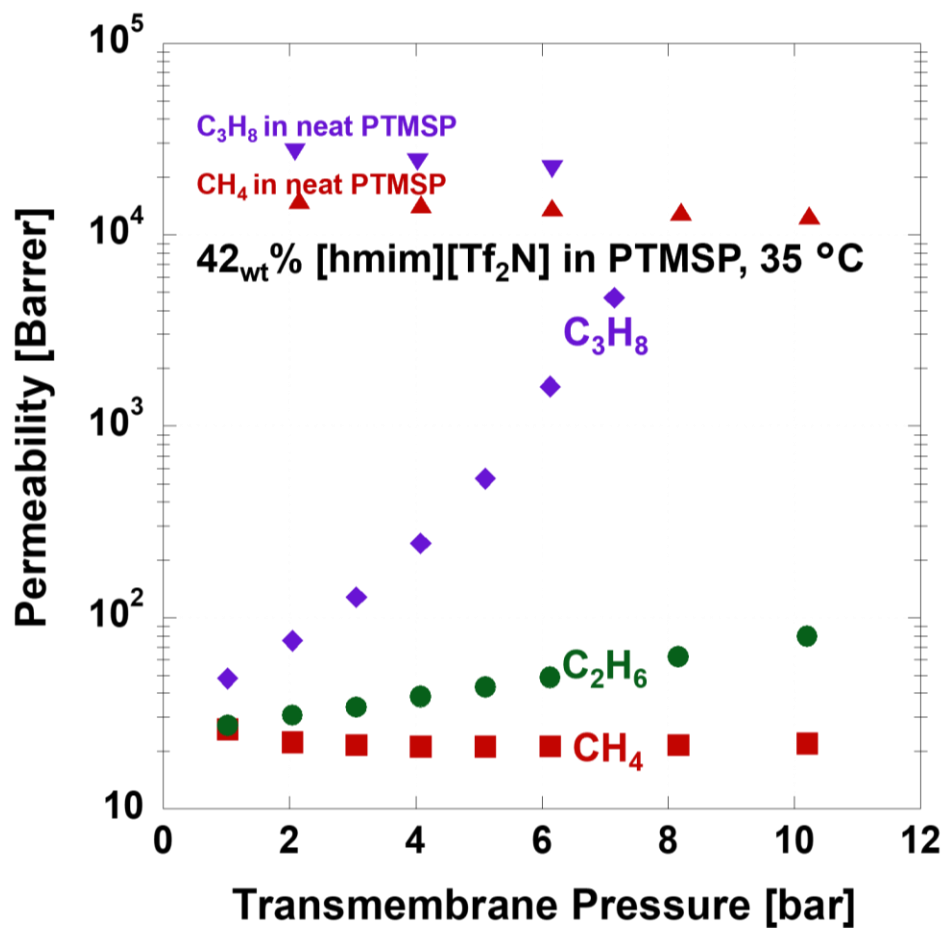
Figure 5.2: Pure-gas permeability in $42_{wt}\%$ [hmim][Tf$_2$N] in PTMSP at 35 °C and comparison with the neat PTMSP permeation results.

Notably, propane permeability (above 2 bar of transmembrane pressure) increases with increasing IL loading, and as a result the pure-gas C_3H_8/CH_4 selectivity increases with increasing IL content. Figure 5.3 shows the pure-gas C_3H_8/CH_4 selectivity of the hydrocarbon gas species as a function of IL loading.
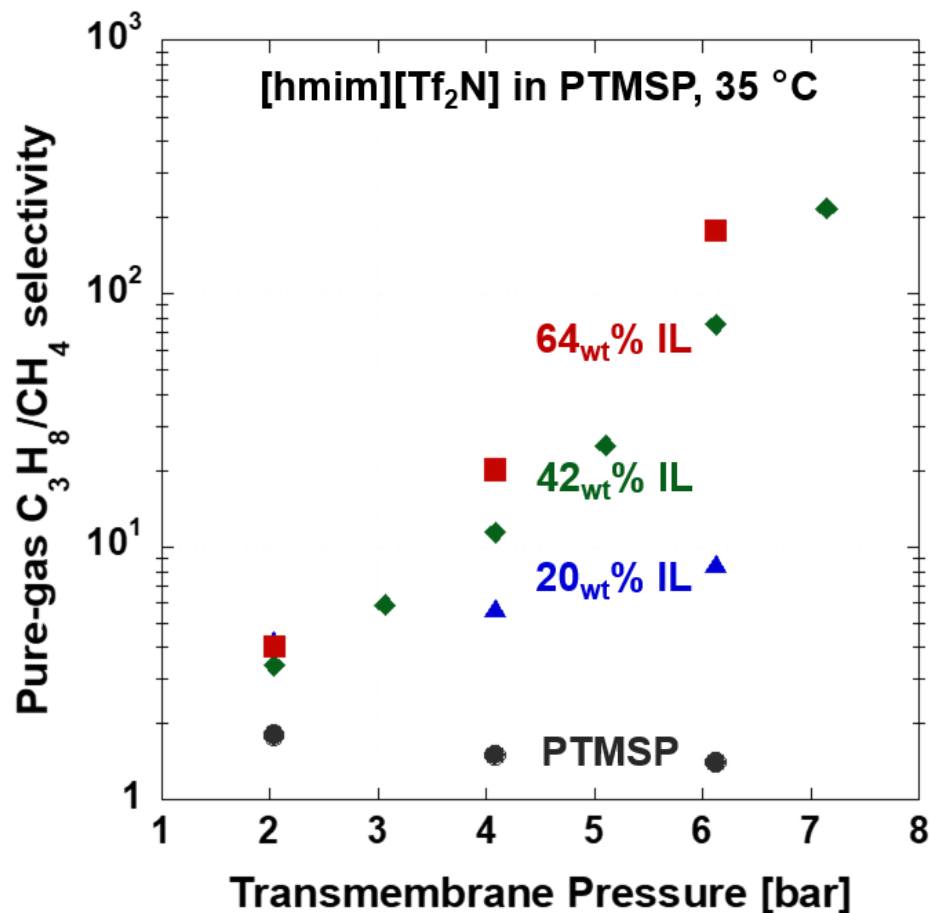
Figure 5.3: Pure-gas C_3H_8/CH_4 selectivity in 20, 42, and 64_{wt}% [hmim][Tf_2N] in PTMSP SILMs at 35 °C at a range of transmembrane pressures.
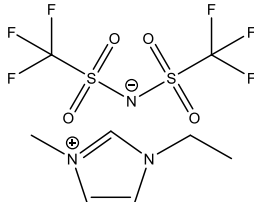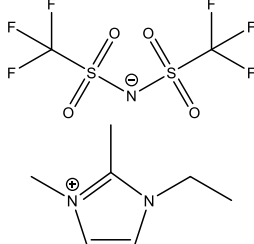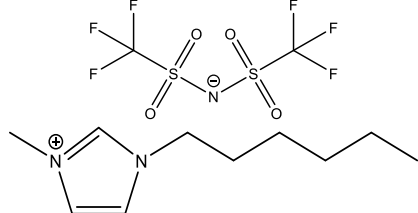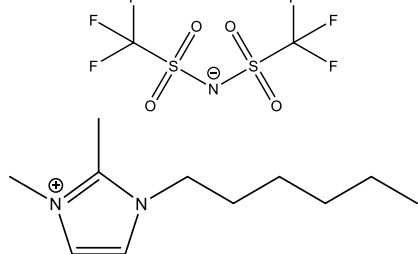
It was observed that the C_3H_8 plasticization constant, $\beta_{C_3H_8}$, was larger for SILMs of higher IL loading. This is further discussed in section 7.2.
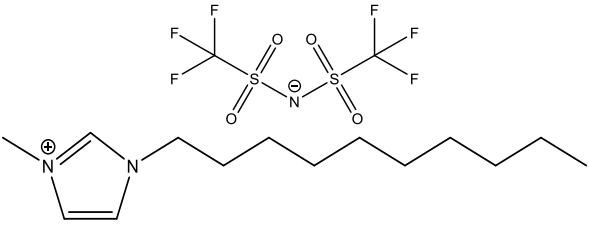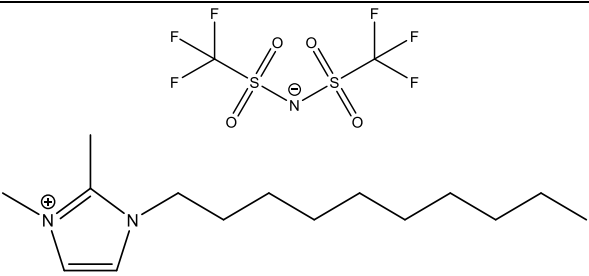
5.1.2: [$C_x$mim][Tf_2N] and [$C_x$mmim][Tf_2N] in PTMSP SILMs

The two series of imidazolium-based cation ILs listed in Table 5.1 were selected to better understand the effects of alkyl chain length and the presence of a secondary

alkyl group on properties such as viscosity, molar volume, and, ultimately, gas permeability in SILMs. The six ionic liquids were synthesized and purified by Dr. Oscar Morales (see Chapter 3.1).

Table 5.1: Molecular structure, molar mass, and molar volume of $[C_x mim][Tf_2N]$ and $[C_x mmim][Tf_2N]$ ionic liquids, where x =2, 6 or 10. The molar volumes were calculated by dividing the molar mass over the densities in Table 5.2.

IL	Structure	Molar mass [g/mol]	Molar volume (at 35 °C) [cm³/mol]
[emim][Tf₂N] or [C₂mim][Tf₂N]		391.3	259
[emmim][Tf₂N] or [C₂mmim][Tf₂N]		405.3	273
[hmim][Tf₂N] or [C₆mim][Tf₂N]		447.4	327
[hmmim][Tf₂N] or [C₆mmim][Tf₂N]		461.4	341

IL	Structure		
[dmim][Tf$_2$N] or [C$_{10}$mim][Tf$_2$N]		503.5	397
[dmmim][Tf$_2$N] or [C$_{10}$mmim][Tf$_2$N]		517.6	-

Maximilian Strauss characterized the viscosities and densities of the [C$_x$mim][Tf$_2$N] and the [C$_x$mmim][Tf$_2$N] IL series, as well as the H$_2$, CH$_4$, and C$_3$H$_8$ permeabilities at similar loadings using a constant-volume, variable pressure system in PTMSP SILMs made with these ILs. The relevant density and viscosity data is summarized in Table 5.2.

Table 5.2: Density and viscosity data of [C$_x$mim][Tf$_2$N] and [C$_x$mmim][Tf$_2$N] ionic liquids were measured with an Anton Paar DMA 4500 and an SVM 3001.

IL	Density at 35 °C [g/cm^3]	Viscosity at 25 °C [mPa s]	Viscosity at 35 °C [mPa s]	Viscosity at 50 °C [mPa s]
[emim][Tf$_2$N]	1.513 ±0.005	33.18 ±0.03	23.93 ±0.19	15.6 ±0.6
[emmim][Tf$_2$N]	1.483 ±0.006	66.11 ±0.02	44.83 ±0.10	27.06 ±0.57
[hmim][Tf$_2$N]	1.368 ±0.005	70.65 ±0.03	46.02 ±0.27	24.9 ±1.5
[hmmim][Tf$_2$N]	1.352 ±0.007	131.2 ±0.25	78.04 ±0.40	-
[dmim][Tf$_2$N]	1.269 ±0.004	89.07 ±0.29	56.96 ±0.12	36.2 ±0.57
[dmmim][Tf$_2$N]	-	206.2 ±0.54	117.2 ±0.47	-

Morgan and Scovazzo developed a simplified gas diffusivity correlation of the form of Equation 2.20 specific to imidazolium-cation ionic liquids at 30 °C supported in

1 μm nominal pore diameter glass fiber filters and a 0.5 μm nominal pore diameter Zefluor (hydrophobic PTFE) backing [2]:

$$D_{A,0} = A \frac{V_{IL}^a}{\mu_{IL}^b V_A^c} \tag{5.1}$$

where $A = 0.00266$ cm^2/s, $a = 0$, $b = 0.66 \pm 0.03$, and $c = 1.04 \pm 0.08$.

Although both viscosity and molar volume of the ILs are increased by adding more carbons to the primary alkyl chain or adding a secondary methyl group, we hypothesize (based on Equation 5.1 and the molar volumes and viscosities from Table 5.1 and Table 5.2) that the permeabilities for SILMs of similar IL loadings will decrease with increasing alkyl chain length or addition of a secondary methyl group to the cation. In other words, the decrease in $D_{A,0}$ due to the increase in viscosity is expected to dominate over the increase in $D_{A,0}$ due to the larger molar volume that results from increasing the number of alkyl carbons.

Three observations can be made from the gas permeability and C_3H_8/CH_4 selectivity versus transmembrane pressure plotted in Figure 5.4. First, it illustrates that, indeed, the H_2, CH_4, and C_3H_8 permeabilities can be arranged in decreasing order with increasing alkyl chain length in the SILM cations. Second, comparing [hmim][Tf$_2$N] and [hmmim][Tf$_2$N] containing SILMs reveals that the H_2 and C_3H_8 permeabilities are smaller for SILMs made with the IL containing a secondary methyl group. Curiously, this is true only for CH_4 permeability at transmembrane pressures of 3 bar or lower, as the plasticization constant for CH_4 in the [hmmim]-based SILM appears to be much larger than that for the [hmim]-based SILM. Third, the inflection points on the semi-log C_3H_8 permeability curve occur at lower transmembrane pressures for SILMs made from denser ILs (at similar IL$_{wt}$% loadings). Note that C_3H_8 permeability approaches a plateau at

around 8000 Barrer for the [emim][Tf$_2$N] and [emmim][Tf$_2$N]-containing SILMs. The data in Figure 5.4 is shown in tabular form in Table E.4 (see Appendix E).
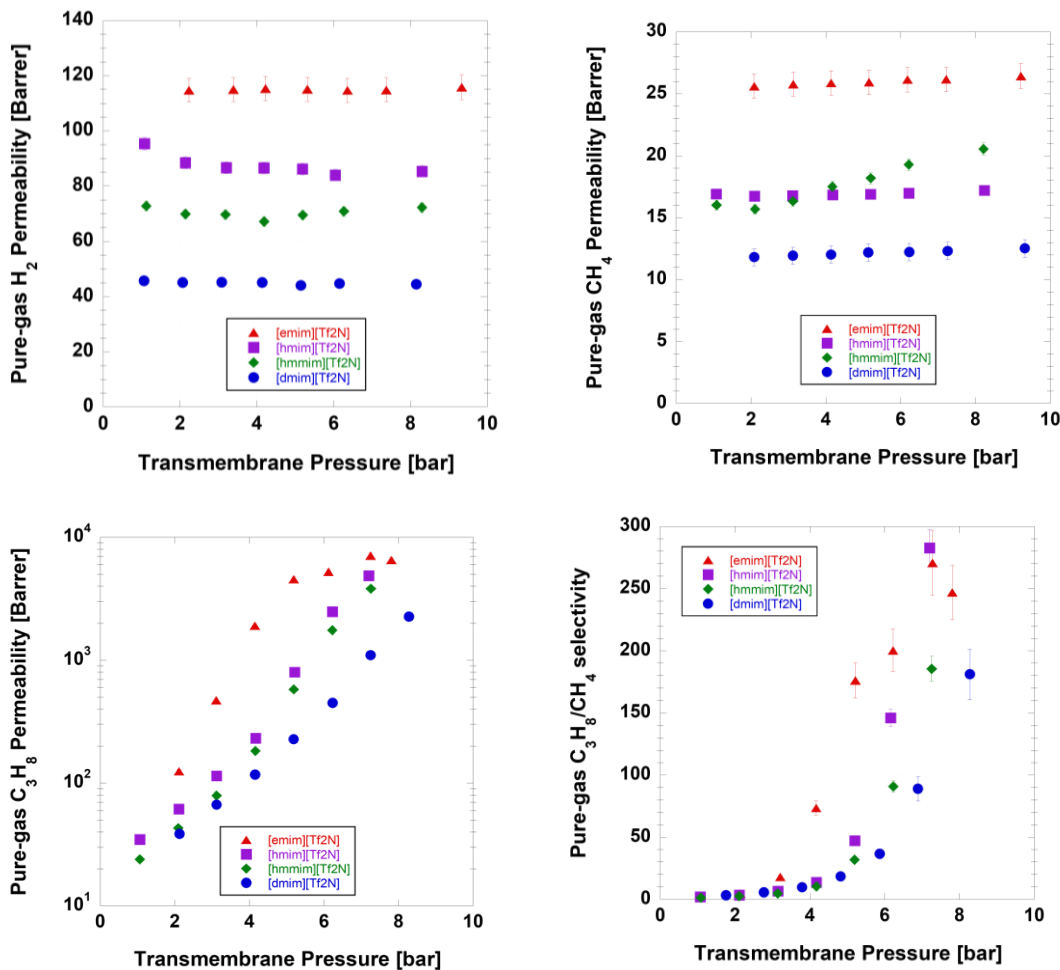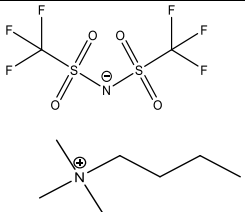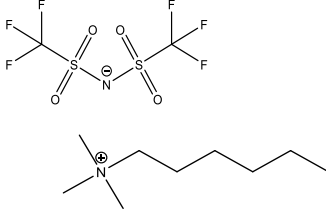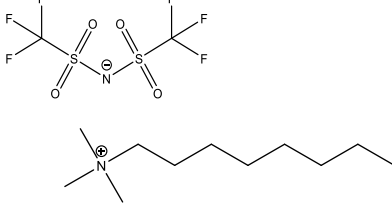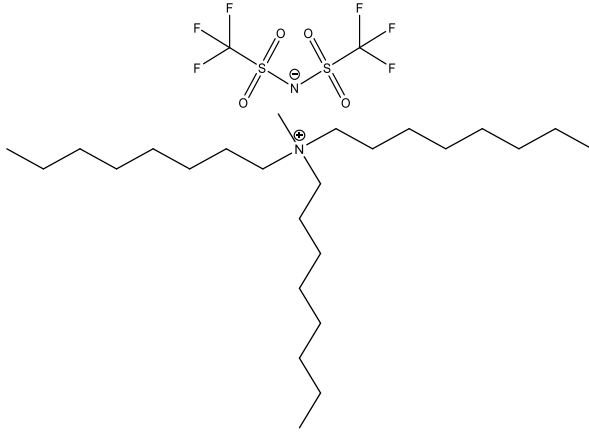
Figure 5.4:   Pure-gas permeability measured at 35 °C in selected [C$_x$mim][Tf$_2$N] and [C$_x$mmim][Tf$_2$N] in PTMSP SILMs of similar IL mass loadings of 42$_{wt}$%. All data were collected in a constant-volume, variable pressure system by Maximilian Strauss following the protocol in Table E.2.

5.1.3: [N$_{xxxy}$][Tf$_2$N] in PTMSP SILMs

An analogous study to that presented in section 5.1.2 was done with the ammonium-based ILs shown in Table 5.3 with the aid of Sarah Sam and Mikaela Rey.

Table 5.3: IL structure, molar volume, density, and viscosity data of [N$_{xxxy}$][Tf$_2$N] and ionic liquids. The densities and viscosities were obtained from [3-7].

IL	Structure	Density (25 °C)	Molar volume (25 °C) [cm^3/mol]	Viscosity (25 °C) [mPa s]
[N$_{1114}$][Tf$_2$N]		1.393 ±0.001 [3]	284	105.4 ±1.5 [3]
[N$_{1116}$][Tf$_2$N]		1.311 ±0.026 [4]	324	153 ±17 [5]
[N$_{1118}$][Tf$_2$N]		1.260 ±0.01 [5,6]	359	181 ±20 [5]
[N$_{8881}$][Tf$_2$N]		1.101 ±0.001 [4]	589	601 ±48 [7]

For similar IL loading SILMs, the decreasing permeability trend with increasing primary alkyl chain length was also observed in the ammonium-ILs series. The $[N_{1114}]$, $[N_{1116}]$, and $[N_{1118}]$-based SILMs are also prone to plasticization by C_3H_6 and C_3H_8.
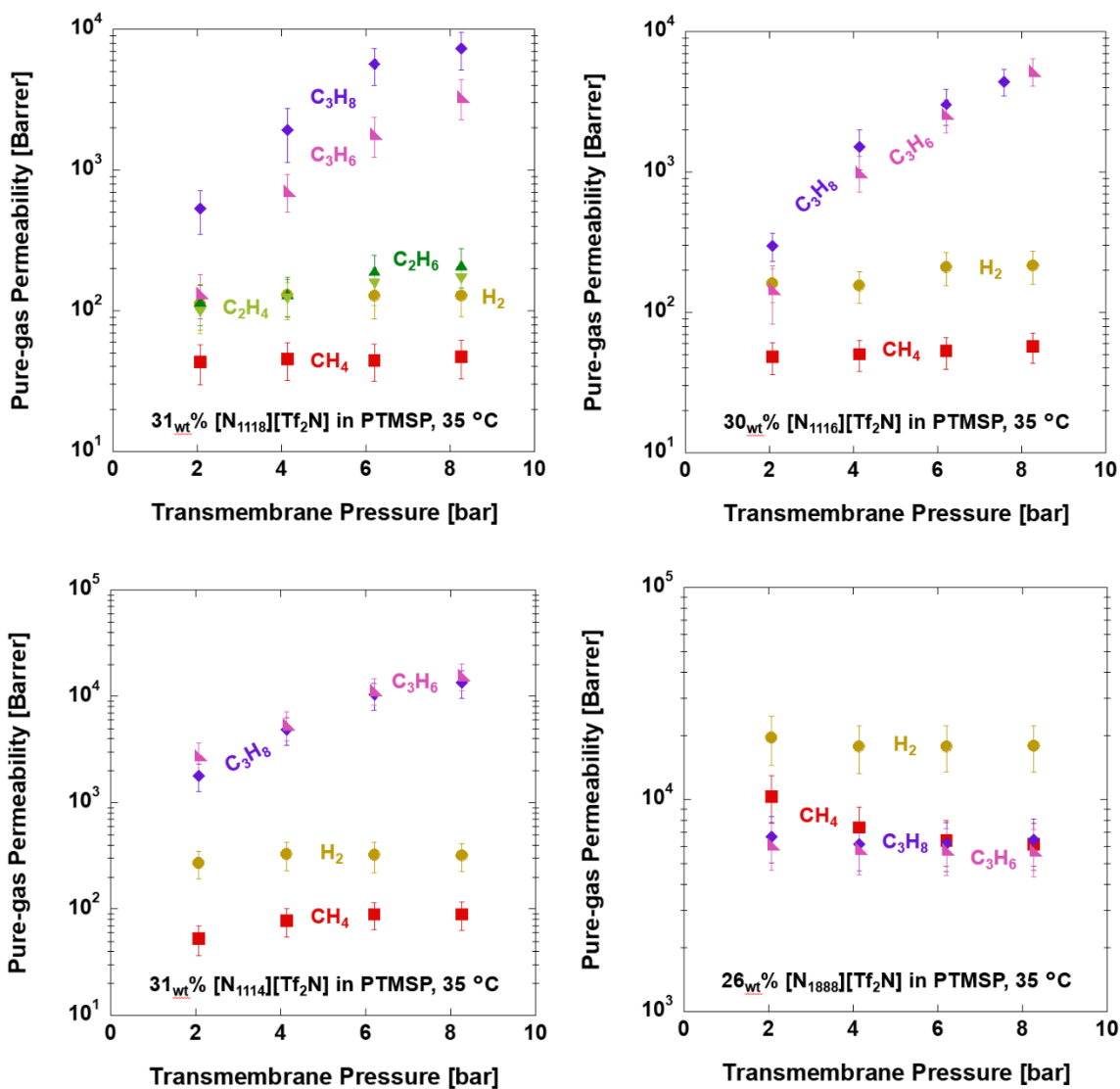
Figure 5.5:   Pure-gas permeability in selected $[N_{xxxy}][Tf_2N]$-PTMSP SILMs of similar IL loadings at 35 °C.

However, this was not the case in the [N_{1888}]-containing SILM. Curiously, the C_3H_6 and C_3H_8 permeabilities in this sample were constant with increasing transmembrane pressure and were lower than the H_2 permeabilities. In fact, the H_2 permeabilities in this sample were higher than in neat PTMSP.

Given that [N_{1888}][Tf_2N] is the most hydrophobic IL in the series, it is hypothesized that the IL can plasticize the PTMSP matrix without the presence of a condensable gas. All of the data is shown in tabular form in Table E.5 (see Appendix E).

5.2 PMP AND PMP SILMS

Figure 5.6 presents H_2, CH_4, C_3H_6, and C_3H_8 permeation data for neat poly(4-methyl-2-pentyne), or PMP, and a 27_{wt}% [hmim][Tf_2N] in PMP SILM. The neat PMP permeabilities were consistent with previously reported data [9-10]. Much like in the case of the PTMSP study, all gas permeabilities (absent plasticization) were over two orders of
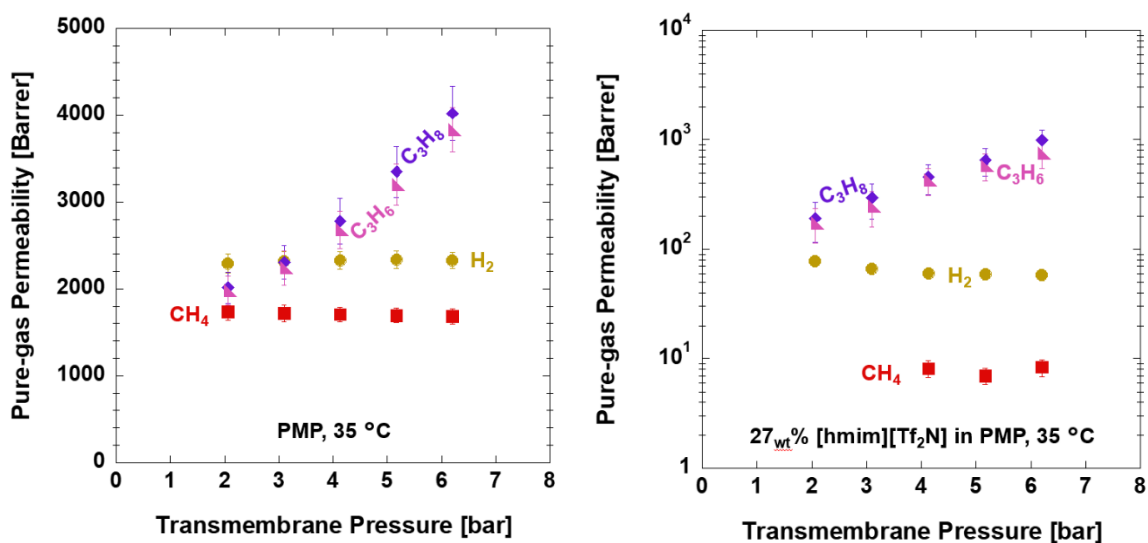
Figure 5.6:   Pure-gas permeability in neat PMP (cast in CCl_4) and a 26.6_{wt}% [hmim][Tf_2N] in PMP SILM at 35 °C was measured with a constant-pressure, variable-volume system, with help from Maximilian Strauss.

magnitude lower for the SILM than for neat PMP, and the NGL vapors plasticize the SILM but not the neat PMP support at 35 °C. Curiously, the pure-gas H_2/CH_4 selectivity is roughly twice that observed in the PTMSP-based SILMs. The data from Figure 5.6 is shown in tabular form in Table E.6 (see Appendix E).

5.3 PDMS AND PDMS-IL COMPOSITES

PDMS is a dense, rubbery material that can be blended with compatible ILs to make composite (rather than supported) membranes. In this section, we compare gas permeation data for neat PDMS and two PDMS-IL composite membranes (each 20_{wt}% IL loading). In addition to a dialkylimidazolium bis(trifluoromethylsulfonyl)imide IL, we investigated a tetraalkylphosphonium bis(2,4,4-trimethylpentyl)phosphinate IL. The structure and some properties of that IL, [P_{1118}][Phos], are shown in Table 5.4.

Table 5.4:   Structure, molar volume, density, and viscosity of [P_{1118}][Phos] [10].
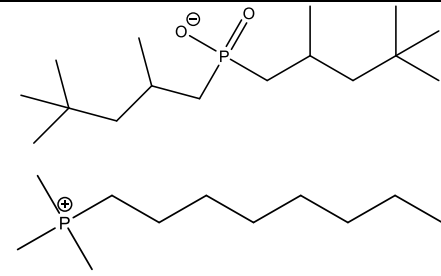
IL	Structure	Density (25 °C)	Molar volume (25 °C) [cm^3/ mol]	Viscosity (25 °C) [mPa s]
[P_{1118}][Phos]		0.8906 ±0.009 [10]	538	804 ±16 [10]

Figure 5.7 shows several gas permeabilities as well as C_3H_8/CH_4 selectivity versus transmembrane pressure for neat PDMS, 20_{wt}% [N_{1118}][Tf$_2$N] in PDMS and 20_{wt}% [P_{1118}][Phos] in PDMS. The data is shown in tabular form in Table E.7 (see Appendix E).

It should be noted that the [N$_{1118}$][Tf$_2$N] made a poor dispersion with PDMS such that macroscopic IL droplets aggregated throughout the crosslinked PDMS phase.
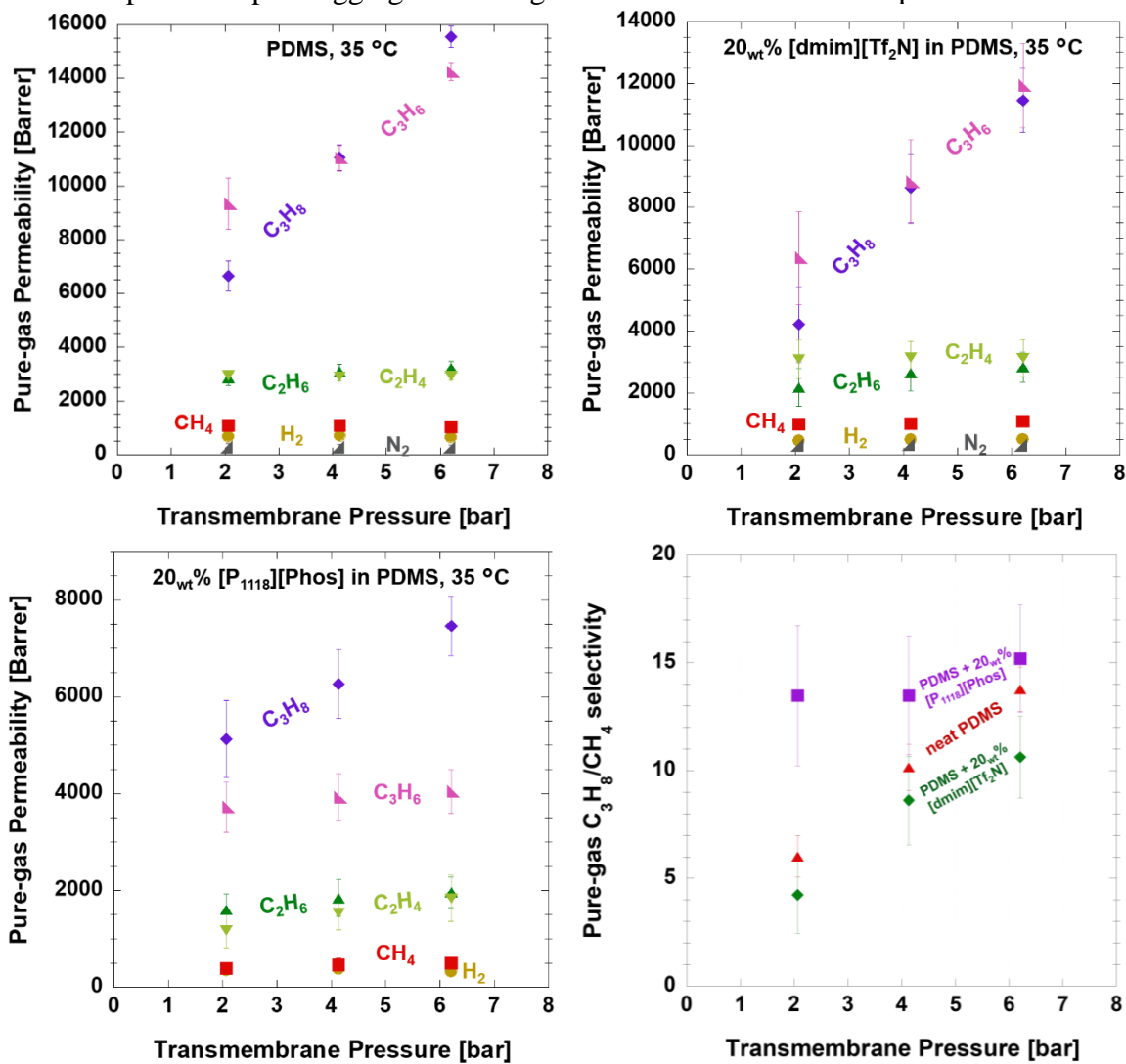
Figure 5.7: Pure-gas permeability in neat PDMS and selected 20$_{wt}$% IL-PDMS composites at 35 °C. The error bars are the standard deviations obtained from 3 samples of each type in a constant-pressure, variable-volume system.

Appropriately, the gas permeabilities in the 20$_{wt}$% [N$_{1118}$][Tf$_2$N]-PDMS membranes are only modestly smaller than those collected from neat PDMS, although with more sample-to-sample variability, and the pure-gas C$_3$H$_8$/CH$_4$ selectivity was

somewhat smaller. In contrast, the 20_{wt}% [P_{1118}][Phos]-PDMS samples were visibly homogeneous at the time of testing, although the samples turned slightly orange after annealing at 160 °C. Gas permeabilities in the 20_{wt}% [P_{1118}][Phos] samples are noticeably smaller, and their pure-gas C_3H_8/CH_4 selectivities are larger than those in neat PDMS.

5.4 Aging of neat PTMSP and a 10_{WT}% PTMSP SILM

Lau et al. observed that mixed-matrix membranes made with porous aromatic framework (PAF) filler particles and PTMSP exhibited a smaller permeability reduction over time due to physical aging than did neat PTMSP [11]. It was hypothesized that the presence of an IL in the PTMSP accessible free volume might improve its resistance to physical aging. Given that some minor plasticization was observed in CH_4 permeation in SILMs with IL loadings greater than 20_{wt}%, a 10_{wt}% [emim][Tf_2N] SILM was selected to minimize the contribution of plasticization effects during the aging study. CH_4 at 6 bar of upstream pressure was continuously permeated for 150 hours through a neat PTMSP sample and a 10_{wt}% [emim][Tf_2N] sample, both of which were last conditioned by methanol 72 hours prior to starting the permeation experiments. In order to prevent backflow of pump oil vapor, the cold trap leading the downstream to the vacuum pump was in constant contact with liquid N_2 for the duration of the 150 hours. Figure 5.8 shows that after 150 hours, the CH_4 permeabilities in both samples decreased to roughly 10% of the values measured at time zero, suggesting that the presence of [emim][Tf_2N] in PTMSP does not limit the permeability decrease due to physical ageing. The aging study data is shown in tabular form in Table E.8 (see Appendix E).
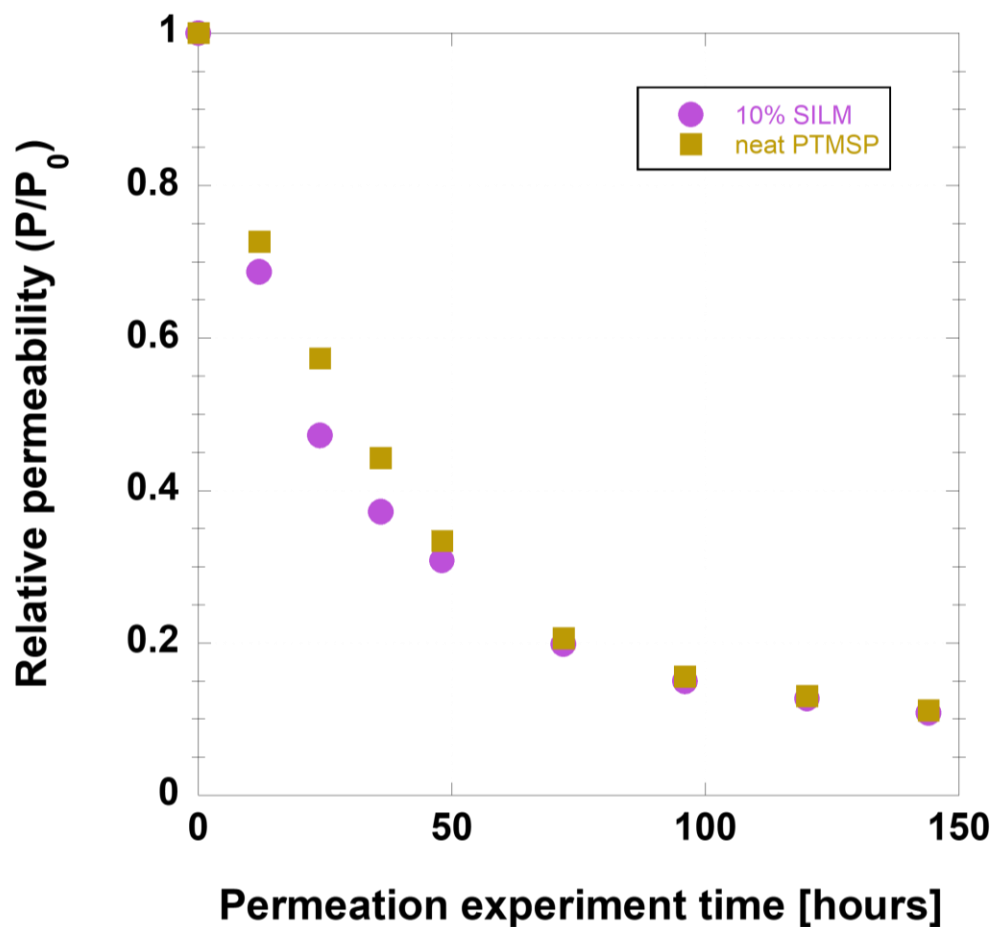
Figure 5.8: 150-hour aging study of neat PTMSP and a $10_{wt}\%$ [emim][Tf_2N] in PTMSP SILM using a constant-volume, variable-pressure permeation system at 35 ^{0}C and 6 bar of upstream (and transmembrane) pressure. The CH_4 permeability at t=0 was 12100 Barrer for the neat PTMSP sample and 3570 Barrer for the $10_{wt}\%$ [emim][Tf_2N] in PTMSP SILM.

5.5 REFERENCES

[1]   T.C. Merkel, V.I. Bondar, K. Nagai, B.D. Freeman, Sorption and Transport of Hydrocarbon and Perfluorocarbon Gases in Poly(1-trimethylsilyl-1-propyne), Journal of Polymer Science Part B: Polymer Physics 38 (2000) 415-434.

[2]   D. Morgan, L. Ferguson, P. Scovazzo, Diffusivities of Gases in Room-Temperature Ionic Liquids: Data and Correlations Obtained Using a Lag-Time Technique, Industrial & Engineering Chemistry Research, 44 (2005) 4815-4823.

[3]   M. Dakkach, F.M. Gaciño, S.K. Mylona, M.J.P. Comuñas, M.J. Assael, J. Fernández, High pressure densities of two nanostructured liquids based on the bis(trifluoromethylsulfonyl)imide anion from (278 to 398) K and up to 120 MPa, The Journal of Chemical Thermodynamics, 118 (2018) 67-76.

[4]   P. Kilaru, G.A. Baker, P. Scovazzo, Density and Surface Tension Measurements of Imidazolium-, Quaternary Phosphonium-, and Ammonium-Based Room-Temperature Ionic Liquids: Data and Correlations, Journal of Chemical & Engineering Data, 52 (2007) 2306-2314.

[5]   J. Sun, M. Forsyth, D.R. MacFarlane, Room-Temperature Molten Salts Based on the Quaternary Ammonium Ion, The Journal of Physical Chemistry B, 102 (1998) 8858-8864.

[6]   M.L.P. Le, N.A. Tran, H.P.K. Ngo, T.G. Nguyen, V.M. Tran, Liquid Electrolytes Based on Ionic Liquids for Lithium-Ion Batteries, Journal of Solution Chemistry, 44 (2015) 2332-2343.

[7]   B. Yoo, W. Afzal, J.M. Prausnitz, Effect of Water on the Densities and Viscosities of Some Ionic Liquids Containing a Phosphonium Cation, Zeitschrift für Physikalische Chemie, 227 (2013) 157-166.

[8]   S. Markova, V. Zhmakin, T. Gries, V. Teplyakov, Combination of the Experimental and Theoretical Approaches for the Estimation of the C_1–C_4 Alkane Permeability Parameters in Poly (4-Methyl-2-Pentyne) and Poly (4-Methyl-1-Pentene), Applied Sciences, 10 (2020) 1735.

[9]   L.G. Toy, K. Nagai, B.D. Freeman, I. Pinnau, Z. He, T. Masuda, M. Teraguchi, Y.P. Yampolskii, Pure-Gas and Vapor Permeation and Sorption Properties of

Poly[1-phenyl-2-[p-(trimethylsilyl)phenyl]acetylene] (PTMSDPA), Macromolecules, 33 (2000) 2516-2524.

[10]   X. Liu, W. Afzal, J.M. Prausnitz, Unusual trend of viscosities and densities for four ionic liquids containing a tetraalkyl phosphonium cation and the anion bis(2,4,4-trimethylpentyl) phosphinate, The Journal of Chemical Thermodynamics, 70 (2014) 122-126.

[11]   C.H. Lau, P.T. Nguyen, M.R. Hill, A.W. Thornton, K. Konstas, C.M. Doherty, R.J. Mulder, L. Bourgeois, A.C.Y. Liu, D.J. Sprouster, J.P. Sullivan, T.J. Bastow, A.J. Hill, D.L. Gin, R.D. Noble, Ending Aging in Super Glassy Polymer Membranes, Angewandte Chemie International Edition, 53 (2014) 5322-5326.

Chapter 6: Mixed-gas permeation in PTMSP and PTMSP-based SILMs

6.1 VALIDATION WITH 30%-70% PEGDA-PEGMEA AND CO_2-C_2H_6 BINARY MIXTURE

The constant-pressure, mixed-gas sweep permeation system was built and validated in collaboration with Maximilian Strauss, Dr. Kristofer Gleason and Dr. Tangqiumei Song. The system was validated with a standard sample of fully crosslinked 30-70% PEGDA-PEGMEA, which was prepared in our laboratory following the procedure detailed by Ribeiro et al. [1]. Binary mixtures of CO_2-C_2H_6 of the same compositions as in a prior study were prepared *in situ* through mass flow control [2]. The mixed-gas permeabilities of CO_2 and C_2H_6 were calculated using Equation 2.21 and plotted vs fugacity, as shown in Figure 6.1.
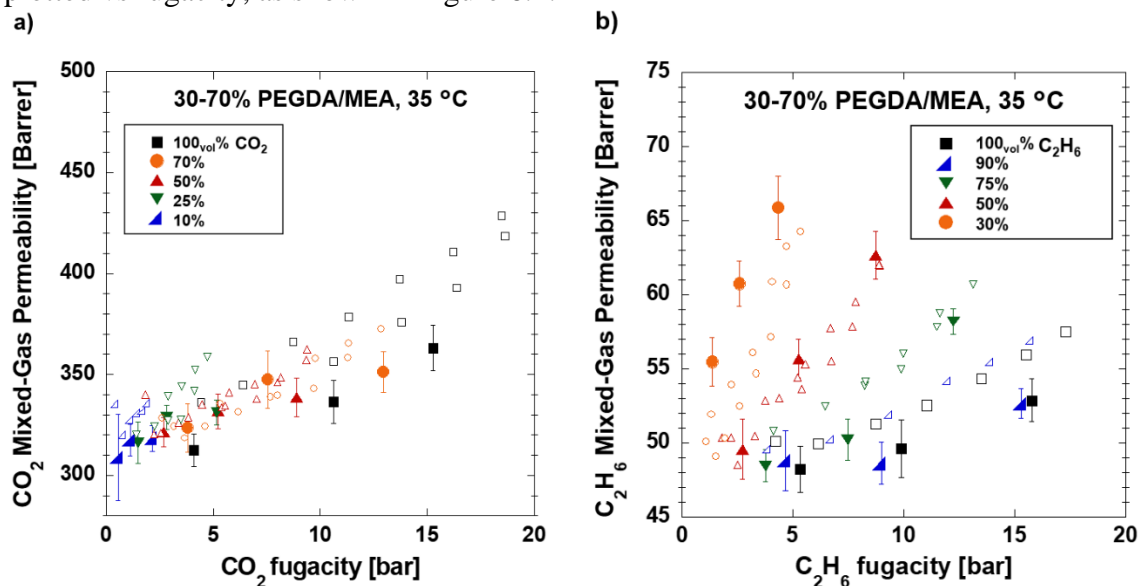
Figure 6.1:   Mixed-gas a) CO_2 and b) C_2H_6 permeabilities versus fugacity of binary mixtures in 30-70% PEGDA/MEA copolymer at 35 °C. The unfilled datapoints were reproduced from the literature for reference [2].

Mixture fugacities were computed using the density form of the virial equation of state truncated to the 3rd term as was done by Ribeiro *et al.* [1]. Calculations are described

in detail in Appendix C. Relevant virial coefficients have been tabulated by Dymond *et al.* for various species, including CH_4, C_2H_6, CO_2 and C_3H_8 and some of their cross coefficients [3]. The mixed-gas data from Figure 6.1 are tabulated in Table F.1 (see Appendix F).

6.2 MIXED-GAS PERMEATION IN PTMSP

To more fairly compare permeabilities from pure-gas and mixed-gas experiments, we expressed the pure-gas permeabilities in terms of fugacity rather than pressure (*i.e.,* using Equation 2.21 instead of Equation 2.1). The unfilled symbols in Figure 6.2a are the partial pressure-derived permeabilities plotted vs pressure (previously shown in Figure 5.1), while the filled symbols are the fugacity-derived permeabilities plotted vs paraffin fugacity. Although accounting for mixture fugacities makes a modest difference for CH_4, it makes a significant difference for C_2H_6 and C_3H_8 permeability calculations at the pressures investigated.

Figure 6.2b shows the mixed-gas permeabilities for 3 compositions of CH_4-C_2H_6 and CH_4-C_3H_8 mixtures (in one of the neat PTMSP standards previously tested in the constant-volume, variable-pressure permeation system) at a total pressure of 6 bar plotted vs the fugacity of the more condensable species in the mixture (C_{2+}), as calculated from the truncated virial EOS. Measurements for each binary mixture system were made from lower to higher composition of C_{2+}. The CH_4-C_2H_6 mixture was tested before the CH_4-C_3H_8 experiments were performed.

Permeabilities at 35 °C follow the dual-mode behavior in both cases. Notably, the CH_4 permeabilities in the CH_4-C_3H_8 mixtures are smaller than in the CH_4-C_2H_6 mixtures, and both are smaller than CH_4 permeabilities in the pure-gas experiments. Competitive sorption effects, albeit not as dramatic as in the CH_4-C_4H_{10} case, are likely the primary

reason for this difference between pure and mixed-gas permeability values [4]. This hypothesis could be verified with binary and ternary mixed-gas sorption analysis. Interestingly, mixed-gas C_2H_6-CH_4 and C_3H_8-CH_4 selectivities are significantly larger than those predicted from the pure-gas data, as shown in Figure 6.5. The raw mixed-gas data for neat PTMSP are tabulated in Table F.2 (see Appendix F).
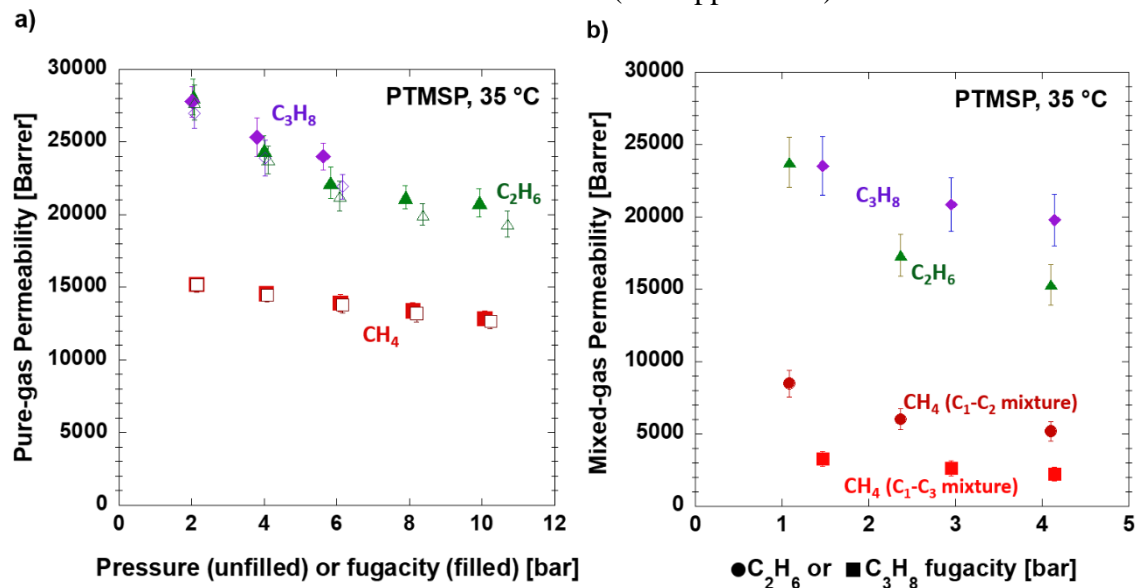
Figure 6.2:   Comparison of a) pure and b) mixed-gas CH_4, C_2H_6 and C_3H_8 permeabilities at 35 °C in neat PTMSP cast from cyclohexane and conditioned with methanol at least 72 hours prior to the permeation experiment. Note that the unfilled datapoints were shown previously in Figure 5.1 (and Table E.1).

6.3 MIXED-GAS PERMEATION IN 42_{WT}% [HMIM][TF$_2$N] IN PTMSP SILM

In addition to the pure-gas feeds, three different compositions of a CH_4-C_2H_6 binary mixture were tested at three total pressures, 4.1, 8.3, and 16.5 bar, in order of increasing C_2H_6 composition. Each data point in Figures 6.3a has a matching point in Figure 6.3b. For instance, the 10% C_2H_6 at 1.8 bar in Figure 6.3a corresponds to the same GC injection as the 90% CH_4 at 15.4 bar point in Figure 6.3b.

Much like in the case of CO_2 in Figure 6.1a, the C_2H_6 permeability is solely a function of C_2H_6 fugacity. The same is observed for the CH_4 permeability, which is especially evident when it is plotted versus C_2H_6 fugacity, as in Figure F.1 (see Appendix F). The CH_4-C_2H_6 mixed-gas $42_{wt}\%$ SILM data are tabulated in Table F.3 (see Appendix F).
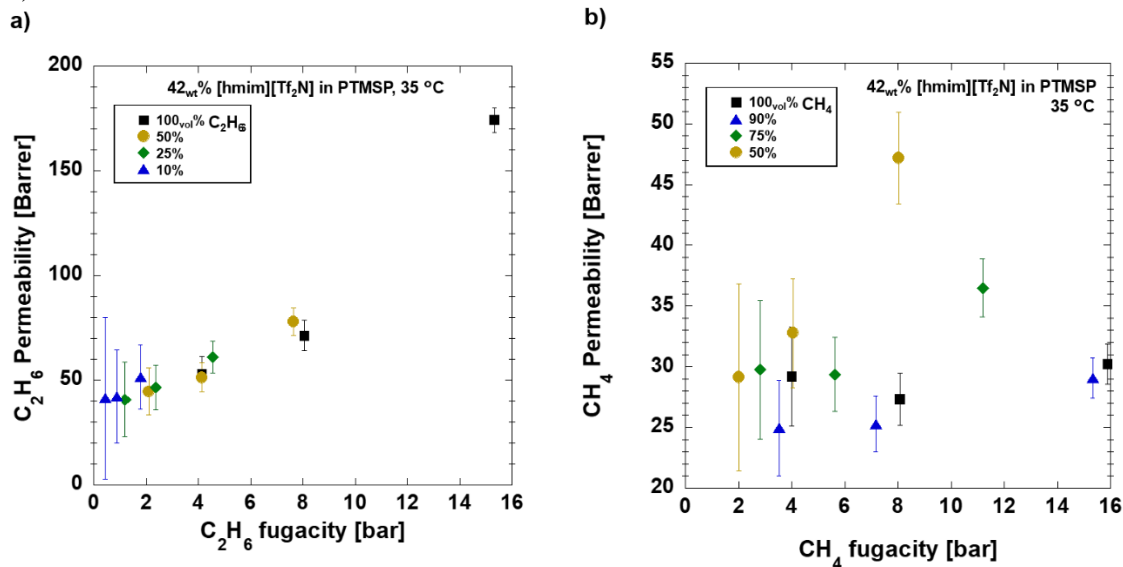
Figure 6.3:   Mixed-gas a) C_2H_6 permeability vs C_2H_6 fugacity and b) CH_4 permeability vs CH_4 fugacity in $42_{wt}\%$ [hmim][Tf_2N] in PTMSP SILM measured at 35 °C.

A similar study was done for pure CH_4, pure C_3H_8 and several CH_4-C_3H_8 binary mixtures at 4.1 and 7.2 bar of total gas pressure. Because a 1 bar pressure difference is needed across the mass flow controllers and across the gas mixing zone and the upstream side of the permeation cell, it was difficult to measure mixed-gas permeabilities at higher pressures than 7.3 bar, given that the vapor pressure of propane is only 9.3 bar at room temperature (23 °C) [5].

The mixed-gas C_3H_8 permeabilities are plotted against C_3H_8 fugacity in Figure 6.4a. The mixed-gas CH_4 permeabilities are plotted versus both C_3H_8 fugacity in Figure

6.4a and CH_4 fugacity in Figure 6.4b. Unlike in the pure-gas experiments, the CH_4 permeability increases with rising total pressure and C_3H_8 composition in the gas mixture, while the C_3H_8/CH_4 selectivity only marginally increases. More generally, all gas permeabilities increase with increasing C_3H_8 fugacity or activity. The activity can be defined as $\hat{f}_{C_3H_8}/\hat{f}^0_{C_3H_8}$, where $\hat{f}^0_{C_3H_8} = \phi_{C_3H_8} p^0_{C_3H_8}(35\,°C) = (0.827)(12.2\,\text{bar}) = 10.1\,\text{bar}$ [5]. The tabulated data are shown in Table F.4 (see Appendix F).
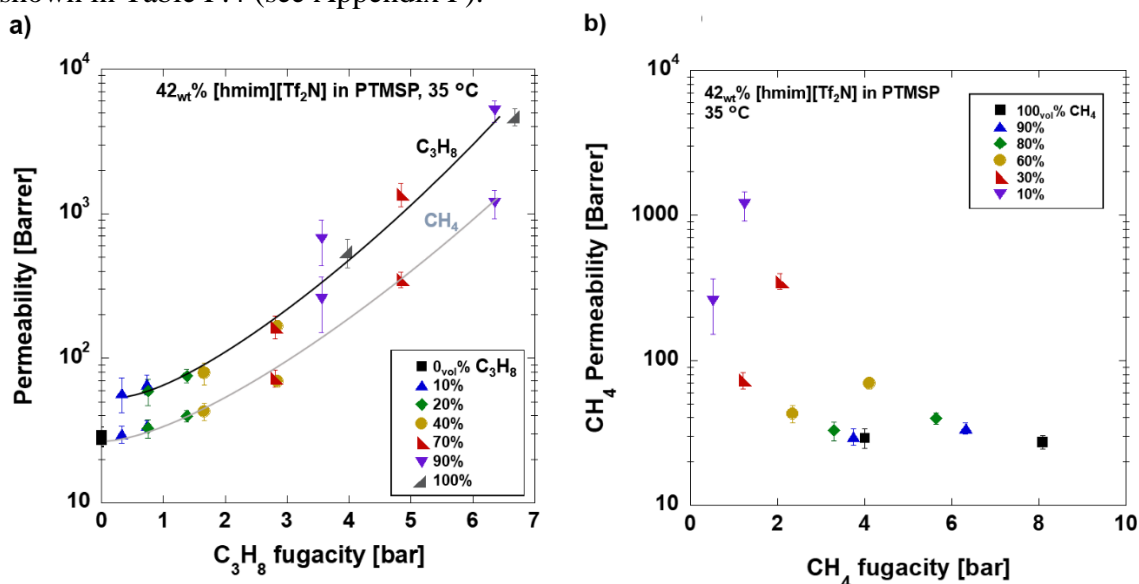
Figure 6.4: Mixed-gas a) CH_4 and C_3H_8 permeability vs C_3H_8 fugacity and b) CH_4 permeability vs CH_4 fugacity in 42_{wt}% [hmim][Tf$_2$N] in PTMSP SILM measured at 35 °C

Figure 6.5 was constructed to more easily compare pure and mixed-gas selectivity in neat PTMSP and the 42_{wt}% SILM. Figure 6.5a displays the C_2H_6/CH_4 selectivity results, and Figure 6.5b shows the results for C_3H_8/CH_4 selectivity. In both cases, the mixed-gas PTMSP selectivity was higher than that for the 42_{wt}% SILM and that predicted from the pure-gas measurements for neat PTMSP. In contrast, the mixed-gas selectivity results for the 42_{wt}% SILM were much more modest than the pure-gas predictions at high

C_{2+} fugacity, due chiefly to the lack of plasticization effects on the pure-gas CH_4 permeabilities. The selectivity data are compared in Table F.5 (see Appendix F).
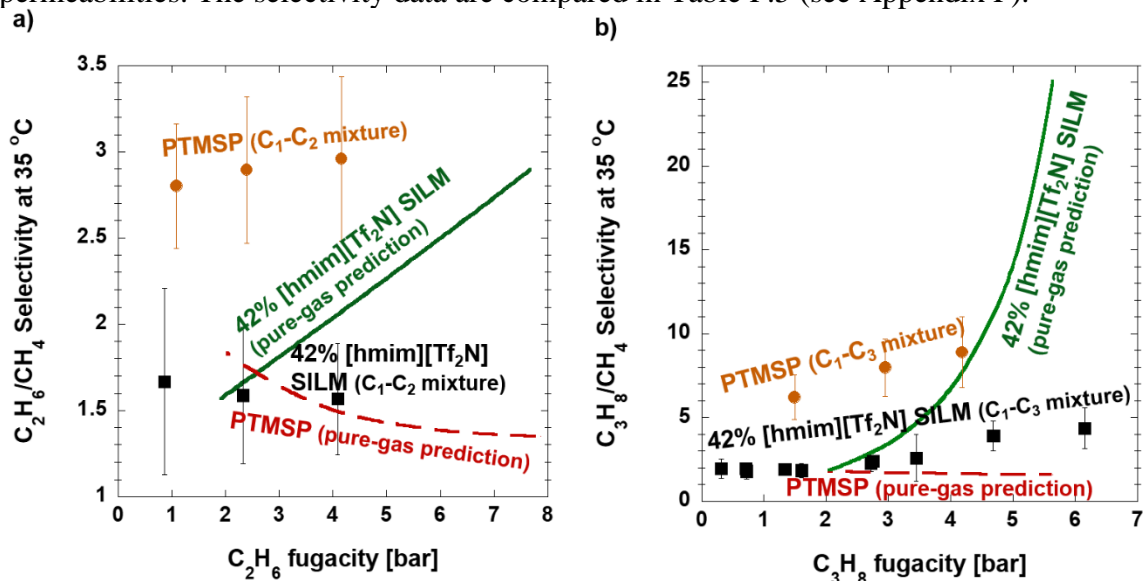
Figure 6.5: Pure and mixed-gas permeability selectivities in neat PTMSP and a $42_{wt}\%$ [hmim][Tf$_2$N] in PTMSP SILM at 35 °C for a) the CH_4-C_2H_6 binary system and b) the CH_4-C_3H_8 binary system.

The findings from this section can also be summarized on the reverse-selective upper bound plots, which were shown previously in Figure 2.2c and Figure 2.2d with expanded axes. The pure- and mixed-gas C_2H_6/CH_4 selectivities for both neat PTMSP and $42_{wt}\%$ SILM are presented in the C_2H_6/CH_4 upper bound plot in Figure 6.6a; those for C_3H_8/CH_4 selectivity are overlayed on the C_3H_8/CH_4 upper bound in Figure 6.6b. In the latter, the discrepancy between pure-gas predicted and mixed-gas selectivities is especially evident. Figure 6.6b also shows that the C_3H_8 permeability spans nearly 2 orders of magnitude, depending on the pressure studied. The pressure labels across both figures correspond to partial pressures of C_2H_6 or C_3H_8 rather than total mixture pressures and that the upper bounds (dotted lines) were drawn by eye, as was done previously [6].
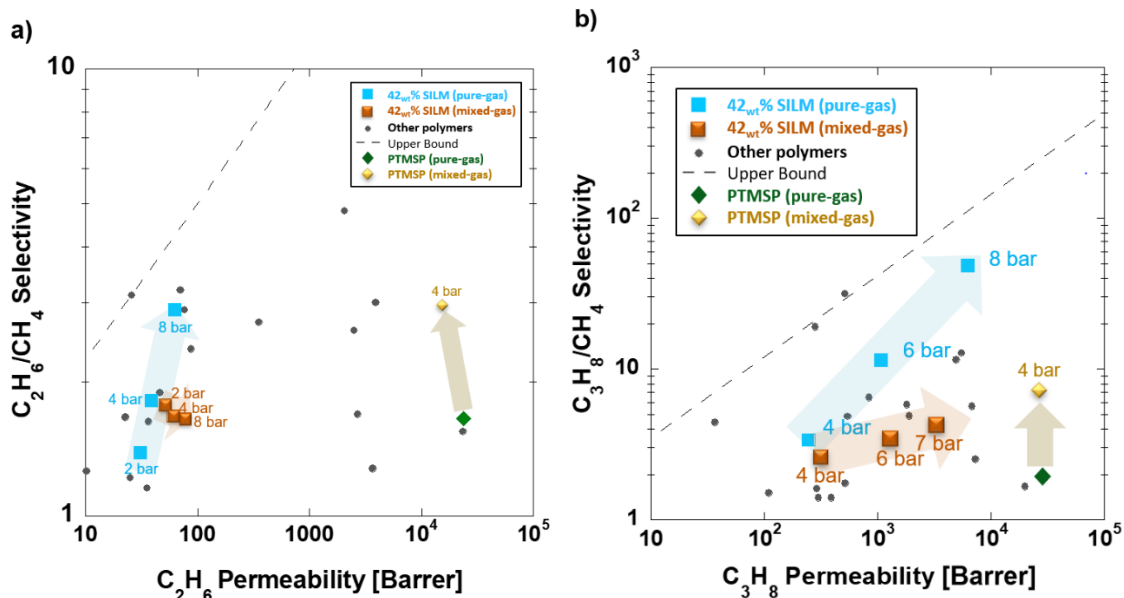
Figure 6.5: Reverse selective a) C_2H_6/CH_4 and b) C_3H_8/CH_4 upper bound plots. The gray points represent literature data from references [6-25]

6.4 REFERENCES

[1]   C.P. Ribeiro, B.D. Freeman, Carbon dioxide/ethane mixed-gas sorption and dilation in a cross-linked poly(ethylene oxide) copolymer, Polymer, 51 (2010) 1156-1168.

[2]   C.P. Ribeiro, B.D. Freeman, D.R. Paul, Pure- and mixed-gas carbon dioxide/ethane permeability and diffusivity in a cross-linked poly(ethylene oxide) copolymer, Journal of Membrane Science, 377 (2011) 110-123.

[3]   J.H. Dymond, K.N. Marsh, R.C. Wilhoit, K.C. Wond, The Virial Coefficients of Pure Gases and Mixtures, Springer, Darmstadt, 2001.

[4]   R.D. Raharjo, B.D. Freeman, D.R. Paul, E.S. Sanders, Pure and mixed gas CH_4 and n-C_4H_{10} permeability and diffusivity in poly(1-trimethylsilyl-1-propyne), Polymer, 48 (2007) 7329-7344.

[5]   N.L. Helgeson, B.H. Sage, Latent heat of vaporization of propane, Journal of Chemical & Engineering Data, 12 (1967) 47-49.

[6]   B.D. Freeman, I. Pinnau, Separation of gases using solubility-selective polymers, Trends in Polymer Science 5 (1997) 167-173.

[7]   Y. Alqaheem, A. Alomair, M. Vinoba, A. Pérez, Polymeric Gas-Separation Membranes for Petroleum Refining, International Journal of Polymer Science, 2017 (2017) 4250927.

[8]   F.I Alghunaimi, The Performance of a Thermally Cross-Linked Polymer of Intrinsic Microporosity (PIM-1) for Gas Separation, M.S. Thesis, King Abdullah University of Science and Technology, Thuwal, Saudi Arabia, 2013.

[9]   K. Haraya, K. Obata, T. Hakuta, H. Yoshitom, The permeation of gases through a new type polyimide membrane, Membrane 11 (1986) 48-52.

[10]   L. Starannikova, Y. Yampol'skii, K. Makovet'skii, T. Golenko, A novel high permeability rubbery membrane material – cis-polypentenamer, Desalination, 200 (2006) 18-19.

[11]   I. Pinnau, Z. He, Pure- and mixed-gas permeation properties of polydimethylsiloxane for hydrocarbon/methane and hydrocarbon/hydrogen separation, Journal of Membrane Science, 244 (2004) 227-233.

[12]   A. Khosravi, M. Sadeghi, H.Z. Banadkohi, M.M. Talakesh, Polyurethane-silica nanocomposite membranes for separation of propane/methane and ethane/methane, Industrial Engineering and Chemistry Research 53 (2014) 2011-2021.

[13]   M.B. Rao, S. Sircar, Nanoporous carbon membranes for separation of gas mixtures by selective surface flow, Journal of Membrane Science, 85 (1993) 253-264.

[14]   T.C. Merkel, V.I. Bondar, K. Nagai, B.D. Freeman, Sorption and Transport of Hydrocarbon and Perfluorocarbon Gases in Poly(1-trimethylsilyl-1-propyne), Journal of Polymer Science Part B: Polymer Physics 38 (2000) 415-434.

[15]   S. Thomas, I. Pinnau, N. Du, M.D. Guiver, Hydrocarbon/hydrogen mixed-gas permeation properties of PIM-1, an amorphous microporous spirobisindane polymer, Journal of Membrane Science, 338 (2009) 1-4.

[16]   N.Y. Alaslai, Gas Sorption, Diffusion and Permeation in a Polymer of Intrinsic Microporosity (PIM-7), M.S. Thesis, King Abdullah University of Science and Technology, Thuwal, Saudi Arabia, 2013.

[17]   M.V. Bermeshev, A.V. Syromolotov, L.E. Starannikova, M.L. Gringolts, V.G. Lakhtin, Y.P. Yampolskii, E.S. Finkelshtein, Glassy Polynorbornenes with Si–O–Si Containing Side Groups. Novel Materials for Hydrocarbon Membrane Separation, Macromolecules, 46 (2013) 8973-8979.

[18]   A. Morisato, B.D. Freeman, I. Pinnau, C.G. Casillas, Pure hydrocarbon sorption properties of poly(1-trimethylsilyl-1-propyne) (PTMSP), poly(1-phenyl-1-propyne) (PPP), and PTMSP/PPP blends, Journal of Polymer Science Part B: Polymer Physics, 34 (1996) 1925-1934.

[19]   E.A. Grushevenko, I.L. Borisov, D.S. Bakhtin, G.N. Legkov, G.N. Bondarenko, A.V. Volkov, Membrane Material Based on Octyl-Substituted Polymethylsiloxane for Separation of C_3/C_1 Hydrocarbons, Petroleum Chemistry 57 (2017) 334-340.

[20]   S.S. Chang, R. Wang, T.-S. Chung, Y. Liu, C_2 and C_3 hydrocarbon separations in poly(1,5-naphthalene-2,2′-bis(3,4-phthalic) hexafluoropropane)diimide (6FDA-1,5-NDA) dense membranes, Journal of Membrane Science 210 (2002) 55–64.

[21]   L.G. Toy, K. Nagai, B.D. Freeman, I. Pinnau, Z. He, T. Masuda, M. Teraguchi, Y.P. Yampolskii, Pure-Gas and Vapor Permeation and Sorption Properties of Poly[1-phenyl-2-[p-(trimethylsilyl)phenyl]acetylene]   (PTMSDPA), Macromolecules, 33 (2000) 2516-2524.

[22]   M.E. Arnold, K. Nagai, B.D. Freeman, R.J. Spontak, D.E. Betts, J.M. DeSimone, I. Pinnau, Gas Permeation Properties of Poly(1,1'-dihydroperfluorooctyl acrylate), Poly(1,1'-dihydroperfluorooctyl methacrylate), and Poly(styrene)-b-poly(1,1'-dihydroperfluorooctyl acrylate) Block Copolymers, Macromolecules, 34 (2001) 5611-5619.

[23]   K. Nagai, L.G. Toy, B.D. Freeman, M. Teraguchi, G. Kwak, T. Masuda, I. Pinnau, Gas permeability and n-butane solubility of poly(1-trimethylgermyl-1-propyne), Journal of Polymer Science Part B: Polymer Physics, 40 (2002) 2228-2236.

[24]   C. Altintas, S. Keskin, Molecular simulations of MOF membranes for separation of ethane/ethene and ethane/methane mixtures, RSC Advances, 7 (2017) 52283-52295.

[25]   O. Shekhah, V. Chernikova, Y. Belmabkhout, M. Eddaoudi, Metal–Organic Framework Membranes: From Fabrication to Gas Separation, Crystals, 8 (2018).

Chapter 7: Light Paraffin Sorption, Diffusion, and Dilation in SILMs

7.1 SORPTION

Sorption measurements were performed to elucidate the solubility (thermodynamic) and diffusivity (kinetic) components of the gas permeabilities in PTMSP and [hmim][Tf$_2$N] SILMs. Literature CH$_4$ sorption data in neat PTMSP was replicated with both the pressure-decay method and the gravimetric method using a magnetic suspension balance (see Section 3.5). Given its lower uncertainties, the gravimetric method was selected for the rest of the sorption measurements.

Sorption isotherms were fitted with either the dual-mode model, Equation 2.12, or the Berens-Hopfenberg sorption model, Equation 2.18. The concentration version of the latter is Equation 7.1:

$$C_A = k_{D,A} p_A \exp\left[2(1+\chi)\frac{\bar{V}_A}{V_{STP}^{ig}} C_A\right] + \frac{C_{H,A}^{\prime,*} b_A^* p_A}{1 + b_A^* p_A} \tag{7.1}$$

where the Henry's constant, $k_{D,A}$, can be related to the Flory-Huggins χ parameter [1]:

$$k_{D,A} = \frac{V_{STP}^{ig}}{\bar{V}_A \, p_A^0} \exp\left(-(1+\chi)\right) \tag{7.2}$$

where V_{STP}^{ig} is 22414 cm^3/mol, $\bar{V}_A$ is the partial molar volume of penetrant A in the sorbing sample (assumed constant for the purposes of these fits) and p_A^0 is the saturation vapor pressure or, if above the critical temperature, the hypothetical saturation vapor pressure of A at 35 °C. Values of these parameters used with Equation 7.2 are shown in Table 7.1. Critical volumes were obtained from the NIST chemistry webbook (available at www.NIST.gov). The partial molar volumes were estimated from critical volumes by a correlation suggested by Kamiya *et al.* [3]. Also shown in Table 7.1 are the Chung diameters, which were used for calculating the size-selective upper bounds in Figure 2.2

and are also estimated from critical volumes [2].

Table 7.1: Light paraffin critical volumes (V_C), Chung diameters (d_C), vapor pressures (p_A^0), and partial molar volumes, $(\bar{V}_A)$, as estimated from [3].

Gas	$V_C \left[\frac{cm^3}{mol}\right]$	d_C [Å]	$\bar{V}_A \left[\frac{cm^3}{mol}\right]$	p_A^0 [bar] (35 °C)
CH_4	98.63	3.737 [2]	54 [3]	322 [4,5]
C_2H_6	141.3	4.27 [2]	66 [3]	51.7 [6]
C_3H_8	198.4	4.731 [2]	82 [3]	12.2 [7]

The vapor pressure for C_3H_8 was obtained from the Antoine's-type correlation developed by Helgeson and Sage [7]. In the case of CH_4, a Frost-Kalkwarf-type equation was used to extrapolate its hypothetical vapor pressure at 35 °C [4] and was found to deviate somewhat with the prediction from the more typical Antoine-type correlation developed by Prydz and Goodwin of 354 bar [5]. The C_2H_6 hypothetical vapor pressure was estimated from the equation proposed by Straty and Tsumura [6] (though its form required neglecting the last term, as it became imaginary for $T > T_C$).

Figure 7.1 shows the concentration versus pressure, pure-gas CH_4 sorption isotherms in neat PTMSP and SILMs of various IL loadings, as well as the extrapolation from the Henry's Law constant at 35 °C for bulk [hmim][Tf$_2$N]. An Arrhenius linearization was used to obtain a [hmim][Tf$_2$N] Henry's Law constant for CH_4 (and C_2H_6) at the appropriate temperature of 35 °C. Uncertainties in the MSB sorption data are less than 0.1%, and the raw data is tabulated in Table G.1 (see Appendix G).

All CH_4 isotherms were well fit by the dual-mode model, although the Berens-Hopfenberg model was also used to fit CH_4 SILM isotherms. Both models use three

fitting parameters: $k_{D,A}$, $C'_{H,A}$ and b_A for the dual-mode model and χ, $C'^{,*}_{H,A}$, and b^*_A for the Berens-Hopfenberg model. The former are shown in Table 7.2, while the latter are displayed in Table 7.3 along with the corresponding $k_{D,A}(\chi)$. Note that the CH$_4$ concentration (and, therefore, solubility) is lower the higher the IL content, while their Langmuir parameters become smaller.
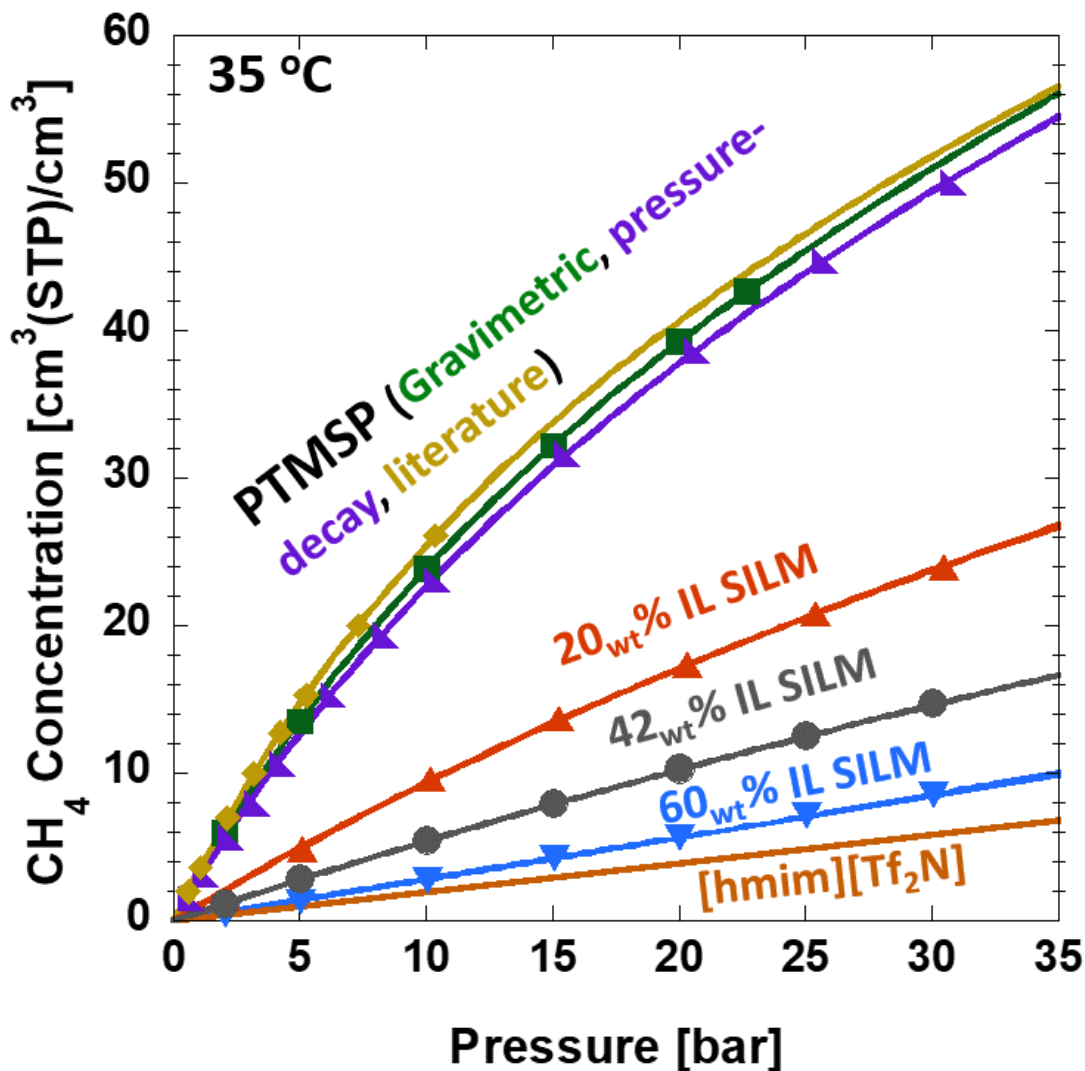
Figure 7.1:   Pure-gas CH$_4$ sorption isotherms in [hmim][Tf$_2$N], PTMSP and PTMSP SILMs with 20, 42, and 60$_{wt}$% [hmim][Tf$_2$N] loading measured at 35 °C. Neat PTMSP and [hmim][Tf$_2$N] literature sorption data retrieved from [8,9]

In the case of the C_2H_6 isotherms shown in Figure 7.2 and tabulated in Table G.2, the neat PTMSP data gathered were somewhat higher than the literature values at higher pressures, which is consistent with our observation of the higher-than-expected ethane permeabilities (shown in Figure 7.4a). More notably, the isotherms for all SILMs display an inflection point, which moves to lower pressures with increasing IL loading.
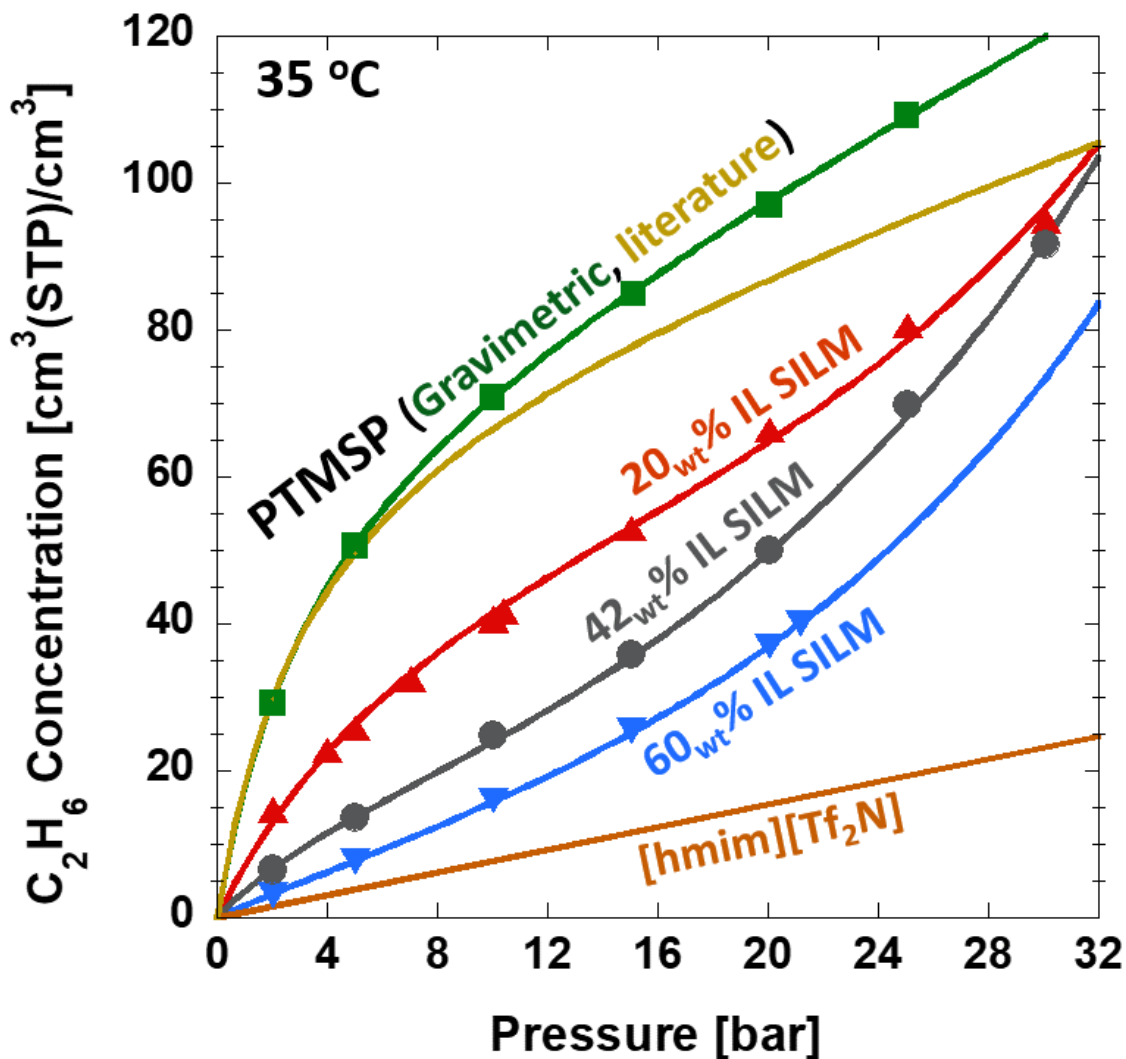
Figure 7.2: Pure-gas C_2H_6 sorption isotherms in [hmim][Tf$_2$N], PTMSP and PTMSP SILMs with 20, 42, and 60$_{wt}$% [hmim][Tf$_2$N] loading measured at 35 °C. Neat PTMSP, [hmim][Tf$_2$N] literature sorption data retrieved from [8,10].

Similar trends are observed for the C_3H_8 isotherms shown in Figure 7.3 and tabulated in Table G.3. In this case, the neat PTMSP sorption data closely matched that in the literature. From Table 7.3, it is noted that the χ parameter decreases with increasing IL loading, while the corresponding Henry's parameters increase with rising IL loading.
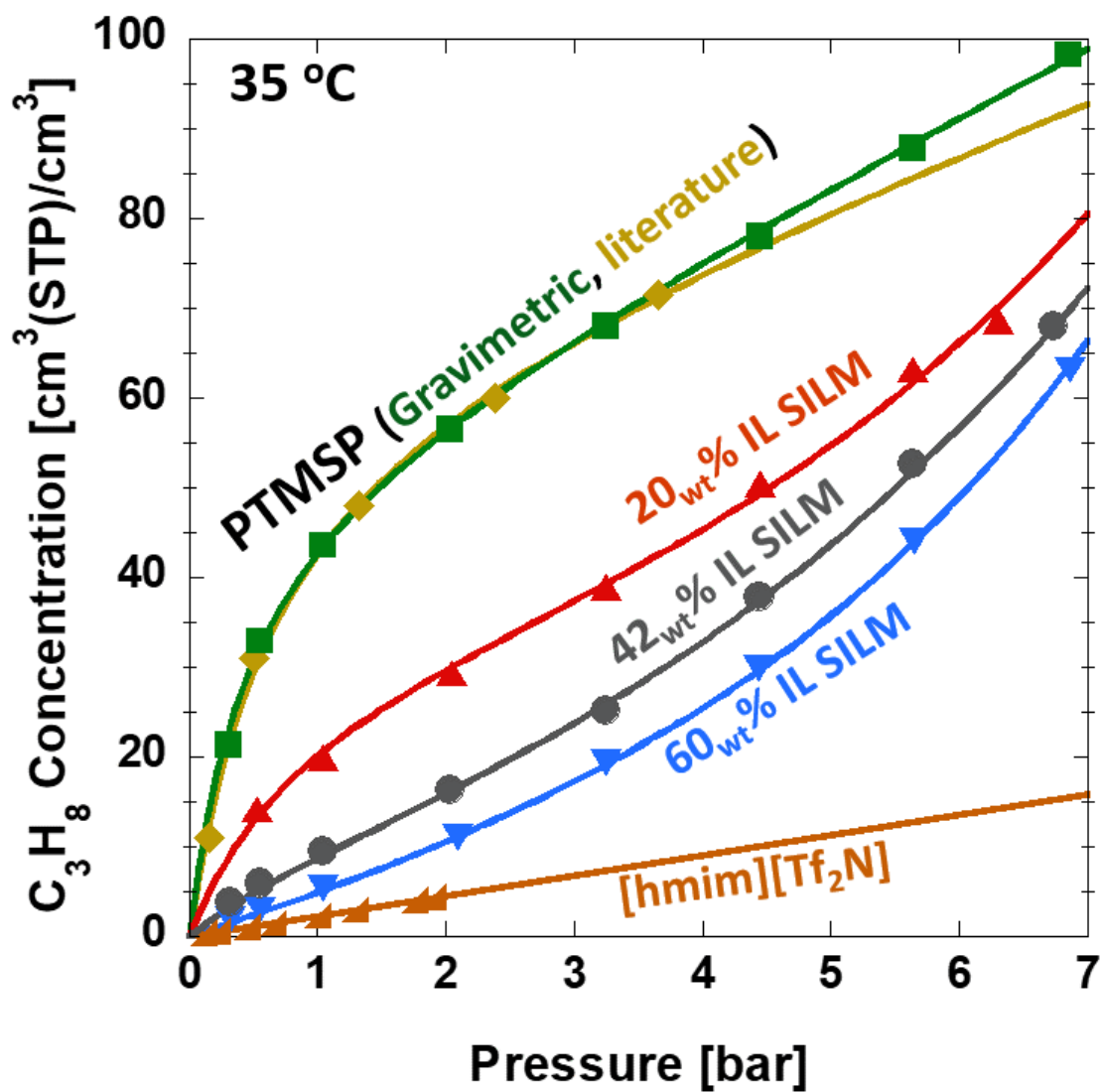
Figure 7.3: Pure-gas C_3H_8 sorption isotherms in [hmim][Tf$_2$N], PTMSP and PTMSP SILMs with 20, 42, and 60$_{wt}$% [hmim][Tf$_2$N] loading measured at 35 °C. Neat PTMSP, [hmim][Tf$_2$N] literature sorption data retrieved from [8,11].

Table 7.2: Dual-mode model fitting parameters for sorption isotherms in Figure 7-1, Figure 7-2, and Figure 7-3. All fits have an R^2 of at least 0.999.

Sample	Gas	$k_{D,A} \left[\dfrac{cm^3(STP)}{cm^3\,bar}\right]$	$C'_{H,A} \left[\dfrac{cm^3(STP)}{cm^3}\right]$	$b_A \left[\dfrac{1}{bar}\right]$
PTMSP (Merkel) [8]	CH_4	0.49	62	0.049
PTMSP (PD)	CH_4	0.53	63	0.038
PTMSP (MSB)	CH_4	0.56	60	0.043
20$_{wt}$% SILM (MSB)	CH_4	0.19	63	0.014
42$_{wt}$% SILM (MSB)	CH_4	0.17	53	0.008
60$_{wt}$% SILM (MSB)	CH_4	0.23	47	0.001
[hmim][Tf$_2$N] [9]	CH_4	0.20	-	-
PTMSP (Merkel) [8]	C_2H_6	1.28	71	0.31
PTMSP (MSB)	C_2H_6	1.94	68	0.30
[hmim][Tf$_2$N] [10]	C_2H_6	0.77	-	-
PTMSP (Merkel) [8]	C_3H_8	5.23	60	1.09
PTMSP (MSB)	C_3H_8	7.30	51	2.29
[hmim][Tf$_2$N] [11]	C_3H_8	2.27	-	-

The concave-down region in the 60$_{wt}$% SILM isotherm is small enough that a Flory Huggins fit (i.e., Equation 7.1 with $C'^{,*}_{H,A} = 0 = b^*_A$) could also fit the data reasonably well.

Because the concentration, C_A, is a function of itself in Equation 7.1, and to facilitate the regression, the concentration data was first fit with a simple polynomial (*e.g.,* a quadratic) function of pressure. This function was written in place of the C_A inside the argument of the exponential in Equation 7.1.

One should be cautious when comparing the Henry's and Langmuir's parameters between Tables 7.2 and 7.3, as these are obtained from different, albeit related, sorption model fits.

Table 7.3: Berens-Hopfenberg model fitting parameters for sorption isotherms in Figure 7-1, Figure 7-2, and Figure 7-3. The $k_{D,A}$ values were obtained from χ using equation 7.2. All fits have an R^2 of at least 0.998.

Sample	Gas	$k_{D,A} \left[\dfrac{cm^3(STP)}{cm^3\ bar}\right]$	$C_{H,A}^{\prime,*} \left[\dfrac{cm^3(STP)}{cm^3}\right]$	$b_A^* \left[\dfrac{1}{bar}\right]$	χ
20$_{wt}$% SILM (MSB)	CH$_4$	0.09	68	0.014	1.68
42$_{wt}$% SILM (MSB)	CH$_4$	0.08	57	0.009	1.79
60$_{wt}$% SILM (MSB)	CH$_4$	0.14	63	0.002	1.2
20$_{wt}$% SILM (MSB)	C$_2$H$_6$	0.45	62	0.12	1.69
42$_{wt}$% SILM (MSB)	C$_2$H$_6$	1.08	14	0.23	0.80
60$_{wt}$% SILM (MSB)	C$_2$H$_6$	1.19	3.1	0.11	0.71
20$_{wt}$% SILM (MSB)	C$_3$H$_8$	2.26	35	0.98	1.29
42$_{wt}$% SILM (MSB)	C$_3$H$_8$	3.93	12	0.57	0.74
60$_{wt}$% SILM (MSB)	C$_3$H$_8$	4.18	5.9	0.26	0.68

While the Berens-Hopfenberg model adequately fits the sorption data, note that the χ parameter in this framework is assumed constant. The χ parameter would be better described by a model that accounts for its dependence on the gas concentration in the sample. Another shortcoming is that the partial molar volumes used have likely been overestimated and assumed constant, rather than behaving as functions of pressure and concentration, which provides further motivation for doing dilation measurements.

7.2 DIFFUSION

Equation 7.3 was used to calculate the effective concentration-averaged diffusivities in Figure 7.4e and f. Note that for SILM samples (which were tested with a constant-volume, variable-pressure system) the downstream pressure and concentration are assumed to be zero, and the expression simplifies to permeability over upstream solubility [2, 12-13]:

$$\bar{D}_A = P_A \frac{p_{us,A} - p_{ds,A}}{C_{us,A} - C_{ds,A}} \cong \frac{P_A}{S_{us,A}} \tag{7.3}$$

For the neat PTMSP samples, this simplification was not made, as the downstream gas concentrations in PTMSP (at 1.013 bar) are significant for samples

111

measured in a constant-pressure, variable-volume system. For this same reason, the permeability equation used to fit the data in Figure 7.4a has a downstream pressure contribution; that is, the dual- mode transport model has the form [8]:

$$P_A = k_{D,A}\bar{D}_{D,A} + \frac{C'_{H,A}b_A\bar{D}_{H,A}}{(1 + b_A p_{us,A})(1 + b_A p_{ds,A})} \tag{7.4}$$

where $\bar{D}_{D,A}$ and $\bar{D}_{H,A}$ are fitting parameters meant to represent the effective concentration-averaged diffusion coefficient of penetrant A in the dense (Henry's law) and nonequilibrium excess free volume (Langmuir), respectively. Once these parameters are known, they can be used in conjunction with Equation 7.5 [8] to model concentration-averaged diffusivities for any given pressure, as was done for the curves in Figure 7.4e.

$$\bar{D}_A = \frac{k_{D,A}\bar{D}_{D,A} + \dfrac{C'_{H,A}b_A\bar{D}_{H,A}}{(1 + b_A p_{us,A})(1 + b_A p_{ds,A})}}{k_{D,A} + \dfrac{C'_{H,A}b_A}{(1 + b_A p_{us,A})(1 + b_A p_{ds,A})}} \tag{7.5}$$

Since we observed a strong concentration-dependence on the gas diffusivities in SILMs (*i.e.,* increasing gas diffusivities with increasing pressure), the data in Figure 7.4f was fit with Equation 7.6 to obtain the plasticization constant, β, and the infinite-dilution effective concentration-averaged diffusivities, $\bar{D}_{0,A}$ [2, 8, 13]:

$$\bar{D}_A = \bar{D}_{0,A}\exp(\beta_A\bar{C}_A) = \bar{D}_{0,A}\exp\big(\beta_A\big[C_{us,A} + C_{ds,A}\big]/2\big) \tag{7.6}$$

where $\bar{C}_A$ is the average concentration of species A throughout the membrane thickness. The fitting parameters relevant to Figure 7.4 are summarized in Table 7.4. The data from Figure 7.4 is tabulated in Table G.4 (see Appendix G). The 64wt% SILM permeation data was used as an approximation of a 60wt% SILM in this section.
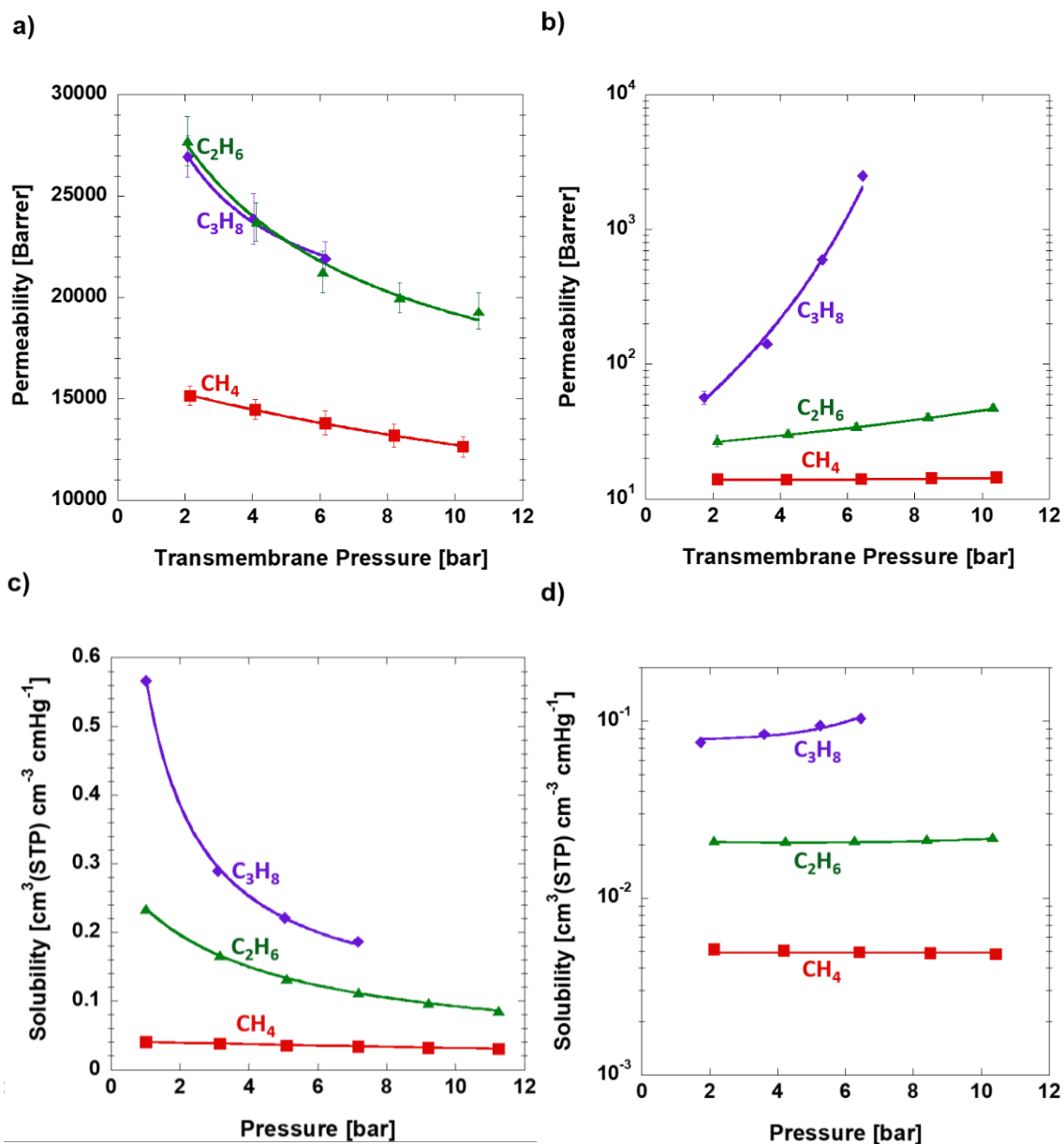
Figure 7.4: Pure-gas CH_4, C_2H_6 and C_3H_8 a) and b) permeabilities, c) and d) solubilities, and e) and f) diffusivities in PTMSP and $60_{wt}\%$ [hmim][Tf$_2$N] PTMSP SILM, respectively. All data was obtained at 35 °C.
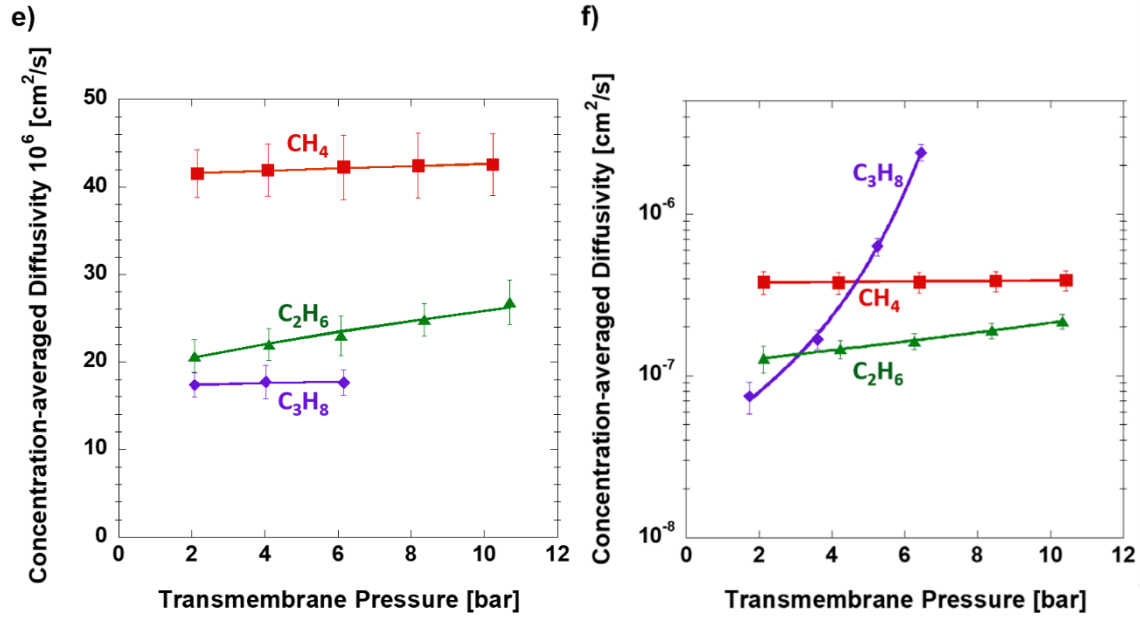
Figure 7.4   (continued)

Lastly, considering that the downstream concentration is negligible for the SILM permeation measurements, permeabilities at any pressure can be modeled with Equation 7.7, as is shown by the curves in Figure 7.4b.

$$P_A = \left(k_{D,A} \exp\left[2(1+\chi)\frac{\bar{V}_A}{V_{STP}^{ig}}C_A\right] + \frac{C_{H,A}^{\prime,*}b_A^*}{1+b_A^* p_A}\right)\bar{D}_{0,A} \exp\left(\beta C_{us,A}/2\right) \qquad (7.7)$$

Although the C_3H_8 diffusivity curve in Figure 7.4f crosses over the C_2H_6 and CH_4 diffusivity curves, it should be noted that these trends are derived from pure-gas measurements and thus are biased by large plasticization effects inherent in the pure-gas C_3H_8 measurements, small plasticization effects in the C_2H_6 measurements, and negligible plasticization effects in the CH_4 measurements.

114

Table 7.4: Dual-mode transport model diffusivities (in the Henry's law and Langmuir regions), plasticization model infinite-dilution diffusivity, plasticization parameter, and infinite-dilution permeabilities at 35 °C.

A = CH$_4$	$D_{D,A} \cdot 10^6$ [cm^2/s]	$D_{H,A} \cdot 10^6$ [cm^2/s]	$D_{0,A} \, 10^6$ [cm^2/s]	β_A	$P_{0,A}$ [Barrer]
Neat PTMSP	61	37	41.3	-	17000
20$_{wt}$% SILM	-	-	6.9	0.010	920
42$_{wt}$% SILM	-	-	0.28	0.037	21
60$_{wt}$% SILM	-	-	0.37	0.030	14
A = C$_2$H$_6$	$D_{D,A} \cdot 10^6$ [cm^2/s]	$D_{H,A} \cdot 10^6$ [cm^2/s]	$D_{0,A} \, 10^6$ [cm^2/s]	β_A	$P_{0,A}$ [Barrer]
Neat PTMSP	48	14	19.3	-	35000
20$_{wt}$% SILM	-	-	1.38	0.044	1300
42$_{wt}$% SILM	-	-	0.05	0.13	30
60$_{wt}$% SILM	-	-	0.11	0.076	24
A = C$_3$H$_8$	$D_{D,A} \cdot 10^6$ [cm^2/s]	$D_{H,A} \cdot 10^6$ [cm^2/s]	$D_{0,A} \, 10^6$ [cm^2/s]	β_A	$P_{0,A}$ [Barrer]
Neat PTMSP	18	16	17.2	-	41000
20$_{wt}$% SILM	-	-	1.06	0.049	2900
42$_{wt}$% SILM	-	-	0.030	0.12	48
60$_{wt}$% SILM	-	-	0.036	0.13	27

7.3 DILATION

In its simplest sense, dilatometry allows us to quantify the volume change of a sample due to sorption of a penetrant. This information is valuable in and of itself, but it

may also be essential in accurately determining other properties. As was alluded to in section 3.5.2, for instance, determination of the sorption isotherms by gravimetric methods often assumes that the volume of the sample is constant throughout the measurement. When studying a highly soluble species such as C_3H_8, however, this assumption may result in a significant underestimation of the buoyancy correction and skew the reported sorption isotherms accordingly. Additionally, because measuring thickness (z-direction) dilation is often challenging and involves larger uncertainties, samples are often assumed to dilate isotropically, such that Equation 7.8 is valid [14,15]:

$$\Delta V = V_0 \left[\left(\frac{L_x}{L_{0,x}} \right)^3 - 1 \right] \tag{7.8}$$

Kamiya *et al.* suggest that the elongation in the x and y directions (length and width, respectively) may become less than the fractional change in thickness when thin polymer samples dilate above $10_{vol}\%$, as was observed with various penetrants in rubbery PDMS but not in glassy LDPE, where the dilation was well below $10_{vol}\%$ [3]. Pope et al. also observed a subtle difference in the length and thickness dilation of PTMSP by CO_2 at pressures up to 62 bar, and this was also observed, albeit to a lesser extent, below $10_{vol}\%$ and after three equilibrium dilation cycles.

Dilation studies also permit the quantitative determination of partial molar volumes via Equation 7.9. As was discussed in section 7.1, the gas partial molar volume in PTMSP and SILMs was assumed to be constant and near the gas molar volume at its normal boiling point, but it would be much more helpful to know the partial molar volume in the material of interest as a function of pressure and concentration [3,14-15]:

$$\bar{V}_A = V_{STP}^{ig} \left[\frac{d}{dp} \left(\frac{\Delta V}{V_0} \right) + \kappa \right] \frac{dp}{dC} \tag{7.9}$$

Where the isothermal compressibility, $\kappa = -\frac{1}{V_0} \left(\frac{\partial V}{\partial p} \right)_{T,n_i}$, has a negligible contribution.

The raw CH_4 dilation data for PTMSP and $20_{wt}\%$ [hmim][Tf_2N] in PTMSP SILM at 35 °C is presented in Figure 7.5a. Figure 7.5b shows that the partial molar volume of CH_4 in neat PTMSP is very modest compared to that in PDMS (on the range of 54-59 cm^3/mol at 35 °C) [3,16-17], that in 5 organic liquids (on average 53 cm^3/mol at 25 °C) [18], or that in [hmim][Tf_2N] (36 ±7 cm^3/mol) [19]. In the SILM samples, the CH_4 partial molar volume increases with increasing IL and is near that in bulk [hmim][Tf_2N] for the $60_{wt}\%$ sample. Note that isotropic volume expansion was assumed for calculating the partial molar volumes.

a)   **b)**
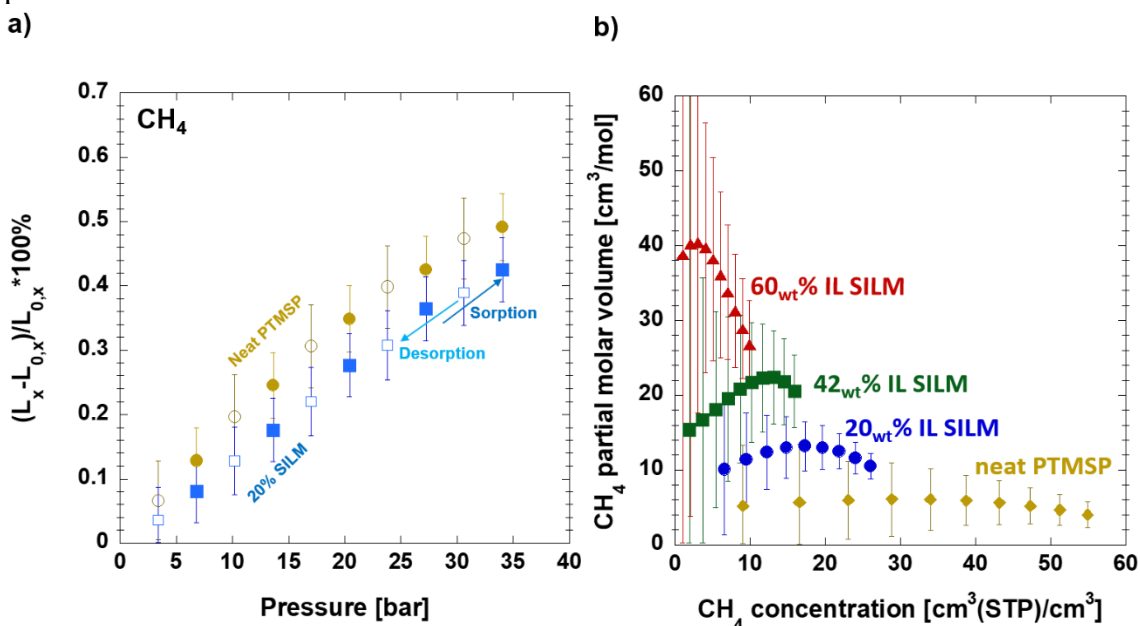
Figure 7.5: Pure-gas CH_4 a) dilation in the x-direction (length) and b) partial molar volumes in PTMSP and SILMs of various loadings at 35 °C.

The volume expansion was at most $1.5_{vol}\%$ in the case of CH_4, so the added contribution from the buoyancy correction in the sorption isotherms has only a small effect. One can expect the volume expansion in C_2H_6 and C_3H_8 dilation experiments to be larger (as much as $18_{vol}\%$ with 8 bar of C_3H_8 in neat PTMSP). Thus, accounting for the

effect of volume expansion in the sample during the sorption measurements has a more significant impact on the reported isotherms and partial molar volumes, as shown in Figure 7.6. Note the inherent assumption of isotropic volume expansion.
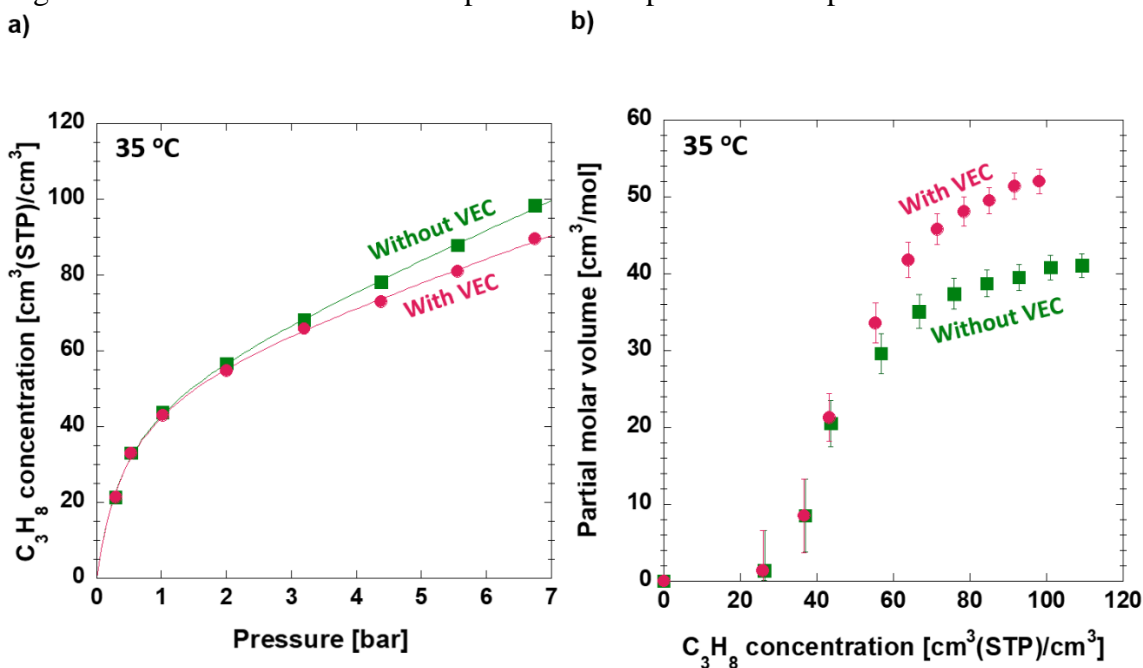
Figure 7.6:   Impact of the volume expansion correction (VEC) on the C_3H_8 sorption isotherm of neat PTMSP and on the partial molar volume of C_3H_8 in neat PTMSP at 35 °C.

Now let us discuss the shortcomings of this length dilation data. Each pressure step was held for 10 minutes, which is considerably shorter than the longer steps (4-12 hours) used when measuring equilibrium sorption. The dilation kinetics in PTMSP are such that 10-minute steps may be a good approximation of the equilibrium dilation, but this is a less appropriate assumption for dilation measurements of the SILM samples. Figure 7.7 shows that, for a C_3H_8 dilation step at 6 bar held for 12 hours, the measured length (past the initial 5 minutes of C_3H_8 exposure) decreases significantly over time for the 60_{wt}% SILM sample, while it varies only modestly for the neat PTMSP. Therefore, to

reconcile the volume dilation and partial molar volume data with the sorption data, it is important that the dilation data is gathered under the same conditions as the sorption data.
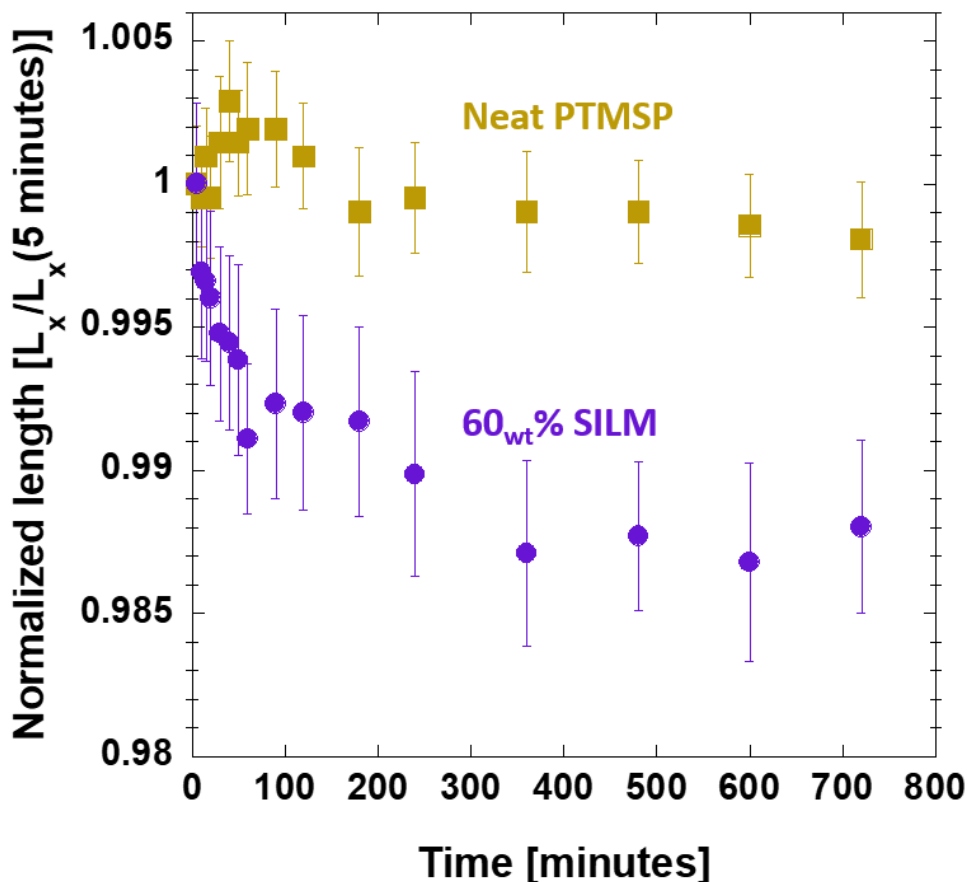
Figure 7.7: Pure-gas C_3H_8 dilation in the x-direction (length) as a function of time, normalized by the length after 5 minutes exposure to 6 bar of C_3H_8 at 35 °C.

In some preliminary C_3H_8 dilation measurements, SILM samples were observed to shrink in length and width when exposed to sufficiently high C_3H_8 or C_2H_6 pressures, and an optical change in the dilation samples was observed. Over the range of pressures indicated in Table 7.5, SILM dilation samples turned from translucent to completely opaque. Although the observed transition was reversible upon evacuation of the C_{2+}, the transition from translucent to cloudy occurred very rapidly, while the transition from

opaque back to translucent could take from several hours (for the $20_{wt}\%$ SILM samples) to multiple days (for the $60_{wt}\%$ SILM samples). Presumably, the SILMs still experience an overall volume increase, but the increase in thickness would have to more than compensate for the decrease in length and width during these transitions. An apparatus capable of quantifying thickness dilation measurements must be used for cases where the isotropic volume expansion assumption is not appropriate.

Table 7.5: Range of C_2H_6 and C_3H_8 pressures where an optical change in SILMs was observed for various [hmim][Tf$_2$N] loadings in PTMSP at 35 °C.

Sample	C_2H_6 pressure [bar]	C_3H_8 pressure [bar]
$20_{wt}\%$ SILM	20-26	6.2-7.6
$42_{wt}\%$ SILM	17-20.5	3.1-4.1
$60_{wt}\%$ SILM	4.5-7	0.7-1.4

7.4 REFERENCES

[1]   M.S. Suwandi, T. Hirose, S.A. Stern, Permeation, diffusion, and solution of cyclopropane in silicone rubber, Journal of Polymer Science Part B: Polymer Physics, 28 (1990) 407-423.

[2]   S. Matteucci, Y. Yampol'skii, B.D. Freeman, I. Pinnau, Transport of gases and vapors in glassy and rubbery polymers, in: Y. Yampol'skii, I. Pinnau, B.D. Freeman (Eds.) Materials Science of Membranes, John Wiley & Sons, Chichester, 2006.

[3]   Y. Kamiya, Y. Naito, K. Terada, K. Mizoguchi, A. Tsuboi, Volumetric Properties and Interaction Parameters of Dissolved Gases in Poly(dimethylsiloxane) and Polyethylene, Macromolecules, 33 (2000) 3111-3119.

[4]   H. Fatoorehchi, R. Rach, H. Sakhaeinia, Explicit Frost-Kalkwarf type equations for calculation of vapour pressure of liquids from triple to critical point by the Adomian decomposition method, The Canadian Journal of Chemical Engineering, 95 (2017) 2199-2208.

[5]   R. Prydz, R.D. Goodwin, Experimental melting and vapor pressures of methane, The Journal of Chemical Thermodynamics, 4 (1972) 127-133.

[6]   G.C. Straty, R. Tsumura, PVT and Vapor Pressure Measurements on Ethane, Journal of research of the National Bureau of Standards. Section A, Physics and chemistry, 80A (1976) 35-39.

[7]   N.L. Helgeson, B.H. Sage, Latent heat of vaporization of propane, Journal of Chemical & Engineering Data, 12 (1967) 47-49.

[8]   T.C. Merkel, V.I. Bondar, K. Nagai, B.D. Freeman, Sorption and Transport of Hydrocarbon and Perfluorocarbon Gases in Poly(1-trimethylsilyl-1-propyne), Journal of Polymer Science Part B: Polymer Physics 38 (2000) 415-434.

[9]   A. Finotello, J.E. Bara, D. Camper, R.D. Noble, Room-Temperature Ionic Liquids: Temperature Dependence of Gas Solubility Selectivity, Industrial & Engineering Chemistry Research, 47 (2008) 3453-3459.

[10]   L.J. Florusse, S. Raeissi, C.J. Peters, High-Pressure Phase Behavior of Ethane with 1-Hexyl-3-methylimidazolium Bis(trifluoromethylsulfonyl)imide, Journal of Chemical & Engineering Data, 53 (2008) 1283-1285.

[11]   C. Miguel Sanchez, T. Song, J.F. Brennecke, B.D. Freeman, Hydrogen Stable Supported Ionic Liquid Membranes with Silver Carriers: Propylene and Propane Permeability and Solubility, Industrial & Engineering Chemistry Research, 59 (2020) 5362-5370.

[12]   G. Genduso, B.S. Ghanem, I. Pinnau, Experimental Mixed-Gas Permeability, Sorption and Diffusion of CO_2-CH_4 Mixtures in 6FDA-mPDA Polyimide Membrane: Unveiling the Effect of Competitive Sorption on Permeability Selectivity, Membranes, 9 (2019).

[13]   R.D. Raharjo, B.D. Freeman, D.R. Paul, E.S. Sanders, Pure and mixed gas CH_4 and n-C_4H_{10} permeability and diffusivity in poly(1-trimethylsilyl-1-propyne), Polymer, 48 (2007) 7329-7344

[14]   R.D. Raharjo, B.D. Freeman, E.S. Sanders, Pure and mixed gas CH_4 and n-C_4H_{10} sorption and dilation in poly(1-trimethylsilyl-1-propyne), Polymer, 48 (2007) 6097-6114.

[15]   D.S. Pope, W.J. Koros, H.B. Hopfenberg, Sorption and Dilation of Poly(1-(trimethylsilyl)-1-propyne) by Carbon Dioxide and Methane, Macromolecules, 27 (1994) 5839-5844.

[16]   R.D. Raharjo, B.D. Freeman, E.S. Sanders, Pure and mixed gas CH_4 and n-C_4H_{10} sorption and dilation in poly(dimethylsiloxane), Journal of Membrane Science, 292 (2007) 45-61.

[17]   M.G. De Angelis, T.C. Merkel, V.I. Bondar, B.D. Freeman, F. Doghieri, G.C. Sarti, Hydrocarbon and fluorocarbon solubility and dilation in poly(dimethylsiloxane): Comparison of experimental data with predictions of the Sanchez–Lacombe equation of state, Journal of Polymer Science Part B: Polymer Physics, 37 (1999) 3011-3026.

[18]   J. Horiuti, The solubility of gas and coefficient of dilation by adsorption, Scientific Papers of the Institute of Physical and Chemical Research, 17 (1931) 125-256.

[19]   J. Kumełan, D. Tuma, G. Maurer, Partial molar volumes of selected gases in some ionic liquids, Fluid Phase Equilibria, 275 (2009) 132-144.

Chapter 8: Conclusions and Recommendations

8.1 CONCLUSIONS

The ionic liquid [hmim][Tf$_2$N] is effectively supported in the disubstituted polyacetylenes PTMSP and PMP by equilibrating the polymer supports in an IL-methanol solution and drying, rather than equilibrating the supports in bulk IL. This greatly reduces equilibration time, from the order of days to the order of minutes.

Prior to exposure to C$_{2+}$, the [hmim][Tf$_2$N] is evenly dispersed across the SILM thickness from this casting process, as determined from SEM-EDX spectroscopy. The IL is effectively confined in the SILM supports given no IL crystallization transition, and only weakened IL glass and melting transition features were observed in DSC scans.

When the IL loading in the PTMSP SILM is increased, its density increases rapidly at first, with minimal volume expansion until a critical loading (19$_{wt}$% IL) is reached, after which the density increase becomes akin to the predictions from volume additivity of the density of bulk [hmim][Tf$_2$N] and the skeletal density of neat PTMSP.

42$_{wt}$% SILMs have a lower elastic modulus and yield strength but are tougher and more ductile than the neat PTMSP support. Overall, the SILMs were found to have adequate mechanical properties for their application as membrane materials.

Gas permeability decreases considerably with increasing IL loading. For instance, CH$_4$ permeability in 64$_{wt}$% [hmim][Tf$_2$N] in PTMSP SILMs is 3 orders of magnitude lower than in neat PTMSP. Unlike in neat PTMSP, C$_2$H$_6$ and C$_3$H$_8$ plasticize SILMs at 35 °C such that gas diffusivities increase exponentially with increasing concentration of the plasticizing gas. As a result, pure-gas C$_2$H$_6$/CH$_4$ and C$_3$H$_8$/CH$_4$ selectivities appear to be pressure-dependent, such that in 42$_{wt}$% SILMs the C$_2$H$_6$/CH$_4$ selectivity triples over the range of 10 bar studied, and the C$_3$H$_8$/CH$_4$ selectivity increases a hundred-fold over

123

the studied range of 7 bar. In contrast, the binary mixed-gas C_3H_8/CH_4 selectivity increases from 2 to only 4 over the same C_3H_8 pressure range, and the binary mixed-gas C_2H_6/CH_4 selectivity only marginally changes over the studied pressure range.

For neat PTMSP at 35 °C, mixed-gas C_2H_6/CH_4 selectivity was up to twice that of the pure-gas selectivity prediction. Similarly, mixed-gas C_3H_8/CH_4 selectivity in neat PTMSP was four to six times larger than the prediction from pure-gas measurements.

A mixed-gas constant-pressure, variable-volume sweep permeation system was built and validated to conduct mixed-gas permeation experiments. Ultimately, it was found that supporting [hmim][Tf$_2$N] in PTMSP was detrimental to light paraffin gas permeability and was not justified by the minor enhancement in the mixed-gas C_{2+}/CH_4 selectivity.

In both the [C$_x$mim][Tf$_2$N] and the [N$_{xxxy}$][Tf$_2$N] IL series, gas permeabilities in PTMSP SILMs with similar IL loadings were lower for ILs with longer primary alkyl chains. Gas permeabilities were also slightly lower for SILMs made with [hmmim][Tf$_2$N] than for those made with [hmim][Tf$_2$N]. Longer primary alkyl chains or the presence of a secondary methyl group on cations also decreased the pressure at which an inflection point was observed in the C_3H_8 permeability curves.

In testing $20_{wt}\%$IL-PDMS blends, the imidazolium-based [dmim][Tf$_2$N] IL-PDMS membranes showed a modest decrease in pure-gas C_3H_8/CH_4 selectivity (from 6 to 4.5 at 2 bar transmembrane pressure), whereas a more desirable pure-gas C_3H_8/CH_4 selectivity increase (from 6 to 13.5 at 2 bar of transmembrane pressure) was observed for the [P$_{1118}$][Phos]-PDMS blends. This result suggests that blending ILs with large solubility-selectivities compared to that of the PDMS matrix can effectively enhance permeability-selectivity if the IL is compatible with and well dispersed in the polymer

124

matrix (and if its addition does not significantly increase the size-sieving character of the composite material).

A sorption model combining a Langmuir term and a simplified Flory-Huggins term was developed and shown to effectively fit sorption isotherm data. Solubility predictions from this model for SILMs and the dual-mode sorption model for neat PTMSP were used to infer effective concentration-averaged gas diffusivities. An empirical exponential model was used to fit the SILM diffusion data and to determine plasticization constants for each of the light paraffins in PTMSP SILMs of various [hmim][Tf_2N] loadings. The dual-mode transport model was used to fit gas permeabilities in neat PTMSP and to predict effective concentration-averaged diffusivities at any transmembrane pressure.

Dilation studies revealed that the CH_4 partial molar volume in SILMs increases with increasing IL content up to that measured in bulk [hmim][Tf_2N]. Particularly for C_{2+} studies, it is imperative to use equilibrium dilation data to accurately account for the volume expansion contribution to the buoyancy correction of sorption isotherms and thus compute appropriate partial molar volumes. A reversible optical change was observed at specific pressure ranges during C_{2+} dilation measurements of SILMs of various IL loadings. It was determined that the isotropic volume expansion assumption is not best suited for characterizing C_{2+} dilation of SILMs, particularly above the pressures where the optical transition was observed.

8.2 RECOMMENDATIONS FOR FUTURE WORK

A complete characterization of the SILMs or other membrane materials of interest will require detailed studies of the transport properties at other temperatures to obtain enthalpies of sorption and activation energies of diffusion of each gas and, ultimately, to

predict transport properties at any temperature [1]. Additionally, mixed-gas sorption studies could be coupled with mixed-gas permeation results to quantify the mixed-gas solubility (e.g., competitive sorption via a mixture dual mode model) and diffusivity (e.g., diffusion path blocking via an inverse C_{2+} exponential dependence on CH_4 diffusivity) effects on the observed mixed-gas permeability, as has been done for the CH_4-n-C_4H_{10} binary system in PTMSP and PDMS [2-3]. Gas diffusivities are related to the fractional free volume of the material, so future efforts to model fractional free volume as a function of plasticizing penetrant concentration could enhance our understanding of plasticization [4].

Thickness equilibrium dilation measurements are needed to accurately determine sorption isotherms when volume expansion is significant ($>2_{vol}\%$) and not isotropic. The same is true for reporting accurate partial molar volumes of highly condensable species.

Future work will better elucidate the optical transition observed in SILMs in C_{2+} atmospheres. For instance, to test whether the transition is due to phase separation, one could investigate the phase equilibrium of bulk [hmim][Tf_2N] with C_{2+}, as has been done with the ionic liquid [emim][FAP] and C_3H_8 [5] and with [emim][Tf_2N] and 1,1,1,2-tetrafluoroethane (R-134a) [6]. The potential for SILMs to work as sensors of small amounts of C_{2+} paraffins and VOCs can also be evaluated.

Another avenue of interest for future work involves supporting chemisorbing ionic liquids in highly open, mechanically robust supports (such as polyacetylenes) for CO_2 separations, as these are likely to yield high selectivity at even small concentration gradients [7-8]. Additional efforts include characterizing other promising substituted polyacetylenes, such as poly(1-hexyne) and poly(1-tetradecyne), whose transport properties have only been sparingly studied [9]. There are also opportunities to study

126

ionic liquids with higher C_{2+}/CH_4 solubility selectivity in gas separation membrane systems, including [P$_{1118}$][Phos] and [bHim][Ac] [10-11].

8.3 REFERENCES

[1]   D. Craster, T.G.J. Jones, Permeation of a Range of Species through Polymer Layers under Varying Conditions of Temperature and Pressure: In Situ Measurement Methods, Polymers, 11 (2019).

[2]   R.D. Raharjo, B.D. Freeman, D.R. Paul, E.S. Sanders, Pure and mixed gas CH_4 and n-C_4H_{10} permeability and diffusivity in poly(1-trimethylsilyl-1-propyne), Polymer, 48 (2007) 7329-7344.

[3]   R.D. Raharjo, B.D. Freeman, D.R. Paul, G.C. Sarti, E.S. Sanders, Pure and mixed gas CH_4 and n-C_4H_{10} permeability and diffusivity in poly(dimethylsiloxane), Journal of Membrane Science, 306 (2007) 75-92.

[4]   T. Corrado, R. Guo, Macromolecular design strategies toward tailoring free volume in glassy polymers for high performance gas separation membranes, Molecular Systems Design & Engineering, 5 (2020) 22-48.

[5]   M. Althuluth, M.T. Mota-Martinez, A. Berrouk, M.C. Kroon, C.J. Peters, Removal of small hydrocarbons (ethane, propane, butane) from natural gas streams using the ionic liquid 1-ethyl-3 -methylimidazolium tris(pentafluoroethyl)trifluorophosphate, The Journal of Supercritical Fluids, 90 (2014) 65-72.

[6]   R. Wei, High-Pressure Phase Equilibria of Ionic Liquids and Compressed Gases for Applications in Reactions and Absorption Refrigeration, PhD Dissertation, The University of Kansas, Lawrence, Kansas, 2009.

[7]   S. Kasahara, E. Kamio, A. Otani, H. Matsuyama, Fundamental Investigation of the Factors Controlling the CO_2 Permeability of Facilitated Transport Membranes Containing Amine-Functionalized Task-Specific Ionic Liquids, Industrial & Engineering Chemistry Research, 53 (2014) 2422-2431.

[8] F. Moghadam, E. Kamio, A. Yoshizumi, H. Matsuyama, An amino acid ionic liquid-based tough ion gel membrane for CO_2 capture, Chemical Communications, 51 (2015) 13658-13661.

[9] H. Balcar, P. Topka, J. Sedláček, J. Zedník, J. Čejka, Polymerization of aliphatic alkynes with heterogeneous Mo catalysts supported on mesoporous molecular sieves, Journal of Polymer Science Part A: Polymer Chemistry, 46 (2008) 2593-2599.

[10] X. Liu, W. Afzal, M. He, J.M. Prausnitz, Solubilities of small hydrocarbons, viscosities of diluted tetraalkylphosphonium bis(2,4,4-trimethylpentyl) phosphinates, AIChE Journal, 60 (2014) 2607-2612.

[11] X. Liu, E. Ruiz, W. Afzal, V. Ferro, J. Palomar, J.M. Prausnitz, High Solubilities for Methane, Ethane, Ethylene, and Propane in Trimethyloctylphosphonium Bis(2,4,4-trimethylpentyl) Phosphinate ([P8111][TMPP]), Industrial & Engineering Chemistry Research, 53 (2014) 363-368.

Appendix A: Nomenclature of chemicals

This appendix lists the chemicals referenced in this thesis by abbreviation and full name, in order of appearance:

PTMSP	Poly(1-trimethylsilyl-1-propyne)
[hmim][Tf$_2$N] or [C$_6$mim][Tf$_2$N]	1-hexyl-3-methylimidazolium bis(trifluoromenthylsulfonyl)imide
PDMS	Poly(dimethylsiloxane)
PEO	Poly(ethylene oxide)
PIM-1	Polymer of intrinsic microporosity 1, a 5,5',6,6'-tetrahydroxy-3,3,3',3'-tetramethyl-1,1'-spirobisindane and tetrafluoroterephthalonitrile derived dibenzodioxin polymer
6FDA-mPDA	4,4'-(hexafluoroisopropylidene)diphthalic anhydride and m-phenylene diamine derived polyimide
PMP	Poly(4-methyl-2-pentyne)
PTMGP	Poly(1-methylgermyl-1-pentyne)
PTMSDPA	Poly(1-phenyl-2(4-trimethylsilyl)phenylacetylene)
PCIPA	Poly(1-chloro-2-phenylacetylene)
PTBA	Poly(terbutylacetylene)
PPP	Poly(1-phenyl-1-propyne)
PVTMS	Poly(vinyltrimethylsilane)
PBTMST	Poly(bis(trimethylsilyl)tricyclononene)
PTMST	Poly(1-(trimethylsilyl)phenyl-2-phenylacetylene)
[omim][Cl]	1-octyl-3-methylimidazolium chloride
[bmim][Ac]	1-butyl-3-methylimidazolium acetate

[bmim][DCA]	1-butyl-3-methylimidazolium dicyanamide
[bmim][Tf$_2$N]	1-butyl-3-methylimidazolium bis(trifluoromethylsulfonyl)imide
PMPentene	Poly(4-methyl-1-pentene)
POMS	Poly(octylmethylsiloxane)
cis-PPM	cis-poly(pentenamer)
[emim][Tf$_2$N] or [C$_2$mim][Tf$_2$N]	1-ethyl-3-methylimidazolium bis(trifluoromethylsulfonyl)imide
[emmim][Tf$_2$N] or [C$_2$mmim][Tf$_2$N]	1-ethyl-2,3-dimethylimidazolium bis(trifluoromethylsulfonyl)imide
[hmmim][Tf$_2$N] or [C$_6$mmim][Tf$_2$N]	1-hexyl-2,3-methylimidazolium bis(trifluoromethylsulfonyl)imide
[dmim][Tf$_2$N] or [C$_{10}$mim][Tf$_2$N]	1-decyl-3-methylimidazolium bis(trifluoromethylsulfonyl)imide
[dmmim][Tf$_2$N] or [C$_{10}$mmim][Tf$_2$N]	1-decyl-2,3-dimethylimidazolium bis(trifluoromethylsulfonyl)imide
[N$_{1114}$][Tf$_2$N]	Trimethylbutylammonium bis(trifluoromethylsulfonyl)imide
[N$_{1116}$][Tf$_2$N]	Trimethylhexylammonium bis(trifluoromethylsulfonyl)imide
[N$_{1118}$][Tf$_2$N]	Trimethyloctylammonium bis(trifluoromethylsulfonyl)imide
[N$_{1888}$][Tf$_2$N]	Trioctylmethylammonium bis(trifluoromethylsulfonyl)imide
[P$_{1118}$][Phos]	Trimethyloctylphosphonium bis(2,4,4-trimethylpentyl)phosphinate
PEGDA/MEA	Poly(ethylene glycol)diacrylate-co-poly(ethylene glycol)methylether acrylate
[emim][FAP]	1-ethyl-3-methylimidazolium tris(perfluoroethyl)trifluorophosphate

R-134a   1,1,1,2-tetrafluoroethane

[bHim][Ac]   1-butyl-3-H-imidazolium acetate or 1-butylimidazolium acetate

Appendix B: Gas solubility unit conversions and comparisons

This appendix shows example solubility unit conversions and a comparison of gas solubilities in selected polymers and liquids.

Henry's constant can be defined as a limit, analogously to Raoult's law [1]:

$$k_{D,A} = \log_{x_A \to 0} \frac{p}{x_A} \tag{B.1}$$

where $k_{D,A}$ is typically reported in units of [bar], [MPa], or [atm] and x is the mole fraction of gas in the liquid. Near the infinite dilution limit, solubility can be estimated from the Henry's constant [1]:

$$S_{D,A} \cong \frac{M_l}{\rho_l} k_{D,A} \tag{B.2}$$

where M_l is the molar mass of the liquid, ρ_l is the density of the liquid, and $S_{D,A}$ typically has units of $[\frac{\text{mol}}{\text{L bar}}]$ in ionic liquids literature or $\left[\frac{\text{cm}^3 (\text{STP})}{\text{cm}^3 \text{ cmHg}}\right]$ in membrane science literature.

The two can be related through the unit conversion:

$$\left[\frac{\text{cm}^3 (\text{STP})}{\text{cm}^3 \text{ cmHg}}\right] = 3.35 \left[\frac{\text{mol}}{\text{L bar}}\right] \tag{B.3}$$

Of course, when interested in determining solubilities outside the Henry's law valid range (a good rule of thumb for deciding what is far from infinite dilution is when the Henry's law solubility deviates more than 2% from the experimental solubility), solubilities should be determined with a more appropriate model, such as those presented in section 7.1.

Some light paraffin solubilities in selected soft materials with common units are compared in Table B.1.

Table B.1: CH$_4$ and C$_3$H$_8$ solubilities and C$_3$H$_8$/CH$_4$ solubility selectivity at 25 °C in selected polymers and liquids.

Material	CH$_4$ Solubility [mmol L^{-1} bar^{-1}]	C$_3$H$_8$ Solubility [mmol L^{-1} bar^{-1}]	C$_3$H$_8$/CH$_4$ Solubility Selectivity
Water [2]	0.0014	0.0017	1.2
Acetone [2]	27	425	16
n-heptane [2,3]	46	1017	22
[hmim][Tf$_2$N] [4]	8.9	98	11
[bHim][Ac] [5]	10	153	15
[P$_{1118}$][Phos] [6]	15	254	17
PDMS (∞ dilution) [7]	19	331	17
PTMSP (∞ dilution)	209	2720	13
PTMSP (Δp=6 bar) [8]	125	740	6
Amorphous PE (∞ dilution) [9]	9	175	19

APPENDIX B REFERENCES

[1]   R. Sander, Compilation of Henry's law constants (version 4.0) for water as solvent, Atmos. Chem. Phys., 15 (2015) 4399-4981.

[2]   P.G.T Fogg, W. Gerrard, Solubility of Gases in Liquids, John Wiley & Sons, Chichester, 1991.

[3]   W. Hayduk, E.B. Walter, P. Simpson, Solubility of propane and carbon dioxide in heptane, dodecane, and hexadecane, Journal of Chemical & Engineering Data, 17 (1972) 59-61.

[4]   M. Althuluth, M.C. Kroon, C.J. Peters, Solubility of Methane in the Ionic Liquid 1-Ethyl-3-methylimidazolium Tris(pentafluoroethyl)trifluorophosphate, Industrial & Engineering Chemistry Research, 51 (2012) 16709-16712.

[5]   X. Liu, W. Afzal, M. He, J.M. Prausnitz, Solubilities of small hydrocarbons, viscosities of diluted tetraalkylphosphonium bis(2,4,4-trimethylpentyl) phosphinates, AIChE Journal, 60 (2014) 2607-2612.

[6]   X. Liu, E. Ruiz, W. Afzal, V. Ferro, J. Palomar, J.M. Prausnitz, High Solubilities for Methane, Ethane, Ethylene, and Propane in Trimethyloctylphosphonium Bis(2,4,4-trimethylpentyl) Phosphinate ([P8111][TMPP]), Industrial & Engineering Chemistry Research, 53 (2014) 363-368.

[7]   Y. Kamiya, Y. Naito, K. Terada, K. Mizoguchi, A. Tsuboi, Volumetric Properties and Interaction Parameters of Dissolved Gases in Poly(dimethylsiloxane) and Polyethylene, Macromolecules, 33 (2000) 3111-3119.

[8]   T.C. Merkel, Z. He, I. Pinnau, B.D. Freeman, P. Meakin, A.J. Hill, Effect of Nanoparticles on Gas Sorption and Transport in Poly(1-trimethylsilyl-1-propyne), Macromolecules, 36 (2003) 6844-6855.

[9]   A.S. Michaels, H.J. Bixler, Flow of gases through polyethylene, Journal of Polymer Science, 50 (1961) 413-439.

Appendix C: Compressibility factor and fugacity coefficient calculations

This appendix summarizes the two primary methods for calculating nonidealities in this work.

The NIST Reference Fluid Thermodynamic and Transport Properties Database, originally named after REFrigerant PROPerties, is a standardized collection of thermodynamic models for the purpose of calculating reliable thermophysical properties (e.g., densities, vapor pressures, enthalpies, fugacity coefficients, etc.) within the uncertainties of experimental measurements. For light paraffins and other natural gases, the current standard (i.e., ISO 20765-2/3) adopted the use of the GERG 2008 mixture equation of state (EOS), described in detail by Kunz and Wagner [1]. The pure gas properties for methane and ethane follow a Klimeck EOS while propane is modeled with a Span and Wagner EOS. The NIST REFPROP database is ubiquitous in the industry and widely available in chemical engineering modeling software such as Aspen PLUS, ProMax, MATLAB or MS Excel, among others.

For simplicity, properties for an isothermal pure-component system can be modeled for a range of pressures of interest. The resulting compressibility factors can be fit with a pressure-based virial expansion type polynomial [2]. In this work, a 4th degree polynomial (*i.e.,* truncated to 5 terms) was used for pure-gas systems at 35 °C:

$$Z \equiv \frac{pV_m}{RT} = 1 + Bp + Cp^2 + Dp^3 + Ep^4 \qquad (C.1)$$

where Z is the compressibility factor, p is pressure, V_m is the molar volume, R is the universal gas constant, T is absolute temperature, and B, C, D, and E are the second, third, fourth, and fifth pseudo-virial coefficients. Fugacity coefficients, ϕ, were derived from Equation C.2 [2]:

$$\ln \phi = \int_0^p \frac{Z-1}{p} dp \qquad (C.2)$$

Example compressibility factors and fugacity coefficients for methane, ethane, propane, and propylene are shown in Figure C.1. It is recognized that this virial fit inherently makes higher error predictions than the Klimeck EOS or the Span and Wagner EOS. Nonetheless, this fit was found to match the predictions from NIST REFPROP for the temperature and pressure range of interest more closely than alternative EOS of similar complexity (e.g., the density-based virial EOS or the Peng-Robinson EOS). The 35 °C pseudo-virial coefficients are listed in Table C.1.

Table C.1: Pseudo-virial coefficients of select light hydrocarbons at 35 °C.

Species	$B \ 10^3$ $[cm^3/mol]$	$C \ 10^5$ $[cm^6/mol^2]$	$D \ 10^7$ $[cm^9/mol^3]$	$E \ 10^8$ $[cm^{12}/mol^4]$
CH_4	-1.53	0.117	0.123	-0.0138
C_2H_6	-6.64	-5.00	9.16	-2.88
C_3H_6	-12.6	-16.9	30.5	-44.9
C_3H_8	-14.2	-20.5	29.2	-67.7
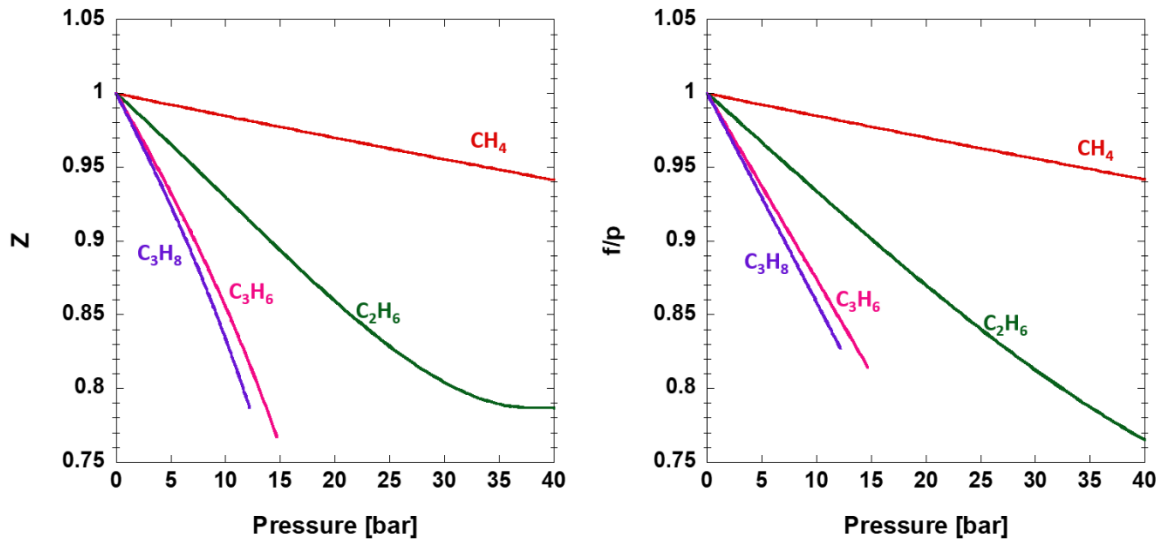
Figure C.1: Pure-component compressibility factor and fugacity coefficient of select light hydrocarbons at 35 °C obtained from Equations C.1 and C.2 and the coefficients listed in Table C.1. Note the C_3H_6 and C_3H_8 curves become discontinuous at their saturation point.

Analogously to Equation C.1, we can define compressibility by a 2nd degree molar density version of the virial EOS [2-3]:

$$Z \equiv \frac{p}{RT\rho} = 1 + B\rho + C\rho^2 \tag{C.3}$$

where ρ is the gas molar density. The pure-gas fugacity coefficient can be obtained from [4-5]:

$$\ln \phi = Z - 1 - \ln Z + \int_0^\rho Z - 1 \frac{d\rho}{\rho} \tag{C.4}$$

Substituting Equation C.1 into Equation C.4 yields [3]:

$$\phi = \exp(2B\rho + \frac{3}{2}C\rho^2 - \ln Z) \tag{C.5}$$

For predicting nonidealities in mixtures, such as in Chapter 6, the density version of the virial EOS truncated to 3 terms was employed, given its relative simplicity and the availability of second and third virial coefficients in the compendium compiled by

137

Dymond *et al.* [4]. B and C are replaced by B_m and C_m, the second and third virial coefficients of the mixture, respectively. These are defined generally by [2-6]:

$$B_m(T, y) = \sum_{i=1}^{n} \sum_{j=1}^{n} y_i y_j B_{ij}(T) \tag{C.6}$$

$$C_m(T, y) = \sum_{i=1}^{n} \sum_{j=1}^{n} \sum_{k=1}^{n} y_i y_j y_k C_{ijk}(T) \tag{C.7}$$

where y are mol fraction of gas and the indices represent different species. Therefore, the binary (*i.e.,* B_{ii} and B_{jj}) and ternary (*i.e.,* C_{iii}, C_{jjj} and C_{kkk}) "mixture" coefficients with equal indices indicate intraspecies interactions and are equivalent to pure-component coefficients, while mixture coefficients with at least 2 different indices are interspecies interactions. Note that $C_{iij} = C_{iji} = C_{jii}$ are all equivalent.

For binary-systems, Equation C.7 simplifies to [6]:

$$C_m(T, y) = y_1^3 C_{111}(T) + 3y_1^2 y_2 C_{112}(T) + 3y_1 y_2^2 C_{122}(T) + y_2^3 C_{222}(T) \tag{C.8}$$

For the methane-ethane (CH_4-C_2H_6) binary system, Hou *et al.* correlate the second virial cross coefficient temperature dependence [5]:

$$B_{12}(T) = 109.86 - \frac{59748}{T} \tag{C.9}$$

where the units of B_{12} are [cm^3/mol] and the units of T are [K]. As no temperature correlation was available, the third virial cross coefficients were interpolated from Table 5 of Hou *et al.* [5].

For the methane-propane (CH_4-C_3H_8) binary system, the following correlations developed by Richter *et al.* were employed [6]:

$$B_{12}(T) = 0.0035903 \, T^2 + 3.0962 \, T - 736.73 \tag{C.10}$$

$$C_{112}(T) = -46.044 \, T + 20514 \tag{C.11}$$

$$C_{122}(T) = 7.3896 \, T + 11688 \tag{C.12}$$

where the third virial cross coefficients have units of [cm^6/mol^2] and those of T are [K].

The mixture fugacity coefficients for component i can then be computed by [3]:

$$\ln \hat{\phi}_i = 2\rho \sum_{j=1}^{n} y_j B_{ji} + \frac{3}{2}\rho^2 \sum_{j=1}^{n} \sum_{k=1}^{n} y_j y_k C_{jki} - \ln Z \qquad (C.13)$$

APPENDIX C REFERENCES

[1]   O. Kunz, W. Wagner, The GERG-2008 Wide-Range Equation of State for Natural Gases and Other Mixtures: An Expansion of GERG-2004, Journal of Chemical & Engineering Data, 57 (2012) 3032-3091.

[2]   H.C. Van Ness, M.M. Abbott, Thermodynamics, in: R.H. Perry, D.W. Green (Eds.), Perry's Chemical Engineer's Handbook, 8th Edition, McGraw-Hill Professional, New York, 2008, pp. 4-19-4-21.

[3]   C.P. Ribeiro, B.D. Freeman, Carbon dioxide/ethane mixed-gas sorption and dilation in a cross-linked poly(ethylene oxide) copolymer, Polymer, 51 (2010) 1156-1168.

[4]   J.H. Dymond, K.N. Marsh, R.C. Wilhoit, K.C. Wond, The Virial Coefficients of Pure Gases and Mixtures, Springer, Darmstadt, 2001.

[5]   H. Hou, J.C. Holste, K.R. Hall, K.N. Marsh, B.E. Gammon, Second and Third Virial Coefficients for Methane + Ethane and Methane + Ethane + Carbon Dioxide at (300 and 320) K, Journal of Chemical & Engineering Data, 41 (1996) 344-353.

[6]   M. Richter, M.O. McLinden, Vapor-Phase (p, ρ, T, x) Behavior and Virial Coefficients for the (Methane + Propane) System, Journal of Chemical & Engineering Data, 59 (2014) 4151-4164.

Appendix D: Additional characterization data

This appendix presents additional PTMSP characterization data, namely, gel permeation chromatography (GPC) analysis, proton nuclear magnetic resonance (H-NMR) results and, for the in-house batches, synthesis yields. The [hmim][Tf$_2$N] and TMSP H-NMR spectra are also included.

In-house batches of PTMSP were synthesized with the assistance of Dr. Oscar Morales Collazo, Maximilian Strauss and Edwin Torres Cuevas following the procedure described in section 3.1.2. The 1 µg/mL PTMSP in GPC-grade chloroform samples were prepared by Edwin Torres Cuevas, while Adrian Rylski and Malgorzata Chwatko kindly ran the GPC analyses. A sample GPC spectrum is shown in Figure D.1, while a summary of the properties is shown in Table D.1.

Figure D.2, Figure D.3 and Figure D.4 present the H-NMR spectra for [hmim][Tf$_2$N], TMSP, and PTMSP, respectively.
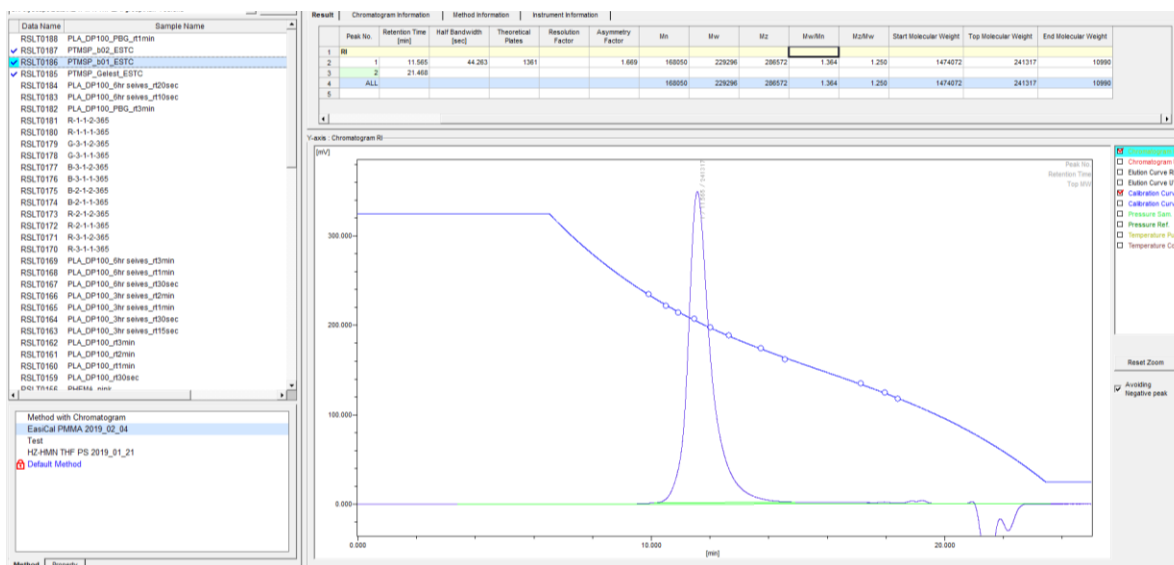
Figure D.1:   Sample PTMSP in chloroform GPC spectrum.

Table D.1:   PTMSP properties across four batches. All data in Chapters 4 through 7 of this thesis was collected from samples made with batch 4: Gelest 2019.

PTMSP batch	Weight-averaged molar mass [g/mol]	Polydispersity index	Catalyst	Yield [%]
1: Gelest 2018	353700	1.61	-	-
2: In-house 6/5/2019	229300	1.36	$NbCl_5$	96
3: In-house 6/8/2019	228600	1.22	$NbCl_5$	92
4: Gelest 2019	300900	2.28	-	-
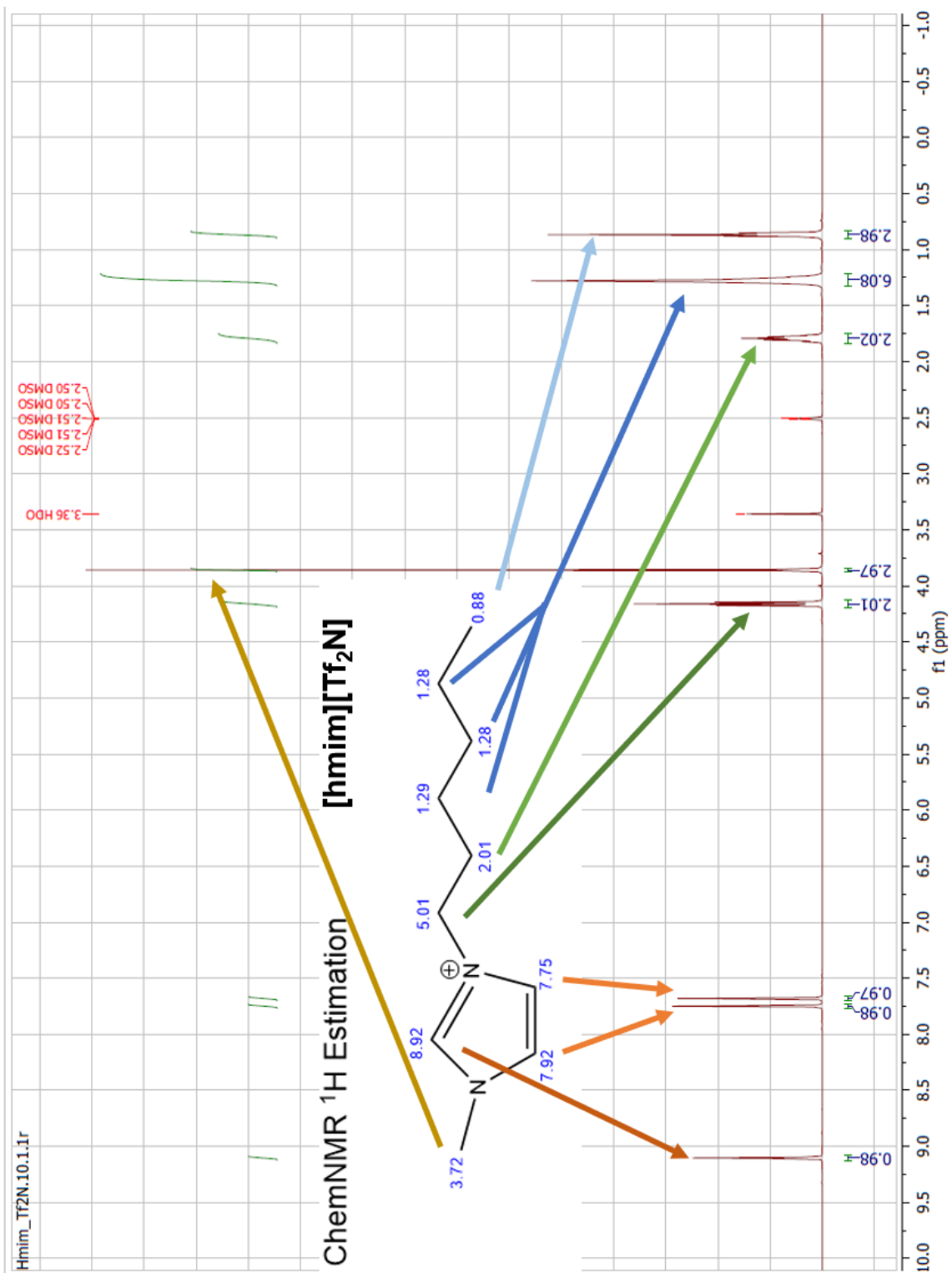
Figure D.2: H-NMR spectrum of [hmim][Tf$_2$N] in deuterated DMSO.
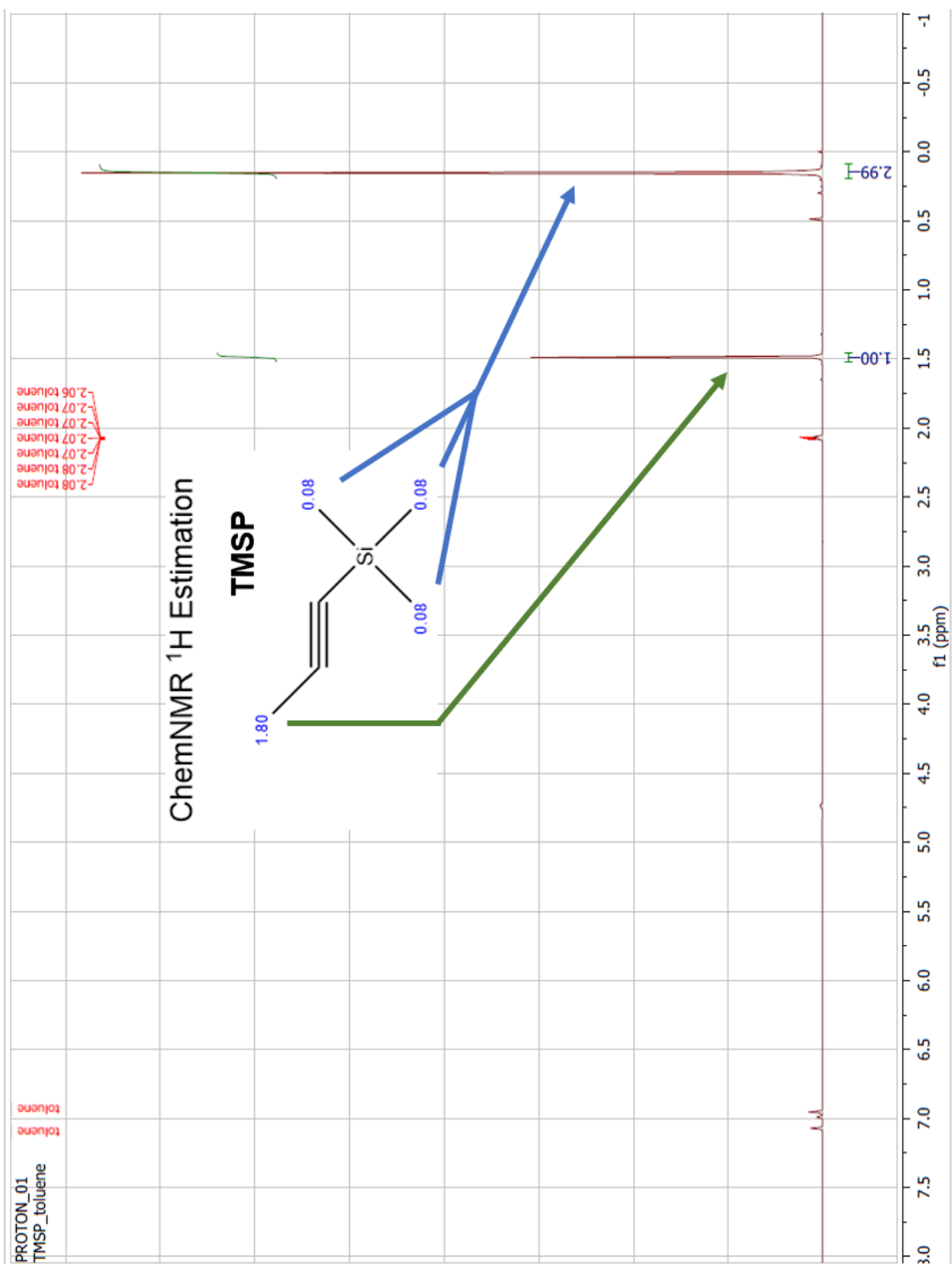
Figure D.3: H-NMR spectrum of TMSP monomer in deuterated toluene.
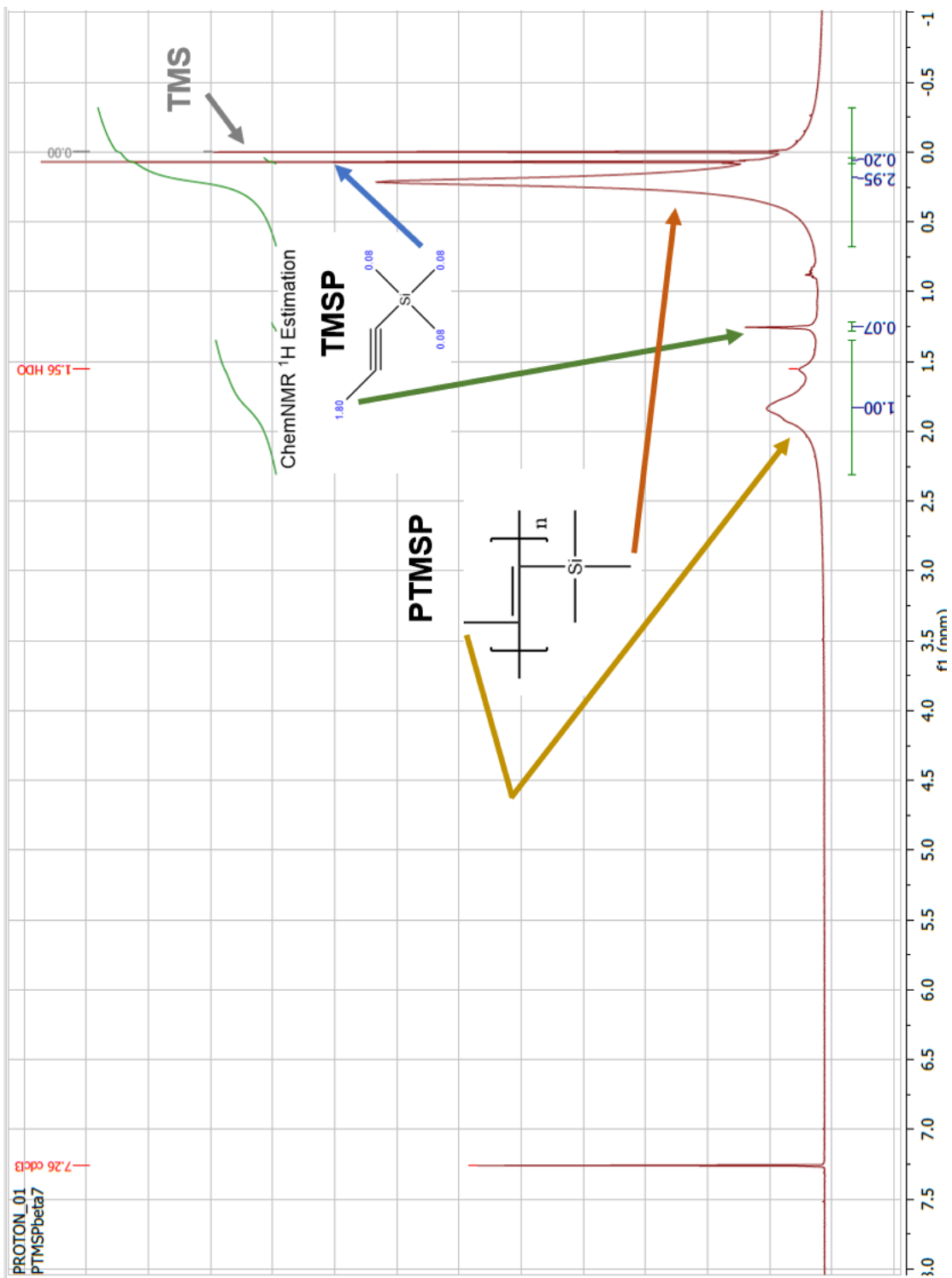
Figure D.4: H-NMR spectrum of PTMSP in deuterated chloroform (CDCl$_3$) with tetramethylsilane (TMS) reference trace.

Appendix E: Tabulated pure-gas permeabilities

This appendix presents the tabulated data from the Figures in Chapter 5 and an additional permeability data Figure for 20$_{wt}$% and 64$_{wt}$% [hmim][Tf$_2$N] in PTMSP SILMs.

Table E.1: Neat PTMSP, 20$_{wt}$% and 64$_{wt}$% [hmim][Tf2N] in PTMSP SILM gas permeabilities versus transmembrane pressure at 35 ºC.

0% SILM (neat PTMSP)					
Δp H2 [bar]	2.07	4.14	6.21	8.27	10.34
Permeability H2 [Barrer]	16901	16664	16567	15998	16025
P error H2 [Barrer]	741	689	701	869	957
Δp N2 [bar]	2.15	4.09	6.16	8.20	10.24
Permeability N2 [Barrer]	2.28	4.08	6.44	8.43	10.38
P error N2 [Barrer]	6945.9	6315.1	5980.2	5808.4	5604.5
Δp CH4 [bar]	617.62	539.41	493.99	545.04	478.03
Permeability CH4 [Barrer]	15146	14463	13797	13187	12638
P error CH4 [Barrer]	476	492	587	566	504
Δp C2H6 [bar]	2.08	4.12	6.09	8.37	10.70
Permeability C2H6 [Barrer]	27718	23736	21264	19988	19326
P error C2H6 [Barrer]	1208	946	1030	742	901
Δp C3H8 [bar]	2.08	4.03	6.16		
Permeability C3H8 [Barrer]	26951	23875	21916		
P error C3H8 [Barrer]	1025	1250	834		
Δp C2H4 [bar]	2.10	4.10	6.15		
Permeability C2H4 [Barrer]	25971	24209	23574		
P error C2H4 [Barrer]	1241.2	1275	1319.1		
Δp C3H6 [bar]	2.08	4.07	6.16		
Permeability C3H6 [Barrer]	31394	28124	26311		
P error C3H6 [Barrer]	1530	1458.7	1383.2		

Table E.1   (continued)

20% SILM (20wt% [hmim][Tf2N] supported in PTMSP)					
Δp H2 [bar]	2.07	4.28	6.33	8.44	10.49
Permeability H2 [Barrer]	2123.5	2081.2	1940.6	2002.5	1968.3
P error H2 [Barrer]	181.36	92.42	64.11	55.45	48.99
Δp CH4 [bar]	2.55	4.45	6.34	8.51	10.50
Permeability CH4 [Barrer]	881.89	944.41	873.77	878.53	864.54
P error CH4 [Barrer]	61.88	40.64	28.82	24.21	21.51
Δp C2H6 [bar]	2.24	4.18	6.21	8.34	10.21
Permeability C2H6 [Barrer]	1646.8	1660.4	1778.1	1888.9	2003.1
P error C2H6 [Barrer]	130.36	75.21	59.49	52.66	50.46
Δp C3H8 [bar]	1.94	4.05	6.25		
Permeability C3H8 [Barrer]	3799.9	5418.9	7471.3		
P error C3H8 [Barrer]	344.28	251.69	248.85		
64% SILM (64wt% [hmim][Tf2N] supported in PTMSP)					
Δp H2 [bar]	2.22	4.27	6.39	8.37	10.34
Permeability H2 [Barrer]	43.32	43.12	43.15	43.42	43.54
P error H2 [Barrer]	4.01	2.79	2.48	2.37	2.32
Δp CH4 [bar]	2.12	4.19	6.41	8.50	10.43
Permeability CH4 [Barrer]	14.01	13.90	14.06	14.26	14.41
P error CH4 [Barrer]	1.34	0.91	0.81	0.78	0.77
Δp C2H6 [bar]	2.13	4.23	6.26	8.39	10.33
Permeability C2H6 [Barrer]	27.11	30.77	34.67	40.92	47.94
P error C2H6 [Barrer]	2.59	2.00	2.00	2.24	2.56
Δp C3H8 [bar]	1.73	3.60	5.25	6.45	
Permeability C3H8 [Barrer]	56.68	141.63	598.65	2497.1	
P error C3H8 [Barrer]	6.33	9.87	36.13	143.00	

Table E.2: $42_{wt}\%$ [hmim][Tf$_2$N] in PTMSP SILM gas permeabilities versus transmembrane pressure at 35 ºC.

Δp H2 [bar]	1.02	2.04	3.06	4.08		6.12		8.16	10.20
Permeability H2 [Barrer]	94.63	95.40	95.65	95.96		96.23		96.34	96.46
P error H2 [Barrer]	2.34	2.16	2.11	2.11		2.10		2.07	2.08
Δp CH4 [bar]	1.03	2.10	3.13	4.14	5.11	6.15		8.26	10.30
Permeability CH4 [Barrer]	26.07	22.22	21.56	21.24	21.22	21.30		21.59	22.03
P error CH4 [Barrer]	0.41	0.41	0.41	0.41	0.41	0.41		0.42	0.42
Δp C2H6 [bar]	1.04	2.10	3.07	4.10	5.11	6.16		8.24	10.25
Permeability C2H6 [Barrer]	27.32	30.84	33.84	38.51	43.37	48.68		62.47	79.74
P error C2H6 [Barrer]	0.57	0.62	0.67	0.79	0.87	0.95		1.19	1.90
Δp C3H8 [bar]	1.04	2.06	3.08	4.09	5.11	6.13	7.11		
Permeability C3H8 [Barrer]	48.07	75.34	127.89	243.05	531.58	1609.7	4679.1		
P error C3H8 [Barrer]	0.85	1.49	2.78	5.66	19.50	64.03	139.31		

Table E.3: 42$_{wt}$% [emim], [hmim], [hmmim] and [dmim][Tf$_2$N] in PTMSP SILM gas permeabilities versus transmembrane pressure at 35 °C.

42% [emim][Tf2N] in PTMSP							
Δp H2 [bar]	2.2338	3.3935	4.2203	5.3123	6.3625	7.3725	9.3362
Permeability H2 [Barrer]	114.78	115	115.3	115.14	114.69	114.89	115.85
P error H2 [Barrer]	4.3305	4.3388	4.3514	4.346	4.3289	4.3371	4.3964
Δp CH4 [bar]	2.0833	3.1251	4.1371	5.1518	6.1798	7.2137	9.2126
Perm. CH4 [Barrer]	25.616	25.774	25.872	25.933	26.152	26.168	26.425
P error CH4 [Barrer]	0.98269	0.98877	0.99327	0.99593	1.0067	1.0058	1.0172
Δp C3H8 [bar]	2.1107	3.1131	4.1489	5.1913	6.1221	7.2534	7.8034
Perm. C3H8 [Barrer]	124.68	470.3	1906.4	4564.7	5238.7	7079.9	6523
P error C3H8 [Barrer]	4.7704	18.081	73.884	192.03	248.02	402.3	328.25
42% [hmim][Tf2N] in PTMSP							
Δp H2 [bar]	1.078	2.1424	3.2016	4.1832	5.1899	6.0437	8.2992
Perm. H2 [Barrer]	95.432	88.469	86.692	86.619	86.226	84.036	85.38
P error H2 [Barrer]	2.3408	2.1564	2.1128	2.113	2.1024	2.0701	2.0795
Δp CH4 [bar]	1.0714	2.0902	3.1146	4.1803	5.1979	6.2175	8.2376
Perm. CH4 [Barrer]	16.93	16.735	16.777	16.828	16.906	16.985	17.21
P error CH4 [Barrer]	0.41253	0.40766	0.40863	0.40986	0.41176	0.41369	0.41971
Δp C3H8 [bar]	1.0676	2.1025	3.1218	4.1647	5.2129	6.2214	7.2035
Perm. C3H8 [Barrer]	34.913	61.258	114.21	232.2	798.35	2481.4	4866
P error C3H8 [Barrer]	0.85089	1.4924	2.7822	5.6579	19.503	64.026	139.31
42% [hmmim][Tf2N] in PTMSP							
Δp H2 [bar]	1.1197	2.1378	3.1809	4.1883	5.1948	6.2655	8.2959
Permeability H2 [Barrer]	72.854	69.867	69.76	67.209	69.544	70.853	72.227
P error H2 [Barrer]	1.7864	1.7057	1.7032	1.6407	1.6976	1.7296	1.7631
Δp CH4 [bar]	1.0775	2.1078	3.1183	4.1758	5.2028	6.2186	8.2166
Perm. CH4 [Barrer]	16.024	15.687	16.329	17.495	18.182	19.292	20.546
P error CH4 [Barrer]	0.39135	0.38296	0.39891	0.4271	0.44386	0.47094	0.50294
Δp C3H8 [bar]	1.0653	2.0953	3.1189	4.1579	5.1873	6.2203	7.2556
Perm. C3H8 [Barrer]	23.959	43.057	78.961	182.13	579.04	1752.5	3811.4
P error C3H8 [Barrer]	0.59668	1.0677	1.9571	4.5319	14.469	45.932	117.15
42% [dmim][Tf2N] in PTMSP							
Δp H2 [bar]	1.0607	2.0693	3.0835	4.1386	5.1459	6.1553	8.1552
Permeability H2 [Barrer]	45.739	45.123	45.231	45.115	44.036	44.71	44.431
P error H2 [Barrer]	1.7256	1.7024	1.707	1.7029	1.662	1.6878	1.6862
Δp CH4 [bar]	2.0854	3.1204	4.1421	5.1361	6.2291	7.2565	9.3192
Perm. CH4 [Barrer]	11.808	11.936	12.025	12.194	12.231	12.323	12.519
P error CH4 [Barrer]	0.67334	0.6805	0.6857	0.69599	0.69777	0.7031	0.71697
Δp C3H8 [bar]	2.1243	3.1182	4.1542	5.1856	6.2346	7.2489	8.2809
Perm. C3H8 [Barrer]	38.571	66.678	117.07	227.66	449.84	1095.1	2265.9
P error C3H8 [Barrer]	1.9625	3.3947	5.9671	11.588	22.947	58.404	124.31

Table E.4: Constant-volume, variable-pressure permeation experiments sample testing protocol. The criterion for reaching pseudo-steady state is 6 times the time lag.

Step	Upstream pressure [psia]	Hold time [hrs]
Degas	0 (active vacuum)	22
Leak test (step 0)	0 (hold)	1
1	15	2.5
2	30	2.5
3	45	2.5
4	60	2.5
5	75	2.5
6	90	2.5
7	105	2.5
8	120	2.5
9	0 (vent, then vacuum)	1

Table E.5: [N$_{xxxy}$][Tf$_2$N] in PTMSP SILM gas permeabilities versus transmembrane pressure at 35 °C.

31% [N1118][Tf2N] in PTMSP					
Δp [bar]	2.0684	4.1368	6.2053		8.2737
Permeability H2 [Barrer]	111.53	128.13	127.72		127.88
P error H2 [Barrer]	39.104	38.64	40.458		37.475
Permeability CH4 [Barrer]	43.459	45.629	44.523		47.07
P error CH4 [Barrer]	13.813	13.768	13.072		14.301
Permeability C2H6 [Barrer]	115.67	131.58	192.16		210.16
P error C2H6 [Barrer]	37.035	41.157	54.959		65.191
Permeability C3H8 [Barrer]	531.78	1929.5	5663.4		7343
P error C3H8 [Barrer]	182.01	808.34	1659.2		2202
Permeability C2H4 [Barrer]	98.012	122.35	155.32		168.95
P error C2H4 [Barrer]	29.107	35.92	46.293		49.548
Permeability C3H6 [Barrer]	133.99	715.65	1804.7		3320.3
P error C3H6 [Barrer]	46.672	216.15	570.56		1035.8
30% [N1116][Tf2N] in PTMSP					
Δp [bar]	2.0684	4.1368	6.2053	7.5842	8.2737
Permeability H2 [Barrer]	160.27	154.91	210.33		215.98
P error H2 [Barrer]	43.798	38.79	56.089		56.215
Permeability CH4 [Barrer]	48.218	50.507	53.053		57.288
P error CH4 [Barrer]	12.082	12.674	13.607		13.973
Permeability C3H8 [Barrer]	297.55	1518.7	3027.7	4413.9	
P error C3H8 [Barrer]	67.82	484.06	887.85	954.57	
Permeability C3H6 [Barrer]	148.05	1005.7	2583.4		5238.6
P error C3H6 [Barrer]	65.279	279.51	683.45		1181.1
31% [N1114][Tf2N] in PTMSP					
Δp [bar]	2.0684	4.1368	6.2053		8.2737
Permeability H2 [Barrer]	270.5	326.29	320.79		318.04
P error H2 [Barrer]	77.015	96.425	100.55		90.967
Permeability CH4 [Barrer]	52.68	77.564	89.231		89.376
P error CH4 [Barrer]	16.324	23.269	25.174		26.442
Permeability C3H8 [Barrer]	1782.4	4878.7	10387		13447
P error C3H8 [Barrer]	513.65	1395.7	2923.4		3869
Permeability C3H6 [Barrer]	2784	5494.5	11519		15845
P error C3H6 [Barrer]	861.49	1680.7	3172.6		4445.6

Table E.5   (continued)

26% [N1888][Tf2N] in PTMSP					
Δp [bar]	2.0684	4.1368	6.2053		8.2737
Permeability H2 [Barrer]	19561	17784	17823		17847
P error H2 [Barrer]	5106.5	4500.3	4343.7		4375.1
Permeability CH4 [Barrer]	10369	7395.7	6418.3		6182.8
P error CH4 [Barrer]	2563.3	1834.2	1586.2		1519
Permeability C3H8 [Barrer]	6663.2	6179.9	6188.2		6478.2
P error C3H8 [Barrer]	1651.6	1575.8	1617.2		1647.5
Permeability C3H6 [Barrer]	6170.5	5860.6	5835.1		5772.4
P error C3H6 [Barrer]	1541.5	1433.7	1468		1461.9

Table E.6:   Neat PMP and 27_{wt}% [hmim][Tf$_2$N] in PMP SILM gas permeabilities versus transmembrane pressure at 35 ºC.

PMP					
Δp [bar]	2.0684	3.1026	4.1368	5.1711	6.2053
Permeability H2 [Barrer]	2292.4	2315.7	2327	2338.1	2326.5
P error H2 [Barrer]	107.51	117.06	98.629	98.454	92.405
Permeability CH4 [Barrer]	1732.4	1720.3	1705.7	1696.2	1686.1
P error CH4 [Barrer]	96.028	93.707	84.493	85.726	89.509
Permeability C3H8 [Barrer]	2013.9	2309.8	2779.2	3347.5	4021.8
P error C3H8 [Barrer]	181.47	193.73	263.08	294.16	312.18
Permeability C3H6 [Barrer]	1979.4	2243.5	2681.8	3206	3832.7
P error C3H6 [Barrer]	166.21	197.05	215.19	235.06	252.74
27% [hmim][Tf2N] in PMP					
Δp [bar]	2.0684	3.1026	4.1368	5.1711	6.2053
Permeability H2 [Barrer]	77.167	66.223	59.952	58.43	57.735
P error H2 [Barrer]	7.3815	6.0119	6.1299	5.9854	5.8684
Permeability CH4 [Barrer]			8.1176	6.9418	8.3605
P error CH4 [Barrer]			1.4453	1.1696	1.4959
Permeability C3H8 [Barrer]	192.58	292.34	455.85	651.85	990.02
P error C3H8 [Barrer]	76.404	103.47	138.73	185.86	239.28
Permeability C3H6 [Barrer]	173.56	247.29	426.18	578.93	750.98

P error C3H6 [Barrer]	60.182	89.143	115.52	155.86	210.35

Table E.7: Neat PDMS, $20_{wt}\%$ [dmim][Tf_2N]-PDMS, and [P1118][Phos]-PDMS gas permeabilities versus transmembrane pressure at 35 ℃.

PDMS			
Δp [bar]	2.0684	4.1368	6.2053
Permeability H2 [Barrer]	679.27	707.8	650.43
P error H2 [Barrer]	82.91	68.02	41.46
Permeability CH4 [Barrer]	1103.7	1087.4	1034.1
P error CH4 [Barrer]	85.37	69.43	50.39
Permeability C2H6 [Barrer]	2851.9	3106.2	3224.6
P error C2H6 [Barrer]	281.4	253.09	241.4
Permeability C3H8 [Barrer]	6643.6	11065	15560
P error C3H8 [Barrer]	553.1	475.6	387.6
Permeability N2 [Barrer]	278.45	289	271.65
P error N2 [Barrer]	129.86	108.13	98.39
Permeability C2H4 [Barrer]	2958.6	2900.6	2927.5
P error C2H4 [Barrer]	190.96	150.2	141.7
Permeability C3H6 [Barrer]	9342.3	11044	14250
P error C3H6 [Barrer]	961.8	471.8	339.4
20% [dmim][Tf2N]-PDMS			
Δp [bar]	2.0684	4.1368	6.2053
Permeability H2 [Barrer]	455.47	498.24	507.81
P error H2 [Barrer]	90.3	84.2	73.7
Permeability CH4 [Barrer]	995.6	1000.6	1077
P error CH4 [Barrer]	125.2	109.77	95.4
Permeability C2H6 [Barrer]	2177.6	2641.9	2836.8
P error C2H6 [Barrer]	614.4	578.1	492.89
Permeability C3H8 [Barrer]	4214.5	8626.8	11455
P error C3H8 [Barrer]	1229.8	1104.1	1030
Permeability N2 [Barrer]	309.03	328.67	313.68
P error N2 [Barrer]	83.95	75.43	64.32
Permeability C2H4 [Barrer]	3083.4	3143.9	3131.1
P error C2H4 [Barrer]	626.17	523.97	602
Permeability C3H6 [Barrer]	6368.7	8821.6	11941
P error C3H6 [Barrer]	1504.3	1354.7	1363.1

Table E.7   (continued)

20% [P1118][Phos]-PDMS			
Δp [bar]	2.0684	4.1368	6.2053
Permeability H2 [Barrer]	356.02	380.75	323.04
P error H2 [Barrer]	109.23	77.912	55.096
Permeability CH4 [Barrer]	380.11	464.17	491.19
P error CH4 [Barrer]	125.15	135.8	122.21
Permeability C2H6 [Barrer]	1592.5	1839.3	1962.3
P error C2H6 [Barrer]	331.79	378.77	314.97
Permeability C3H8 [Barrer]	5128	6259.6	7465.1
P error C3H8 [Barrer]	790.9	716.4	613.5
Permeability C2H4 [Barrer]	1174.5	1536.9	1833
P error C2H4 [Barrer]	362.04	348.62	471.55
Permeability C3H6 [Barrer]	3717	3922.9	4045.2
P error C3H6 [Barrer]	517.18	484.4	455.1

Table E.8: CH_4 aging study in neat PTMSP and 10_{wt}% [emim][Tf2N] in PTMSP SILM at 35 ℃.

	neat PTMSP		10wt% [emim][Tf2N] in PTMSP	
Time [hrs]	Perm. CH4 [Barrer]	P/P0	Perm. CH4 [Barrer]	P/P0
0	12103	1	3572.3	1
12	8794	0.7266	2454.2	0.68701
24	6941	0.57349	1687.9	0.4725
36	5361	0.44295	1330.6	0.37248
48	4044	0.33413	1103	0.30876
72	2497	0.20631	709.49	0.19861
96	1889.6	0.15608	536.52	0.15019
120	1578.8	0.13045	454.36	0.12719
144	1358	0.1122	387.85	0.10857
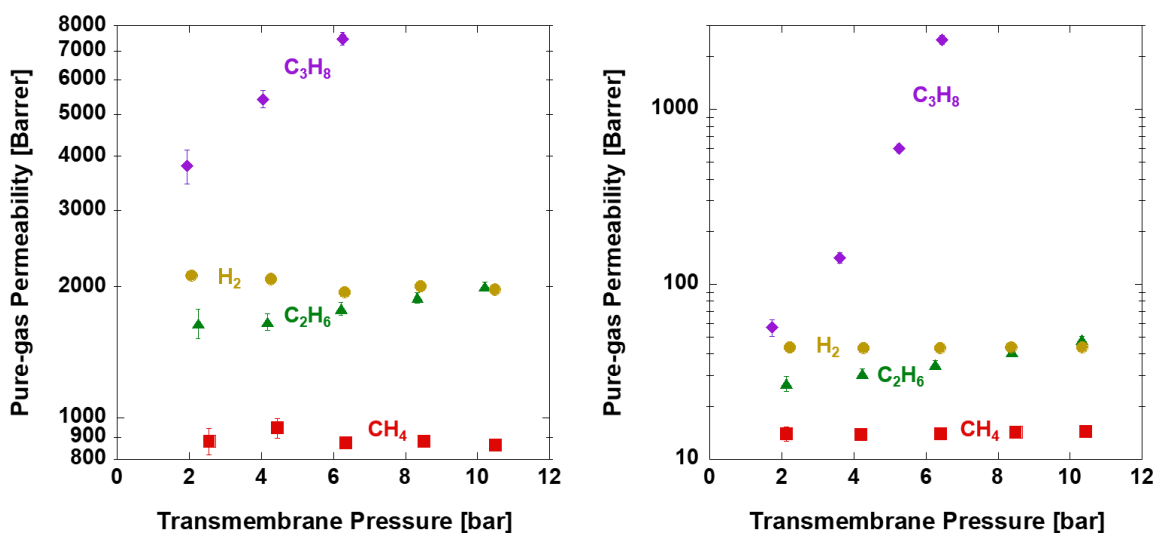
Figure E.1: Pure-gas permeabilities versus transmembrane pressure in 20_{wt}% (left) and 64_{wt}% [hmim][Tf$_2$N] in PTMSP SILM (right) at 35 °C. Thanks to Dr. Jaesung Park, who graciously assisted with these measurements.

Appendix F: Tabulated mixed-gas permeabilities

This appendix presents the tabulated data from Figure 6-1 through Figure 6-4 in Chapter 6.

Table F.1: CO_2-C_2H_6 mixed-gas permeabilities versus mixture component fugacity at 35 ℃. All permeabilities are in [Barrer] and all fugacities are in [bar].

This study										
	100% CO2		70% CO2		50% CO2		25% CO2		10% CO2	
CO2 fugacity	Perm.	Error	Perm.	Error	Perm.	Error	Perm.	Error	Perm.	Error
4.1034	312.54	8.174								
10.635	336.54	10.76								
15.283	363.17	11.301								
3.8104			323.51	12.117						
7.5484			347.57	14.182						
12.963			351.17	10.103						
2.6843					321.52	7.2309				
5.2243					331.79	8.6381				
8.8986					338.7	9.5067				
1.4847							316.21	10.276		
2.8166							328.95	5.944		
5.1626							331.31	6.1681		
0.5551									308.95	21.466
1.1285									317.4	7.8363
2.1738									318.48	6.3818
Ribeiro, 2011 SI: data at 35 °C [1]										
	100% CO2		70% CO2		50% CO2		25% CO2		10% CO2	
CO2 fugacity	Perm.	Error	Perm.	Error	Perm.	Error	Perm.	Error	Perm.	Error
4.4385	336.5									
6.3864	344.98									
8.7401	366.29									
11.337	378.51									
10.627	356.48									
13.813	375.95									
13.732	397.37									
16.207	410.63									
16.369	392.91									
18.642	418.6									
18.479	428.66									

Table F.1   (continued)

CO2 fugacity	100% CO2 Perm.	Error	70% CO2 Perm.	Error	50% CO2 Perm.	Error	25% CO2 Perm.	Error	10% CO2 Perm.	Error
2.5921			328.6							
3.1602			324.17							
3.6675			318.54							
4.6211			324.17							
5.3313			335.36							
6.1835			331.4							
7.6647			338.98							
8.0096			339.56							
9.6937			343.03							
9.7749			358.1							
11.297			358.3							
11.337			365.47							
12.839			372.56							
1.8414					339.94					
2.2472					320.52					
2.5515					321.07					
3.3834					326.01					
3.8298					328.79					
4.4791					334.98					
5.3922					333.85					
5.5545					334.6					
5.7371					341.1					
7.0154					337.83					
6.9545					345.17					
8.0096					346.15					
8.1719					348.51					
9.3488					357.29					
9.3894					362.38					
1.4153							320.16			
2.2674							324.17			
2.8964							327.3			
3.5052							327.49			
4.1139							341.87			
4.1545							352.47			
4.7226							358.71			
3.5255							344.2			
2.8964							339.17			
0.78625									320.16	
1.1109									327.49	
1.4355									330.84	
1.679									331.96	
1.9225									335.74	
0.42103									335.36	

Table F.1   (continued)

This study										
	100% C2H6		90% C2H6		75% C2H6		50% C2H6		30% C2H6	
C2H6 fugacity	Perm.	Error	Perm.	Error	Perm.	Error	Perm.	Error	Perm.	Error
5.355	48.239					1.5426				
9.9003	49.614					1.9256				
15.776	52.861					1.4511				
4.6874		48.788					2.0274			
8.9866		48.614					1.4082			
15.297		52.656					0.98664			
3.7692			48.466					1.0643		
7.4705			50.234					1.3988		
12.247			58.189					0.87763		
2.7446				49.563					2.0379	
5.2656				55.67					1.3126	
8.7372				62.65					1.6071	
1.3835					55.449					1.6422
2.603					60.735					1.5086
4.3572					65.856					2.1297
Ribeiro, 2011 SI: data at 35 °C [1]										
	100% C2H6		90% C2H6		75% C2H6		50% C2H6		30% C2H6	
C2H6 fugacity	Perm.	Error	Perm.	Error	Perm.	Error	Perm.	Error	Perm.	Error
4.2318	50.118									
6.1391	49.941									
8.7219	51.298									
11.027	52.537									
13.51	54.366									
15.517	55.959									
17.305	57.493									
3.8345			49.587							
6.6954			50.236							
9.3179			51.888							
11.94			54.189							
13.907			55.457							
15.715			56.903							
4.1126					50.767					
6.457					52.478					
8.2451					53.835					

Table F.1　　(continued)

C2H6 fugacity	100% C2H6		90% C2H6		75% C2H6		50% C2H6		30% C2H6	
	Perm.	Error	Perm.	Error	Perm.	Error	Perm.	Error	Perm.	Error
8.2848					54.13					
9.8742					54.956					
9.9736					56.047					
11.503					57.847					
11.623					58.732					
13.133					60.678					
2.5232							48.525			
1.808							50.354			
2.2053							50.354			
3.298							50.472			
3.755							52.832			
4.3709							53.009			
5.404							53.628			
5.2252							54.425			
5.5629							55.31			
6.7351							55.546			
6.6954							57.788			
7.6689							57.876			
7.8279							59.528			
8.9206							61.976			
8.8808							62.035			
1.0927									50.059	
1.5497									49.086	
1.947									50.295	
1.3311									51.888	
2.6027									52.478	
2.245									53.953	
3.3576									54.661	
3.1987									56.077	
4.0331									57.139	
4.7086									60.678	
4.0729									60.855	
4.7086									63.274	
5.3444									64.277	

Table F.2: CH_4, C_2H_6, and C_3H_8 pure-gas permeabilities versus fugacity and CH_4-C_2H_6 or CH_4-C_3H_8 mixed-gas permeabilities versus C_{2+} fugacity at 35 ºC. All permeabilities have units of [Barrer] and fugacities have units of [bar].

Pure-component fugacity	Perm. CH4	Error CH4	Perm. C2H6	Error C2H6	Perm. CH4	Error CH4	Perm. C3H8	Error C3H8
2.1431	15196	477.58			15196	477.58		
4.062	14553	495.07			14553	495.07		
6.1025	13928	592.57			13928	592.57		
8.0931	13357	573.28			13357	573.28		
10.077	12841	512.1			12841	512.1		
2.0509			28110	1225.1				
4.0016			24416	973.09				
5.8346			22180	1074.4				
7.8944			21187	786.5				
9.9295			20828	971				
2.0209							27768	1056.1
3.7988							25317	1325.5
5.6221							24005	913.51
	CH4 (mixed with C2H6)				CH4 (mixed with C3H8)			
C2+ mixture component fugacity	Perm. CH4	Error CH4	Perm. C2H6	Error C2H6	Perm. CH4	Error CH4	Perm. C3H8	Error C3H8
1.0874	8490.2	916	23776	1705				
2.3692	6000.2	721	17362	1460				
4.1058	5178.6	688	15323	1396				
2.9528					2626.8	515	20851	1842
1.4694					3265.3	538	23522	2012
4.1457					2227.3	487	19792	1771

Table F.3: CH_4-C_2H_6 mixed-gas permeabilities versus mixture component fugacity in $42_{wt}\%$ [hmim][Tf_2N] in PTMSP SILM at 35 °C. Permeabilities have units of [Barrer] and fugacities have units of [bar].

	100% CH4		90% CH4		75% CH4		50% CH4	
CH4 fugacity	Perm. CH4	Error CH4	Perm. CH4	Error CH4	Perm. CH4	Error CH4	Perm. CH4	Error CH4
4.0027	29.217	4.0629						
3.5298			24.959	3.8992				
2.8238					29.747	5.6767		
2.0167							29.146	7.6848
8.082	27.325	2.1503						
7.1649			25.305	2.2704				
5.6213					29.358	3.0355		
4.0442							32.782	4.4977
15.893	30.225	1.6769						
15.331			29.083	1.6417				
11.191					36.49	2.3747		
8.0364							47.192	3.7447
	100% C2H6		50% C2H6		25% C2H6		10% C2H6	
C2H6 fugacity	Perm. C2H6	Error C2H6	Perm. C2H6	Error C2H6	Perm. C2H6	Error C2H6	Perm. C2H6	Error C2H6
4.1349	52.897	8.496						
2.1167			44.606	11.268				
1.2074					40.767	17.785		
0.44669							41.474	38.686
8.053	71.321	7.1152						
4.1412			51.343	6.8988				
2.3661					46.591	10.538		
0.87869							42.173	22.31
15.329	174.26	5.8529						
7.6501			77.942	6.4531				
4.5596					61.016	7.5618		
1.7919							51.569	15.256

Table F.4: CH_4-C_3H_8 mixed-gas permeabilities versus mixture component fugacity in $42_{wt}\%$ [hmim][Tf_2N] in PTMSP SILM at 35 °C. Permeabilities have units of [Barrer] and fugacities have units of [bar].

C3H8 fugacity	100% CH4		10% C3H8		90% CH4		20% C3H8		80% CH4		40% C3H8		60% CH4		70% C3H8		30% CH4		90% C3H8		10% CH4		100% C3H8		CH4 fugacity
	Perm. CH4	Error CH4	Perm. C3H8	Error C3H8	Perm. CH4	Error CH4	Perm. C3H8	Error C3H8	Perm. CH4	Error CH4	Perm. C3H8	Error C3H8	Perm. CH4	Error CH4	Perm. C3H8	Error C3H8	Perm. CH4	Error CH4	Perm. C3H8	Error C3H8	Perm. CH4	Error CH4	Perm. C3H8	Error C3H8	
3.9782	29.132	4.3681																					543.05	121.5	4.0027
3.5589			57.491	15.58	29.892	4.0007																			3.7435
2.8057							59.041	12.092	32.835	4.8791															3.298
1.6567											79.183	14.086	42.882	5.8334											2.3473
0.75189															165.14	29.251	72.946	9.8079							1.2116
0.32492																			668.57	234.9	258.15	107.15			0.52466
6.6836	27.325	3.0418																					4679.1	630.14	8.082
6.3561			66.103	10.466	34.036	2.984																			6.3198
4.841							75.627	8.1438	39.796	3.4352															5.639
2.8468											166.67	15.994	69.327	5.9483											4.111
1.3809															1368.6	258.09	350.93	43.512							2.0628
0.73479																			5177	878.8	1187.7	268.49			1.2434

163

Figure F.1: Expanded a) CH$_4$-C$_2$H$_6$ and b) CH$_4$-C$_3$H$_8$ size-selective and c) C$_2$H$_6$-CH$_4$ and d) C$_3$H$_8$-CH$_4$ reverse-selective upper bound plots in black and white.

APPENDIX F REFERENCES

[1]   C.P. Ribeiro, B.D. Freeman, D.R. Paul, Pure- and mixed-gas carbon dioxide/ethane permeability and diffusivity in a cross-linked poly(ethylene oxide) copolymer, Journal of Membrane Science, 377 (2011) 110-123.

Appendix G: Tabulated pure-gas sorption and diffusion data

This appendix presents the tabulated data from Figure 7.1 through Figure 7.4 in Chapter 7.

Table G.1: CH$_4$ pure-gas raw concentration data versus pressure for neat PTMSP and 20$_{wt}$%, 42$_{wt}$%, and 60$_{wt}$% [hmim][Tf$_2$N] in PTMSP SILMs at 35 ºC.

	p [bar]	2	4.99	9.99	15	19.99	22.68						
PTMSP (MSB)	C [cm^3(STP)/cm^3]	5.9787	13.522	23.827	32.238	39.251	42.66						
	p [bar]	0.53	1.06	2.10	3.12	4.13	6.12	8.20	10.24	15.37	20.48	25.595	30.67
PTMSP (P-D)	C [cm^3(STP)/cm^3]	1.5205	3.0898	5.6097	7.9174	10.675	15.316	19.341	23.086	31.67	38.694	44.753	50.05
	p [bar]	0.57	1.05	2.13	3.17	4.20	5.22	7.28	10.36				
PTMSP [1]	C [cm^3(STP)/cm^3]	1.97	3.58	6.95	9.95	12.71	15.27	19.99	26.09				
	p [bar]	2.02	5.02	10.03	15.03	20.04	25.04	30.04					
20% SILM	C [cm^3(STP)/cm^3]	1.4949	4.824	9.5904	13.723	17.406	20.785	23.939					
	p [bar]	2.02	5.04	10.04	15.03	20.04	25.04	30.04					
42% SILM	C [cm^3(STP)/cm^3]	1.0857	2.8109	5.4237	7.8991	10.263	12.504	14.654					
	p [bar]	2.02	5.02	10.03	15.03	20.04	25.04	30.04					
60% SILM	C [cm^3(STP)/cm^3]	0.3764	1.2773	2.7378	4.2447	5.6823	7.1282	8.5344					

Table G.2: C$_2$H$_6$ pure-gas raw concentration data versus pressure for neat PTMSP and 20$_{wt}$%, 42$_{wt}$%, and 60$_{wt}$% [hmim][Tf$_2$N] in PTMSP SILMs at 35 ºC.

	p [bar]	2	4.99	9.99	15.1	20.03	25.03						
PTMSP (MSB)	C [cm^3(STP)/cm^3]	29.281	50.728	70.933	85.023	97.139	109.23						
	p [bar]	2	5	10	15	20	25						
PTMSP [1]	C [cm^3(STP)/cm^3]	29.73	49.56	66.48	77.63	86.74	94.886						
	p [bar]	2	2.03	4.01	5.03	7.02	10.02	10.03	10.42	15.04	20.05	25.06	30.07
20% SILM	C [cm^3(STP)/cm^3]	14.644	14.606	22.805	25.795	32.525	40.738	40.534	41.747	53.044	66.418	80.598	94.968
	p [bar]	2.02	5.03	10.03	15.04	20.06	21.16						
42% SILM	C [cm^3(STP)/cm^3]	3.1301	7.6474	16.026	25.524	36.986	40.073						
	p [bar]	2.02	5.03	10.03	15.04	20.06	21.16						
60% SILM	C [cm^3(STP)/cm^3]	3.1301	7.6474	16.026	25.524	36.986	40.073						

Table G.3: C_3H_8 pure-gas raw concentration data versus pressure for neat PTMSP and $20_{wt}\%$, $42_{wt}\%$, and $60_{wt}\%$ [hmim][Tf$_2$N] in PTMSP SILMs at 35 ºC.

	p [bar]	0.29662	0.54	1.03	2.03	3.24	4.44	5.63	6.84
PTMSP (MSB)	C [cm³(STP)/cm³]	21.391	32.999	43.718	56.604	68.107	78.084	87.842	98.316
	p [bar]	0.15199	0.50662	1.3172	2.3811	3.6477			
PTMSP [1]	C [cm³(STP)/cm³]	11	31	48	60	71.5			
	p [bar]	0.52	1.04	2.04	3.25	4.45	5.64	6.3	
20% SILM	C [cm³(STP)/cm³]	14.144	19.913	29.31	38.976	50.423	63.221	68.521	
	p [bar]	0.46353	0.97299	1.8865	2.8352	3.8189	4.8027	5.7161	6.6034
42% SILM	C [cm³(STP)/cm³]	4.7713	8.8268	14.314	20.994	26.958	32.206	38.409	46.281
	p [bar]	0.30995	0.55	1.04	2.09	3.24	4.44	5.6499	6.8597
60% SILM	C [cm³(STP)/cm³]	1.8768	3.0028	5.4429	11.098	19.37	29.905	44.047	63.206
	p [bar]	0.144	0.248	0.489	0.689	1.029	1.324	1.797	1.934
[hmim][Tf2N] [2]	C [cm³(STP)/cm³]	0.4	0.6	1.1	1.5	2.3	3	4.1	4.4

Table G.4: CH_4, C_2H_6, and C_3H_8 permeabilities in [Barrer], solubilities in [cm³(STP) cm^{-3} cmHg^{-1}] and diffusivities in [cm²/s] in $60_{wt}\%$ [hmim][Tf$_2$N] in PTMSP SILMs at 35 ºC. The $64_{wt}\%$ SILM permeability raw data was used as an approximation of a $60_{wt}\%$ SILM.

CH4						
p [bar]	P	P error	S	S error	D	D error
2.1229	14.01	1.3407	0.003692	4.90E-04	3.80E-07	6.21E-08
4.1851	13.9	0.90735	0.00369	5.16E-04	3.77E-07	5.81E-08
6.4149	14.06	0.80606	0.003689	5.02E-04	3.81E-07	5.63E-08
8.504	14.26	0.77787	0.003688	4.95E-04	3.87E-07	5.60E-08
10.428	14.41	0.76766	0.003687	4.90E-04	3.91E-07	5.60E-08
C2H6						
p [bar]	P	P error	S	S error	D	D error
2.1263	27.11	2.5912	0.021122	3.49E-03	1.28E-07	2.45E-08
4.2341	30.77	1.9994	0.020988	2.34E-03	1.47E-07	1.89E-08
6.257	34.67	1.9988	0.021133	2.11E-03	1.64E-07	1.89E-08
8.3909	40.92	2.2363	0.021502	2.04E-03	1.90E-07	2.08E-08
10.333	47.94	2.5562	0.021992	2.04E-03	2.18E-07	2.33E-08
C3H8						
p [bar]	P	P error	S	S error	D	D error
1.7333	56.68	6.3253	0.075899	1.46E-02	7.47E-08	1.66E-08
3.6025	141.63	9.8675	0.084208	1.03E-02	1.68E-07	2.37E-08
5.2524	598.65	36.127	0.094583	9.89E-03	6.33E-07	7.64E-08
6.4486	2497.1	143	0.10374	1.03E-02	2.41E-06	2.76E-07

Table G.5: CH_4, C_2H_6, and C_3H_8 permeabilities in [Barrer], solubilities in [cm^3(STP) cm^{-3} $cmHg^{-1}$] and diffusivities in [10^{-6} cm^2/s] in neat PTMSP at 35 ºC.

CH4						
p [bar]	P	P error	S	S error	D	D error
1.0132			0.040427	8.89394E-05		
2.1502	15146	476			41.518	2.7385
3.1634			0.037744	8.30368E-05		
4.0873	14463	492			41.924	2.973
5.1005			0.035676	9.27576E-05		
6.1604	13797	587			42.249	3.693
7.1736			0.033754	0.000084385		
8.1972	13187	566			42.434	3.7402
9.2104			0.032105	7.38415E-05		
10.239	12638	504			42.582	3.5015
11.252			0.030647	6.74234E-05		
C2H6						
p [bar]	P	P error	S	S error	D	D error
1.0132			0.23444	0.00304772		
2.0799	27718	1208			20.677	1.8491
3.1634			0.16694	0.001469072		
4.1162	23736	946			21.974	1.8058
5.1005			0.13299	0.001303302		
6.0858	21264	1030			22.986	2.2738
7.1736			0.11277	0.000733005		
8.3679	19988	742			24.815	1.9081
9.2104			0.097168	0.00069961		
10.701	19326	901			26.816	2.5573
11.252			0.086113	0.000602791		
C3H8						
p [bar]	P	P error	S	S error	D	D error
1.0132			0.56627	0.0113254		
2.0822	26951	1025			17.354	1.3649
3.0954			0.28983	0.0057966		
4.0283	23875	1250			17.724	1.8895
5.0415			0.22144	0.00287872		
6.1581	21916	834			17.64	1.3881
7.1713			0.1867	0.00028005		

167
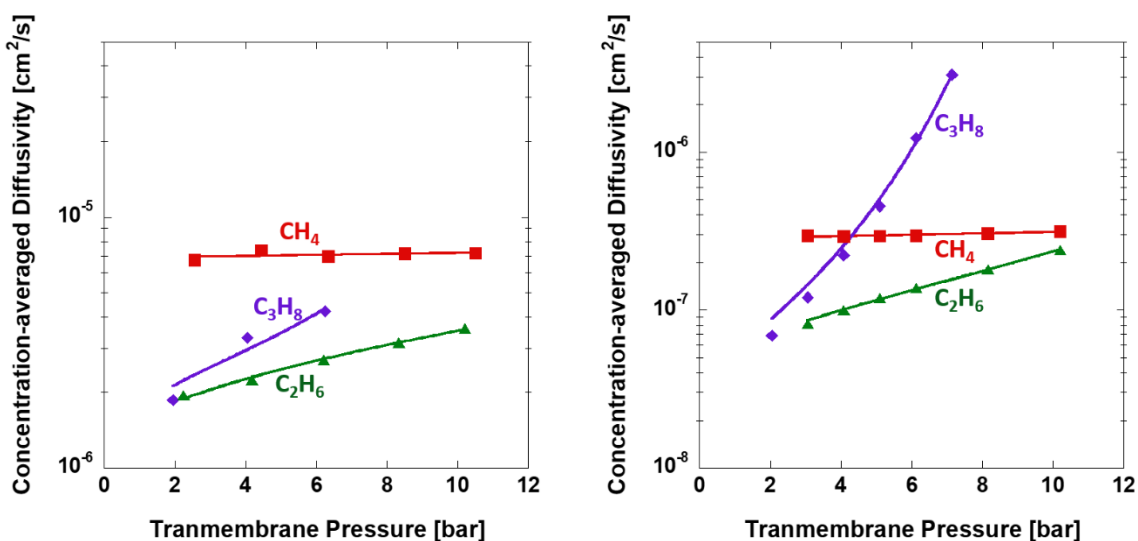
Figure G.1: Pure-gas effective concentration-averaged diffusivities versus transmembrane pressure in $20_{wt}\%$ (left) and $42_{wt}\%$ [hmim][Tf$_2$N] in PTMSP SILM (right) at 35 °C.

APPENDIX G REFERENCES

[1] T.C. Merkel, V.I. Bondar, K. Nagai, B.D. Freeman, Sorption and Transport of Hydrocarbon and Perfluorocarbon Gases in Poly(1-trimethylsilyl-1-propyne), Journal of Polymer Science Part B: Polymer Physics 38 (2000) 415-434.

[2] C. Miguel Sanchez, T. Song, J.F. Brennecke, B.D. Freeman, Hydrogen Stable Supported Ionic Liquid Membranes with Silver Carriers: Propylene and Propane Permeability and Solubility, Industrial & Engineering Chemistry Research, 59 (2020) 5362-5370.

Bibliography

Y. Agata, H. Yamamoto, Determination of Hansen solubility parameters of ionic liquids using double-sphere type of Hansen solubility sphere method, Chemical Physics, 513 (2018) 165-173.

A. Ahosseini, A.M. Scurto, Viscosity of Imidazolium-Based Ionic Liquids at Elevated Pressures: Cation and Anion Effects, International Journal of Thermophysics, 29 (2008) 1222-1243.

A. Ahosseini, B. Sensenich, L.R. Weatherley, A.M. Scurto, Phase Equilibrium, Volumetric, and Interfacial Properties of the Ionic Liquid, 1-Hexyl-3-methylimidazolium Bis(trifluoromethylsulfonyl)amide and 1-Octene, Journal of Chemical & Engineering Data, 55 (2010) 1611-1617.

N.Y. Alaslai, Gas Sorption, Diffusion and Permeation in a Polymer of Intrinsic Microporosity (PIM-7), M.S. Thesis, King Abdullah University of Science and Technology, Thuwal, Saudi Arabia, 2013.

F.I Alghunaimi, The Performance of a Thermally Cross-Linked Polymer of Intrinsic Microporosity (PIM-1) for Gas Separation, M.S. Thesis, King Abdullah University of Science and Technology, Thuwal, Saudi Arabia, 2013.

A.T. Alhazmi, Tröger's Base Ladder Polymer for Membrane-Based Hydrocarbon Separation, M.S. Thesis, King Abdullah University of Science and Technology, Thuwal, Saudi Arabia, 2017.

Y. Alqaheem, A. Alomair, M. Vinoba, A. Pérez, Polymeric Gas-Separation Membranes for Petroleum Refining, International Journal of Polymer Science, 2017 (2017) 4250927.

M. Althuluth, M.C. Kroon, C.J. Peters, Solubility of Methane in the Ionic Liquid 1-Ethyl-3-methylimidazolium Tris(pentafluoroethyl)trifluorophosphate, Industrial & Engineering Chemistry Research, 51 (2012) 16709-16712.

M. Althuluth, M.T. Mota-Martinez, A. Berrouk, M.C. Kroon, C.J. Peters, Removal of small hydrocarbons (ethane, propane, butane) from natural gas streams using the

ionic liquid 1-ethyl-3 -methylimidazolium tris(pentafluoroethyl)trifluorophosphate, The Journal of Supercritical Fluids, 90 (2014) 65-72.

M. Althuluth, J.P. Overbeek, H.J. van Wees, L.F. Zubeir, W.G. Haije, A. Berrouk, C.J. Peters, M.C. Kroon, Natural gas purification using supported ionic liquid membrane, Journal of Membrane Science, 484 (2015) 80-86.

C. Altintas, S. Keskin, Molecular simulations of MOF membranes for separation of ethane/ethene and ethane/methane mixtures, RSC Advances, 7 (2017) 52283-52295.

M.E. Arnold, K. Nagai, B.D. Freeman, R.J. Spontak, D.E. Betts, J.M. DeSimone, I. Pinnau, Gas Permeation Properties of Poly(1,1'-dihydroperfluorooctyl acrylate), Poly(1,1'-dihydroperfluorooctyl methacrylate), and Poly(styrene)-b-poly(1,1'-dihydroperfluorooctyl acrylate) Block Copolymers, Macromolecules, 34 (2001) 5611-5619.

R.W. Baker, K. Lokhandwala, Natural Gas Processing with Membranes: An Overview, Industrial Engineering Chemistry Research 47 (2008) 2109-2121.

H. Balcar, P. Topka, J. Sedláček, J. Zedník, J. Čejka, Polymerization of aliphatic alkynes with heterogeneous Mo catalysts supported on mesoporous molecular sieves, Journal of Polymer Science Part A: Polymer Chemistry, 46 (2008) 2593-2599.

L.A. Banu, D. Wang, R.E. Baltus, Effect of Ionic Liquid Confinement on Gas Separation Characteristics, Energy & Fuels, 27 (2013) 4161-4166.

S. Bazhenov, A. Malakhov, D. Bakhtin, V. Khotimskiy, G. Bondarenko, V. Volkov, M. Ramdin, T.J.H. Vlugt, A. Volkov, CO_2 stripping from ionic liquid at elevated pressures in gas-liquid membrane contactor, International Journal of Greenhouse Gas Control, 71 (2018) 293-302.

C.L. Bentley, T. Song, B.J. Pedretti, M.J. Lubben, N.A. Lynd, J.F. Brennecke, Effects of Poly(glycidyl ether) Structure and Ether Oxygen Placement on CO2 Solubility, Journal of Chemical & Engineering Data, 66 (2021) 2832-2843.

A.R. Berens, Gravimetric and volumetric study of the sorption of gases and vapors in poly(vinyl chloride) powders, Polymer Engineering & Science, 20 (1980) 95-101.

M.V. Bermeshev, A.V. Syromolotov, L.E. Starannikova, M.L. Gringolts, V.G. Lakhtin, Y.P. Yampolskii, E.S. Finkelshtein, Glassy Polynorbornenes with Si–O–Si Containing Side Groups. Novel Materials for Hydrocarbon Membrane Separation, Macromolecules, 46 (2013) 8973-8979.

P. Bernardo, E. Drioli, G. Golemme, Membrane Gas Separation: A Review/State of the Art, Industrial Engineering and Chemistry Research, 48 (2009) 4638-4663.

A. Bondi, van der Waals volumes and radii. The Journal of Physical Chemistry 68 (1964) 441-451.

R.I. Canales, J.F.; Brennecke, Comparison of Ionic Liquids to Conventional Organic Solvents for Extraction of Aromatics from Aliphatics. Journal of Chemical Engineering Data, 61 (2016) 1685-1699.

C. Casado-Coterillo, M. Del Mar López-Guerrero, Á. Irabien, Synthesis and Characterisation of ETS-10/Acetate-based Ionic Liquid/Chitosan Mixed Matrix Membranes for CO_2/N_2 Permeation, Membranes, 4 (2014) 287-301.

P. Chandra, Multi-Component Transport of Gases and Vapors in Poly(ethylene terephthalate), M.S. Thesis, Georgia Institute of Technology, Atlanta, GA, 2006.

S.S. Chang, R. Wang, T.-S. Chung, Y. Liu, C_2 and C_3 hydrocarbon separations in poly(1,5-naphthalene-2,2′-bis(3,4-phthalic) hexafluoropropane)diimide (6FDA-1,5-NDA) dense membranes, Journal of Membrane Science 210 (2002) 55–64.

Y. Changtao, L. Shuyuan, W. Hailong, Y. Fei, x. Xu, Pore structure characteristics and methane adsorption and desorption properties of marine shale in Sichuan Province, China, RSC Advances, 8 (2018) 6436-6443.

A. Chapeaux, L.D. Simoni, T.S. Ronan, M.A. Stadtherr, J.F. Brennecke, Extraction of alcohols from water with 1-hexyl-3-methylimidazolium bis(trifluoromethylsulfonyl)imide, Green Chemistry, 10 (2008) 1301-1306.

171

M.W. Conder, K.A. Lawlor, Production Characteristics Of Liquids-Rich Resource Plays Challenge Facility Design, American Oil & Gas Reporter (2014).

T. Corrado, R. Guo, Macromolecular design strategies toward tailoring free volume in glassy polymers for high performance gas separation membranes, Molecular Systems Design & Engineering, 5 (2020) 22-48.

M.G. Cowan, D.L. Gin, R.D. Noble, Poly(ionic liquid)/Ionic Liquid Ion-Gels with High "Free" Ionic Liquid Content: Platform Membrane Materials for CO2/Light Gas Separations, Accounts of Chemical Research, 49 (2016) 724-732.

D. Craster, T.G.J. Jones, Permeation of a Range of Species through Polymer Layers under Varying Conditions of Temperature and Pressure: In Situ Measurement Methods, Polymers, 11 (2019).

Z. Dai, R.D. Noble, D.L. Gin, X. Zhang, L. Deng, Combination of ionic liquids with membrane technology: A new approach for CO_2 separation, Journal of Membrane Science, 497 (2016) 1-20.

M. Dakkach, F.M. Gaciño, S.K. Mylona, M.J.P. Comuñas, M.J. Assael, J. Fernández, High pressure densities of two nanostructured liquids based on the bis(trifluoromethylsulfonyl)imide anion from (278 to 398) K and up to 120 MPa, The Journal of Chemical Thermodynamics, 118 (2018) 67-76.

M.G. De Angelis, T.C. Merkel, V.I. Bondar, B.D. Freeman, F. Doghieri, G.C. Sarti, Hydrocarbon and fluorocarbon solubility and dilation in poly(dimethylsiloxane): Comparison of experimental data with predictions of the Sanchez–Lacombe equation of state, Journal of Polymer Science Part B: Polymer Physics, 37 (1999) 3011-3026.

K. De Sitter, P. Winberg, J. D'Haen, C. Dotremont, R. Leysen, J.A. Martens, S. Mullens, F.H.J. Maurer, I.F.J. Vankelecom, Silica filled poly(1-trimethylsilyl-1-propyne) nanocomposite membranes: Relation between the transport of gases and structural characteristics, Journal of Membrane Science, 278 (2006) 83-91.

M.T. Demko, J.C. Cheng, A.P. Pisano, Rigid, Vapor-Permeable Poly(4-methyl-2-pentyne) Templates for High Resolution Patterning of Nanoparticles and Polymers, ACS Nano, 6 (2012) 6890-6896.

172

S.E. DeRosa, D.T. Allen, Impact of Natural Gas and Natural Gas Liquids Supplies on the United States Chemical Manufacturing Industry: Production Cost Effects and Identification of Bottleneck Intermediates, ACS Sustainable Chemistry and Engineering, 3 (2015) 451-459.

S.V. Dixon-Garrett, K. Nagai, B.D. Freeman, Sorption, diffusion, and permeation of ethylbenzene in poly(1-trimethylsilyl-1-propyne), Journal of Polymer Science Part B: Polymer Physics, 38 (2000) 1078-1089.

J.H. Dymond, K.N. Marsh, R.C. Wilhoit, K.C. Wond, The Virial Coefficients of Pure Gases and Mixtures, Springer, Darmstadt, 2001.

S. Elhenawy, M. Khraisheh, F. AlMomani, M. Hassan, Key Applications and Potential Limitations of Ionic Liquid Membranes in the Gas Separation Process of CO_2, CH_4, N_2, H_2 or Mixtures of These Gases from Various Gas Streams, Molecules, 25 (2020).

J.R. Elliot and C.T. Lira, Introductory Chemical Engineering Thermodynamics, 2nd Ed, Prentice Hall, Upper Saddle River, NJ, 2012.

S. Faramawy, T. Zakib, A.A.-E. Sakr, Natural gas origin, composition, and processing: A review, Journal of Natural Gas Science and Engineering, 34 (2016) 34-54.

H. Fatoorehchi, R. Rach, H. Sakhaeinia, Explicit Frost-Kalkwarf type equations for calculation of vapour pressure of liquids from triple to critical point by the Adomian decomposition method, The Canadian Journal of Chemical Engineering, 95 (2017) 2199-2208.

H. Feng, Modeling of vapor sorption in glassy polymers using a new dual mode sorption model based on multilayer sorption theory, Polymer, 48 (2007) 2988-3002.

A. Finotello, J.E. Bara, S. Narayan, D. Camper, R.D. Noble, Ideal Gas Solubilities and Solubility Selectivities in a Binary Mixture of Room-Temperature Ionic Liquids, The Journal of Physical Chemistry B, 112 (2008) 2335-2339.

A. Finotello, J.E. Bara, D. Camper, R.D. Noble, Room-Temperature Ionic Liquids: Temperature Dependence of Gas Solubility Selectivity, Industrial & Engineering Chemistry Research, 47 (2008) 3453-3459.

L.J. Florusse, S. Raeissi, C.J. Peters, High-Pressure Phase Behavior of Ethane with 1-Hexyl-3-methylimidazolium Bis(trifluoromethylsulfonyl)imide, Journal of Chemical & Engineering Data, 53 (2008) 1283-1285.

P.J. Flory, Principles of polymer chemistry. Cornell University Press, Ithaca, NY, 1953.

P.G.T. Fogg, W. Gerrard, Solubility of gases in liquids, John Wiley & Sons, Chichester, 1991.

M. Franklin, K. Chau, L.J. Cushing and J.E. Johnston, Characterizing Flaring from Unconventional Oil and Gas Operations in South Texas Using Satellite Observations, Environmental Science & Technology, 53 (2019) 2220-2228.

B.D. Freeman, I. Pinnau, Separation of gases using solubility-selective polymers, Trends in Polymer Science 5 (1997) 167-173.

B.D. Freeman, Basis of Permeability/Selectivity Tradeoff Relations in Polymeric Gas Separation Membranes, Macromolecules, 32 (1999) 375-380.

M. Galizia, W.S. Chi, Z.P. Smith, T.C. Merkel, R.W. Baker, B.D. Freeman, 50th Anniversary Perspective: Polymers and Mixed Matrix Membranes for Gas and Vapor Separation: A Review and Prospective Opportunities, Macromolecules, 50 (2017) 7809-7843.

G. Genduso, B.S. Ghanem, I. Pinnau, Experimental Mixed-Gas Permeability, Sorption and Diffusion of CO_2-CH_4 Mixtures in 6FDA-mPDA Polyimide Membrane: Unveiling the Effect of Competitive Sorption on Permeability Selectivity, Membranes, 9 (2019).

G.S. Golubev, I.L. Borisov, V.V. Volkov, Performance of Commercial and Laboratory Membranes for Recovering Bioethanol from Fermentation Broth by Thermopervaporation, Russian Journal of Applied Chemistry, 91 (2018) 1375-1381.

A.S.L. Gouveia, M. Yáñez, V.D. Alves, J. Palomar, C. Moya, D. Gorri, L.C. Tomé, I.M. Marrucho, CO_2/H_2 separation through poly(ionic liquid)–ionic liquid membranes: The effect of multicomponent gas mixtures, temperature and gas feed pressure, Separation and Purification Technology, 259 (2021) 118113.

E.A. Grushevenko, I.L. Borisov, D.S. Bakhtin, G.N. Legkov, G.N. Bondarenko, A.V. Volkov, Membrane Material Based on Octyl-Substituted Polymethylsiloxane for Separation of C_3/C_1 Hydrocarbons, Petroleum Chemistry 57 (2017) 334-340.

K. Haraya, K. Obata, T. Hakuta, H. Yoshitom, The permeation of gases through a new type polyimide membrane, Membrane 11 (1986) 48-52.

T. Harlacher, M. Wessling, Gas–gas separation by membranes. In Progress in Filtration and Separation, Elsevier: New York, NY, USA (2015) 557–584.

W. Hayduk, E.B. Walter, P. Simpson, Solubility of propane and carbon dioxide in heptane, dodecane, and hexadecane, Journal of Chemical & Engineering Data, 17 (1972) 59-61.

N.L. Helgeson, B.H. Sage, Latent heat of vaporization of propane, Journal of Chemical & Engineering Data, 12 (1967) 47-49.

J. Horiuti, The solubility of gas and coefficient of dilation by adsorption, Scientific Papers of the Institute of Physical and Chemical Research, 17 (1931) 125-256.

H. Hou, J.C. Holste, K.R. Hall, K.N. Marsh, B.E. Gammon, Second and Third Virial Coefficients for Methane + Ethane and Methane + Ethane + Carbon Dioxide at (300 and 320) K, Journal of Chemical & Engineering Data, 41 (1996) 344-353.

S.O. Ilyin, V.V. Makarova, M.P. Arinina, E.G. Litvinova, V.S. Khotimskii, V.G. Kulichikhin, Phase equilibrium and rheology of poly(1-trimethylsilyl-1-propyne) solutions, Polymer Science, Series A, 59 (2017) 1-11.

A. Ito, T. Yasuda, T. Yoshioka, A. Yoshida, X. Li, K. Hashimoto, K. Nagai, M. Shibayama, M. Watanabe, Sulfonated Polyimide/Ionic Liquid Composite Membranes for CO_2 Separation: Transport Properties in Relation to Their Nanostructures, Macromolecules, 51 (2018) 7112-7120.

A. Iulianelli, E. Drioli, Membrane engineering: Latest advancements in gas separation and pre-treatment processes, petrochemical industry and refinery, and future perspectives in emerging applications, Fuel Processing Technology, 206 (2020) 106464.

T. James, S. Phil, M. Erin, Natural Gas Processing, Energy Information Administration, Office of Oil and Gas, 2006.

Y. Kamiya, Y. Naito, K. Terada, K. Mizoguchi, A. Tsuboi, Volumetric Properties and Interaction Parameters of Dissolved Gases in Poly(dimethylsiloxane) and Polyethylene, Macromolecules, 33 (2000) 3111-3119.

S. Kanehashi, K. Nagai, Analysis of dual-mode model parameters for gas sorption in glassy polymers, Journal of Membrane Science, 253 (2005) 117-138.

E.J. Kappert, M.J.T. Raaijmakers, K. Tempelman, F.P. Cuperus, W. Ogieglo, N.E. Benes, Swelling of 9 polymers commonly employed for solvent-resistant nanofiltration membranes: A comprehensive dataset, Journal of Membrane Science, 569 (2019) 177-199.

S. Kasahara, E. Kamio, A. Otani, H. Matsuyama, Fundamental Investigation of the Factors Controlling the CO_2 Permeability of Facilitated Transport Membranes Containing Amine-Functionalized Task-Specific Ionic Liquids, Industrial & Engineering Chemistry Research, 53 (2014) 2422-2431.

A. Keller, The Lower Carbon Hydrocarbons Leading a US Manufacturing Renaissance, Wood Mackenzie, 2018, 5-12.

S.D. Kelman, B.W. Rowe, C.W. Bielawski, S.J. Pas, A.J. Hill, D.R. Paul, B.D. Freeman, Crosslinking poly[1-(trimethylsilyl)-1-propyne] and its effect on physical stability, Journal of Membrane Science, 320 (2008) 123-134.

A. Khakpay, P. Scovazzo, Reverse-selective behavior of room temperature ionic liquid-based membranes for natural gas processing. Journal of Membrane Science, 545 (2018) 204-212.

A. Khosravi, M. Sadeghi, H.Z. Banadkohi, M.M. Talakesh, Polyurethane-silica nanocomposite membranes for separation of propane/methane and

ethane/methane, Industrial Engineering and Chemistry Research 53 (2014) 2011-2021.

P. Kilaru, G.A. Baker, P. Scovazzo, Density and Surface Tension Measurements of Imidazolium-, Quaternary Phosphonium-, and Ammonium-Based Room-Temperature Ionic Liquids: Data and Correlations, Journal of Chemical & Engineering Data, 52 (2007) 2306-2314.

M. Klepić, K. Setničková, M. Lanč, M. Žák, P. Izák, M. Dendisová, A. Fuoco, J.C. Jansen, K. Friess, Permeation and sorption properties of CO2-selective blend membranes based on polyvinyl alcohol (PVA) and 1-ethyl-3-methylimidazolium dicyanamide ([EMIM][DCA]) ionic liquid for effective CO_2/H_2 separation, Journal of Membrane Science, 597 (2020) 117623.

J. Kumełan, D. Tuma, G. Maurer, Partial molar volumes of selected gases in some ionic liquids, Fluid Phase Equilibria, 275 (2009) 132-144.

O. Kunz, W. Wagner, The GERG-2008 Wide-Range Equation of State for Natural Gases and Other Mixtures: An Expansion of GERG-2004, Journal of Chemical & Engineering Data, 57 (2012) 3032-3091.

R.J. Lahiere, M.W. Hellums, J.G. Wijmans, J. Kaschemekat, A Membrane Vapor Separation: Recovery of Vinyl Chloride Monomer from PVC Reactor Vents, Industrial Engineering and Chemistry Research, 32 (1993) 2236-2241.

Y. Lan, M.G. Corradini, X. Liu, T.E. May, F. Borondics, R.G. Weiss, M.A. Rogers, Comparing and Correlating Solubility Parameters Governing the Self-Assembly of Molecular Gels Using 1,3:2,4-Dibenzylidene Sorbitol as the Gelator, Langmuir, 30 (2014) 14128-14142.

C.H. Lau, P. Li, F. Li, T. Chung, D.R. Paul, Reverse-selective polymeric membranes for gas separations, Progress in Polymer Science, 38 (2013) 740-766.

C.H. Lau, P.T. Nguyen, M.R. Hill, A.W. Thornton, K. Konstas, C.M. Doherty, R.J. Mulder, L. Bourgeois, A.C.Y. Liu, D.J. Sprouster, J.P. Sullivan, T.J. Bastow, A.J. Hill, D.L. Gin, R.D. Noble, Ending Aging in Super Glassy Polymer Membranes, Angewandte Chemie International Edition, 53 (2014) 5322-5326.

M.L.P. Le, N.A. Tran, H.P.K. Ngo, T.G. Nguyen, V.M. Tran, Liquid Electrolytes Based on Ionic Liquids for Lithium-Ion Batteries, Journal of Solution Chemistry, 44 (2015) 2332-2343.

S. Lee, N. V.D. Long, M.Lee, Design and Optimization of Natural Gas Liquefaction and Recovery Processes for Offshore Floating Liquefied Natural Gas Plants, Industrial & Engineering Chemistry Research, 51 (2012) 10021-10030.

Z. Lei, C. Dai, B. Chen, Gas Solubility in Ionic Liquids, Chemical Reviews, 114 (2014) 1289-1326.

X. Li, J. Li, Fluxes and Driving Forces in Membrane Separation Processes, in: E. Drioli, L. Giorno (Eds.) Encyclopedia of Membranes, Springer Berlin Heidelberg, Berlin, Heidelberg, 2015, pp. 1-3.

H. Lin, B.D. Freeman, Chapter 7: Permeation and Diffusion, in: Springer Handbook of Materials Measurement Methods, 2006, pp. 371-387.

X. Liu, E. Ruiz, W. Afzal, V. Ferro, J. Palomar, J.M. Prausnitz, High Solubilities for Methane, Ethane, Ethylene, and Propane in Trimethyloctylphosphonium Bis(2,4,4-trimethylpentyl) Phosphinate ([P8111][TMPP]), Industrial & Engineering Chemistry Research, 53 (2014) 363-368.

X. Liu, W. Afzal, J.M. Prausnitz, Unusual trend of viscosities and densities for four ionic liquids containing a tetraalkyl phosphonium cation and the anion bis(2,4,4-trimethylpentyl) phosphinate, The Journal of Chemical Thermodynamics, 70 (2014) 122-126.

X. Liu, W. Afzal, M. He, J.M. Prausnitz, Solubilities of small hydrocarbons, viscosities of diluted tetraalkylphosphonium bis(2,4,4-trimethylpentyl) phosphinates, AIChE Journal, 60 (2014) 2607-2612.

R.P. Lively, D.S. Scholl, Seven Separations to Change the World, Nature 532 (2016) 435-437.

H.A. Mannan, D.F. Mohshim, H. Mukhtar, T. Murugesan, Z. Man, M.A. Bustam, Synthesis, characterization, and CO_2 separation performance of polyether

sulfone/[EMIM][Tf$_2$N] ionic liquid-polymeric membranes (ILPMs), Journal of Industrial and Engineering Chemistry, 54 (2017) 98-106.

S. Markova, V. Zhmakin, T. Gries, V. Teplyakov, Combination of the Experimental and Theoretical Approaches for the Estimation of the C$_1$–C$_4$ Alkane Permeability Parameters in Poly (4-Methyl-2-Pentyne) and Poly (4-Methyl-1-Pentene), Applied Sciences, 10 (2020) 1735.

T. Masuda, E. Isobe, T. Higashimura, K. Takada, Poly[1-(trimethylsilyl)-1-propyne]: A new high polymer synthesized with transition-metal catalysts and characterized by extremely high gas permeability. Journal of the American Chemical Society, 105 (1983) 7473-7474.

T. Masuda, Substituted Polyacetylenes: Synthesis, Properties, and Functions, Polymer Reviews, 57 (2016) 1-14.

S. Matteucci, Y. Yampol'skii, B.D. Freeman, I. Pinnau, Transport of gases and vapors in glassy and rubbery polymers, in: Y. Yampol'skii, I. Pinnau, B.D. Freeman (Eds.) Materials Science of Membranes, John Wiley & Sons, Chichester, 2006.

T.C. Merkel, V.I. Bondar, K. Nagai, B.D. Freeman, Sorption and Transport of Hydrocarbon and Perfluorocarbon Gases in Poly(1-trimethylsilyl-1-propyne), Journal of Polymer Science Part B: Polymer Physics 38 (2000) 415-434.

T.C. Merkel, B.D. Freeman, R.J. Spontak, Z. He, I. Pinnau, P. Meakin, A.J. Hill, Sorption, Transport, and Structural Evidence for Enhanced Free Volume in Poly(4-methyl-2-pentyne)/Fumed Silica Nanocomposite Membranes, Chemistry of Materials, 15 (2003) 109-123.

T.C. Merkel, B.D. Freeman, R.J. Spontak, Z. He, I. Pinnau, P. Meakin, A.J. Hill, Ultrapermeable, Reverse-Selective Nanocomposite Membranes, Science, 296 (2002) 519.

T.C. Merkel, Z. He, I. Pinnau, B.D. Freeman, P. Meakin, A.J. Hill, Effect of Nanoparticles on Gas Sorption and Transport in Poly(1-trimethylsilyl-1-propyne), Macromolecules, 36 (2003) 6844-6855.

A.S. Michaels, H.J. Bixler, Flow of gases through polyethylene, Journal of Polymer Science, 50 (1961) 413-439.

C. Miguel Sanchez, T. Song, J.F. Brennecke, B.D. Freeman, Hydrogen Stable Supported Ionic Liquid Membranes with Silver Carriers: Propylene and Propane Permeability and Solubility, Industrial & Engineering Chemistry Research, 59 (2020) 5362-5370.

B.S. Minhas, D.W. Staubs, Membrane process for LPG recovery U.S. Patent 7,799,964 B2 (April 2006).

F. Moghadam, E. Kamio, A. Yoshizumi, H. Matsuyama, An amino acid ionic liquid-based tough ion gel membrane for CO_2 capture, Chemical Communications, 51 (2015) 13658-13661.

J.D. Moon, Impact of Humidity and Polymer Blending on the Gas Transport Properties of Polybenzimidazoles, PhD dissertation, The University of Texas at Austin, Austin, TX, 2019.

D. Morgan, L. Ferguson, P. Scovazzo, Diffusivities of Gases in Room-Temperature Ionic Liquids: Data and Correlations Obtained Using a Lag-Time Technique, Industrial & Engineering Chemistry Research, 44 (2005) 4815-4823.

A. Morisato, B.D. Freeman, I. Pinnau, C.G. Casillas, Pure hydrocarbon sorption properties of poly(1-trimethylsilyl-1-propyne) (PTMSP), poly(1-phenyl-1-propyne) (PPP), and PTMSP/PPP blends, Journal of Polymer Science Part B: Polymer Physics, 34 (1996) 1925-1934.

A. Morisato, B.D. Freeman, I. Pinnau, C.G. Casillas, Pure hydrocarbon sorption properties of poly(1-trimethylsilyl-1-propyne) (PTMSP), poly(1-phenyl-1-propyne) (PPP), and PTMSP/PPP blends, Journal of Polymer Science Part B: Polymer Physics, 34 (1996) 1925-1934.

K. Nagai, T. Masuda, T. Nakagawa, B.D. Freeman, I. Pinnau, Poly[1-(trimethylsilyl)-1-propyne] and related polymers: synthesis, properties and functions, Progress in Polymer Science, 26 (2001) 721-798.

K. Nagai, A. Sugawara, S. Kazama, B.D. Freeman, Effects of physical aging on solubility, diffusivity, and permeability of propane and n-butane in poly(4-

methyl-2-pentyne), Journal of Polymer Science Part B: Polymer Physics, 42 (2004) 2407-2418.

K. Nagai, L.G. Toy, B.D. Freeman, M. Teraguchi, G. Kwak, T. Masuda, I. Pinnau, Gas permeability and n-butane solubility of poly(1-trimethylgermyl-1-propyne), Journal of Polymer Science Part B: Polymer Physics, 40 (2002) 2228-2236.

T. Nakagawa, T. Watanabe, M. Mori, K. Nagai, Aging of Gas Permeability in Poly[1-(trimethylsilyl)-1-propyne] (PTMSP) and PTMSP-Poly(tert-butylacetylene) Blends. ACS Symposium Series Polymer Membranes for Gas and Vapor Separation, 733 (1999) 68-84.

R.D. Noble, D.L. Gin, Perspective on ionic liquids and ionic liquid membranes, Journal of Membrane Science, 369 (2011) 1-4.

W. Ogieglo, H. Wormeester, M. Wessling, N. E. Benes, Effective medium approximations for penetrant sorption in glassy polymers accounting for excess free volume, Polymer (Guildf), 55 (2014) 1737-1744.

K. Ohlrogge, J. Wind, A Method and Apparatus for reducing Emissions from Breather lined Storage Tanks, U.S. Patent 6,059,856 (May 2000).

J. Park, H. Ha, H.W. Yoon, J. Noh, H.B. Park, D.R. Paul, C.J. Ellison, B.D. Freeman, Gas sorption and diffusion in poly(dimethylsiloxane) (PDMS)/graphene oxide (GO) nanocomposite membranes, Polymer, 212 (2021) 123185.

D.R. Paul, Y.P. Yampol'skii, Gas Separation Membranes, CRC Press, Boca Raton, 2018, 116-118.

A. Pederstad, Improving utilization of associated gas in US tight oil fields (Rep. No. 988 457 930), Carbon Limits, Oslo, Norway, 2015.

I. Pinnau, C. G. Casillas, A. Morisato, B.D. Freeman, Hydrocarbon/Hydrogen Mixed Gas Permeation in Poly(1 -trimethylsilyl-1 -propyne) (PTMSP), Poly(1 -phenyl-1 -propyne) (PPP), and PTMSP/PPP Blends. Journal of Polymer Science: Part B: Polymer Physics, 34 (1996) 2613-2621.

I. Pinnau, Z. He, Pure- and mixed-gas permeation properties of polydimethylsiloxane for hydrocarbon/methane and hydrocarbon/hydrogen separation, Journal of Membrane Science, 244 (2004) 227-233.

I. Pinnau, L.G. Toy, Transport of organic vapors through poly(1-trimethylsilyl-1-propyne), Journal of Membrane Science, 116 (1996) 199-209.

V. Polevaya, V. Geiger, G. Bondarenko, S. Shishatskiy, V. Khotimskiy, Chemical Modification of Poly(1-Trimethylsylil-1-Propyne) for the Creation of Highly Efficient CO_2-Selective Membrane Materials, Materials, 12 (2019) 2763.

V. Polevaya, A. Vorobei, A. Gavrikov, S. Matson, O. Parenago, S. Shishatskiy, V. Khotimskiy, Modification of Poly(4-methyl-2-pentyne) in the Supercritical Fluid Medium for Selective Membrane Separation of CO_2 from Various Gas Mixtures, Polymers, 12 (2020) 2468.

C.F. Poole, S.K. Poole, Ionic liquid stationary phases for gas chromatography, Journal of Separation Science, 34 (2011) 888-900.

D.S. Pope, W.J. Koros, H.B. Hopfenberg, Sorption and Dilation of Poly(1-(trimethylsilyl)-1-propyne) by Carbon Dioxide and Methane, Macromolecules, 27 (1994) 5839-5844.

R. Prydz, R.D. Goodwin, Experimental melting and vapor pressures of methane, The Journal of Chemical Thermodynamics, 4 (1972) 127-133.

D.G. Pye, H.H. Hoehn, M. Panar, Measurement of gas permeability of polymers. I. Permeabilities in constant volume/variable pressure apparatus, Journal of Applied Polymer Science, 20 (1976) 1921-1931.

R.D. Raharjo, B.D. Freeman, D.R. Paul, E.S. Sanders, Pure and mixed gas CH_4 and n-C_4H_{10} permeability and diffusivity in poly(1-trimethylsilyl-1-propyne), Polymer, 48 (2007) 7329-7344.

R.D. Raharjo, B.D. Freeman, D.R. Paul, G.C. Sarti, E.S. Sanders, Pure and mixed gas CH_4 and n-C_4H_{10} permeability and diffusivity in poly(dimethylsiloxane), Journal of Membrane Science, 306 (2007) 75-92.

R.D. Raharjo, B.D. Freeman, E.S. Sanders, Pure and mixed gas CH_4 and n-C_4H_{10} sorption and dilation in poly(1-trimethylsilyl-1-propyne), Polymer, 48 (2007) 6097-6114.

R.D. Raharjo, B.D. Freeman, E.S. Sanders, Pure and mixed gas CH_4 and n-C_4H_{10} sorption and dilation in poly(dimethylsiloxane), Journal of Membrane Science, 292 (2007) 45-61.

R.D. Raharjo, H. Lin, D.F. Sanders, B.D. Freeman, S. Kalakkunnath, D.S. Kalika, Relation between network structure and gas transport in crosslinked poly(propylene glycol diacrylate), Journal of Membrane Science, 283 (2006) 253-265.

R.D. Raharjo, Mixed Gas Sorption and Transport Study in Solubility Selective Polymers, PhD dissertation, The University of Texas at Austin, Austin, TX, 2007.

M.B. Rao, S. Sircar, Nanoporous carbon membranes for separation of gas mixtures by selective surface flow, Journal of Membrane Science, 85 (1993) 253-264.

C.P. Ribeiro, B.D. Freeman, D.R. Paul, Pure- and mixed-gas carbon dioxide/ethane permeability and diffusivity in a cross-linked poly(ethylene oxide) copolymer, Journal of Membrane Science, 377 (2011) 110-123.

C.P. Ribeiro, B.D. Freeman, Carbon dioxide/ethane mixed-gas sorption and dilation in a cross-linked poly(ethylene oxide) copolymer, Polymer, 51 (2010) 1156-1168.

C.P. Ribeiro, B.D. Freeman, Sorption, Dilation, and Partial Molar Volumes of Carbon Dioxide and Ethane in Cross-Linked Poly(ethylene oxide), Macromolecules, 41 (2008) 9458-9468.

M. Richter, M.O. McLinden, Vapor-Phase (p, ρ, T, x) Behavior and Virial Coefficients for the (Methane + Propane) System, Journal of Chemical & Engineering Data, 59 (2014) 4151-4164.

T. Ridha, Y. Li, E. Gençer, J, Siirola, J. Miller, F. Ribeiro, R. Agrawal, Valorization of Shale Gas Condensate to Liquid Hydrocarbons through Catalytic Dehydrogenation and Oligomerization, Processes, 6 (2018) 139.

L.M. Robeson, The upper bound revisited, Journal of Membrane Science, 320 (2008) 390-400.

M. Rungta, C. Zhang, W.J. Koros, L. Xu, Membrane-based ethylene/ethane separation: The upper bound and beyond, AIChE Journal, 59 (2013) 3475-3489.

I.C. Sanchez, R.H. Lacombe, Statistical Thermodynamics of Polymer Solutions, Macromolecules, 11 (1978) 1145–1156.

R. Sander, Compilation of Henry's law constants (version 4.0) for water as solvent, Atmos. Chem. Phys., 15 (2015) 4399-4981.

C.A. Scholes, G.W. Stevens, S.E. Kentish, Membrane gas separation applications in natural gas processing, Fuel 96 (2012) 15-28.

C.A. Scholes, G.W. Stevens, S.E. Kentish, Modeling syngas permeation through a poly dimethyl siloxane membrane by Flory–Rehner theory, Separation and Purification Technology, 116 (2013) 13-18.

P. Scovazzo, Determination of the upper limits, benchmarks, and critical properties for gas separations using stabilized room temperature ionic liquid membranes (SILMs) for the purpose of guiding future research, Journal of Membrane Science, 343 (2009) 199-211.

M.S. Shannon, J.M. Tedstone, S.P.O. Danielsen, M.S. Hindman, A.C. Irvin, J.E. Bara, Free Volume as the Basis of Gas Solubility and Selectivity in Imidazolium-Based Ionic Liquids, Industrial & Engineering Chemistry Research, 51 (2012) 5565-5576.

V.P. Shantarovich, I.B. Kevdina, Y.P. Yampol'skii, A.Y. Alentiev, Positron Annihilation Lifetime Study of High and Low Free Volume Glassy Polymers: Effects of Free Volume Sizes on the Permeability and Permselectivity, Macromolecules, 33 (2000) 7453-7466.

O. Shekhah, V. Chernikova, Y. Belmabkhout, M. Eddaoudi, Metal–Organic Framework Membranes: From Fabrication to Gas Separation, Crystals, 8 (2018).

J.-J. Shieh, T.S. Chung, Gas permeability, diffusivity, and solubility of poly(4-vinylpyridine) film, Journal of Polymer Science Part B: Polymer Physics, 37 (1999) 2851-2861.

M.B. Shiflett, E.J. Maginn, The solubility of gases in ionic liquids. AIChE Journal, 63 (2017) 4722-4737.

T. Song, O. Morales-Collazo, J.F. Brennecke, Solubility and Diffusivity of Oxygen in Ionic Liquids, Journal of Chemical & Engineering Data, 64 (2019) 4956-4967.

L.E. Starannikova, N.A. Belov, V.P. Shantorovich, T. Suzuki, T.G. Golenko, K.L. Makovetskii, Y.P. Yampol'skii, Transport and physicochemical parameters of polypentenamer, Polymer Science Series A, 49 (2007) 509-516.

L. Starannikova, Y. Yampol'skii, K. Makovet'skii, T. Golenko, A novel high permeability rubbery membrane material – cis-polypentenamer, Desalination, 200 (2006) 18-19.

G.C. Straty, R. Tsumura, PVT and Vapor Pressure Measurements on Ethane, Journal of research of the National Bureau of Standards. Section A, Physics and chemistry, 80A (1976) 35-39.

E.Y. Sultanov, A.A. Ezhov, S.M. Shishatskiy, K. Buhr, V.S. Khotimskiy, Synthesis, Characterization, and Properties of Poly(1-trimethylsilyl-1-propyne)-block-poly(4-methyl-2-pentyne) Block Copolymers, Macromolecules, 45 (2012) 1222-1229.

E.Y. Sultanov, M.Y. Gorshkova, E.N. Semenistaya, V.S. Khotimsky, Living polymerization of 4-methyl-2-pentyne and 1-trimethylsilyl-1-propyne initiated by $NbCl_5-Ph_4Sn$ catalyst, Polymer Science Series B, 50 (2008) 330-333.

J. Sun, M. Forsyth, D.R. MacFarlane, Room-Temperature Molten Salts Based on the Quaternary Ammonium Ion, The Journal of Physical Chemistry B, 102 (1998) 8858-8864.

M.S. Suwandi, T. Hirose, S.A. Stern, Permeation, diffusion, and solution of cyclopropane in silicone rubber, Journal of Polymer Science Part B: Polymer Physics, 28 (1990) 407-423.

185

V.P. Talluri, P. Patakova, T. Moucha, O. Vopicka, Transient and Steady Pervaporation of 1-Butanol–Water Mixtures through a Poly[1-(Trimethylsilyl)-1-Propyne] (PTMSP) Membrane, Polymers, 11 (2019) 1943.

D. Tammaro, L. Lombardi, G. Scherillo, E. Di Maio, N. Ahuja, G. Mensitieri, Modelling Sorption Thermodynamics and Mass Transport of n-Hexane in a Propylene-Ethylene Elastomer, Polymers 13 (2021) 1157.

S. Thomas, I. Pinnau, N. Du, M.D. Guiver, Hydrocarbon/hydrogen mixed-gas permeation properties of PIM-1, an amorphous microporous spirobisindane polymer, Journal of Membrane Science, 338 (2009) 1-4.

S. Thomas, I. Pinnau, N. Du, M.D. Guiver, Pure- and mixed-gas permeation properties of a microporous spirobisindane-based ladder polymer (PIM-1), Journal of Membrane Science, 333 (2009) 125-131.

L.C. Tomé, I.M. Marrucho, Ionic liquid-based materials: a platform to design engineered CO_2 separation membranes, Chemical Society Reviews, 45 (2016) 2785-2824.

L.G. Toy, K. Nagai, B.D. Freeman, I. Pinnau, Z. He, T. Masuda, M. Teraguchi, Y.P. Yampolskii, Pure-Gas and Vapor Permeation and Sorption Properties of Poly[1-phenyl-2-[p-(trimethylsilyl)phenyl]acetylene] (PTMSDPA), Macromolecules, 33 (2000) 2516-2524.

G. Tu, Z. Liao, Z. Huang, B. Jiang, J. Wang, Y. Yang, Strategy of effluent recovery technology selection in polyolefin plants, Process Safety and Environmental Protection, 103 (2016) 405-412.

U.S. Energy Information Administration, Petroleum Supply Annual, 2017.

U.S. Energy Information Administration, Monthly Crude Oil and Natural Gas Production, 2020.

H.C. Van Ness, M.M. Abbott, Thermodynamics, in: R.H. Perry, D.W. Green (Eds.), Perry's Chemical Engineer's Handbook, 8th Edition, McGraw-Hill Professional, New York, 2008, pp. 4-19-4-21.

D.W. van Krevelen, Properties of Polymers, 3rd Ed, Elsevier, Amsterdam, 1990.

A.V. Volkov, D.S. Bakhtin, L.A. Kulikov, M.V. Terenina, G.S. Golubev, G.N. Bondarenko, S.A. Legkov, G.A. Shandryuk, V.V. Volkov, V.S. Khotimskiy, A.A. Belogorlov, A.L. Maksimov, E.A. Karakhanov, Stabilization of gas transport properties of PTMSP with porous aromatic framework: Effect of annealing, Journal of Membrane Science, 517 (2016) 80-90.

A. Volkov, A. Yushkin, A. Grekhov, A. Shutova, S. Bazhenov, S. Tsarkov, V. Khotimsky, T.J.H. Vlugt, V. Volkov, Liquid permeation through PTMSP: One polymer for two different membrane applications, Journal of Membrane Science, 440 (2013) 98-107.

V. Volkov, Free Volume Structure and Transport Properties of Glassy Polymers— Materials for Separating Membranes, Nature Polymer, 23 (1991) 457–466.

X. Wang, R. Daniels, R.W. Baker, A Recovery of VOCs from High-Volume Low Concentration Air Streams, AIChE Journal 47 (2001) 1094-1097.

X. Wang, A. Hill, B.D. Freeman, I.C. Sanchez, Structural, sorption and transport characteristics of an ultrapermeable polymer. Journal of Membrane Science 314 (2008) 15–23.

J. Wang, J. Luo, S. Feng, H. Li, Y. Wan, X. Zhang, Recent development of ionic liquid membranes, Green Energy & Environment, 1 (2016) 43-61.

R. Wei, High-Pressure Phase Equilibria of Ionic Liquids and Compressed Gases for Applications in Reactions and Absorption Refrigeration, PhD Dissertation, The University of Kansas, Lawrence, Kansas, 2009.

L.C. Witchey-Lakshmanan, H.B. Hopfenberg, R.T. Chern, Sorption and transport of organic vapors in poly[1-(trimethylsilyl)-1-propyne], Journal of Membrane Science, 48 (1990) 321-331.

Y. Yampol'skii, A Current Position of Polyacetylenes Among Other Highly Permeable Membrane Materials, Polymer Reviews, 57 (2017) 200-212.

S. Yi, B. Ghanem, Y. Liu, I. Pinnau, W.J. Koros, Ultraselective glassy polymer membranes with unprecedented performance for energy-efficient sour gas separation, Science Advances, 5 (2019) eaaw5459.

B. Yoo, W. Afzal, J.M. Prausnitz, Effect of Water on the Densities and Viscosities of Some Ionic Liquids Containing a Phosphonium Cation, Zeitschrift für Physikalische Chemie, 227 (2013) 157-166.

A. Yushkin, A. Grekhov, S. Matson, M. Bermeshev, V. Khotimsky, E. Finkelstein, P.M. Budd, V. Volkov, T.J.H. Vlugt, A. Volkov, Study of glassy polymers fractional accessible volume (FAV) by extended method of hydrostatic weighing: Effect of porous structure on liquid transport, Reactive and Functional Polymers, 86 (2015) 269-281.

H. Zhao, X. Ding, Z. Wei, Q. Xie, Y. Zhang, X. Tan, H_2/CO_2 Gas Transport Performance in Poly (Ethylene Oxide) Reverse-selective Membrane with Star-like Structures, Journal of Wuhan University of Technology-Mater. Sci. Ed., 34 (2019) 195-200.

H. Zhao, Z. Lai, A. Firoozabadi, Sorption Hysteresis of Light Hydrocarbons and Carbon Dioxide in Shale and Kerogen, Scientific Reports, 7 (2017) 16209.

Vita

Jose Carlos Davila Labastida was born to Laura Imelda Labastida Michel and Jose Manuel Davila Sastrias in Querétaro, México. He began high school at Monterrey Tech in Querétaro, moved to Texas in 2011 and graduated from Round Rock High School in 2013. Jose Carlos attended Texas A&M University in College Station, where he earned a Bachelor of Science in Chemical Engineering along with three minors in 2017. He subsequently enrolled in The University of Texas at Austin under guidance of Professor Joan F. Brennecke and Professor Benny D. Freeman and graduated with a Master of Science in Engineering in 2021.

Permanent email address: jc.davilabas@gmail.com

This thesis was typed by Jose Carlos Davila Labastida.